DOCTOR OF SCIENCES

Hunting modifications of gravity from the lab to cosmology via compact objects

Schlogel, Sandrine

Award date:
2016

Awarding institution:
University of Namur

UNIVERSITÉ DE NAMUR

FACULTÉ DES SCIENCES
DÉPARTEMENT DE MATHÉMATIQUE

Hunting modifications of gravity:

from the lab to cosmology via compact objects

Thèse présentée par
Sandrine Schlögel
pour l'obtention du grade
de Docteur en Sciences

Composition du Jury:

Ruth DURRER
André FÜZFA (Promoteur)
Anne LEMAÎTRE (Président du Jury)
David F. MOTA
Christophe RINGEVAL (Promoteur)

Octobre 2016

Imprimé en Belgique

ISBN : 978-2-87037-939-4
Dépôt légal: D / 2016/ 1881/27

Université de Namur
Faculté des Sciences
rue de Bruxelles, 61, B-5000 Namur (Belgique)

Hunting modifications of gravity:
from the lab to cosmology via compact objects

by Sandrine Schlögel

Abstract: Modifications of gravity have been considered to model the primordial inflation and the late-time cosmic acceleration. Provided that modified gravity models do not suffer from theoretical instabilities, they must be confronted with observations, not only at the cosmological scales, but also with the local tests of gravity, in the lab and in the Solar System, as well as at the astrophysical scales. Considering in particular sub-classes of the Horndeski gravity, we study their observational predictions at different scales. In order to pass the local tests of gravity while allowing for long-range interactions in cosmology, Horndeski gravity exhibits screening mechanisms, among them the chameleon. The chameleon screening mechanism has been tested recently using atom interferometry in a vacuum chamber. Numerical simulations are provided in this thesis in order to refine the analytical predictions. At the astrophysical scale, Horndeski gravity predicts a variation of the gravitational coupling inside compact stars. Focusing on Higgs inflation, we discuss to what extent the Higgs vacuum expectation value varies inside stars and conclude whether the effect is detectable in gravitational and nuclear physics. Finally, the covariant Galileon model exhibits non-linearities in the scalar field kinetic term such that it might pass the local tests of gravity thanks to the Vainshtein screening mechanism. We discuss if a sub-class of the covariant Galileon theory dubbed the Fab Four model leads to a viable inflationary phase and provide combined analysis with neutron stars and Solar System observables.

Ph.D. thesis in Physics
Date: October 7th, 2016
Department of Mathematics
Advisors: André FÜZFA (UNamur), Christophe RINGEVAL (UCLouvain)

À la poursuite de modifications de la gravitation:
du laboratoire à la cosmologie en passant par les objets compacts

par Sandrine Schlögel

Résumé : Dans le cadre de la cosmologie moderne, des modifications de la théorie d'Einstein ont été étudiées pour expliquer l'inflation primordiale et l'accélération actuelle de l'expansion de l'Univers. Pourvu que ces modèles de gravitation modifiée soient bien posés théoriquement, ils sont confrontés aux observations, non seulement en cosmologie, mais aussi en laboratoire et dans le Système Solaire ainsi qu'en astrophysique. Nous étudions dans cette thèse les prédictions de quelques sous-classes de la théorie d'Horndeski à différentes échelles. Ces théories font en général appel à des mécanismes d'écrantage afin de modéliser des interactions à longue portée tout en étant conformes aux contraintes observationnelles aux échelles locales. Parmi ces mécanismes d'écrantage, le caméléon a été récemment testé en laboratoire grâce à l'interférométrie atomique. Des simulations numériques de cette expérience sont développées dans cette thèse afin de raffiner les prédictions dérivées analytiquement. Aux échelles astrophysiques, la théorie d'Horndeski prévoit une variation du couplage gravitationnel à l'intérieur des objets compacts. Nous nous attardons dans cette thèse sur la 'Higgs inflation' en particulier. Nous discutons les variations de la valeur moyenne dans le vide du champ de Higgs prédites par ce modèle afin d'établir si celles-ci sont détectables dans des objets astrophysiques. Finalement, nous étudions une sous-classe du modèle du 'Galileon covariant', le modèle des 'Fab Four', qui fait appel au mécanisme d'écrantage de Vainshtein pour passer les contraintes locales. Nous analysons si le modèle des 'Fab Four' peut donner lieu à une phase d'inflation conforme aux observations. Nous étudions également les prédictions de ce dernier modèle aux échelles astrophysiques, en particulier dans les étoiles à neutron et le Système Solaire, et mettont en évidence les déviations du couplage gravitationnel prédites par les 'Fab Four'.

Thèse de doctorat en Sciences Physiques
Date: 07/10/2016
Département de Mathématique
Promoteurs: André FÜZFA (UNamur), Christophe RINGEVAL (UCLouvain)

Thank you...

"Des chercheurs qui cherchent,
On en trouve.
Des chercheurs qui trouvent,
On en cherche.
Inventrices et vous inventeurs,
De tous les pays unissez-vous.
L'homme n'a pas été au bout
De tous ses possibles."

Julos Beaucarne

"Chercher n'est pas une chose
et trouver une autre,
mais le gain de la recherche,
c'est la recherche elle-même."

St-Grégoire de Nysse

I like to say that my PhD thesis was most of the time a solitary work, but that I did it not alone. I met a lot of people during those four years. Some of them taught me the job of researcher, others allowed me to take distance from my research topics (breaks are important too) and some of them have finally become friends.

I would like to thank first Ruth Durrer and David F. Mota for having accepted to be the rapporteurs of this thesis. Their reflections, suggestions and the ensuing discussion allowed me to bring a fresh perspective to my thesis. Merci aussi à Ruth de m'avoir accueillie dans le groupe de recherche à Genève pendant quelques mois. Même si notre projet de recherche n'aura donné lieu à aucun résultat publiable, certains fruits de ce travail se trouvent entre les lignes de cette thèse.

Merci à Anne Lemaître d'avoir présidé ce jury... et d'avoir repéré des fautes d'orthographe et d'anglais qui m'avaient échappées !

Cette thèse n'aurait pas pu voir le jour sans mes deux directeurs de thèse. Merci à André Füzfa de m'avoir guidée dans la recherche en relativité générale et en cosmologie. Je le remercie pour la confiance qu'il m'a accordée tout au long de ces quatres années, non seulement dans mon travail de recherche, mais aussi lors d'expériences de vulgarisation scientifique. Enfin, je lui suis reconnaissante de m'avoir permis de m'essayer à l'astronomie. Je pense que nous nous souviendrons pendant longtemps de ces nuits passées en compagine de Jean-Pol, Eve, Chapi Chapo et bien d'autres, les pieds glacés guettant l'amas de la ruche (M44 pour les intimes) entre deux nuages en partageant un *Pick Up!*. Merci à Christophe Ringeval pour la relecture de ce manuscrit alors que ce dernier était encore à l'état d'ébauche. Ses remarques m'auront permis d'acquérir une plus grande rigueur et d'approfondir mes idées.

Je tiens aussi à remercier l'ensemble des chercheurs avec qui j'ai eu la chance de collaborer, de près ou de loin, durant ma thèse. Merci à Max Rinaldi de m'avoir accompagnée dans l'apprentissage du métier de chercheur. Merci aussi de m'avoir incitée à découvrir d'autres univers de recherche, d'abord en me poussant à aller à Genève, ensuite en m'invitant à Trento.

Merci à Sébastien Clesse d'avoir donné une nouvelle impulsion au "groupe cosmo" de Namur. Je me souviendrai non seulement de l'élevage de caméléons lancé ensemble, mais aussi des différentes activités du Printemps des Sciences, comme les contes d'Alice et d'Umitou, ou encore le spectacle du Pr Big et du Dr Bang.

Thanks to Karel Van Acoleyen for the guidance of my first steps in modified gravity when I was still a master student. The tools I developed then have been proven very useful all along my thesis. Thanks also for having accepted to be part of my "comité d'accompagnement" during the last four years.

Merci à Jean-Philippe Bruneton pour nos discussions scientifiques annuelles autour d'une bonne bière, à Paris ou à Namur... c'est également ainsi qu'avance la science. Merci encore à Aurélien Hees et Olivier Minazzoli pour cette dernière année de collaboration. Si le Higgs ne nous a pas encore révélé toutes ses subtilités, c'est sans doute que nous n'en avons pas encore assez discuté autour d'un verre. Thanks to Holger Müller to have contacted me during the Marcel Grossmann meeting. It was really great to have the oppotunity to discuss with experimentalists about chameleons.

Nevertheless, my PhD thesis also strongly benefits from what I did with the university in addition to scientific research. I have already mentionned scientific outreach but that's not all!

Le voyage en Inde organisé par l'ONG de l'Université de Namur m'aura permis de me donner un second souffle au milieu de ces quatre années, de voir "autre chose" (par exemple, découvrir le jack fruit). Merci à tout le groupe Dinde ainsi qu'à ceux qui nous ont aidés à préparer ce voyage. In particular, I thank John for the corrections of some selected parts of this thesis.

Thanks to all the researchers I met during my research stays at the University of Geneva. Thanks for having adopted me as a member of the research group for a few months. I not only appreciated the discussions about science,

but also about our respective cultures, for instance smashing the traditional Genevan marmite together or celebrating the German (and Belgian!) St. Nikolaus.

Thanks to all my office mates for one week, one month, one year (Aurélie, Marco and Giovanni, Alexis, Ioannis, Marie-Hélène and Adrien). I strongly enjoyed to share time with you and I took advantage of the opportunity to learn some words in Italian (I would not mention which ones here)!

As I said, at the end of those four years, some of my colleagues have become friends. Merci à Evallou et Marou pour les Megagigantorigolades et autres Poussinmontagnes[(1)]. Merci aussi pour ce merveilleux pélerinage cosmologique à Rome à l'occasion du Marcel Gross'blague. Merci à Alexis pour le voyage sur la Lune. Nos débats passionnés sur la politique et la philosophie des sciences qui nous ont occupés de longues heures, me manqueront très certainement ! Thanks also to Yérali, Delphinou, Mara, Vivi,... for the great breaks spent in their company.

Merci à mes très-proches, mes amis de longue date et ma famille pour leur soutien ; pour leur compréhension, car ils se sont toujours intéressés à ce que je faisais ; et pour leur incompréhension, car le monde de la recherche est un monde à part qui a ses propres règles, parfois incongrues. Merci à Manu, pour sa présence de tous les jours. Cette thèse lui doit beaucoup, à commencer par la qualité des figures et de la mise en page de ce manuscrit que j'aurais eu bien du mal à faire toute seule.

Thanks to you who reads this thesis...

[(1)] Pour des informations complémentaires, voir par exemple [Ponti07].

Contents

Introduction

Over the last century, general relativity has emerged as the theory of gravitation. It not only allowed the explanation of phenomena that are not in the Newton's theory of gravitation, but also has opened up new perspectives in predictions, especially in astrophysics and cosmology. Indeed, when the gravitational field is very strong, i.e. in compact objects like black holes and neutron stars, relativistic effects are expected. The existence of compact objects is favored by the observations today, using either electromagnetic or gravitational wave signals.

During the last decades, the observations of the sky at large scales have made the study of precision cosmology possible. According to our current understanding, the Universe has a history and is expanding over time. Only 5% of its matter-energy content is described by the standard model of particle physics. Around 68% of the Universe is responsible for the late-time cosmic acceleration which can be modelled thanks to the cosmological constant Λ. The remaining 27% of the matter-energy content of the Universe is composed of cold (i.e. non-relativistic) dark matter (CDM) whose nature is still unknown. The $\Lambda-$CDM concordance picture reproduces the current observations.

Despite of the successes of general relativity and the standard model of particle physics, there are at least two reasons to look for theories beyond this paradigm:

1. At high energy and small distances, quantum effects are expected in general relativity, like other fundamental interactions. Since general relativity is not renormalizable, its quantization is therefore problematic, it should be considered rather as an effective classical theory of gravity emerging from its quantum counterpart. A viable quantum theory of gravitation should first be well-defined and second, conform to current observations. Compact objects and cosmology provide the most promising observational tests of quantum gravity.

2. In cosmology the nature of dark matter and the late-time cosmic acceleration is still debated. Today research for dark matter has shifted to particle physics. The detection of a new particle could reveal an extension of the standard model of particle physics although the distribution

of dark matter in the sky should also be explained. The cosmological constant raises some theoretical issues, in particular why is its value fine-tuned to such a tiny value while still non-zero? Finally, within the $\Lambda-$CDM paradigm, the initial conditions in the early Universe appear to be fine-tuned. An exponentially accelerated phase of expansion in the early Universe referred to as primordial inflation, around 10^{-43} s after the Big Bang, is able to give an explanation of the current observations. The late-time cosmic acceleration and inflation can be modelled either by a) invoking new particles and fields beyond the standard model of particle physics, the scalar fields being privileged for the sake of simplicity, or by b) calling on modifications of gravity.

Since the conception of general relativity, modifications and extensions of the Einstein's theory have been extensively studied, devoted to quantum gravity, the explanation of observations in cosmology or the unification of the fundamental interactions. However, modified gravity is challenging from the theoretical point of view since general relativity has a privileged status as highlighted in Chap. 1: this is the only well-defined theory (for instance it exhibits second-order equations of motion) which guarantees that the physical laws are valid in all coordinate systems in a four dimensional spacetime. In particular, this result is based on the fact that the metric is the only field describing gravity.

Alternative theories must thus first be well-defined and then compared to present observations in order to establish whether they are viable. In Chap. 2, the current observational tests of gravitation are briefly reviewed. We propose to classify them depending on the tested regime given by the strength of the gravitational field and the presence of energy-momentum sources. Today, general relativity has been tested with very good accuracy in the vacuum, either in the weak field regime, i.e. in the Solar System and in the lab, or in the strong field regime, thanks to indirect and direct detection of gravitational waves coming from binary systems.

The presence of sources renders the tests of general relativity trickier since there are uncertainties about the modeling of the sources. This is the case for neutron stars and in cosmology where the cosmological fluid can be considered as a source, possibly of unknown nature like dark energy, dark matter or scalar fields responsible for primordial inflation. Meanwhile the current cosmic expansion and primordial inflation could also reveal modifications of gravity at large scales. In Chap. 3, alternative models to general relativity are introduced and classified depending on which underlying assumptions of general relativity they violate. In particular, we focus on alternatives to general relativity invoking a scalar field counterpart to the metric in order to describe gravity, i.e. scalar-tensor theories. Initially, those theories were devoted to testing the constancy of gravitational coupling in spacetime. Today, scalar-tensor theories have been found to give rise to models for inflation and late-time cosmic expansion in agreement with cosmological observations. Meanwhile, they must be confronted with other observations, like experiments on

the Earth as well as observations in the Solar System and around compact objects, in order to conclude if they are viable alternatives to general relativity.

The first scalar-tensor theory we focus on, is the chameleon model. This model was first proposed by Khoury and Weltman in 2004 [Khoury04b, Khoury04a] in order to reproduce the current cosmic acceleration and to pass the weak-field constraints. This model is based on a screening mechanism: the chameleon effective mass is small in low density environment, the scalar field mediating long range interaction like the late-time cosmic acceleration, while the chameleon becomes massive in high density environment, the effects are so short ranged that they are difficult to measure.

In Chap. 4, we briefly comment the current status of the chameleon model. It has been tested in cosmology, in the Solar System, and recently in astrophysics; a part of the parameter space of the chameleon model remains unconstrained. The most promising test today comes from lab experiments using atom interferometry, as first proposed by Burrage, Copeland and Hinds in 2014 [Burrage15]. Indeed, if the atom interferometer is placed inside a vacuum chamber in the presence of a test mass, the acceleration induced by the chameleon field can be determined with very good accuracy by measuring the interference fringes. A first experiment has been developed in Berkeley. It shows that almost all the chameleon parameter space should be reachable with this experimental set-up in the near future. However, the forecasts for the acceleration due to the chameleon were computed only analytically, neglecting the effects of the vacuum chamber geometry. In Chap. 4, we provide numerical simulations for the on-going experiment in Berkeley in order to refine the analytical constraints and to take into account the effects of the chamber geometry.

In general, scalars mediating gravity are not assumed to be detected in nature as yet and are only considered as hypothetical degrees of freedom. In 2012, the first elementary scalar field, the Higgs field, was detected in the Large Hadron Collider [Aad12, Chatrchyan12]. The question then arises, could the Higgs field be a partner of the Einstein metric for describing gravity? In 2008, Bezrukov and Shaposhnikov propose a model where the Higgs field is the inflaton, provided it is nonminimally coupled to gravity, within the framework of modified gravity [Bezrukov09b]. This model reviewed in Chap. 5 is favored by the latest cosmological observations.

Because of the nonminimal coupling of the Higgs field to gravity, the distribution of the Higgs field around compact objects in the presence of matter is expected to be non trivial, contrary to general relativity (i.e. with a minimally coupled Higgs field) where the Higgs field has settled to its vacuum expectation value (vev) everywhere. If the distribution is not trivial, it implies that the vev varies in spacetime and the Higgs field is not necessarily settled to it, for instance inside compact objects. Because of these variations, the question arises if this model is able to pass current constraints in the Solar System and if the nuclear physics inside neutron stars is affected. These questions are discussed in Chap. 5.

In 1974, Horndeski derived the most general Lagrangian for the extension of general relativity invoking an additional scalar field [Horndeski74]. Scalar-tensor theory is one particular case in the general class highlighted by Horndeski. In Chap. 6, we focus on another theory dubbed the Fab Four model in reference to the four general Lagrangian terms arising in Horndeski gravity, which were rediscovered in 2012 by Copeland, Padilla and Saffin [Copeland12]. This model appears to be well posed from the theoretical point of view. In Chap. 6, the predictions of two of the Fab Four are discussed for primordial inflation as well as in the Solar System and around compact objects.

Finally, we draw some conclusions and perspectives in Part III.

Conventions

Unit system, We use natural units in which $c = \hbar = 1$ such that all quantities are expressed in powers of GeV. The Newton's constant is given by $G_{\rm N} = 1/m_{\rm pl}^2$, $m_{\rm pl}$ being the Planck mass.

Notations, The most used notations are reported in Tab. 0.1. Furthermore, the Greek indices refer to spacetime coordinates, x^μ with $\mu = 0, 1, 2, 3$, while the Latin ones to space coordinates, $x^{\rm i}$ with $i = 1, 2, 3$. The covariant and partial derivatives for any function or tensor $\mathbf{T}$ are respectively denoted by,

$$\nabla_\mu \mathbf{T} = \mathbf{T}_{;\mu}, \tag{0.0.1}$$

$$\partial_\mu \mathbf{T} = \mathbf{T}_{,\mu}. \tag{0.0.2}$$

Time and radial derivatives are respectively denoted by the dot $\mathrm{d}f/\mathrm{d}t \equiv \dot{f}$ and the prime $\mathrm{d}f/\mathrm{d}r \equiv f'$. Vector fields are in bold characters.

Differential geometry, We follow the convention of Misner *et al.*'s reference book [Misner73]. In particular, we adopt the Einstein's implicit summation for repeated indices and the mostly plus signature for the metric $(-,\ +,\ +,\ +)$. Following this convention, the covariant derivative of a tensor $\mathbf{T}$ is given by,

$$\nabla_\lambda T^{\nu_1 \ldots \nu_{\rm q}}_{\mu_1 \ldots \mu_{\rm p}} = \partial_\lambda T^{\nu_1 \ldots \nu_{\rm q}}_{\mu_1 \ldots \mu_{\rm p}} + \Gamma^{\nu_1}_{\lambda\rho} T^{\rho \ldots \nu_{\rm q}}_{\mu_1 \ldots \mu_{\rm p}} \ldots + \Gamma^{\nu_{\rm q}}_{\lambda\rho} T^{\nu_1 \ldots \rho}_{\mu_1 \ldots \mu_{\rm p}} - \Gamma^{\rho}_{\lambda\mu_1} T^{\nu_1 \ldots \nu_{\rm q}}_{\rho \ldots \mu_{\rm p}} - \Gamma^{\rho}_{\lambda\mu_{\rm p}} T^{\nu_1 \ldots \nu_{\rm q}}_{\mu_1 \ldots \rho}. \tag{0.0.3}$$

The components of the Levi-Civita connection are,

$$\left\{ \begin{matrix} \rho \\ \mu\nu \end{matrix} \right\} = \frac{1}{2} g^{\lambda\rho} \left(\partial_\mu g_{\lambda\nu} + \partial_\nu g_{\lambda\mu} - \partial_\lambda g_{\mu\nu} \right), \tag{0.0.4}$$

the Riemann tensor,

$$R^\alpha_{\mu\beta\nu} = \left(\partial_\beta \Gamma^\alpha_{\mu\nu} + \Gamma^\alpha_{\sigma\beta} \Gamma^\sigma_{\mu\nu} \right) - (\beta \leftrightarrow \nu), \tag{0.0.5}$$

the Ricci tensor,

$$R_{\mu\nu} = R^\alpha_{\mu\alpha\nu}, \tag{0.0.6}$$

and the Ricci scalar $R = R^\mu_\mu$. The Einstein tensor is $G_{\mu\nu} = R_{\mu\nu} - \frac{1}{2} g_{\mu\nu} R$ and the Einstein equations read,

$$G_{\mu\nu} = 8\pi G_{\rm N} T_{\mu\nu}. \tag{0.0.7}$$

Symbols and acronyms, The list of symbols and acronyms are reported in Tabs. 0.1 and 0.2.

Symbols	Signification
$a(t)$	scale factor
$\beta_{\rm PPN}$, $\gamma_{\rm PPN}$	post-Newtonian parameters β, γ
c, $G_{\rm N}$	speed of light, Newton's constant
$E_{\rm b}$	binding energy
ϵ, η	slow-roll parameters
$\eta_{\mu\nu}$	Minkowski metric
$g_{\mu\nu}$, g	metric tensor, determinant of $g_{\mu\nu}$
$h_{\mu\nu}$	perturbations of the metric
$\Gamma^{\rho}_{\mu\nu}$	connection coefficients
$G_{\mu\nu}$	Einstein tensor
G	bare gravitational constant
$\mathcal{G}$	Gauss-Bonnet combination
H, H_0	Hubble parameter, Hubble constant
$\kappa \equiv 8\pi/m_{\rm pl}^2$	parameter (action)
Λ	cosmological constant
L, $\mathcal{L}$	Lagrangian, Lagrangian density
$\lambda_{\rm sm}$, v	SM Higgs self-interaction coupling and vev
$\nu(r)$, $\lambda(r)$	metric fields (Schwarzschild gauge)
$\mathcal{M}$	manifold
$m_{\rm pl}$, $M_{\rm pl} = m_{\rm pl}/\sqrt{8\pi}$	Planck mass, reduced Planck mass
$m_{\rm i}$, $m_{\rm g}$	inertial mass, gravitational mass
$M_\odot$, $R_\odot$	Solar mass, Solar radius
$N(t)$	number of e-folds
$n_{\rm s}, r$	spectral index, tensor-to-scalar ratio (inflation)
$\Omega(x)$	conformal factor
$\mathrm{d}\Omega^2 \equiv \mathrm{d}\theta^2 + \sin^2\theta \mathrm{d}\varphi^2$	infinitesimal solid angle
Φ, $U \equiv -\Phi/G_{\rm N}$	Newtonian gravitational potential
ϕ, π	scalar fields
$\psi_{\rm M}$	matter fields
$q(t)$, $\Omega(t)$	deceleration parameter, density parameters
ρ, p	energy density, pressure
$\mathcal{R}$, $r_{\rm s}$	radius of compact objects, Schwarzschild radius
$R^{\mu}_{\nu\lambda\kappa}$, $R_{\mu\nu}$, R	Riemann tensor, Ricci tensor, Ricci scalar
s	compactness
t, 0 subscript	cosmic time, (cosmology) for today
$T_{\mu\nu}$	stress-energy-momentum tensor
$\mathbf{u}$	four-velocity
$V(\phi)$	potential
w	equation of state
ξ	nonminimal coupling constant in Higgs inflation
z	redshift

Table 0.1: List of symbols appearing in this thesis and their signification.

Acronyms	Signification
BAO	Baryon Acoustic Oscillations
BBN	Big Bang Nucleosynthesis
BH	Black Hole
BVP	Boundary Value Problem
CDM	Cold Dark Matter
C.L.	Confidence Level
CMB	Cosmic Microwave Background
DE	Dark Energy
DM	Dark Matter
EF	Einstein frame
EH	Einstein-Hilbert
EoS	Equation of State
FLRW	Friedmann-Lemaître-Robertson-Walker
GR	General Relativity
GW	Gravitational Wave
IVP	Initial Value Problem
JF	Jordan frame
LHC	Large Hadron Collider
LLI	Local Lorentz Invariance
LPI	Local Position Invariance
LSS	Large-Scale Structure
MOND	MOdified Newton Dynamics
NS	Neutron Star
PN	Post-Newtonian
PPN	Parametrized Post-Newtonian
QCD	Quantum Chromodynamics
SgrA*	Sagittarius A*
SEP	Strong Equivalence Principle
SM	Standard Model of particle physics
SN	Supernovae
SR	Special Relativity
STT	Scalar-Tensor theories
TOV	Tolmann-Oppenheimer-Volkoff
UFF	Universality of Free Fall
vev	Vacuum Expectation Value
WEP	Weak Equivalence Principle

Table 0.2: List of acronyms appearing in this thesis and their signification.

Part I

General context

Chapter 1

The Theory of General Relativity

This first chapter is devoted to General Relativity (GR) and its foundations, the action formalism being privileged. The theoretical pillars of GR, among them Lorentz invariance and causality, locality, general covariance as well as second-order equations of motion are introduced. Then the Lovelock theorem is formulated in order to highlight the particular status of GR in 4-dimensional spacetime. Finally, the equivalence principles are discussed in the light of the previous analysis of GR.

1.1 The Mach principle

The concepts of space and time dramatically change from the Newton's theory to the Einstein's one, revealing two philosophical stances. In the XVIIIth century (see also [Rovelli04]), Clarke (and Newton after him) claimed that *"space exists as a substance or as an absolute being and absolute motion is present"* [Alexander77] while Leibniz (and Descartes before him) maintained that *"the space is constituted only in relation to co-existent things allowing for relativism in motions only"* [Alexander77]. During the foundations of GR, Einstein was inspired by the Mach's principle[(1)] [Mach83], which is descended from the Leibniz's point of view, stating that [Brans61],

> MACH PRINCIPLE - *"The geometrical and the inertial properties of space are meaningless for an empty space, [...] the physical properties of space have their origin in the matter contained therein and [...] the only meaningful notion of a particle is motion relative to other matter in the Universe."*

[(1)] We would like to point out here that many different formulations of the Mach principle have been proposed in the literature (see [Rovelli04] for a summary), some of them being fulfilled by GR. In this manuscript, we will follow Brans and Dicke's formulation [Brans61].

In GR, matter affects the gravitational field according to the Mach principle [Rovelli04]. Also position and motion are fully relational in the sense that they are not determined with respect to a fixed non-dynamical background like in Newton's theory [Gaul00]. The local inertial frame is even fully determined by the dynamical fields [Rovelli04]. However, it is clear that GR does not implement the Mach's principle entirely since it admits many vacuum solutions, like the Schwarzschild, Kerr and de Sitter ones. Those aspects will be further discussed in the rest of this chapter. The Mach's point of view on gravity has not only inspired GR but also ways to test GR as well as modified gravity, as we will see in Chap. 2 and 3.

1.2 General picture of General Relativity

Even if GR and the Newton's theory of gravity do not follow from the same philosophical stances, GR must reduce to the Newton's laws in the non-relativistic limit where the gravitational field is weak and velocities are small $v \ll c$, c being the speed of light, according to the **correspondence principle**. In this section, the mathematical aspects of GR are briefly reviewed as well as their weak-field Newtonian counterparts.

1.2.1 Field equations

GR is a classical field theory which can be formulated with an action principle. The most general action is divided into a geometrical part known as the Einstein-Hilbert (EH) action $S_{\rm EH}$ and in the matter action $S_{\rm M}$,

$$S = S_{\rm EH} + S_{\rm M} \tag{1.2.1}$$

$$= \frac{1}{2\kappa}\int \mathrm{d}^4x\sqrt{-g}\,(R-2\Lambda) + S_{\rm M}\left[\psi_{\rm M}; g_{\mu\nu}\right], \tag{1.2.2}$$

with $\kappa \equiv 8\pi/m_{\rm pl}^2$, $m_{\rm pl}$ being the Planck mass; $g_{\mu\nu}$ the metric and g its determinant; R the Ricci scalar; Λ the cosmological constant; and $\psi_{\rm M}$ the matter fields. The equations of motion or Einstein equations are then derived from the action variation with respect to $g_{\mu\nu}$ or equivalently by the **Euler-Lagrange equations**[(2)],

$$\frac{\partial}{\partial x^\rho}\left[\frac{\partial L}{\partial g_{\mu\nu,\,\rho}} - \frac{\partial}{\partial x^\lambda}\left(\frac{\partial L}{\partial g_{\mu\nu,\,\rho\lambda}}\right)\right] - \frac{\partial L}{\partial g_{\mu\nu}} = 0. \tag{1.2.3}$$

[(2)]This Ricci scalar is function of second-order derivatives of the metric (see also Secs. 1.3.4 and 1.4 for a discussion), leading to the definition of the Euler-Lagrange equations given by Eq. (1.2.3).

Reminding the following relations,

$$\delta g^{\mu\nu} = -g^{\alpha\mu}g^{\beta\nu}\delta g_{\alpha\beta}, \tag{1.2.4}$$

$$\frac{1}{\sqrt{-g}}\frac{\delta\sqrt{-g}}{\delta g^{\mu\nu}} = -\frac{1}{2}g_{\mu\nu}, \tag{1.2.5}$$

$$\frac{\delta R}{\delta g^{\mu\nu}} = R_{\mu\nu} + g_{\mu\nu}\Box - \nabla_\mu\nabla_\nu, \tag{1.2.6}$$

the Einstein equations read,

$$G_{\mu\nu} + \Lambda g_{\mu\nu} = \kappa T^{(\mathrm{M})}_{\mu\nu}, \tag{1.2.7}$$

with the stress-energy-momentum tensor $T^{(\mathrm{M})}_{\mu\nu}$[3],

$$T^{(\mathrm{M})}_{\mu\nu} \equiv -\frac{2}{\sqrt{-g}}\frac{\delta S_{\mathrm{M}}}{\delta g^{\mu\nu}}. \tag{1.2.8}$$

The Einstein equations are of second-order in the metric and their solutions determine the metric field $g_{\mu\nu}$ up to a diffeomorphism[4]. The Einstein equations describe the dynamics of the spacetime predicted by GR, that is how the spacetime is curved (left-hand side of Eq. (1.2.7)) depending on the matter-energy composition of the spacetime (right-hand side of Eq. (1.2.7)). According to the correspondence principle, GR reduces to the Newton's theory in the non-relativistic limit if,

$$g_{\mu\nu} = \eta_{\mu\nu} + h_{\mu\nu}, \tag{1.2.9}$$

with $\eta_{\mu\nu}$ the Minkowski metric and $h_{\mu\nu}$ the perturbation ($h \ll 1$). So, the Einstein equations generalize the Poisson equation[5] of the classical mechanics,

$$\nabla^2\Phi = 4\pi G_{\mathrm{N}}\rho, \tag{1.2.10}$$

with $\Phi = -2h_{00}$, the Newtonian gravitational potential. Indeed, the left-hand side of Eq. (1.2.10) is related to the second-order derivative of Φ (more precisely $R_{00} = \nabla^2\Phi$ [Misner73]) while the right-hand side is related to the energy distribution in space.

The conservation of the stress-energy tensor[6],

$$\nabla^\mu T^{(\mathrm{M})}_{\mu\nu} = 0, \tag{1.2.11}$$

generalizes the Eulerian equations of hydrodynamics in the case of a perfect fluid (see Sec. 2.2.1) to curved spacetime. On the other hand, the Einstein

[3] Following standard practice, we will abbreviate "stress-energy-momentum tensor" as "stress-energy tensor".

[4] Notice that the metric is not determined univocally because of the diffeomorphism-invariance of GR. This is because metric fields are potentials rather than observables (see also Sec. 1.3.3 for a discussion). Einstein was troubled with this characteristic of GR during its conception (see e.g. [Rovelli04, Norton93]).

[5] If $\Lambda \neq 0$, it is rather a Helmholtz equation.

[6] The conservation of $T_{\mu\nu}$ can be also derived from the Noether theorem, as shown in App. A

tensor is automatically conserved $\nabla^\mu G_{\mu\nu} = 0$ according to the second Bianchi identity,

$$(\nabla_\kappa R)^\rho_{\lambda\mu\nu} + (\nabla_\nu R)^\rho_{\lambda\kappa\mu} + (\nabla_\mu R)^\rho_{\lambda\nu\kappa} = 0, \tag{1.2.12}$$

by contracting twice Eq. (1.2.12) provided that the affine connection Γ defined as the covariant derivative of basis vectors e_μ,

$$\nabla_\mu e_\nu \equiv \Gamma^\lambda_{\mu\nu} e_\lambda. \tag{1.2.13}$$

is the so-called Levi-Civita one, i.e. is only determined by the metric.

1.2.2 The Levi-Civita connection

The metric has non-trivial properties in GR: it is symmetric $g_{\mu\nu} = g_{\nu\mu}$ such that it has 10 degrees of freedom (provided that the spacetime is four-dimensional), and its covariant derivative vanishes $\nabla^\mu g_{\mu\nu} = 0$, the parallel transport preserving thus distances and angles, so that the second Bianchi identity (1.2.12) holds.

In general, the affine connection (1.2.13) has $4^3 = 64$ degrees of freedom in a four-dimensional spacetime, raising the question where these degrees of freedom come from. In GR, it reduces to the **Levi-Civita connection** which is fully determined by the metric and has no independent degrees of freedom. In particular, the path along which the particles are freely falling i.e. the geodesics (see Sec. 1.2.3), is also fully determined by the metric.

In the case of the general affine connection, the **non-metricity** tensor $Q_{\lambda\mu\nu}$,

$$\nabla_\lambda g_{\mu\nu} = Q_{\lambda\mu\nu}, \tag{1.2.14}$$

is responsible for $4 \times 10 = 40$ degrees of freedom, assuming $g_{\mu\nu} = g_{\nu\mu}$. The remaining 24 degrees of freedom are related to the antisymmetric part of the connection ($4 \times 6 = 24$ degrees of freedom) given by the **torsion tensor**,

$$T^\lambda_{\mu\nu} \equiv \Gamma^\lambda_{\mu\nu} - \Gamma^\lambda_{\nu\mu}. \tag{1.2.15}$$

We can derive the components of the general affine connection $\Gamma^\lambda_{\mu\nu}$ by computing the combination,

$$\begin{aligned} \nabla_\mu g_{\alpha\beta} + \nabla_\alpha g_{\beta\mu} - \nabla_\beta g_{\mu\alpha} &= Q_{\mu\alpha\beta} + Q_{\alpha\beta\mu} - Q_{\beta\mu\alpha} && (1.2.16)\\ &= \partial_\mu g_{\alpha\beta} + \partial_\alpha g_{\beta\mu} - \partial_\beta g_{\mu\alpha} \\ &\quad + \left(\Gamma^\lambda_{\beta\alpha} - \Gamma^\lambda_{\alpha\beta}\right) g_{\lambda\mu} + \left(\Gamma^\lambda_{\beta\mu} - \Gamma^\lambda_{\mu\beta}\right) g_{\lambda\alpha} \\ &\quad - \left(\Gamma^\lambda_{\mu\alpha} + \Gamma^\lambda_{\alpha\mu}\right) g_{\lambda\beta}. && (1.2.17) \end{aligned}$$

Using the definitions of the Levi-Civita connection (0.0.4) as well as the definition of the torsion (1.2.15), we obtain,

$$\begin{aligned} Q_{\mu\alpha\beta} + Q_{\alpha\beta\mu} - Q_{\beta\mu\alpha} &= 2\left\{ \beta\, \mu\, \alpha \right\} + T^\lambda_{\beta\alpha} g_{\lambda\mu} + T^\lambda_{\beta\mu} g_{\lambda\alpha} - T^\lambda_{\alpha\mu} g_{\lambda\beta} \\ &\quad - 2\Gamma_{\beta\mu\alpha}, \end{aligned} \tag{1.2.18}$$

such that the components of the general affine connection read,

$$\Gamma^{\lambda}_{\mu\nu} = \left\{ {\lambda \atop \mu\nu} \right\} + K^{\lambda}_{\mu\nu} + \frac{1}{2}\left(Q^{\lambda}_{\mu\nu} - Q_{\mu\nu}{}^{\lambda} - Q_{\nu}{}^{\lambda}{}_{\mu}\right), \tag{1.2.19}$$

where $K^{\lambda}_{\mu\nu}$ is the contortion tensor,

$$K^{\lambda}_{\mu\nu} = \frac{1}{2}\left(T^{\lambda}_{\mu\nu} + T_{\mu}{}^{\lambda}{}_{\nu} + T_{\nu}{}^{\lambda}{}_{\mu}\right). \tag{1.2.20}$$

1.2.3 Geodesics equations

The Einstein equations only determine the spacetime dynamics. The motion of a body in spacetime derives from the so-called geodesics equations which generalize the Newton's second law for the gravitational force ($\mathbf{F}_{\rm g} = -m\,\nabla\Phi$, m being the test mass),

$$\nabla\Phi = -\frac{\mathrm{d}\mathbf{p}}{\mathrm{d}t}, \tag{1.2.21}$$

with the momentum $\mathbf{p}$.

In GR, because of the spacetime curvature, the notions of straight line and parallelism are adapted by introducing the parallel transport along a curve. A freely falling body takes the shortest path, and moves along the so-called **geodesics**. The general definition of geodesics states that they are the curves whose tangent vector $\mathbf{V}$ is parallel propagated along itself [Wald84], that is satisfying,

$$\nabla_{\mathbf{V}}\mathbf{V} = 0. \tag{1.2.22}$$

In terms of spacetime components, the geodesics equations read,

$$\frac{\mathrm{d}^2x^{\mu}}{\mathrm{d}\lambda^2} + \Gamma^{\mu}_{\nu\rho}\frac{\mathrm{d}x^{\nu}}{\mathrm{d}\lambda}\frac{\mathrm{d}x^{\rho}}{\mathrm{d}\lambda} = 0, \tag{1.2.23}$$

with λ the affine parameter and $\Gamma^{\mu}_{\nu\rho}$ either the affine connection or the Levi-Civita one[(7)]. The geodesics equations can also be derived from the action variation by extremizing the infinitesimal path length $\mathrm{d}s$,

$$S_{\rm geo} = \int \mathrm{d}s = \int \sqrt{-g_{\mu\nu}\mathrm{d}x^{\mu}\mathrm{d}x^{\nu}} = \int \sqrt{-g_{\mu\nu}\frac{\mathrm{d}x^{\mu}}{\mathrm{d}\lambda}\frac{\mathrm{d}x^{\nu}}{\mathrm{d}\lambda}}\mathrm{d}\lambda, \tag{1.2.24}$$

where λ is the affine parameter.

Both the geodesics and the Einstein equations implement the GR theory: on the one hand, spacetime curvature depends on the presence of matter-energy and on the other hand, body motion depends on spacetime curvature. If the motion is considered for test particles with negligible mass, one can solve first Einstein equations to determine spacetime shape and then solve

[(7)] The torsion does not affect the geodesics because of the symmetry over the indices ν and ρ, such that only the non-metricity makes the affine connection different than the Levi-Civita one in this case [Misner73].

geodesics (which correspond to the conservation of $T_{\mu\nu}$ in this case) to characterize the geometry. However, if one considers a large number of test particles whose contribution to curvature cannot be neglected, the problem is hard to handle since no clear starting point exists. This is the reason why a mean field approach is used in general, for instance by assuming a fluid approximation (see Chap. 2).

1.3 The underlying assumptions of GR

After reviewing the usual point of view on GR, we will question in this section what its underlying assumptions are in order to understand why the EH action is so special at some point[8]. Those assumptions are not trivial and have inspired theories of gravity beyond GR.

1.3.1 Lorentz invariance and causality

In classical mechanics, equations of motion are of second order (see Sec. 1.3.4 for a discussion). Initial conditions for the position and the velocity then univocally determine how the system evolves - at least locally - in both direction in time according to the Cauchy theorem.

In Special Relativity (SR), Lorentz invariance implies that the maximal speed of the information propagation, corresponds to the speed of light in the vacuum[9] $c = 1$ and that there exists no closed timelike curve in spacetime. An event is said to be causally connected to another one if and only if points of the spacetime can be joined by non-spacelike curves [Hawking73]. Because of the Lorentzian signature of the metric, the time coordinate has a privileged status [Bruneton07]. Hence, considering a four dimensional spacetime with one time dimension, the equations of motion are hyperbolic. The Cauchy problem is not necessarily well-defined globally in GR due to the fact that Einstein equations are hyperbolic and non-linear. Whether it can be done or not must be decided on a case by case basis [Friedrich00]. In GR, even if the spacetime signature is Lorentzian such that SR can be recovered locally (see also Sec. 1.5), there exist solutions of the Einstein equations with closed timelike curves, for instance the Gödel spacetime [Gödel49], the question of causality being thus not trivial.

Three requirements allow to define **causality** in GR [Bruneton07],

1. *Global chronology*, No global chronology exists in relativity since any field defines its own chronology locally on the spacetime manifold. However,

[8] The requirement of a Lagrangian formulation is also not trivial [Durrer08b, Uzan11] since the evolution of every functions appearing in the Lagrangian must be determined self-consistently via the equations of motion.

[9] Note that Lorentz-invariance does not always ensures the absence of superluminal motion (see [Durrer08b, Bruneton07]).

in order to impose a global chronology, the spacetime is (in general) required to be **globally hyperbolic** [Bruneton07], that is it can be decomposed into the three space components and one time component, a procedure called 3+1 decomposition. In order to define this notion in more detail, let us introduce the concept of Cauchy surface [Gourgoulhon12],

> CAUCHY SURFACE - *"a Cauchy surface is a spacelike hypersurface Σ in [the manifold] $\mathcal{M}$ such that each causal (i.e. timelike or null) curve without end point intersects Σ once and only once."*

A spacetime equipped of a metric $(\mathcal{M},\ g)$ that admits a Cauchy surface is by definition globally hyperbolic and satisfies the 3+1 decomposition. Most of the relevant spacetimes for cosmology and astrophysics admits this property, the Gödel spacetime being an exception (see e.g. [Hawking73]). The topology of such a spacetime $\mathcal{M}$ is necessarily $\Sigma \times \mathbb{R}$.

2. *No superluminal motion*, In GR, no signal propagates faster than the graviton speed (which corresponds to c) since superluminality would break the equivalence of all inertial frames [Durrer08b] (see also Sec. 1.3.3). In some cases, for instance when the dominant energy condition reading,

$$T_{\mu\nu}t^\mu t^\nu \geq 0 \qquad \text{and} \qquad T_{\mu\nu}T^\nu_\lambda t^\mu t^\lambda \leq 0, \tag{1.3.1}$$

with t^μ any timelike vector[(10)], is not satisfied, GR admits solutions with superluminal motion and closed loops, like the wormholes.

3. *Cauchy problem*, The Cauchy problem is well-posed for globally hyperbolic spacetime in the absence of superluminality (see [Hawking73, Wald84] for a rigorous treatment of this question), provided that the gauge freedom due to general covariance (see Sec. 1.3.3 for the definition) is fixed.

1.3.2 Locality

In classical field theory, **locality** refers to the fact that interactions at one point of the spacetime depend only on the infinitesimal vicinity of this point. In non-local theories, the dynamics of a field at the spacetime point x is not only determined by its neighborhood $x + \delta x$, but also by the values of the field in a region of spacetime possibly infinite. As an example, in case of time non-localities, fields can exhibit memory effects [Mitsou15]. Mathematically, it means that the field dynamics is given by integro-differential equations rather than differential ones.

Locality is preserved in GR since equations of motion are differential equations which derive from a Lagrangian formulation and are identified to the Euler-Lagrange equations. Indeed, the Lagrangian formalism is unable

[(10)] This condition is equivalent to $\rho > |p|$ for a perfect fluid given by Eq. (2.2.2).

to account directly for either non-conservative interaction or causal history-dependence processes, that is for non-local interactions, since they are time-symmetric and necessarily energy conserving provided that $\partial\mathcal{L}/\partial t = 0$ [Galley13, Galley14]. However, in some cases, it is possible to formulate the Lagrangian in such a way that non-conservative forces are included, their equations of motion being given by the Euler-Lagrange equations [José98].

While causality and locality are sometimes confused, it is possible to build non-local theories which preserve causality (see e.g. [Tsamis14]). In this case, the equations of motion cannot derive from an action and an arrow of time exists.

1.3.3 General covariance

Einstein defines general covariance by the following statement [Einstein16]:

> GENERAL COVARIANCE - *"All physical laws have to be expressed by equations that are valid in all coordinate systems, i. e., which are covariant under arbitrary substitutions (or generally covariant)".*

Contrary to the Newton's second law where fictious forces have to be invoked in non-inertial frame, Einstein equations are now valid in all coordinate systems, gravity acting like a fictious force in GR. Indeed, at each point of the spacetime, there exists a frame where gravity is vanishing and the laws of SR thus apply.

As any dynamical field theory based on tensorial quantities, GR can be formulated in such a way that it is invariant under coordinate transformation $x^\mu \longrightarrow y^\mu = y^\mu\left(x^\alpha\right)$, that is under **passive diffeomorphism**, the diffeomorphism being defined as [Gaul00],

> DIFFEOMORPHISM - *"A infinitely differentiable (C^∞) map between manifolds that is one-to-one, onto and has a C^∞ inverse."*

In GR, the spacetime is a differential manifold and passive diffeomorphism corresponds to a mapping between two differential charts on the manifold. In particular, the EH action in the presence of the cosmological constant is invariant under coordinate transformation since it involves only scalars: the Ricci scalar, the cosmological constant and the volume element $\sqrt{-g}\,\mathrm{d}^4x$. Indeed, the volume element transforms under a change of coordi-

nates $x^\mu \longrightarrow y^\mu = y^\mu\left(x^\alpha\right)$ as,

$$\begin{aligned} \mathrm{d}^4 y &= \mathrm{d}^4 x \left(\det \frac{\partial y}{\partial x}\right), && (1.3.2)\\ \sqrt{-g(y)} \equiv \sqrt{-\tilde{g}} &= \sqrt{-\det \tilde{g}_{\mu\nu}}, && (1.3.3)\\ \det \tilde{g}_{\mu\nu} &= \det\left(\frac{\partial x^\alpha}{\partial y^\mu}\frac{\partial x^\beta}{\partial y^\nu} g_{\alpha\beta}\right), && (1.3.4)\\ &= \det\left(g_{\alpha\beta}\right) \det\left(\frac{\partial x^\alpha}{\partial y^\mu}\frac{\partial x^\beta}{\partial y^\nu}\right), && (1.3.5)\\ \Rightarrow \qquad \mathrm{d}^4 y\sqrt{-\tilde{g}} &= \mathrm{d}^4 x \left(\det \frac{\partial y}{\partial x}\right) \sqrt{-g\left(\det \frac{\partial x}{\partial y}\right)^2} && (1.3.6)\\ &= \mathrm{d}^4 x\sqrt{-g} && (1.3.7) \end{aligned}$$

where $(\partial y/\partial x)$ is the Jacobian matrix of the transformation and the property of determinant $\det(AB) = \det(A)\det(B)$, A and B being two matrices, is used. It results that the EH action is invariant under change of coordinates,

$$S \propto \int \mathrm{d}^4 x\, \sqrt{-g}\, \left[R(x) - 2\Lambda\right] = \int \mathrm{d}^4 y\, \sqrt{-\tilde{g}(y)}\, \left[\tilde{R}(y) - 2\tilde{\Lambda}\right] \propto \tilde{S}, \quad (1.3.8)$$

where the tilde denotes quantities expressed in the coordinate system y^μ.

However, since position and motion are fully relational in GR according to the Mach principle, GR is also invariant under **active diffeomorphism**: if all physical dynamical objects are shifted at once on the spacetime manifold $\mathcal{M}$ (without change of coordinate system), nothing is generated but an equivalent mathematical description [Gaul00]. From the mathematical point of view, active diffeomorphism is a smooth displacement of any dynamical fields along an integral curve of vector field $\xi \in T_P(\mathcal{M})$, $T_P(\mathcal{M})$ being the tangent space to the spacetime manifold at point P. Such a transformation is generated by the **pushforward** $(\phi^*\xi) : T_P(\mathcal{M}) \longrightarrow T_{\phi(P)}(\mathcal{M})$ which carries the tangent vectors ξ along the C^∞ map $\phi : \mathcal{M} \longrightarrow \mathcal{M}$ between two tangent spaces of the spacetime manifold,

$$\left(\phi^*\xi\right)(f) = \xi\left(f \circ \phi\right), \quad (1.3.9)$$

the smooth function $f : \mathcal{M} \longrightarrow \mathbb{R}$ being "pushed forward" to $f \circ \phi : \mathcal{M} \longrightarrow \mathbb{R}$ by composing f with ϕ.

In GR, general covariance does not only refer to passive diffeomorphism invariance but also on active diffeomorphism invariance which is made possible by the **lack of prior geometry**. By prior geometry, one means [Misner73],

> PRIOR GEOMETRY - *"Any aspect of the spacetime geometry that is fixed immutably, i.e. that cannot be changed by changing the distribution of the gravitational sources."*

The lack of prior geometry implies that the spacetime geometry is purely dynamical and that gravity is entirely described in terms of the geometry, the active diffeomorphism invariance being rendered equivalent to the passive one,

revealing an additional symmetry [Bertschinger02]. As an example, the Nordstrøm theory where $g_{\mu\nu} = \varphi^2 \eta_{\mu\nu}$ with φ a scalar field, admits a prior geometry since the Minkowski spacetime is fixed a priori. Contrary to the passive diffeomorphism invariance, the active one is far from obvious considering the EH action since the Lagrangian does not only depend on coordinates, but also on the metric field which is affected by the pushforward.

In App. A, we show that the invariance of tensor fields under active diffeomorphism in GR implies that the second Bianchi identity holds, as long as the connection is Levi-Civita. As a result, a shift of the metric field does not affect the Einstein equations which only determine the spacetime geometry [Misner73].

Finally, general covariance implies that rods and clocks measurements depend on the reference frame where the observer is located because of the gauge freedom of the metric. The interpretation of the measurements is thus much more tricky in GR than in classical mechanics where the spacetime is in addition euclidean. It is thus crucial to work with **gauge-invariant** quantities, that is quantities which do not depend on the coordinate system. Over the ten degrees of freedom of the metric, four are gauge degrees of freedom and must be fixed by the four Bianchi identities, the six remaining ones being dynamical. It results that, in the Hamiltonian formulation of GR, Einstein equations reduce to four elliptic constraint equations and six hyperbolic Hamilton equations. This is the reason why metric fields are not observables, since they are defined up to the gauge transformation. However, some quantities are gauge-invariant like the proper time $\mathrm{d}\tau$. They constitute the useful quantities to be computed in order to confront the theory with the observations.

1.3.4 Second order equations of motion

Since the Newton's theory, equations of motion are of second order, two initial conditions determining the solution univocally (see also Sec. 1.3.1). Actually, the laws of physics must involve no more than second-order time derivatives of the fundamental dynamical variables or generalized coordinates q^i in order to preserve the stability of the solution [Woodard15] as stated by the **Ostrogradsky theorem** [Ostrogradsky50].

For the sake of simplicity[(11)], let us introduce the Ostrogradsky's result in classical mechanics for a point particle in one dimension. In general, the Lagrangian $L = T - V$ with T and V the kinetic and potential energies, depends upon the point particle position and its derivative, $L(q,\ \mathrm{d}q/\mathrm{d}t \equiv \dot{q})$ with a quadratic dependence on $\dot{q}$ coming from the kinetic term. In this case, the equation of motion is derived from the usual Euler-Lagrange equation and is of second order, $\ddot{q} = \mathcal{F}(q,\ \dot{q})$, provided that the system is **nondegenerate**, i. e. $\partial L/\partial q^{(n)}$ depends on up to $q^{(n)}$ with n the order of time derivative. The evolution of $q(t)$ is then univocally determined by two initial conditions, q_0 and

[(11)] This result is so general that applies to all classical field theory.

$\dot{q}_0$. In this case, the phase space transformation $(q,\ \dot{q}) \longleftrightarrow (Q,\ P)$ with Q and P the two canonical coordinates, is invertible,

$$Q \equiv q \qquad \text{and} \qquad P \equiv \frac{\partial L}{\partial \dot{q}}, \tag{1.3.10}$$

since P can be solved for determining $\dot{q} = v(Q,\ P)$.

The canonical Hamiltonian is given by the Legendre transformation of the Lagrangian,

$$\begin{aligned} H &= \dot{q}\frac{\partial L}{\partial \dot{q}} - L(q,\ \dot{q}), & (1.3.11)\\ &= Pv(Q,\ P) - L\left[Q,\ v(Q,\ P)\right], & (1.3.12) \end{aligned}$$

the time evolution of the canonical coordinates being given by the Hamilton's equations.

Let us now assume a Lagrangian with second order derivative $L(q, \dot{q}, \ddot{q})$. Since the Euler-Lagrange reads now,

$$\frac{\partial L}{\partial q} - \frac{\mathrm{d}}{\mathrm{d}t}\frac{\partial L}{\partial \dot{q}} + \frac{\mathrm{d}^2}{\mathrm{d}t^2}\frac{\partial L}{\partial \ddot{q}} = 0, \tag{1.3.13}$$

and because of the assumption of nondegeneracy i. e. $\partial L/\partial \ddot{q}$ depends upon $\ddot{q}$, the equation of motion is of fourth order $q^{(4)} = \mathcal{F}\left(q,\ \dot{q},\ \ddot{q},\ q^{(3)}\right)$. It means that four initial conditions must be fixed in order to get the solution $\left(q_0,\ \dot{q}_0,\ ,\ddot{q}_0,\ ,q_0^{(3)}\right)$ and four canonical variables have to be defined, for instance,

$$Q_1 \equiv q, \qquad P_1 \equiv \frac{\partial L}{\partial \dot{q}} - \frac{\mathrm{d}}{\mathrm{d}t}\frac{\partial L}{\partial \ddot{q}}, \tag{1.3.14}$$

$$Q_2 \equiv \dot{q}, \qquad P_2 \equiv \frac{\partial L}{\partial \ddot{q}}. \tag{1.3.15}$$

The assumption of nondegeneracy guarantees that the system is invertible, so P_2 can be inverted in order to determine $\ddot{q} = a(Q_1, Q_2, P_2)$. Only three of the four canonical coordinates are needed since $L(q, \dot{q}, \ddot{q})$ only depends on three phase space coordinates. The Hamiltonian is then derived by the usual Legendre transformation,

$$\begin{aligned} H(Q_1, Q_2, P_1, P_2) &\equiv \sum_{i=1}^{2} q^{(\mathrm{i})} P_i - L(q, \dot{q}, \ddot{q}) & (1.3.16)\\ &= P_1 Q_2 + P_2\, a(Q_1, Q_2, P_2) \\ &\qquad - L[Q_1, Q_2, a(Q_1, Q_2, P_2)]. & (1.3.17) \end{aligned}$$

As for the previous case, the time evolution is given by the Hamilton's equations.

However, the Hamiltonian (1.3.17) is ill-defined because of the linear term in P_1. Indeed, whereas P_2 is constrained by $(q,\ \dot{q},\ \ddot{q})$, there is no constraint

among the element of P_1 due to the fact that there are three phase space coordinates for four canonical variables. It results that P_1 can take any values and that the Hamiltonian can take arbitrary positive or negative values, leading to the so-called **Ostrogradsky instability** [Motohashi15]. If the system is free, it is not pathological. However, as soon as it is interacting with a 'normal' system with positive energy, the total system will lower its energy [Durrer08b] and will quickly develop into excitation of positive and negative degrees of freedom [Motohashi15] even if the energy is conserved (the Hamiltonian being constant provided that the system is autonomous, i. e. $\partial L/\partial t = 0$).

In general, the Ostrogradsky's result constitutes a no-go theorem in the sense that equations of motion up to more than the second order leads to an instability in the theory assuming the nondegeneracy of the system. In the case of a degenerate system, then $\ddot{q}$ can be integrated out and the Ostrogradsky's instability is evaded (see Chap. 3).

In GR, the Lagrangian density of the EH action is function of up to second order derivatives of $g_{\mu\nu}$. It results that the equations of motion could be of fourth order in $g_{\mu\nu}$. Necessary and sufficient conditions for these Euler-Lagrange equations to be of second order are given by the Lovelock theorem.

1.4 The Lovelock theorem

The underlying assumptions of GR developed in the last sections, i.e. the general covariance and the second-order equations of motion, are summarized in the **Lovelock theorem** [Lovelock69, Berti15],

> LOVELOCK THEOREM - *"In four spacetime dimensions the only divergence free symmetric rank-2 tensor* (general covariance) *constructed solely from the metric* $g_{\mu\nu}$ (lack of prior geometry and the Levi-Civita connection) *and its derivative up to second differential order* (second-order equations of motion)*, is the Einstein tensor plus a cosmological term"*.

Mathematically the Lovelock theorem implies that if the action is assumed to depend only on $g_{\mu\nu}$ up to second order derivative,

$$S = \int \mathrm{d}^4x L\left(g_{\mu\nu};\ g_{\mu\nu,\rho};\ g_{\mu\nu,\rho\sigma}\right), \tag{1.4.1}$$

the equations of motion $E^{\mu\nu}$ reading (see Eq. (1.3.13)),

$$E^{\mu\nu}\left[L\right] = \frac{\partial}{\partial x^\rho}\left[\frac{\partial L}{\partial g_{\mu\nu,\,\rho}} - \frac{\partial}{\partial x^\lambda}\left(\frac{\partial L}{\partial g_{\mu\nu,\,\rho\lambda}}\right)\right] - \frac{\partial L}{\partial g_{\mu\nu}}, \tag{1.4.2}$$

then the only second order equations of motion in $D = 4$ (assuming the Levi-Civita connection) correspond to the Einstein equations with the cosmological constant [Lovelock69],

$$\frac{E^{\mu\nu}}{\sqrt{-g}} = \alpha m_{\mathrm{pl}}^2\left(R^{\mu\nu} - \frac{1}{2}\,g^{\mu\nu}\,R\right) + \Lambda\, g_{\mu\nu}, \tag{1.4.3}$$

with α and Λ two arbitrary constants.

This result is false for $D > 4$ since in that case, the Lagrangian density with the Gauss-Bonnet term $\mathcal{G}$ defined as,

$$\mathcal{L} = \sqrt{-g}\,\mathcal{G} = \sqrt{-g}\left(R_{\mu\nu\alpha\beta}R^{\mu\nu\alpha\beta} - 4R_{\mu\nu}R^{\mu\nu} + R^2\right), \tag{1.4.4}$$

gives also rise to second-order equations of motion [Lovelock69]. Indeed, for $D = 4$, the Gauss-Bonnet term is related to the Euler characteristic χ which is a topological invariant of the spacetime manifold $\mathcal{M}$,

$$\int \mathrm{d}^4x\sqrt{-g}\,\mathcal{G} = \frac{1}{8\pi^2}\chi(\mathcal{M}), \tag{1.4.5}$$

such that the Gauss-Bonnet term is not dynamical.

1.5 The equivalence principles

From a phenomenological point of view, equivalence principles are fundamental in GR. Thanks to our current understanding, gravitation seems to be different than the three others fundamental interactions since it couples to test-particles and fields universally at all scales. The classical mechanics had already called on the Galileo's equivalence principle, usually referred to as the **universality of free fall** (UFF). Indeed two concepts of mass, apparently not related to each other, are invoked in classical mechanics, the inertial m_{i} and the gravitational m_{g} ones. In particular the acceleration inside a gravitational field,

$$\mathbf{a} = -\frac{m_{\mathrm{g}}}{m_{\mathrm{i}}}\nabla\Phi, \tag{1.5.1}$$

is independent of the composition and the amplitude of the involved test mass provided that $m_{\mathrm{i}} = m_{\mathrm{g}}$.

In GR the UFF derives from a novel formulation of the equivalence principle dubbed the **weak equivalence principle** (WEP)[(12)] [Carroll04],

> WEAK EQUIVALENCE PRINCIPLE - *"It is impossible to detect the existence of a gravitational field by means of nongravitational experiments, at least locally in small enough regions of spacetime, where the gravitational field is homogeneous and there is no tidal effect. In the presence of an arbitrary gravitational field, it is possible to find out a local inertial frame where the physical laws are those of SR."*

Thus gravitation does not universally couple to the rest mass only, but also to the energy and momentum, photons being also affected by the gravitational

[(12)] The definitions of the different equivalence principles in GR differ from an author to another one. Some authors distinguish the weak and Einstein equivalence principles (see e.g. [Carroll04] where the WEP guarantees the UFF while the Einstein equivalence principle is related to the existence of local inertial frame). Throughout this thesis, we will consider that they overlap.

field in GR. This first version of the equivalence principle is related to pseudo-Riemannian nature of spacetime. Because of the existence of a metric on the spacetime manifold, there exists a set of differential charts which are compatible with each other such that diffeomorphism-invariance is guaranteed. The WEP is explicitly assumed in the Lovelock theorem since $g_{\mu\nu}$ is the only tensor appearing in the Lagrangian (1.4.1). The UFF is thus guaranteed whatever objects, gravitationally bounded or not.

In addition to the WEP, GR implements an even stronger version of the equivalence principle as first noticed by Dicke [Brans08] when he looked after the possibility of testing GR. The **strong equivalence principle** (SEP) states that [Carroll04],

> STRONG EQUIVALENCE PRINCIPLE - *It is impossible to detect the existence of a gravitational field by means of local experiments, either gravitational or nongravitational.*

This means that the gravitational binding energy contributes equally to gravitational and inertial mass. The effect of a violation of the SEP would be especially sensible in compact objects (see Sec. 2.3.4) where the gravitational self-binding energy is non-negligible. Indeed, GR predicts that compact objects fall in the same way as light particles like photons. Moreover, the fluid approach for describing the matter fields is also questionable since the bunch of test particles composing the fluid self-gravitates and backreacts on spacetime curvature, contrary to point particles. In summary, the SEP implies that the only effect of gravity is the gravity acceleration which is universal. Mathematically, the metric only mediates gravity and the affine connection is the Levi-Civita one, the second Bianchi identity being guaranteed.

The mathematical formulation of the WEP and the SEP can be identified at the level of the action. Matter fields $\psi_{\rm M}$ are universally (and only) coupled to the metric $g_{\mu\nu}$. Hence, gravitation acts universally on all matter contained inside the Universe, so the WEP is guaranteed. Since the gravitational coupling is given by the Newton's constant (or the Planck mass) which does not vary in spacetime, therefore guaranteeing the constancy of the gravitational binding-energy, according to the SEP.

All these assumptions are questionable from the theoretical point of view since the equivalence principles could be broken at some point, leading to variations of the gravitational coupling into spacetime or depending on the relative velocity between observers, or even to a breaking of the universality of the gravitational coupling to all the matter-energy components. In addition, GR is a classical theory of gravity which is not compatible with quantum mechanics. Indeed, gravity in GR is only defined locally according to the differential geometry formulation while quantum mechanics is non-local in the sense that it calls on wave function. In that sense, the equivalence principles should be violated at some point. However, as we will see in Chap. 2, the equivalence principles are tested with very good accuracy today, GR being seemingly well-formulated.

1.6 Conclusion

In this chapter, we proposed an interpretative framework of GR, highlighting the particular status of the Einstein's theory of gravitation. Provided that the connection is the Levi-Civita one and the spacetime is four-dimensional, the most general second-order equations of motion are the Einstein equations in the presence of the cosmological constant. In addition, GR preserves locality and causality (up to some point, for instance assuming the dominant energy condition) and is generally covariant.

At the end of this first chapter, we formulate the following conjecture: in four dimensions, the SEP is valid only if gravitation is mediated by a metric (without prior geometry) and only one metric, with the Levi-Civita connection, equations of motion being of second order (such that the Cauchy problem may be well-posed).

Provided this framework, we will first question how to test GR observationally and experimentally, either the dynamics predicted by the field equations and the geodesics or the equivalence principles. Testing GR is not trivial since the derivation of the observables is tricky because of general covariance.

Moreover, from the theoretical point of view, the underlying assumptions of GR are also questionable since GR has limitations: it is a classical theory of gravity which is expected to break down at high energy scale (usually the cut-off scale of GR is assumed to be the Planck scale). However, some issues appearing in cosmology today could also come from modifications of GR at the low energy scale, in particular due to the difficulty to give a physical interpretation to the cosmological constant.

In Chap. 3, the interpretative framework presented in this chapter will allow one to classify theories of gravity beyond GR in order to establish which assumptions of GR they violate.

Chapter 2

General Relativity under scrutiny

In this chapter, we question how far GR is tested by the current experiments and observations. Indeed, GR has been tested in the regime where the gravitational field is weak like in the lab, in the solar system and in cosmology, either where it is strong, for instance neutron stars (NSs) and black holes (BHs). The recent direct detection of gravitational waves (GWs) enables one to test also the radiative regime. Moreover, testing GR in the vacuum enables one to test directly the spacetime dynamics whereas in the presence of sources, the modeling of the stress-energy tensor is also tested. In particular, NSs and cosmology belong to this regime, the sources being relativistic or not. At the end of this chapter, we propose a classification of the GR tests depending on the presence and the properties of the sources. Even if no strong deviation from GR has been highlighted up to now it enables one to highlight which regimes have been tested.

2.1 Tests of the equivalence principles

Following [Will93], the equivalence principles are tested at three different levels: the UFF, the local position invariance (LPI) and the local Lorentz invariance (LLI). These three statements are tested at different scales, from the lab to cosmology. In this section current constraints are briefly reviewed.

2.1.1 The test of the Universality of Free Fall

GR predicts the UFF for any composition, mass and gravitational binding energy of the test body (see Chap. 1). Experimentally, any deviations from the UFF for two bodies inside the same gravitational field are parametrized by the

Eötvös parameter,

$$\eta_{\text{UFF}} \equiv 2\frac{|a_1 - a_2|}{|a_1 + a_2|}, \tag{2.1.1}$$

with a_1 and a_2, the acceleration of the first and the second body respectively. If $\eta_{\text{UFF}} \neq 0$, then at least one kind of energy contributes differently for the inertial and the gravitational mass [Will93].

The best constraint on the UFF at the Solar System scale is due to the Lunar Laser Ranging experiment [Williams04],

$$\boxed{\eta_{\text{UFF}} = (-1.0 \pm 1.4) \times 10^{-13} \qquad \text{(gravitationally bounded objects)}} \tag{2.1.2}$$

It reveals that the Moon and the Earth, differing in composition and gravitational binding energy, fall in the gravitational field of the Sun by the same way to very good accuracy. The distance of the Moon from the Earth has been measured thanks to a laser beam for several decades, a reflector being planted on the Moon during Apollo space missions, and is currently known at the cm level. Notice that the SEP is tested rather than the WEP in this case because the Moon and the Earth are gravitationally bounded objects.

The UFF has been tested in labs by many sophisticated Eötvös-type experiments, using torsion balance for instance (see [Will08] for more details). The principle of modern torsion balance experiments is the following: two bodies of different compositions are connected by a rod and suspended by a wire. If the gravitational acceleration of the two bodies differ and if this difference has a component perpendicular to the suspension wire, then a torque is induced on the wire. Current best constraints have been obtained by [Schlamminger08] with,

$$\boxed{\eta_{\text{UFF}} = (0.3 \pm 1.8) \times 10^{-13} \qquad \text{(non-gravitationally bounded objects)}} \tag{2.1.3}$$

Eötvös experiments test the WEP since the test mass is not gravitationally bounded, the masses being only bounded by other interactions.

The UFF has been also tested at the atomic level where quantum mechanics comes into play. In 1975, Colella, Overhauser and Werner proposed to test the UFF with neutron interferometry [Colella75], the interferometer being tilted with respect to the Earth gravitational acceleration such that the neutrons are in free fall in the external gravitational field of the Earth. Other experiments are based on atom interferometry: atoms are cooled thanks to laser beams and are then trapped in a precise location. Placing atoms in different atomic levels, differences in acceleration due to the Earth are measured with very good accuracy (see e.g. [Peters99]). The same principle can be used for testing the difference in acceleration for different isotopic species [Fray04], for different spins states [Tarallo14], etc. For instance, the best bounds on the Eötvös parameter for ^{87}Rb and ^{39}K atoms read [Schlippert14],

$$\boxed{\eta_{\text{UFF}} = (0.3 \pm 5.4) \times 10^{-7} \qquad \text{(quantum objects)}} \tag{2.1.4}$$

A similar experiment is described in much more detail in Chap. 4 where numerical simulations are provided for an atom interferometry experiment testing the acceleration due to a scalar field possibly responsible for the current cosmic acceleration. However, the presence of a fifth force is tested in this case (see also Sec. 3.2.5.2) rather than the UFF.

2.1.2 The Local Lorentz Invariance

LLI is one of the cornerstone in SR, and thus in GR and standard model of particle physics (SM). In GR, the WEP guarantees that it is always possible to find a frame at each point of the spacetime where the laws of SR are valid. Active Lorentz invariance[(1)] is maybe not an exact symmetry at all energies; either the Lorentz symmetry is broken since there exists a preferred frame determined by other field(s) than the metric, for instance a vector field [Jacobson01]; or it is deformed such as the Lorentz transformation from one frame to another is modified.

Observing a Lorentz violation implies that observables differ depending on the velocity of the frame. Two laws are thus tested: the constancy of the speed of light c, the best bound being [Michimura13],

$$\boxed{\frac{\delta c}{c} \lesssim 10^{-14}} \tag{2.1.5}$$

as well as the vacuum dispersion relation of SR, $E^2 = mc^2 + p^2c^4$ which can have higher order terms (see e.g. [Mattingly05]). Several formalisms and parametrizations have been proposed, at the classical level like the c^2 formalism or at the quantum one like the Standard Model Extension (see e.g. [Mattingly05, Will08]).

Many experiments have been performed at different scales, none of them highlighting a violation of the LLI (see [Mattingly05, Kostelecky11]). Most of them are realized in conditions where the gravitational effects can be neglected. However, gravitational tests exist too, using the Cosmic Microwave Background (CMB) power spectrum and the polarization of GWs for instance (see also Secs. 2.4.5 and 2.3.3.3 respectively). The direct detection of GWs from coalescing BHs (see Sec. 2.3.3.3) will allow one to improve the constraints on the LLI in the gravity sector [Kostelecký16].

2.1.3 The Local Position Invariance I: gravitational redshift experiments

LPI states that the measure of observables does not depend on the position (in space and in time) where it takes place. The **gravitational redshift** experiment, which consists of measuring the relative difference in frequency $\Delta\nu/\nu$

[(1)] The passive one is always fulfilled provided that the equations of motion are tensorial (a local Lorentz transformation is a subgroup of the general coordinates transformations) [Mattingly05] (see also Sec. 1.3.3).

of two identical frequency clocks placed at two different positions in a static gravitational field, directly tests the LPI. GR predicts that, up to first order,

$$\frac{\Delta\nu}{\nu} = (1+\alpha)\,\frac{\Delta U}{c^2}, \tag{2.1.6}$$

where ΔU is the difference between the gravitational fields at the two different places and $\alpha = 0$ according to GR.

This experiment was first realized by Pound, Rebka and Snider in 1959-1960 at Harvard University [Pound60, Pound64]. They studied the redshift of a photon emitted upwards from the basements of a tower at Harvard to a receiving atom at the top of the building. Since the receiving atom is moving downward, this experiment combines the gravitational redshift and the Doppler redshift predicted by SR. Because of the Mössbauer effect, i.e. the resonant absorption of a photon by an atomic nuclei bounded in a solid, the receiving atom absorbs the photon only if the energy of the photon exactly corresponds to the transition between two atomic energy levels. Using this method, they determined α at the 1% level [Pound64]. The current best constraint was obtained in 1976 by GRAVITY PROBE-A [Vessot80],

$$\boxed{|\alpha| < 2\times10^{-4} \qquad \text{(gravitational redshift)}} \tag{2.1.7}$$

They measured the difference in frequency of two hydrogen maser clocks, one being aloft in a spacecraft 10,000 km away from the Earth and the second one staying on the ground.

LPI has been also tested by **null-redshift experiment** where the difference in frequency between two different clocks at different places in a gravitational field is measured. In this case, the effect of the clocks structure is also tested implying a potential violation of the UFF. Best constraints have been obtained at the Solar System scale by comparing the frequency of atomic clocks in the time-varying gravitational potential of the Earth due to its orbital motion around the Sun [Bauch02]. The measure of α should be improved by the future space missions like the Galileo 5 and 6 satellites ($|\alpha| < 4\times10^{-5}$) [Delva15] as well as the ACES space mission [Cacciapuoti09]. In addition, the test of the gravitational redshift would also be explored in the strong field regime, for example by looking at the bodies orbiting around the central BH of the Milky Way, Sagittarius A* (SgrA*) [Meyer12].

Constraining the variation of the fundamental constants is a second test of the LPI since it would imply a violation of the LPI: depending on where and when the experiment is performed, the measure of the observables would differ. We discuss this second test in Sec. 3.2.4.2. In the following, we will refer to the LPI either for gravitational redshift experiments or the constancy of fundamental constants.

2.2 The weak field regime

The weak field regime describes gravitational systems where the linearization of GR is valid since the gravitational field is weak. The (quasi-)stationarity or slow motion regime is also implicitly assumed, in the sense that the massive bodies motion is slow compared to c. We have already explored the test of the equivalence principles in this regime (see Sec. 2.1). We will now turn to the test of the dynamics predicted by GR either the Einstein or the geodesics equations.

The dynamics predicted by GR has been already tested a lot, for instance with the perihelion precession of Mercury, the deflection of light by the Sun or the Lense-Thirring effect for spinning objects in orbit, for citing only some of them. In order to take into account all the possible deviations from GR, the parametrization of the deviations from the predictions is required. This is the reason why post-Newtonian (PN) formalism [Eddington57] has been developed and extensively used, especially in the Solar system and for binary pulsar.

2.2.1 The Post-Newtonian formalism

The PN formalism is devoted to testing gravity in the weak field regime and, in particular, in the Solar System where the modeling of the Sun and its flock of planets would require many-body system formulated in GR. Assuming the spherical symmetry with the Sun at the center, the expansion of the Einstein equations order by order makes the study of the Solar System possible.

This phenomenological approach consists of expanding all the possible terms of $g_{\mu\nu}$ and $T_{\mu\nu}$ in the weak field and slow motion regime. The PN formalism is perfectly suitable for the Solar System since,

1. *The gravitational field is weak*: $|\Phi|/c^2 \lesssim 10^{-5}$ in the Solar System. The upper limit is at the center of the Sun where $\Phi_\odot/c^2 \lesssim 10^{-5}$ while for the Earth $\Phi_\oplus/c^2 \lesssim 10^{-10}$ [Will93]. The strength of a gravitational field is further defined by the **compactness** s (in spherical symmetry),

$$s = \frac{2G_{\rm N}M}{\mathcal{R}} = 2|\Phi| \equiv \frac{r_{\rm s}}{\mathcal{R}}, \tag{2.2.1}$$

   with M the mass of the object, $\mathcal{R}$ either its radius or its characteristic scale (see Secs. 2.3 and 2.4) and $r_{\rm s} = 2G_{\rm N}M$ its **Schwarzschild radius**,

2. *The matter generating the Solar System gravity is in slow motion* compared to the Solar System center of mass, $v/c \ll 1$ (more precisely $v^2/c^2 \lesssim 10^{-7}$),

3. *The energy density is much larger than the pressure* $\rho c^2 \gg p$: For the sake of simplicity the stress-energy tensor is usually assumed to be a perfect and non viscous fluid,

$$T^{\mu\nu} = (\epsilon + p)\, u^\mu u^\nu + p\, g^{\mu\nu} \tag{2.2.2}$$

with u^μ, the 4-velocity of the perfect fluid, $\epsilon = \rho c^2 (1 + \Pi)$, ϵ, ρ, Π and p being the energy density, the rest-mass energy density, the specific energy density which takes into account other forms of energy than the rest mass one, and the pressure respectively.

These assumptions are no longer valid in the strong field regime which requires other parametrizations of the metric (see Sec. 2.3). Moreover, even for the Solar System, the PN formalism is valid in the limit where the rest of the Universe does not affect it [Misner73].

As stated before, the fields are expanded on the Minkowski background which constitutes the asymptotic solution at spatial infinity. The metric expansion is given by,

$$g_{\mu\nu}(x) = \eta_{\mu\nu} + h_{\mu\nu}(x), \tag{2.2.3}$$

where $h_{\mu\nu} \ll 1$ is developed order by order and can be considered as a field propagating on the Minkowski background where $\eta_{\mu\nu}$ allows for raising/lowering the indices. The **Newtonian limit** is obtained assuming the metric expansion (see also the correspondence principle in Sec. 1.2),

$$g_{00} = -\left(1 + 2\frac{\Phi}{c^2}\right), \qquad g_{i0} = 0, \qquad g_{ij} = \delta_{ij}. \tag{2.2.4}$$

This limit is referred to as the **first order** approximation. The stress-energy tensor must be expanded in the same way, for instance assuming a perfect fluid with $T^{00} = \rho$, $T^{0i} = \rho v^i$ and $T^{ij} = \rho v^i v^j + p\delta^{ij}$. Up to the first order the conservation of $T^{\mu\nu}$ leads to the Eulerian equations of hydrodynamics,

$$\frac{\partial \rho}{\partial t} + \nabla \cdot (\rho \mathbf{v}) = 0, \tag{2.2.5}$$

$$\rho \frac{\mathrm{d}\mathbf{v}}{\mathrm{d}t} = \rho \nabla U - \nabla p, \tag{2.2.6}$$

with $\mathrm{d}/\mathrm{d}t = \partial/\partial t + \mathbf{v} \cdot \nabla$. Indeed up to first order,

$$\nabla_\mu T^{\mu\nu} = 0 \qquad \Rightarrow \qquad \partial_\mu T^{\mu\nu} + \Gamma^\nu_{00} T^{00} \simeq 0, \tag{2.2.7}$$

with $\Gamma^k_{00} = a^k = -\nabla U$ by the Newtonian limit of the geodesics equations, $a^k = \mathrm{d}^2 x^k / \mathrm{d}t^2$ being the acceleration and $U \equiv -\Phi/G_\mathrm{N}$ the gravitational potential[(2)]. The component $\nu = 0$ and $\nu = i$ of Eq. (2.2.7) reduced to Eqs. (2.2.5) and (2.2.6) respectively using the definitions of the total derivative, a^k as well as the relation $\partial_i(\rho v^i v^j) = \nabla \cdot (\rho \mathbf{v}) v^j + \mathbf{v} \cdot \nabla v^j$.

The study of GR requires the **second order** approximation or the 1PN order. The order of smallness of physical quantities ϵ_PN intervening in the equations of motion are evaluated with respect to the gravitational potential U. Keeping in mind that quantities appearing in the Newton's theory like v, ρ and $\eta_{\mu\nu}$ are of 0PN order or ϵ_PN, terms arising in the perturbation theory like

[(2)] In the PN literature, the gravitational potential is referred to as $U \equiv -\Phi/G_\mathrm{N}$ rather than to Φ [Misner73]

$h_{\mu\nu}$ and $\partial/\partial t$ are of the order 1PN. Comparing terms appearing in the Eulerian equations of hydrodynamics as well as the definition of the components of $T_{\mu\nu}$ for a perfect fluid (see [Will93] for details), the bookkeeping of the order of smallness reads[3],

$$U \sim v^2 \sim \frac{p}{\rho} \sim \epsilon_{\rm PN}^2, \tag{2.2.8}$$

and the time derivative which is vanishing in the Newtonian limit, is now of order $\epsilon_{\rm PN}$. The expansion of the metric to the 2PN order implies that the expansion of each component is determined up to,

$$g_{00} = \eta_{00} + h_{00}^{(2)} + h_{00}^{(4)} + ... \simeq -1 + 2U + h_{00}^{(4)}, \tag{2.2.9}$$

$$g_{i0} = \eta_{i0} + h_{i0}^{(3)} + h_{i0}^{(5)} + ... \simeq h_{i0}^{(3)}, \tag{2.2.10}$$

$$g_{ij} = \eta_{ij} + h_{ij}^{(2)} + h_{ij}^{(4)} + ... \simeq \delta_{ij} + h_{ij}^{(2)}. \tag{2.2.11}$$

The relevant even/odd terms in the expansion depend on their change of sign under time reversal: terms whose total v's and $\partial/\partial t$'s are odd like g_{i0} change sign under time reversal contrary to g_{00} and g_{ij}[4] [Misner73].

The stress-energy tensor has to be expanded by the same way. Its expansion requires the definition of some potentials (see also App. B for an example), among them the Newtonian potential [Will93],

$$U(\mathbf{x}, t) \equiv -\frac{\Phi(\mathbf{x}, t)}{G_{\rm N}} \equiv \int \mathrm{d}^3x' \frac{\rho(\mathbf{x}, t)}{|\mathbf{x}' - \mathbf{x}|}. \tag{2.2.12}$$

Einstein equations are then solved order by order.

2.2.2 The Parametrized Post-Newtonian formalism

The PN expansion is dubbed the **parametrized Post-Newtonian** (PPN) formalism when the metric is parametrized in the most general way, including ten parameters depending on ten potentials defined similarly to the Newtonian potential (2.2.12) (see [Nutku69, Will93, Will08] for the whole expansion and technical details). The PPN parameters can be directly constrained from the observations in a model-independent way. We will consider only two PPN parameters in this thesis, namely $\gamma_{\rm PPN}$ and $\beta_{\rm PPN}$. In the Standard PN gauge they read [Will93],

$$g_{00} = -1 + 2\,\bar{G}U - 2\,\beta_{\rm PPN}\,\bar{G}^2U^2, \qquad g_{ij} = \delta_{ij}\left(1 + 2\,\gamma_{\rm PPN}\,\bar{G}U\right), \tag{2.2.13}$$

with $\gamma_{\rm PPN} = \beta_{\rm PPN} = 1$ according to GR ($c = 1$), $\bar{G}$ being the measured gravitational constant. Best constraints today,

$$\boxed{|\gamma_{\rm PPN} - 1| < 2.3 \times 10^{-5}, \qquad |\beta_{\rm PPN} - 1| < 7 \times 10^{-5}} \tag{2.2.14}$$

[3] The cosmological constant does not intervene in the calculations because of its far too low value compared to other terms of the Einstein equations.

[4] This is true up to $\epsilon_{\rm PN}^5$ where other effects like radiation damping come into play.

were obtained by the Cassini spacecraft thanks to Shapiro effect [Bertotti03] and by studying orbital effects in planetary ephemerids [Fienga11] respectively. For the additional PPN parameters, the reader is reported to [Will08]. The constraints on PPN parameters should be improved in the near future thanks to space missions like GAIA (see for example [Hobbs09] and [Hees15]) and BepiColombo [Milani02] which should enable to constrain them up to $\gamma_{\rm PPN} - 1 \sim 10^{-6}$ and $\beta_{\rm PPN} - 1 \sim 10^{-6}$.

The PPN formalism applies to all theories which possess one metric describing spacetime provided this metric satisfies the WEP (see e.g. [Misner73]). In this case the asymptotic behavior of metric fields is polynomial. As an example, if the metric has a massive scalar field counterpart, the gravitational Newtonian potential is of Yukawa type (see also Sec. 3.2.5.2). The asymptotic behavior of the metric field is then exponentially decreasing and the PPN formalism is thus not valid. However, if its mass is sufficiently small, we can consider that it contributes to higher order terms and neglect it in the PPN expansion as for the cosmological constant in GR. Other metric parametrizations have been proposed in order to generalize the PPN parametrization for extended theories of gravity, like the Parametrized Post-Einsteinian formalism [Jaekel05] which takes into account more generalizations of GR. In addition, simulations of observables for general modifications of gravity have been developed [Hees12b].

2.3 The strong field regime

In the limit where $U \sim v^2 \sim p/\rho \sim \epsilon_{\rm PN}^2 \ll 1$ is no more valid everywhere in the gravitational system, strong field regime effects come into play and the linearization of GR, i.e. the 1PN approximation, is no longer appropriate [Will08]. This is the case for compact objects ($s \sim 1$), the most compact objects predicted by GR being BHs with $s \sim 1$ (see the definition of the compactness (2.2.1)). The strong field regime also applies for less compact objects like NSs, $s = 0.2 - 0.4$, and white dwarf, $s = 10^{-2}$. In comparison, $s = 10^{-6}$ for the Sun and $s = 10^{-10}$ for the Earth.

In the case where orbital velocity in binary systems is very large ($v \sim c$), relativistic effects have to be taken into account. Binary pulsar does not belong to this regime so that a kind of PN approximation might work [Will08]. This is no longer true for binary systems of BHs which require other tools like numerical relativity simulations.

Compact objects also enable one to test the SEP because of their non-negligible binding energy. In this section, the GR solution for spacetime around a compact object is briefly reviewed and the current and future tests of GR in the strong field regime are briefly discussed, focusing on BHs, GWs and NSs.

2.3.1 The Schwarzschild solution

Studying spacetime inside and around compact objects, the most simple spacetime symmetry is the spherical one. In this case, the spacetime geometry surrounded compact objects, i.e. in the vacuum, is the Schwarzschild one whether the star is static, vibrating or collapsing, according to the **Birkhoff theorem** [Birkhoff23][(5)],

> BIRKHOFF THEOREM - *"All spherically symmetric solutions of Einstein equations in the vacuum must be static and asymptotically flat (in the absence of a cosmological constant), that is a piece of the Schwarzschild geometry."* [Clifton12, Misner73]

In particular, this theorem implies that far from the compact objects, their gravitational influence is negligible so that the spacetime is asymptotically flat at spatial infinity (neglecting the cosmological constant). The most general metric for a static and spherically symmetric spacetime given here in the **Schwarzschild coordinates**[(6)], is,

$$\mathrm{d}s^2 = -\mathrm{e}^{2\nu(r)}\,\mathrm{d}t^2 + \mathrm{e}^{2\lambda(r)}\,\mathrm{d}r^2 + r^2\,\mathrm{d}\Omega^2, \tag{2.3.1}$$

where ν and λ are both metric fields which have to be determined by solving the Einstein equations, and $\mathrm{d}\Omega^2 \equiv \mathrm{d}\theta^2 + \sin^2\theta\,\mathrm{d}\varphi^2$ is the infinitesimal solid angle. The influence of asymptotically expanding spacetime, taken into account in the Schwarzschild-de Sitter spacetime solution, is neglected in Eq. (2.3.1).

The solution of the Einstein equations in the vacuum for the metric (2.3.1) is the Schwarzschild solution [Schwarzschild16a],

$$\mathrm{d}s^2 = -\left(1 - \frac{r_\mathrm{s}}{r}\right)\mathrm{d}t^2 + \left(1 - \frac{r_\mathrm{s}}{r}\right)^{-1}\mathrm{d}r^2 + r^2\,\mathrm{d}\Omega^2, \tag{2.3.2}$$

with r_s the Schwarzschild radius. Two singularities appear in Eq. (2.3.2). The first one at $r = r_\mathrm{s}$ is only a coordinate system singularity[(7)] while the singularity at $r = 0$ is a true one in the sense that the spacetime curvature becomes infinite. In order to check if the singularities are physical, gauge-invariant observable for the spacetime curvature must be derived, that is the Kretschmann invariant Ξ,

$$\Xi = R_{\mu\nu\rho\sigma}R^{\mu\nu\rho\sigma} = \frac{48M^2}{r^6}, \tag{2.3.3}$$

confirming that the only physical singularity is at $r = 0$.

BH solution implies the existence of an **event horizon** in $r = r_\mathrm{s}$ within which nothing can escape and such as no event inside the horizon affects the

[(5)] This theorem was actually discovered and published two years earlier by Jebsen [Jebsen21, Voje Johansen06]

[(6)] Note that Schwarzschild coordinates apply for any spherical system and do not imply the Schwarzschild solution which is only valid in the vacuum.

[(7)] Change of coordinates to more involved coordinate systems like Eddington-Finkelstein or Kruskal-Szekeres ones, are non-singular in $r = r_\mathrm{s}$.

dynamics outside. Singularities could be created during gravitational collapse without the formation of a horizon [Jacobson96], such that the singularity in $r = 0$ would be "naked". Penrose conjectured that appearance of such a "naked" singularity is forbidden because it would be causally disconnected from the exterior of the event horizon [Penrose65]. This conjecture is referred to as the **cosmic censorship**.

The Schwarzschild solution is sufficient for describing spacetime in the vacuum, i.e. in the absence of matter. In particular, it enables one to study static BHs where only gravity comes into play. Note that most of the BHs rotate (usually slowly enough for assuming the quasi-stationarity), the spacetime being then axisymmetric rather than spherically symmetric [Gourgoulhon14]. A metric is stationary if all its components are time-independent or equivalently if it possesses a timelike Killing vector. If the spacetime is static, then there exists also a time reflection symmetry [Teukolsky15]. Hence, rotating BHs are stationary and modeled by the Kerr metric while non rotating ones are static and modeled by the Schwarzschild metric. The asymptotic flatness has to be imposed for recovering the Minkowski solution at spatial infinity according to the Birkhoff theorem.

2.3.2 The uniqueness theorems for black hole solution

Chandrasekhar wrote [Chandrasekhar83],

> BLACK HOLE - *"The black holes of nature are the most perfect macroscopic objects there are in the Universe: the only elements in their construction are our concepts of space and time. And since the general theory of relativity provides only a single unique family solutions for their descriptions, they are the simplest objects as well."*

From the classical point of view, BHs observations only probe spacetime curvature effects, without any prior knowledge on the matter coupling to gravity. As we will see in the following, GR in the vacuum is directly tested by the recent direct detection of GWs by LIGO [Abbott16b].

In 1967, Israel proved that the only static asymptotically flat solution of the Einstein equations with a regular horizon is the Schwarzschild one in the absence of BH electric charge. This is the beginning of a serie of **uniqueness theorems** (see e.g. the Robinson's contribution of [Wiltshire09]) guaranteeing that there is a very limited family of stationary, asymptotically flat BH solutions in Einstein-Maxwell's theory: the unique spacetime solutions are the Kerr [Kerr63] and Schwarzschild metrics for stationary and static spacetimes respectively (or the Kerr-Newman [Newman65] and the Reissner-Nordström ones [Reissner16, Nordström18] in the presence of an electric field). The mass, the angular momentum and the electric charge are the only three parameters for describing all BHs in nature, all the other properties in the previous stages of the life of the star being not relevant anymore [Thorne94]. In particular, all stellar properties like deviation from spherical symmetry and magnetic

field are not relevant anymore during the collapse of a star since the gravitational field decouples from its matter source in the late stages of collapse [Teukolsky15].

However, the uniqueness theorems assume that there is no additional scalar, vector or spinor field degrees of freedom and that no naked singularity exists[8]. **The no-hair conjecture** states that BHs are completely specified by giving their mass, angular momentum as well as electric and magnetic charges, the "hair" being fields associated with stationary BHs apart from the gravitational and the electromagnetic ones. It has been proven for particular cases only (see e.g. [Bekenstein72, Bekenstein95]). Basically no-hair theorem guarantees that the scalar field is constant outside the horizon, i.e. $|\nabla\phi| = 0 \forall r > r_{\rm H}$, $r_{\rm H}$ being the horizon radius, such that the scalar field is settled to its asymptotic value outside the horizon [Weinberg02]. The proofs of no-hair theorems for more sophisticated models are still under investigation (see e.g. [Berti15]). A lot of models beyond GR violate this theorem [Chrusciel12] [9].

2.3.3 Tests in the vacuum

In this section, the current and future observations in the strong field regime appearing in the vacuum are briefly discussed. Those observations directly probe the spacetime properties since they are performed in the absence of matter.

2.3.3.1 Isolated black holes

Because of the uniqueness theorems, any deviation from the Kerr-Newman family of solutions would invalidate GR. In order to test the dynamics predicted by GR, parametrization of generic spacetimes would be a very useful tool, similarly to PPN expansion in the weak-field regime. However, no unique reference metric exists in the strong-field regime like the Minkowski spacetime in the weak-field one. Some attempts have been developed [Johannsen11] (see also [Berti15] for a summary).

Experimental tests have been proposed, notably by measuring the dynamics of orbiting objects like pulsars around BHs [Sadeghian11], for instance around SgrA* thanks to the telescope General Relativity Analysis via Vlt InTerferometrY (GRAVITY) [Eisenhauer11]. Any deviation from the timelike geodesics of the Kerr spacetime would be an evidence for physics beyond GR. In the forthcoming decades, the radio telescopes Five hundred meter Aperture Spherical Telescope (FAST) and Square Kilometer Array (SKA) will discover

[8] This last assumption which should be unnecessary [Teukolsky15] and is still a limitation of the uniqueness theorem.

[9] For instance hairy BHs are predicted in the presence of non-Abelian gauge fields, like in the Einstein-Yangs-Mills theory where the solution is static and has vanishing Yang-Mills charges whereas it is not characterized by its total mass. However, physical observables remain identical (see e.g. [Volkov99]).

most of the active pulsars beamed toward us in the Milky Way [Kramer04], so that some binary systems of pulsar-BH or pulsar orbiting around SgrA* should be detected.

Some further tests of GR exist too: are all compact objects with a mass $m \gtrsim 3M_\odot$ BHs? Do all BHs have a horizon? Observations in the electromagnetic spectrum are tricky but GWs modes detection should give rise to precision test.

2.3.3.2 Binary pulsar

Pulsars are rotating NSs which emit radio waves due to their intense magnetic field, around 10^8 T. Even if they are compact objects, **binary pulsar systems** only probe GR in the vacuum provided that both compact objects can be considered as "point" masses without complicated tidal effects. Indeed, if the equivalence principles are fully satisfied, the only way to detect gravitational effects is via tides which generate GWs. In order to be detectable, GWs must be generated either by the coalescence of two compact objects either by isolated not perfectly symmetric NSs. Because of the emission of GWs, the orbital period of the binary system decreases over time. In the case of binary pulsar, the orbital velocity is relatively small $v/c \sim 10^{-3} \ll 1$ such that the PN formalism at leading order is still valid and the orbital period changes at an effectively constant rate [Abbott16c].

In 1974, Hulse and Taylor discovered the binary pulsar PSR B1913+16 which enables to test the strong field as well as the radiative regime of GR for the first time. Computation of 3 over the 5 post-keplerian parameters leads to a self-consistent estimation of the 2 remaining parameters, i.e. the mass of the pulsar and of its companion [Will08]. In addition, the variations of the orbital period in time $\dot{P}_\mathrm{b}$ due to the emission of GWs were measured during 30 years (the coalescence process lasts around 10^7 years in the case of binary pulsar systems [Abbott16c]), yielding [Taylor92, Weisberg10],

$$\frac{\dot{P}_\mathrm{b}^\mathrm{obs}}{\dot{P}_\mathrm{b}^\mathrm{GR}} = 1.0013 \pm 0.0021, \tag{2.3.4}$$

GR predictions being tested at 10^{-3} level. Other binary systems have been studied since then, giving rise to even better tests of gravity (see e.g. [Kramer06, Antoniadis13]).

Binary pulsar systems are today able to test GR, either by measuring the emission rate of GWs over decades or by studying the nonradiative strong-gravity effects [Taylor92] by testing the SEP (see Sec. 3.2.5.3). In the future, tests should be improved by detecting a lot of binary systems.

2.3.3.3 Direct detection of gravitational waves

The recent direct detection by LIGO of GWs coming from the coalescence of two binary BHs systems [Abbott16b, Abbott16a] enables one to probe the large

velocity and highly non-linear regime of GR [Abbott16c]. This regime not only requires the PN formalism but also numerical relativity simulations [Gair13] in order to take into account the full non-linearities of GR.

The coalescence process of two BHs is divided into three parts: the inspiral phase during which BHs spiral together on nearly circular orbit; the merger phase where the relative velocity is close to the speed of light, $v/c \sim 1/3$ and the oscillation frequencies of the emitted GWs are very specific [Berti15]; and the ring-downs where any remaining deformity of the final single BH is dissipated in GWs. At the end of the coalescence process, the final BH remnant must settle down to a stable stage, satisfying the Kerr solution according to the uniqueness theorems.

The coalescence process as a whole is found to be in agreement with predictions of Einstein equations in the vacuum. According to the observations during the inspiral phase, i.e. using the low-frequency of the signal, the estimated masses of the primary and secondary BHs are given by $m_1 = 39^{+6}_{-4} m_\odot$ and $m_2 = 32^{+4}_{-5} m_\odot$ for the first event [Abbott16b] and $m_1 = 14.2^{+8.3}_{-3.7} m_\odot$ and $m_2 = 7.5^{+2.3}_{-2.3} m_\odot$ for the second one [Abbott16a]. Moreover, those results are consistent with the estimated mass and the dimensionless spin of the final BH as predicted from the inspiral phase and inferred from the merger and ring-downs phases.

LIGO has given the best upper bound on the graviton mass in the dynamical regime, $m_g < 1.2 \times 10^{-22}$ eV at 90% Confidence Level (C.L.) [Abbott16c], a result which provides constraints on modifications of gravity predicting a massive graviton. Indeed, such theories predict that the massive graviton propagates at a frequency dependent speed [Abbott16b].

Up to now, LIGO has not provided constraints on the polarization states of GWs. Once the other ground based detectors like Advanced Virgo, Kagra and LIGO-India, will be operational, it would be possible to measure the polarization, such that models beyond GR which predict other polarization modes that the quadrupole one (the only mode predicted by GR) could be ruled out.

The advantages of GW astronomy with respect to optical astronomy as well as astroparticle physics, are multiple: their signal is very clean since they are not affected by the presence of matter or electromagnetic fields when they are emitted and as a result, they do not suffer from the uncertainty on the astrophysical matter like NSs (see Sec. 2.3.5). Moreover, GWs enable one to probe some astrophysical phenomenons in the absence of any other signal, for instance BH binary system. However, the inspiral and merger processes are intrinsically transient. The intrinsic feebleness of the signal-to-noise ratio of GWs detection is a second drawback since GWs detection requires complex data analysis for extracting the signal.

2.3.3.4 GWs detection in the future

Experiments like LIGO are dedicated to the coalescence of NSs and stellar BHs at late time, for a redshift $z \sim 1$, since they are able to detect signals

from deca- to hecto-Hz [Yunes13] (the frequency of the first signal detected by LIGO is $\sim 35-150$ Hz). The space mission eLISA (see [Amaro-Seoane13] for the scientific review of the mission) should be launched in the horizon 2034. It would be rather dedicated to the detection of GWs coming from supermassive BH binary system, up to a redshift of $z\sim 10$ [Gair13]. Because of the very large size of its arms, around 10^6 km, such an experiment can detect GWs from 10^{-5} to 1 Hz [Yunes13]. The recent results from LISA-Pathfinder experiment confirmed that the sensitivity of eLISA is reachable [Armano16].

2.3.4 Schwarzschild interior solution

Computing the GR solution for a compact star interior involves the knowledge of the fluid composing the compact stars. In this case, not only the curvature effects are probed but also the composition of the matter sources as well as its coupling to the curvature. As we will see, GR is not tested directly in this case. As for the vacuum solution, we restrict the discussion to the static and spherically symmetric spacetime with the metric ansatz (2.3.1).

The most general stress-energy tensor associated to a spherical distribution of matter bounded by gravitation is locally anisotropic [Lemaître33] such that the radial $p_{\rm r}$ and tangential $p_{\rm t}$ pressures are independent. In the standard perfect fluid limit[(10)], i.e. $p_{\rm r}=p_{\rm t}=p$ (2.2.2), the so-called **Tolman-Oppenheimer-Volkoff (TOV) equation** generalizes the Euler equation of fluid dynamics and is derived from the conservation of the stress-energy tensor, $\nabla_\alpha T^{\alpha\beta}=0$ for $\beta=r$ ($\Gamma^0_{0r}=\nu'$),

$$\nabla_\alpha T^\alpha_r = \frac{{\rm d}p}{{\rm d}r}+\Gamma^\alpha_{r\alpha}p-\Gamma^\alpha_{r\beta}T^\beta_\alpha=0, \tag{2.3.5}$$

$$\frac{{\rm d}p}{{\rm d}r} = -\nu'\left(p+\rho\right), \tag{2.3.6}$$

$$= -(p+\rho)\frac{2m(r)+\kappa r^3 p}{2r\left[r-2m(r)\right]}, \tag{2.3.7}$$

where the second equality derives from the Einstein equations (see e.g. [Wald84] for the detailed calculations) and $m(r)$ is the mass function of the compact object,

$$m(r) = 4\pi\int_0^r {\rm d}r'\, T^0_0\, r'^2, \tag{2.3.8}$$

$$= 4\pi\int_0^r {\rm d}r'\, \rho(r')\, r'^2. \tag{2.3.9}$$

Then the solution of the TOV equation requires an equation of state (EoS) for the star interior $p=p(\rho)$.

[(10)] We emphasize here that perfect fluid is for sure a strong assumption which is only justified by the sake of simplicity. Realistic description of the fluid composing compact objects requires more involved equations of state (see Fig. 2.1).

Starting from the definition of the mass function (2.3.8) and assuming a static and spherically symmetric spacetime, the total mass of the matter distribution is referred to as the **Arnowitt Deser Misner (ADM) mass**,

$$m_{\rm ADM} = 4\pi \int_0^\infty {\rm d}r\, \rho(r)\, r^2. \tag{2.3.10}$$

However, the common sense of the mass that is the density inside a proper volume element $\sqrt{-^{(3)}g}{\rm d}^3x = e^\lambda\, r^2 {\rm d}r{\rm d}\theta{\rm d}\varphi$, is rather referred to as the **proper mass** in GR [Wald84],

$$M_{\rm pr} = \int {\rm d}^3x \sqrt{-^{(3)}g}\rho = 4\pi \int_0^\infty {\rm d}r\, \rho(r)\, {\rm e}^\lambda\, r^2, \tag{2.3.11}$$

the difference between the proper and the total mass being interpreted as the **gravitational binding energy**,

$$E_{\rm b} = M_{\rm pr} - m \quad > \quad 0. \tag{2.3.12}$$

Assuming **top-hat density profile** inside the star,

$$\rho(r) = \left\{ \begin{array}{ll} \rho_0 & \text{if } r \leq \mathcal{R}, \\ 0 & \text{otherwise}, \end{array} \right. \tag{2.3.13}$$

the TOV equation admits an analytical solution, imposing $p(r = \mathcal{R}) = 0$ [Schwarzschild16b, Tolman39],

$$p(r) = \rho_0 \frac{\sqrt{1-s} - \sqrt{1 - \frac{s^3 r^2}{\mathcal{R}^2}}}{\sqrt{1 - \frac{s^3 r^2}{\mathcal{R}^2}} - 3\sqrt{1-s}}. \tag{2.3.14}$$

The central pressure $p_{\rm c} = p(r = 0)$ predicted by GR,

$$p_{\rm c} = \rho_0 \frac{\sqrt{1-s} - 1}{1 - 3\sqrt{1-s}}. \tag{2.3.15}$$

becomes infinite for,

$$1 - 3\sqrt{1-s} = 0 \quad \Leftrightarrow \quad 1 - s = \frac{1}{9} \quad \Leftrightarrow \quad s = \frac{8}{9}, \tag{2.3.16}$$

or equivalently for the critical mass $M_{\rm cr} = (4/9) m_{\rm pl}^2 \mathcal{R}$ (see Eq. (2.2.1)) assuming uniform density stars whatever EoS [Buchdahl59][(11)]. Hence, observations of stars with $s > 8/9$ might reveal either the existence of anisotropic stars with $p_{\rm t} \gtrsim p_{\rm r}$ [Füzfa02] or a deviation from GR.

[(11)] The last two assumptions are not restrictive actually [Wald84].

2.3.5 Tests in the presence of relativistic matter: neutron stars

When the mass of a star is sufficiently large, that is when it reaches the **Chandrasekhar limit** of $m \gtrsim 1.44\,M_\odot$, then electron degeneracy pressure due to the Pauli principle is not sufficient anymore for counterbalancing the gravitational collapse and the star ends up exploding in a supernova (SN) Ib/c or II. The SN remnant can be either a NS or a stellar BH, depending on the mass and the metallicity, i.e. the presence of atomic elements other than hydrogen. The maximal NS mass which has been detected to date, is $2.01 \pm 0.04\,M_\odot$ [Demorest10] (see Fig. 2.1).

In order to be able to test GR with NSs, the EoS should be determined. However, the EoS inside the core of NSs where the density becomes supranuclear around $10^{15}\mathrm{g/cm}^3$, is still largely unknown. The NSs crust is mainly composed of neutrons with electrons and protons while the density in the inner core is so high that it is constituted by a quark-gluon plasma which requires lattice Quantum Chromodynamics (QCD) computations in order to be simulated (see e.g. [Chamel13]). Depending on the EoS, the maximum mass and compactness predicted by GR are different [Berti15]. The mass-radius diagram represented in Fig. 2.1 enables one to represent the different predictions of GR depending on the EoS. If the EoS predicts a maximal mass smaller than the maximal mass detected, i.e. $2.01 \pm 0.04\,M_\odot$, it is rejected (see e.g. [Wex14]).

Hence, the difficulty of testing GR thanks to isolated NSs arises from the fact that the EoS of high-density matter is degenerated with strong-gravity effects [Berti15]. In order to tackle this problem, some strategies have been invoked using almost EoS-independent relations between macroscopic observable properties of NSs [Chamel15] (see e.g. [Yagi13]) like the "I-Love-Q" relation, which is a universal relation between the moment of inertia of the NS I, the Love numbers which measure the tidal deformability and the quadrupole moment of the NS Q (see [Berti15] and references therein for details). More recently a universal relation between I and the compactness has also been highlighted [Breu16]. With such a universal relation, gravity can be tested in the strong-field regime without any prior knowledge of the EoS and astrophysical observations enable one to constrain nuclear physics up to a very large density.

Another axis of research consists of determining the EoS of NSs thanks to **astereoseismology** by observing characteristic NSs oscillation frequency or quasi-normal modes (see [Kokkotas99] for a review). Those oscillations are responsible for the emission of GWs. As an example, the measure of the frequency and the damping time due to GW emission of one particular mode (called the $f-$mode) would give rise to both constraints on mass and radius of the NS up to at least 10% accuracy and could be detected by LIGO up to 20 Mpc[(12)] for supermassive NSs according to [Surace16].

Observations of glitches, i. e. sudden changes in the pulsar rotation rate,

[(12)] 1 pc is the distance at which 1 AU (the averaged distance from the Earth to the Sun) subtends an angle of one arcsecond i. e. $1\,\mathrm{Mpc} \sim 3 \times 10^{22}\mathrm{m}$.

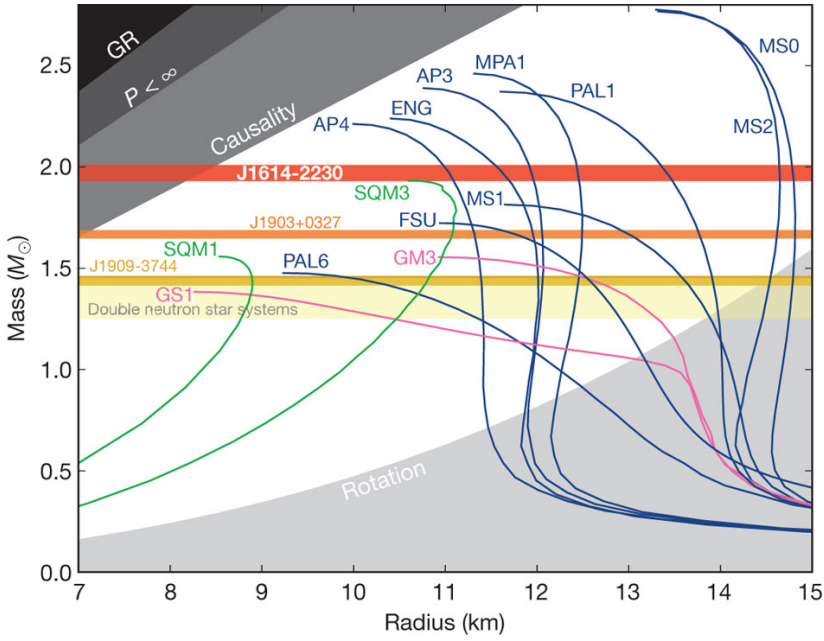

Figure 2.1: NS mass-radius diagram for various EoS (see [Demorest10] for details). The horizontal bands in red, orange and dark yellow show the current observational constraints from several pulsars while in light yellow for double NS binaries. Any EoS line which does not intersect the red band ($m_{\rm NS} = 1.97 \pm 0.04 M_\odot$) is ruled out. Reprinted from [Demorest10] .

thanks to X-ray astronomy [Radhakrishnan69, Espinoza11] also shed light on the pulsars EoS. GWs should be also emitted by those instabilities. Glitches of a few minutes have been observed in some pulsars while the relaxation to the initial rotation period appears to take a few years. This means that the core of NSs has to be made of a non viscous liquid like helium-superfluid [Pines85]. Two X-rays telescopes, CHANDRA and XMM-Newton, observed the evolution of the temperature in time at the surface of quite young NSs in SN remnants. Their observations have confirmed the presence of **superfluid** in NSs (see e.g. [Shternin11]).

2.4 Cosmology

In this section dedicated to cosmology, the solution of the Einstein equations assuming the cosmological principle is briefly reviewed. Similarly to NSs, cosmology not only probes the spacetime curvature because of the presence of a source, that is the cosmological fluid. Depending on the era in the Universe history, the source is either relativistic or not. According to the $\Lambda-$CDM (Cold

Dark Matter) concordance model, the Universe is composed of matter, radiation, Dark Matter (DM) and Dark Energy (DE). Because of the presence of those sources, GR is not tested directly in cosmology.

2.4.1 The cosmological principle

According to the current observations, the Universe is **isotropic** at cosmological scales, i.e. above 100 Mpc. By extending the Copernican principle stating that *"we have no privileged place in the world"* to all observers at cosmological scales, it results that the Universe is supposed to be **homogeneous** at a given cosmic time.

Such a maximally symmetric assumption allows one to predict background cosmology. However, whereas the isotropy is in agreement with the observations, for instance with CMB and galaxy surveys, homogeneity is difficult to test since it requires observations on spatial hypersurfaces [Maartens11].

In order to explain the growth of cosmic structure appearing at smaller scales, the cosmological principle is relaxed to **statistically isotropy and homogeneity**. Several observations today enable one to test GR at the perturbative level and a possible departure from statistical isotropy is still under investigation (see e.g. [Schwarz16]). Most of the cosmological observations today rely on statistical analysis.

2.4.2 The $\Lambda-$CDM concordance picture

The metric for a **maximally symmetric spacetime**, i.e. satisfying the cosmological principle, or Friedmann-Lemaître-Robertson-Walker (FLRW) spacetime reads,

$$\mathrm{d}s^2 = -\mathrm{d}t^2 + a^2(t)\left(\frac{\mathrm{d}r^2}{1-kr^2} + r^2\mathrm{d}\Omega^2\right), \tag{2.4.1}$$

where t is the cosmic time that is the proper time of a comoving observer, r is the radial coordinate and $k = [-1\,;0\,;+1]$ the curvature parameter depending on the spacetime geometry (hyperbolic, flat or spherical respectively). The **scale factor** $a(t)$ is the only metric field to be determined by solving the Friedmann-Lemaître equations,

$$H^2 = \frac{\kappa}{3}\sum_i \rho_i + \frac{\Lambda}{3} - \frac{k}{a^2}, \tag{2.4.2}$$

$$\frac{\ddot{a}}{a} = -\frac{\kappa}{6}\sum_i \rho_i\,(1+3w_i) + \frac{\Lambda}{3}, \tag{2.4.3}$$

with $H = \dot{a}/a$, the **Hubble parameter**[13]. The stress-energy tensor is assumed to be a perfect fluid[14] whose species (DM, dust and radiation) is labeled by i. In cosmology, the EoS w is assumed to be time-independent and barotropic in the most simple case[15],

$$w = \frac{p}{\rho}, \tag{2.4.4}$$

with $w = -1,\ 1/3,\ 0$ for a Universe dominated by Λ, radiation and matter respectively. Assuming a barotropic EoS, the conservation of $T_{\mu\nu}$ gives the evolution of the density during the Universe expansion,

$$\rho(a) \propto a^{-3(1+w)}. \tag{2.4.5}$$

Current observations give rise to stringent constraints on background cosmology. In order to confront the theory with them, Friedmann-Lemaître Eqs. (2.4.2) and (2.4.3) have to be written in terms of dimensionless quantities,

$$1 = \sum_i \Omega_i + \Omega_\Lambda + \Omega_k, \tag{2.4.6}$$

$$q = \frac{1}{2}\sum_i \Omega_i\,(1 + 3\,w_i) - \Omega_\Lambda. \tag{2.4.7}$$

where $\Omega_i(t) = \left[2\kappa/3H^2(t)\right]\rho_i(t) \equiv \rho_i(t)/\rho_{\rm c}(t)$ with ρ_i the energy density of the component i and $\rho_{\rm c}$ the critical density, the label i denoting baryonic matter, DM and radiation (photons and neutrinos); $\Omega_\Lambda \equiv \Lambda/(3\,H^2)$ is the density parameter corresponding to the cosmological constant term is the density parameters; $\Omega_k \equiv -k/(a\,H)^2$ is the density parameter corresponding to the curvature term; and $q = -\ddot{a}a/\dot{a}^2$ is the **deceleration parameter**,

Best bounds on density parameters have been obtained by the Planck satellite probing the CMB [Ade15b] by analyzing the (relative) amplitudes and the positions of the acoustic peaks in the power spectrum of CMB temperature anisotropies. The best-fit of cosmological parameters yields

$$\boxed{\Omega_{\rm k,0} < 0.005, \qquad \Omega_{\Lambda,0} = 0.68, \qquad \Omega_{\rm m,0} = 0.05 \qquad \text{and} \qquad \Omega_{\rm DM,0} = 0.27,} \tag{2.4.8}$$

the radiation being negligible today. The **Hubble constant** is given by $H_0 = 67.80 \pm 0.77$ km Mpc^{-1} s^{-1} [Ade15b]. This is the so-called $\Lambda-$**CDM concordance picture** which is in agreement with all the current observations today (see e.g. [Kowalski08, Ade15c]).

[13] In general, the dimensionless Hubble parameter h yielding $H_0 = h \times 100$ km Mpc^{-1} s^{-1} where the subscript 0 refers to parameters evaluated today, is compared to the observations.

[14] As before, this assumption is only justified by the sake of simplicity and is not valid during all the Universe history.

[15] In general the EoS is time-dependent. Different parametrizations of the EoS exist like the polytropic one $p = K\rho^{(n+1)/n}$ with K a constant and n the polytropic index, and the generalized Chaplygin gas one $p = -A\rho^\alpha$ with A a positive constant and $0 < \alpha \lesssim 1$ [Bento02].

Other observations than the CMB ones enable one to probe the cosmological parameters, among them large galaxy surveys like SDSS-II, BOSS and 6dFGS, which probe the formation of large scale structure (LSS), i.e. groups or filaments of galaxy clusters, during the matter era, by measuring the matter power spectrum. Baryons leave imprints on the matter power spectrum because of their interactions to photons in the early Universe. Before recombination, photons and baryons formed a single fluid because of the Thomson and Coulomb interactions. At the decoupling, photons freely move across spacetime while baryons remained at rest and were attracted by DM gravitational potential wells (see e.g. [Hu01] for details). The distance traveled by the baryons-photons sound-waves from Big Bang to the last scattering surface, of about 150 Mpc, is still observable in the matter power spectrum, through the so-called **baryon acoustic oscillations** (BAO) [Eisenstein05]. BAO is thus a standard ruler enabling to infer cosmological parameters at different redshifts thanks to galaxy surveys, independently of other observations [Anderson14].

In Fig. 2.2a the combined constraint on the cosmological parameters $\Omega_{\mathrm{m},\,0}$ and $\Omega_{\Lambda,\,0}$ obtained by the Wilkinson Microwave Anisotropy Probe (WMAP) and Planck satellites as well as galaxy surveys is represented, assuming the $\Lambda-$CDM model. The prediction of a flat Universe is strongly favored. The observations of SN Ia (see Sec. 2.4.4) are also represented.

In summary, according to our current understanding, the nature of around 95% of the matter-energy content of the Universe is still an open debate: first the cold DM, i.e. non-relativistic matter ($w = 0$) which does not interact with electromagnetic field, and second the DE which is responsible for the current cosmic acceleration. Today DE is compatible with the cosmological constant Λ ($w = -1$).

2.4.3 The nature of Dark Matter

In 1933, Zwicky suggested the existence of DM. He measured the velocity of galaxies inside the Coma cluster [Zwicky33] and compared the underlying total mass of the Coma cluster to the visible matter, concluding that there is a missing mass dubbed DM. Further strong evidences have been obtained in the 1970s by looking at the **galaxy rotation curves** [Rubin70]. Typical velocity distribution does not correspond to visible disk velocity. The presence of a DM halo at the galactic scale must be invoked in order to fulfill the observations.

The evidences for DM are now numerous, at the galactic and cosmological scales. According to our current understanding, temperature fluctuations in the CMB correspond to DM over- and under-densities, which acts as seeds for the formation of LSS hosting galaxies, from the redshift $z \approx 20 - 30$[16]. Without DM, the formation of LSS would be not efficient since primordial fluctuations would vanish because of the diffusion damping. At the scale of clusters of galaxy, gravitational lensing reveals that DM has to be invoked for reconstructing the gravitational potential well [Markevitch04, Clowe06, Massey07].

[16] Rigorously, galaxies are biased tracer of DM.

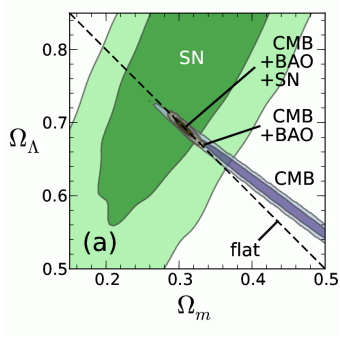

(a) The present DE fraction Ω_Λ vs. matter fraction Ω_m assuming the $\Lambda-$CDM model. Predictions for a flat Universe is denoted by the diagonal dashed line and is strongly favored by CMB+BAO data.

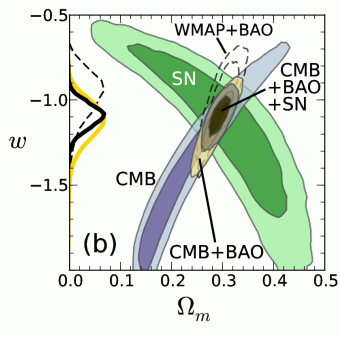

(b) The DE EoS w vs. Ω_m, assuming a constant value for w. The dashed contours show the $1\ \sigma$ and $2\ \sigma$ C.L. regions for the combination of WMAP and BAO data.

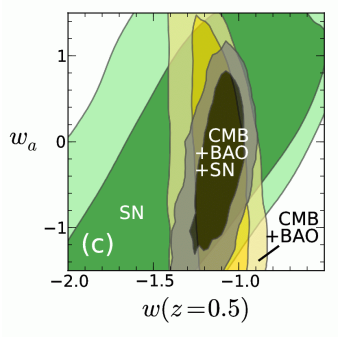

(c) Constraint on the two parameters of the DE model with a time-dependent EoS, for $w(z = 0.5)$.

Figure 2.2: Constraints on the present matter fraction Ω_m (DM+ baryonic matter) and the DE parameters (Ω_Λ, w and $w_a = -\mathrm{d}w/\mathrm{d}a$). Dark and light shaded regions indicate $1\ \sigma$ and $2\ \sigma$ C.L. respectively. "CMB" is Planck+WMAP Polarization, "BAO" is the combination of SDSS-II, BOSS and 6dFGS, and "SN" is Union 2. Reprinted from [Mortonson13].

The $\Lambda-$CDM model does not tell anything about the nature of the DM, the observations only revealing that DM has to be (predominantly) cold or non-relativistic. Strictly speaking, we observe evidences for an extra hidden mass, which is not observed at any wavelengths of electromagnetic signals. Although the evidences of DM come from astronomy and cosmology, most of experimental effort has now been shifted to particle and astroparticle physics. The DM could be a new particle beyond the SM. Several candidates exist, some of them related to issues appearing in the SM: WIMPs and gravitinos (related to supersymmetry), axions (also devoted to the strong CP problem), sterile neutrinos (possibly ruled out [Schneider16]), primordial BHs [Carr74, Carr75], their predicted mass range being in agreement with BHs detected by LIGO [Bird16, Clesse16][(17)], etc. No evidence for new particles has been obtained so far, either by direct or indirect detection. In the presence of a DM signal, one should still justify the observed abundance of DM on cosmological scales.

Alternative models have been proposed, some of them in the framework of modified gravity. For instance, the MOdified Newton Dynamics (MOND) theory [Milgrom83, Famaey12] or its covariant version TeVeS [Bekenstein04], are able to reproduce the galaxy curves whereas they do not fit the CMB observations nor the gravitational lensing ones by invoking baryonic matter only [Angus07, Clowe06]. Others like the Chaplygin gas [Bento02] where DM and DE are both described by a single fluid, are able to reproduce the growth of large-scale structure.

2.4.4 The current accelerated expansion

The first evidence for the acceleration of the spacetime expansion came from the observation of distant galaxies hosting SN Ia by Riess et al. [Riess98] and Perlmutter et al. [Perlmutter99]. They measured the luminosity distance $D_{\rm L}$ and the redshift z defined as,

$$1+z \equiv \frac{\lambda_{\rm obs}}{\lambda_{\rm e}} = \frac{a_0}{a(t)}, \tag{2.4.9}$$

with $\lambda_{\rm e}$, $\lambda_{\rm obs}$, the emitted and the observed wavelengths respectively, the last equality being valid for recessional redshift only, neglecting the local Doppler effects. The relation $D_{\rm L}$-z enables one to probe the expansion up to $z \sim 2$, highlighting the current expansion.

However, the nature of the acceleration is still an open debate. The cosmological constant predicts that the EoS is constant $w = -1$, while more sophisticated models invoking a scalar field for instance, may predict variable EoS, generally parametrized up to first order by,

$$w(z) = w_0 + w_a(1-a), \tag{2.4.10}$$

[(17)]Primordial BHs in this mass range are possibly ruled out according to [Ricotti08], but this result is still controversial.

with $w_0 = w(z=0)$ and $w_a = -\mathrm{d}w/\mathrm{d}a$. Current bounds on the plane $w_0 - w_a$ obtained by combining CMB+BAO+SN data are reported in Figs. 2.2b and 2.2c. There are compatible with $w_0 = -1$ and $w_a = 0$.

Even if Λ is able to reproduce current observations, it leads to a theoretical issue named the **cosmological constant problem** [Weinberg89]. The cosmological constant has the same properties as the vacuum energy of quantum mechanics. Indeed, in order to preserve Lorentz invariance, $T_{\mu\nu}^{(\mathrm{vac})} \propto g_{\mu\nu}$ (see Eq. (2.2.2)) [Weinberg08] such that there exists no preferred direction. It results that $p^{(\mathrm{vac})} = -\rho^{(\mathrm{vac})}$ yielding,

$$T_{\mu\nu}^{(\mathrm{vac})} = -\rho^{(\mathrm{vac})} g_{\mu\nu}, \tag{2.4.11}$$

where $\rho^{(\mathrm{vac})}$ is constant (see Eq. (2.4.5)). A cosmological constant enters in the Einstein equations (1.2.7) exactly in the same way as the contribution of the vacuum energy [Durrer08b], leading to,

$$\rho^{(\mathrm{vac})} = -\frac{\Lambda}{\kappa}. \tag{2.4.12}$$

In general, the cut-off scale for GR is given by the Planck scale $E = m_{\mathrm{pl}}$ such that [Durrer08b],

$$\rho^{(\mathrm{vac})} \sim m_{\mathrm{pl}}^4 \sim 10^{76}\mathrm{GeV}^4, \tag{2.4.13}$$

while the observed value of the cosmological constant yields,

$$\rho_\Lambda \sim \left(10^{-12}\right)^4 \sim 10^{-48}\mathrm{GeV}^4. \tag{2.4.14}$$

It results that a cancellation of the vacuum energy of around 120 orders of magnitude is required for explaining the cosmological observations. This is the so-called **fine-tuning problem**.

In addition the **Weinberg no-go theorem** [Weinberg89] states on very general grounds like the Poincaré invariance at the level of spacetime curvature and fields, that no dynamical adjustment mechanisms could be used to solve the fine-tuning problem [Padilla11].

The second issue arises when looking at the Universe history: the acceleration of the expansion started around $z \sim 0.6$ ($\rho_{\Lambda,\,0} \simeq \rho_{\mathrm{DM},\,0}$), which is referred as **the coincidence problem**. In order to justify Λ, either anthropic or multiverse arguments have been invoked (see e.g. [Carr07]).

In order to face the coincidence issue, it has been proposed that the cosmic acceleration is due to a dynamical scalar field, possibly massive, rather than the cosmological constant. Since this scalar field has an exotic EoS, it has been dubbed Dark Energy. We focus here on one of the simplest models of DE, quintessence [Amendola10]. It invokes a scalar field ϕ minimally coupled to the metric, i.e. there is no modifications of the Einstein's theory, such that the isotropy is not broken,

$$\mathcal{L} = \frac{R}{2\kappa} - \frac{m_{\mathrm{pl}}^2}{2}\left(\partial\varphi\right)^2 + V(\varphi) + \mathcal{L}_{\mathrm{M}}, \tag{2.4.15}$$

with $\phi = m_{\rm pl}\,\varphi$ such that φ is dimensionless, and $V(\varphi)$ the potential of runaway type. Assuming that the Universe is flat and dominated by DE $T^{(\rm M)}_{\mu\nu} \simeq 0$, the Friedmann-Lemaître equations read,

$$H^2 = \frac{\kappa}{3}\rho_\phi, \tag{2.4.16}$$

$$\frac{\ddot{a}}{a} = -\frac{\kappa}{6}\rho_\phi(1+3w_\phi), \tag{2.4.17}$$

where w_ϕ is the EoS of the scalar field,

$$w_\phi = \frac{\rho_\phi}{p_\phi} \qquad \text{with} \qquad \left\{ \begin{array}{l} \rho_\phi = \frac{1}{2}\dot{\phi}^2 + V(\phi), \\ p_\phi = \frac{1}{2}\dot{\phi}^2 - V(\phi). \end{array} \right. \tag{2.4.18}$$

while the Klein-Gordon equation,

$$\ddot{\phi} + 3H\dot{\phi} + \frac{{\rm d}V}{{\rm d}\phi} = 0. \tag{2.4.19}$$

The condition for the acceleration of the expansion is thus given by Eq. (2.4.17)[(18)],

$$\ddot{a} > 0 \qquad \longleftrightarrow \qquad w_\phi < -\frac{1}{3}. \tag{2.4.20}$$

In the case of the cosmological constant ($V(\phi) \propto \Lambda$ and no kinetic term), $w_\phi = -1$ and the solution of Eq. (2.4.16) is de Sitter,

$$a(t) \propto \exp\left(\sqrt{\Lambda}t\right). \tag{2.4.21}$$

Quintessence is able to solve the fine-tuning problem of the initial conditions, for instance if an attractor solution exists. Indeed, for any initial conditions of the scalar field in the early Universe, the scalar field converges to the path given by its attractor by rolling down its potential [Zlatev99]. In addition, quintessence may not suffer from the coincidence problem since it calls on a dynamical mechanism provided that the energy scale of the scalar field today $m_\phi^2 \equiv V_{,\phi\phi}$ is sufficiently small, i.e. $|m_\phi| \lesssim 10^{-33}$ eV [Amendola10]. However, quintessence models rely on the existence of a potential whose parameters must be fixed, introducing additional parameters in the theory.

Scalar fields with a non-standard kinetic term like phantom ($w < -1$) and k-essence, are also able to reproduce the late-time acceleration, but phantom usually suffers from instability because it is a ghost (it has negative kinetic energy density such that its energy density grows with expansion, its quantum vacuum being possibly unstable, see e.g. [Amendola10]) while k-essence violates causality [Durrer08b, Bonvin06].

Infrared modifications of GR (see also Chap. 3) could also be responsible for the acceleration appearing at large scales, for instance by introducing a scalar field nonminimally coupled to the metric (see Sec. 3.2 and

[(18)] We assume that $\rho_\phi > 0$, so there is no violation of the weak energy condition $T_{\mu\nu}t^\mu t^\nu \geq 0$, t^μ being any timelike vector.

[Copeland06, Amendola10] for reviews). The challenge in this latter case, is that those models must pass the local tests of gravity like the PPN parameters in the Solar system (see Sec. 2.2). In order to fulfill this requirement, modified gravity models invoke screening mechanisms (see Sec. 3.1.3), like the chameleon model which nevertheless appears to be fine-tuned (see Chap. 4).

DE and modified gravity models both predict dynamical EoS ($w_a \neq 0$), a prediction which is constrained today using the combined CMB+BAO+SN data sets (see Fig. 2.2c). Those bounds should be improved by future observations, in particular large galaxy surveys, for instance thanks to the Euclid satellite [Amendola16].

Note that, within the general relativistic framework, the current acceleration could be due to the backreaction, i.e. the effect of deviations from exact homogeneity and isotropy coming from the nonlinear growth of matter density perturbations, on the average expansion (see [Buchert12] for a review). Indeed, the timescales at which the cosmic acceleration and the structure formation started, are similar (around 10^{10} years) [Buchert12]. If the nonperturbative effect of the backreaction is so large that it can explain the cosmic acceleration, it could solve the fine-tuning and coincidence problems at once. However, the effect has not been quantified yet in a fully realistic way.

2.4.5 Fine-tuning of the initial conditions

Within the $\Lambda-$CDM concordance model, initial conditions in the early Universe appear to be fine-tuned given the current observations, raising the question of an underlying mechanism.

1. ***The horizon problem***: Since temperature anisotropies of CMB are so tiny, it suggests that the different patches in the sky were in causal contact or inside the so-called Hubble radius H^{-1} before the recombination, so that the thermalisation of the Universe is effective. However, it should not be the case if we assume that the $\Lambda-$CDM model is valid up to the Planck scale. Because of the finite speed of photons, the distance that the photons travel from the early Universe until recombination, corresponds to only 1 deg angular separation in the sky today. How can we explain the temperature isotropy in the CMB for regions much more separated in the sky today?

2. ***The flatness problem***: Why does the Universe appear to be so flat today ($\Omega_{k,0} < 0.005$) although to do so, it has to be even flatter in the past? Initial conditions would be incredibly fine-tuned to $\Omega_k = 0$, for instance $\Omega_k < 10^{-10}$ at the Big Bang nucleosynthesis (BBN)[(19)], which is in addition an unstable point between an open and a closed Universe.

[(19)]The BBN is the stage in the early Universe when temperature and density conditions were such that, during a brief epoch, nuclear reactions were effective in building complex light nuclei, D, ^{3}He, ^{4}He and ^{7}Li (see e.g. [Cyburt16]). By measuring the relic abundances of these nuclei, the physical conditions at BBN are predicted by GR and SM.

3. ***Adiabatic (or curvature) primeval fluctuations***: By definition, adiabatic density fluctuations are identical for each species (photons, baryons and DM) since there is no contribution of entropy ($S = 0$). By opposition, the entropy (or isocurvature) ones are generated in case of entropy inhomogeneities, assuming vanishing spatial curvature (see e.g. [Peter09]). Only adiabatic fluctuations have been detected so far [Ade15e], isocurvature ones being thus negligible in the early Universe. The mechanism generating the initial fluctuations, must thus (mostly) generate adiabatic perturbations.

4. ***The topological defects problem***: The breaking of the gauge group of a Grand Unified Theory to the gauge group of the SM in the early Universe results in a serie of phase transitions induced by spontaneous symmetry breaking (see e.g. [Preskill79, Einhorn80]). Such a process implies the formation of topological defects like monopoles. The annihilation rate of these topological defects is found to be very slow and since they are not observed, it means that a mechanism may be responsible for their disappearance [Zeldovich78].

Up to now, the most powerful mechanism solving all these problems at once, is the **primordial inflation**. This is an almost de Sitter phase in the early Universe, differing in DE since the predicted acceleration is much more larger and inflation requires a **graceful exit**, i.e. inflation must end. The huge acceleration of the expansion in the early Universe explains at once why it appears locally flat today even if it was not the case before inflation and why non causally connected patches in the sky exhibit the same physical properties since they have been in causal contact before inflation. Moreover, the topological defects are diluted due to the huge expansion. The magnitude of the expansion is given by the **number of e-folds** N,

$$N(t) = \ln \frac{a(t)}{a_{\rm i}}, \tag{2.4.22}$$

with $a_{\rm i}$ the scale factor at the onset of inflation. $N(t_{\rm end}) \gtrsim 60 - 70$ solves at once the horizon and the flatness problems.

The most simple inflationary models, first built by Guth [Guth81] and Linde [Linde82][(20)], call on one scalar field, similarly to DE (see Eqs.(2.4.15) to (2.4.19)). Assuming the first **slow-roll condition** (see Eqs. (2.4.20) and (2.4.18)),

$$\dot{\phi}^2 \ll V(\phi), \tag{2.4.23}$$

it results that the scalar field starts to roll slowly down its potential and that the inflation naturally ends when it oscillates around its minimum. This latter

[(20)]There are other precursory papers, among them [Brout78, Sato81, Starobinsky80]. In particular, Starobinsky proposed a model relying on a modifications of the EH action giving rise to an inflationary model which is still viable today (see also Fig. 2.3 and discussion in Chap. 5).

phase is called the **reheating**. The inflationary phase also has to be sufficiently long, providing a second slow-roll condition,

$$\left|\ddot{\phi}\right| \ll \left|\frac{\mathrm{d}V}{\mathrm{d}\phi}\right|. \tag{2.4.24}$$

Both slow-roll conditions (2.4.23) and (2.4.24) are usually quantified by the dimensionless **slow-roll parameters** using Eqs. (2.4.16), (2.4.17), (2.4.18),

$$\epsilon_{\mathrm{V}} \equiv \frac{M_{\mathrm{pl}}^2}{2}\left(\frac{\partial V/\partial\varphi}{V}\right)^2 \ll 1, \qquad |\eta_{\mathrm{V}}| = M_{\mathrm{pl}}^2\left|\frac{\partial^2 V/\partial\varphi^2}{V}\right| \ll 1, \tag{2.4.25}$$

with $M_{\mathrm{pl}} = 1/\sqrt{\kappa}$ the reduced Planck mass. Slow-roll parameters usually constrain background inflation as well as the CMB power spectrum, even if they appear to be restrictive in some cases [Clesse11].

Primordial scalar and metric fluctuations are generated in the early Universe, according to quantum mechanics (see e.g. [Durrer08a, Mukhanov05, Peter09] for technical details). In particular, the scalar field fluctuates around its averaged value at very small scales. However, because of the huge expansion, microscopic regions are stretched so fast that they became larger than the size of the Hubble radius and are then frozen. As a consequence, there are scalar field fluctuations on super-horizon scales at the end of inflation. The scalar field decayed then into particles during reheating. Assuming one-field inflation, the adiabatic initial fluctuations are thus explained since all species fluctuations derive identically from the scalar field ones (provided constant branching ratios),

$$\frac{\delta\rho_\phi}{\rho_\phi} \propto \frac{\delta\rho_{\mathrm{f}}}{\rho_{\mathrm{f}}}, \tag{2.4.26}$$

with ρ_ϕ, the density of the scalar field and ρ_{f}, the density of each species labeled by f. On the contrary, multifield inflation could generate entropy modes.

Because of the quantum nature of the primordial fluctuations, statistical properties only can be derived from the distribution of the temperature fluctuations in the CMB and of matter fluctuations at smaller redshift. In the most simple case, where only one scalar field in slow-roll is assumed, the distribution of the two-point correlation function of $\delta\rho/\rho$ is Gaussian and the two point-correlation function describes all the statistical properties.

However, if **non-gaussianities** are detected, the three- and four-point correlation functions contain additional information. The corresponding parameters are the bispectrum $f_{\mathrm{NL}}^{\mathrm{loc}}$ and the trispectrum amplitude $g_{\mathrm{NL}}^{\mathrm{loc}}$, the current bounds reading [Ade15d],

$$f_{\mathrm{NL}}^{\mathrm{loc}} = 0.8 \pm 5.0 \qquad g_{\mathrm{NL}}^{\mathrm{loc}} = -9.0 \pm 7.0 \times 10^{-4}. \tag{2.4.27}$$

Non-gaussianities are thus negligible even if they could be produced not only during inflation but also during (p)reheating, by cosmic strings or astrophysical processes. It results that single-field inflationary models are favored.

Statistical properties are usually derived in the Fourier space by computing the perturbations of the metric decomposed in scalar, vector and tensor perturbations. The predicted curvature power spectrum $P_\zeta(k)$[21] reads,

$$k^3 P_\zeta(k) \equiv A_\mathrm{s} \left(\frac{k}{k_*}\right)^{n_s - 1}, \tag{2.4.28}$$

with A_s the amplitude of the scalar power spectrum measured at the pivot scale $k_* = 0.05\,\mathrm{Mpc}^{-1}$ and n_s the **scalar spectral index** measuring the departure from scale-invariance. Planck $1\,\sigma$ constraints today yield [Ade15e],

$$\boxed{\ln\left(10^{10}\,A_\mathrm{s}\right) = 3.089 \pm 0.036, \qquad n_\mathrm{s} = 0.9655 \pm 0.0062.} \tag{2.4.29}$$

The fact that the $\mathcal{P}_\zeta(k) \equiv k^3 P_\zeta(k)/(2\pi^2)$ is **almost scale invariant** ($n_\mathrm{s} \simeq 1$), has been probed by the large angular scales of the CMB temperature fluctuations, that is the **Sachs-Wolfe plateau** since, on super-Hubble scales, perturbations are almost constant (up to the Integrated Sachs-Wolfe effect, i.e. how the presence of evolving gravitational potential wells affect the temperature of the CMB photons along their line-of-sight). Indeed, the fluctuations which were super-Hubble at the last scattering surface, were frozen and thus initial conditions are directly probed today by measuring the tilt of $\mathcal{P}_\zeta(k)$.

Perturbations of the metric are not only scalar. Vector perturbations are negligible since they decrease during the expansion, except if they are sourced (locally), for instance by a magnetic field. Tensor modes are related to the generation of primordial GWs during inflation. The **tensor-to-scalar ratio** r [Ade15e],

$$r \equiv \frac{\mathcal{P}_t}{\mathcal{P}_\zeta}, \tag{2.4.30}$$

with $\mathcal{P}_\mathrm{t}$ the power spectrum of tensor perturbations in the metric, has been constrained recently by the observation of the polarization modes of the CMB: only tensor perturbations generate B-modes while E-modes are generated by both tensor and scalar perturbations. The measure of r enables to fix the energy scale of inflation. Up to now, the combined constraints coming from Planck satellite (operating in the range 30-353 GHz) as well as the ground-based telescopes Background Imaging of Cosmic Extragalactic Polarization 2 (BICEP2) and the Keck Array (operating at 150 GHz) give,

$$\boxed{r < 0.10 \qquad (95\%\mathrm{C.L.}).} \tag{2.4.31}$$

Assuming the slow-roll conditions (2.4.23) and (2.4.24), the analytical expression for the power spectrum at the pivot scale $k = k_*$ reads (see e.g. [Peter09]),

$$\mathcal{P}_\zeta(k_*) \simeq \frac{1}{\pi} \frac{H_*^2}{M_\mathrm{pl}^2 \epsilon_{\mathrm{V},\,*}}. \tag{2.4.32}$$

[21] The curvature ζ is used here for describing the scalar perturbations because it is gauge-invariant.

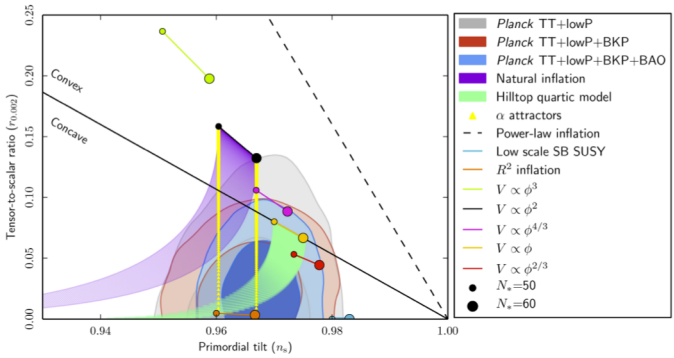

Figure 2.3: Predictions of some inflationary models compared to the Planck observations in terms of n_s and r. Dark and light shaded regions indicate $1\ \sigma$ and $2\ \sigma$ C.L. respectively. Power-law inflation is strongly disfavored while Starobinsky inflation is favored, in the absence of tensor modes detection [Ade15e]. Moreover, in the absence of non-gaussianities, one field inflation is most likely than multifields ones.

In the slow-roll conditions the parameters n_s and r can be determined by expanding the primordial power spectra $\mathcal{P}_\zeta$ and $\mathcal{P}_\mathrm{t}$. To first order they read [Liddle94],

$$n_\mathrm{s} = 1 - 6\epsilon_{\mathrm{V},*} + 2\eta_{\mathrm{V},*}, \qquad r = 16\epsilon_{\mathrm{V},*}, \tag{2.4.33}$$

where the asterisk denotes the pivot scale at which n_s and r are evaluated.

Numerous inflationary models exist and constraints coming from Planck + BICEP2 + Keck Array [Ade15a] allow to rule out some of them. Their results are reported in Fig. 2.3. Bayesian inference analysis has been provided using one of the most favored models as prior, the Higgs inflation [Martin14b, Martin14a] which is equivalent to the Starobinsky model (see also Chap. 5). Future space and ground based missions like BICEP3, LiteBIRD [Matsumura14], COrE+ [Armitage-Caplan11] and PRISM [Andre13] should enable one to constrain r up to 10^{-3}.

Viable alternatives to inflation exist too, among them ekyroptic scenarios [Steinhardt02], string gas cosmology and matter bounces [Brandenberger11, Brandenberger16]. None of them solves all the problems exposed above at once, so inflation is generally considered as the best explanation today even if it remains an effective model valid up to high enough energy scale E, usually $E \simeq m_\mathrm{pl}$ being assumed.

2.5 Conclusion

In this chapter, we discussed some tests of GR. In Fig. 2.4, we propose to classify them depending on the strength of the gravitational field given by the

Newtonian potential $|\Phi|$, as well as the nature of the gravitational source.

In spherically symmetric spacetime, the compactness (2.2.1) provides a natural scale for the strength of the gravitational field. In cosmology, such a parameter cannot be defined. Nevertheless, Baker et al. [Baker15] proposed a definition of the Newtonian potential $|\Phi|$ for cosmology. For that reason, the tests of GR in Fig. 2.4 are classified as a function of this latter parameter.

In order to define the nature of the source, we define the parameter w_*,

$$w_* = -\frac{T^\mu_\mu}{\rho} = 3w - 1. \tag{2.5.1}$$

assuming a perfect fluid (2.2.2). The parameter w_* is equal to 0 for relativistic sources like NSs, -1 in the absence of sources (or sources with negligible pressure), for instance BHs and the Sun, and -4 for vacuum energy sources like DE. Only the diagonal terms of $T_{\mu\nu}$, i.e. the mass-energy density ρ and the isotropic pressure p, are taken into account in the definition of w_*. Relaxing the assumption of perfect fluid, there exist also phenomena invoking the off-diagonal terms, i.e. the momentum transfer and the shear stress. In particular, the classification of the tests proposed in Fig. 2.4 does not take into account gravitomagnetic effects, that is the contribution of moving and rotating material sources to the gravitational field, which are predicted in GR (see e.g.[Will08]). As an example, according to GR, the rotation of a massive body is dragging the local inertial frames of reference around it such that the orbits of moving objects around it are affected. This is the Lense-Thirring effect.

According to the classification of tests represented in Fig. 2.4, best bounds on GR have been obtained in the vacuum. In the presence of sources, GR cannot be directly tested. In the case of NSs, there exists still an uncertainty about the EoS in the core of the stars while the nature of DE and the inflaton is still debated.

In order to complete this chapter, we point out that some issues arising in the SM could also be related to cosmology. Why are the neutrinos massive? What is the origin of matter-anti matter asymmetry? and are the Higgs sector and the cosmological evolution connected? For instance, the existence of mass varying neutrinos could explain the late-time cosmic acceleration [Fardon04]. In Chap. 5, the possible relation between the Higgs field and gravitation will be further developed.

In Chap. 3, the possibility to modify GR is further explored from the theoretical and phenomenological point of views. In the rest of this thesis, we will focus on the phenomenological predictions of some modifications of gravity, keeping in mind the classification of GR tests represented in Fig. 2.4.

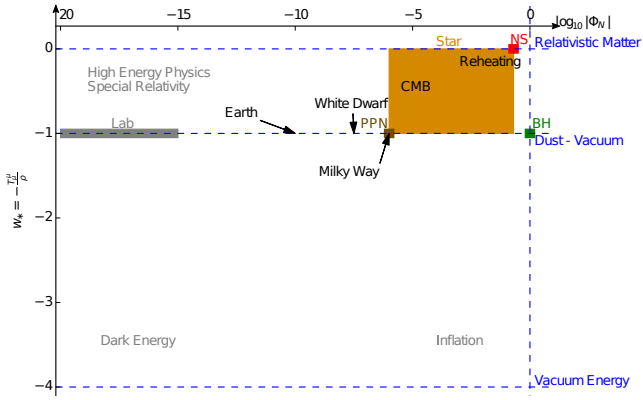

Figure 2.4: Classification of the tests of GR depending on the strength of the Newtonian potential as well as the nature of the sources given by $w_* = -T^\mu_\mu/\rho$. The best bounds on GR have been obtained in the vacuum, i.e. when the gravitational source has negligible pressure, while the modeling of the sources, for instance NSs and DE, is still under progress, the bounds being therefore less stringent.

Chapter 3

Looking beyond General Relativity: Modified Gravity

In Chap. 1, we introduce the underlying assumptions of GR which seem to indicate that GR has a privileged status. However, there are at least two motivations for studying theories of gravitation beyond GR. First, GR is a classical theory which does not include quantum effects since it is not renormalizable. Second, in cosmology, the current cosmic acceleration is of unknown nature and could be due to modifications of gravity (see Sec. 2.4.4 for a discussion). In addition, the initial conditions of the Universe appear to be fine-tuned in the Λ-CDM concordance model. Primordial inflation is able to solve this problem and inflationary models may rely on modifications of gravity.

3.1 Beyond the Lovelock Theorem: Modified Gravity

3.1.1 Classification of Modified Gravity models

The Lovelock theorem (see Sec. 1.4) restricts rather drastically, the possibilities of building theories of gravity beyond GR. At least one of the assumptions of the theorem has to be broken:

- ***The number of dimensions (higher than 4)***: This idea has been widely explored since the Kaluza-Klein theory, giving rise to string and braneworld theories, as well as the Dvali-Gabadadze-Porrati model (DGP). Higher than four dimensions theories are devoted to the unification of the fundamental interactions (for instance, Kaluza-Klein and string theory), quantum gravity (string theory and braneworld) as well as phenomenological considerations like the late-time cosmic acceleration (DGP). When compactified, such theories generally exhibit additional degrees of freedom. As an example, the Kaluza-Klein theory is

an attempt to unify gravitation and electromagnetism by generalizing GR to 5 dimensions [Kaluza21, Klein26b, Klein26a]. The metric in 5 dimensions $g^{(5)}_{AB}$ (with 15 independent components since it is symmetric) is decomposed in the 4-dimensional metric field $g_{\mu\nu}$, a vector field A_μ and a scalar φ (see e.g. [Peter09]),

$$g^{(5)}_{AB} = \begin{pmatrix} g_{\mu\nu} + \mathrm{e}^{2\varphi} A_\mu A_\nu & \mathrm{e}^{2\varphi} A_\mu \\ \mathrm{e}^{2\varphi} A_\nu & \mathrm{e}^{2\varphi} \end{pmatrix}. \tag{3.1.1}$$

When the fifth dimension is compactified, that is the cylinder condition $\partial_y = 0$ applies such that the fifth dimension is ignored, the corresponding action for the equations of motion in four dimensions, reads (see e.g. [Peter09] for the detailed calculations),

$$S = \frac{1}{2\kappa} \int \mathrm{d}^4x \sqrt{-g}\, \mathrm{e}^{2\varphi} \left(R - \frac{\mathrm{e}^{2\varphi}}{4} F_{\mu\nu} F^{\mu\nu} \right), \tag{3.1.2}$$

with $F_{\mu\nu} = \partial_\mu A_\nu - \partial_\nu A_\mu$ the Faraday tensor. As a result, when the Kaluza-Klein theory is compactified, it reduces to a theory of gravitation in four dimensions where the metric has a scalar and a vector counterparts. Another example is Lovelock gravity [Lovelock71] which is an extension of the Lovelock theorem introduced in Sec. 1.4 to higher dimensions where the Gauss-Bonnet term is not trivial anymore.

- ***Additional degree(s) of freedom (not only the spin-2 metric), whether it is scalar, vector or tensor field(s), dynamical or not***: Many theories have been proposed with additional degrees of freedom, either by adding scalar, vector or tensor components, or by making the connexion dynamical, i.e. the assumption on the Levi-Civita connection is relaxed. Those additional degrees of freedom are justified by the compactification of the higher-dimensional theories of gravity like Kaluza-Klein and superstring theory [Lidsey00]. Additional degrees of freedom also enable one to test phenomenological predictions, for instance, do GWs propagate at the speed of light?, and is the gravitational coupling G constant in spacetime? Depending on the way they are formulated, theories with additional degrees of freedom imply violations of the WEP and/or the SEP. Additional scalar fields (Horndeski gravity) lead to the LPI breaking (see Sec. 3.2.4.2), and possibly the UFF if the theory is formulated in such a way that the WEP is violated (see Sec. 3.2.4.3 for a discussion). Additional vector and tensor field(s) (TeVeS, Einstein-Æther, massive gravity,...) (usually) imply Lorentz-violation, breaking thus the LLI, in addition to the LPI. In some cases, general covariance may also be violated (see below).

- ***Equations of motion of higher than second order***: We have already mentioned in Sec. 1.3.4 that equations of motion of higher than second order lead to the Ostrogradsky instability, excepted if the system is degenerate. Some modified gravity theories avoid this instability, for instance

$f(R)$ theories [De Felice10, Sotiriou10],

$$S_{f(R)} = \int \mathrm{d}^4x\sqrt{-g}f(R) + S_{\mathrm{M}}\left[\psi_{\mathrm{M}};\ g_{\mu\nu}\right], \tag{3.1.3}$$

which are found to be equivalent to scalar-tensor theory (STT) (see Sec. 5.2.2 for an example).

- ***Give up general covariance***: As stated in Sec. 1.3.3, general covariance covers the diffeomorphism-invariance and the lack of prior geometry. Some modified gravity theories violate the diffeomorphism-invariance like massive gravity [deRham14], others require prior geometry, among them the Nordstrøm and Rosen's bimetric theories.

- ***Give up Lorentz invariance and/or causality***: Superluminal motion may be allowed either in Lorentz-violating theories at the action level, or by modifying the term responsible for the propagation velocity in the dispersion relation [Bruneton07]. In some cases, the causality is violated. However, such models may rely on higher than second-order equations of motion and therefore may suffer from instabilities. Hence, the Cauchy equation could be not well-posed. In this case, there is no guarantee that either equations of motion admit a solution or this solution is unique.

- ***Give up locality***: Some modified gravity models introducing terms like $f\left(R/\Box\right)$ [Woodard14] or $R(1/\Box^2)R$ at the action level [Maggiore14], are non-local. Indeed, the operator $1/\Box$ is the inversed d'Alembertian operator which is computed by the retarded Green's function (advanced Green's function are avoided in order to preserve causality). It results that non-local effects arise (see also Sec. 1.3.2). Non-local models could explain the late-time cosmic acceleration [Woodard14] and have been studied as effective theories for quantum gravity [Hamber05].

According to the conjecture that we formulated at the end of Chap. 1, the SEP is violated in most of the cases introduced above. Higher dimension theories usually give rise to additional degrees of freedom when they are compactified, such that they violate the SEP. Non-local theories of gravity should avoid our conjecture. Depending on the way the modified gravity theories are formulated, violations of the WEP may arise (see Sec. 3.2.4.3 for the case of STT).

In Fig. 3.1, the directions for going beyond the Lovelock theorem are summarized. Some examples of the models corresponding to the violated assumptions of the Lovelock theorem are indicated. A non-exhaustive list of modified gravity models and their characteristics is reported on Tab. 3.1[(1)]. Although all those models excepted Lovelock gravity predict a violation of the SEP, the WEP can be also violated depending the way the theory is formulated.

The motivations for all these modified gravity models are different. The nature of late-time cosmic acceleration can be explained by DGP, Horndeski

[(1)]This classification is inspired from T. Baker [Baker16], E. Berti *et. al* [Berti15] and the gravity apple tree proposed by M. E. Aldama [Aldama15].

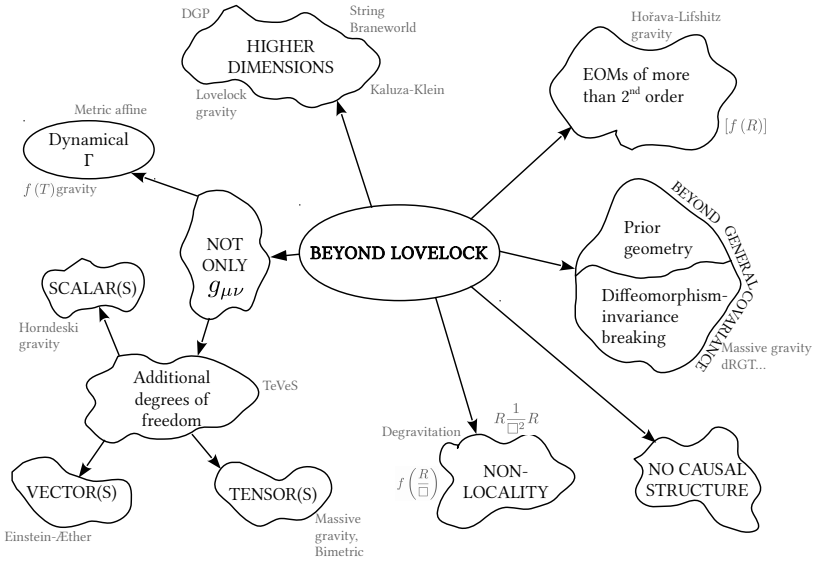

Figure 3.1: Axis of research of modified gravity, depending on the assumptions of the Lovelock theorem which are relaxed (inspired from T. Baker 2013, E. Berti *et al.* [Berti15] and the gravity apple tree proposed by M. E. Aldama [Aldama15]).

gravity and non-local theories for instance. MOND and TeVeS are phenomenological models explaining the matter galactic curves. Inflationary models are often built thanks to scalar field(s) with a large variety of potentials, using Horndeski models for example. We already point out here the large phenomenology of Horndeski gravity which encompasses the generalized STT, $f(R)$, the covariant Galileons, the Fab Four, K-mouflage, in order to cite only some of them. Finally, higher dimension models like string theory, braneworld scenarios, Lovelock gravity, etc. are attempts to unify the four interactions and to renormalize gravity. Quantum gravity has also been investigated in order to solve the problem of BHs and the Big Bang singularities (see Hořava-Lifshitz for instance).

Before confronting the models with the observations, they have to be viable from the theoretical point of view, i.e. they must not suffer from instabilities like ghosts, as further developed in the next section.

MG Theories	Equivalence principles			Add. dofs	General covariance		Causality	Locality	Higher dim.	2nd order EOMs
	UFF	LLI	LPI		No prior geom.	Diffeo.-invar.				
GR	✓	✓	✓	✗	✓	✓	✓	✓	✗	✓
Horndeski gravity										
Brans-Dicke	✓	✓	✗	S	✓	✓	✓	✓	✗	✓
Scalar tensor	✓/✗	✓	✗	S	✓	✓	✓	✓	✗	✓
Fab Four	✓	✓	✗	S	✓	✓	✓	✓	✗	✓
$f(R)$	✓	✓	✗	S	✓	✓	✓	✓	✗	✓
Einstein-Æther	✓	✗	✗	S/V	✓		✗?	✓	✗	✗
Hořava-Lifshitz	✗?	✗	✗	V	✓	✗	✗	✓	✓	✓
Massive gravity	✓	✗	✗	S/V/T	✓	✗?				
Bigravity				T	✗?	✓		✓	✗	
TeVeS	✓	✗	✗	S/V/T				✓		
$f(R/\Box)$							✓	✗		
Kaluza-Klein							✓	✓	✓	✓
DGP							✓	✓	✓	✓
Lovelock gravity	✓	✓	✓	✗	✓	✓	✓	✓	✓	✓
$f(T)$	✓	✗	✗							
Metric affine	?	?	?	Γ	✓	✓	✓	✓	✗	✗

Table 3.1: Comparison of a non-exhaustive list of modified gravity (MG) models depending on which assumption of the Lovelock theorem is violated as well as on the consequences in terms of equivalence principles (see also Chap. 1). Abbreviations: dof=degree of freedom, geom.=geometry, Diffeo. invar.= Diffeomorphism-invariance, S=scalar, V=vector, T=tensor, PS=pseudo-scalar.

3.1.2 Some issues and challenges of Modified Gravity models

While building modified gravity models, the first question raised is whether the theory is well-posed or whether it suffers from some instabilities, like the Ostrogradsky one. As an example, let us consider an alternative to GR with an additional scalar field, $\mathcal{L} = \mathcal{L}(\phi, \partial_\mu \phi)$. The stability of the solution $\phi(x,\ t)$ is established by computing perturbations $\delta\phi(x,\ t)$ around the background solution $\phi_{\rm b}(t)$,

$$\delta\phi(x,\ t) = \phi(x,\ t) - \phi_{\rm b}(t), \tag{3.1.4}$$

up to second order. If the perturbation modes are decaying, then the theory is stable.

A common instability appearing in modified gravity is the **ghost**, especially in theories which attempt to reproduce the late-time cosmic acceleration. In this case, the kinetic term has the "wrong" sign, that is the opposite of the canonical one. From the classical point of view, it means that its kinetic energy is increasing (instead of decreasing) when it climbs up its potential. It is generally accepted that one cannot make sense of such a theory, at least at the quantum level [Durrer08b][(2)]. From the quantum field theory point of view, ghosts can carry out negative energy eigenvalues (if unitarity is imposed [Clifton12]). If the ghost is coupled to conventional matter field, it generates instabilities because of the possible creation of ghost-non-ghost pairs in the vacuum (see also Sec. 1.3.4). Several ways to "exorcise" the ghost have been explored (see e.g. [Clifton12]). Other instabilities exist like tachyons, where the perturbations of the degrees of freedom have negative effective mass $m^2(\phi) < 0$, and the **Laplacian instability** where the perturbations propagate with a negative squared speed [Beltrán Jiménez15]. In all cases, the quantization of the theory is not well-defined and the energy functional is not bounded from below [Durrer08b].

Another pathology of some modified gravity models is the so-called **strong coupling**. When the coupling constants of gravitational fields to matter ones are too strong, there exists a scale Λ where the perturbative quantum field theory approach breaks down for the Minkowski background. It results that the theory can be non renormalizable and, if Λ is too low, the theory is ill-defined at large scale. For instance, this is problematic for DGP where $\Lambda \sim 1000$ km [Clifton12].

3.1.3 Screening mechanisms

In the case where modified gravity is devoted to the explanation of the observations in cosmology like the late-time cosmic acceleration (see Sec. 2.4.4), they have to pass the stringent constraints of the weak-field regime, that is the

[(2)] If gravitation is considered as a low energy effective theory, then it is not necessary to care about its quantization. However, in quantum gravity, the quantization of the theory must be well-defined.

PPN parameters in the Solar system (see Sec. 2.2) and the tests of the equivalence principles (see Sec. 2.1), in order to be viable.

Therefore a common feature of viable modified gravity models is the so-called screening mechanism, that is a mechanism suppressing the modified gravity effects in local environments. Let us consider the sketchy general action for modified gravity models with an extra scalar field[3],

$$\mathcal{L} \supset p(\phi,\ X) - \frac{m^2\ (\phi)}{2}\phi^2 - gW(\phi)T, \tag{3.1.5}$$

where $X = (1/2)\left(\partial\phi\right)^2$, $p(\phi,\ X)$ is a nonminimal coupling function of the kinetic term, $m(\phi)$, the effective mass of the scalar field, g the coupling between the scalar field and matter, $W(\phi)$ a free function of ϕ, and T, the trace of $T_{\mu\nu}$. Three screening mechanisms exist, coming from different terms at the action level:

- *Non-linearities in the kinetic term* $p(\phi,\ X)$: First invoked by Vainshtein in the framework of massive gravity [Vainshtein72], the so-called **Vainshtein mechanism** arises from the non-linearities of the extra degrees of freedom in the kinetic term (coming from higher derivative for instance). Because of the strong kinetic self-coupling, extra degrees of freedom may be hidden and may almost not propagate (see [Babichev13] and references therein). Inside the so-called Vainshtein radius, GR is restored because of the non-linearities, while the linear solution is recovered at large scales, reproducing DE phenomenology. Several modified gravity models exhibit such mechanism, either in the framework of massive gravity (DGP, bigravity, etc) or of STT (Galileons and k-essence), the latter case being referred to as the **k-mouflage** [Babichev09].

- *Large effective mass* $m(\phi)$: In the case of the **chameleon** model [Khoury04b, Khoury04a], the effective potential $V_{\rm eff}$ is defined by,

$$\Box\phi \equiv \frac{\mathrm{d}V_{\rm eff}}{\mathrm{d}\phi}, \tag{3.1.6}$$

  and the corresponding effective mass $m(\phi) = \mathrm{d}^2V_{\rm eff}/\mathrm{d}\phi^2$, depends on the density of the environment. In sparse environment, the scalar field has a low mass and is thus able to mediate long-range force, while it acquires a mass in dense environment. We will detail this mechanism in Chap. 4.

- *Small coupling* g: In the symmetron model [Hinterbichler10, Hinterbichler11], the screening mechanism relies on the symmetry breaking of the effective potential. The coupling g is related to the vacuum expectation value (vev) of the scalar field which varies with the

[3] This action is written in the Einstein frame where there is no explicit coupling to the Ricci scalar (see Sec. 3.2.2 for a formal definition).

environment. In sparse environment, the vev is vanishing and the scalar field acts as a cosmological constant, while the symmetry is restored when the environment is dense, resulting in a non-negligible coupling between the scalar field and matter.

In general, screening mechanisms are studied in the (quasi-)static limit in a spherically symmetric spacetime with a massive object, the Sun for instance, at the center, assuming a Minkowski background.

3.2 Scalar-tensor theories

In the rest of this thesis we will focus on theories where an additional scalar field is the counterpart of the Einstein metric for describing gravity. Among them, STT were first proposed by Jordan in 1955 [Jordan55], and rediscovered independently by Brans and Dicke in 1961 [Brans61]. Since then, they have been studied extensively. On the one hand, STT are one of the most simple extensions of GR in the sense that it invokes only one additional degree of freedom, possibly justified by theories of gravity in higher-dimensions (see the discussion of Sec. 3.1). On the other hand, they have a rich phenomenology, in particular around compact objects and in cosmology. In the next section, the mathematical formulations of STT, in the so-called Jordan and Einstein frames, are introduced.

3.2.1 The Jordan frame

In the so-called Jordan frame, the nonminimal coupling between the scalar field and the Ricci scalar is explicit. In the absence of matter, the action reads,

$$S_{\rm JF} = \int \mathrm{d}^4x \sqrt{-g} \left[\frac{F(\phi)}{2\kappa} R - Z(\phi) \left(\partial\phi\right)^2 - V\left(\phi\right) \right], \tag{3.2.1}$$

where $F\left(\phi\right)$ and $Z(\phi)$ are the nonminimal coupling functions[(4)], R the scalar curvature, $V\left(\phi\right)$, a generic potential. The modified Einstein equations are then given by the variation of the action with respect to $g_{\mu\nu}$ (see Eqs. (1.2.5) and (1.2.6)), assuming vanishing boundary terms[(5)],

$$\begin{aligned} &\left(G_{\mu\nu} + g_{\mu\nu}\Box - \nabla_\mu\nabla_\nu\right) F\left(\phi\right) = \\ &\qquad \kappa \left\{ Z(\phi) \left[2\,\partial_\mu\phi\,\partial_\nu\phi - g_{\mu\nu} \left(\partial\phi\right)^2 \right] - g_{\mu\nu} V\left(\phi\right) \right\}, \end{aligned} \tag{3.2.2}$$

[(4)] The function $Z(\phi)$ can be reabsorbed in a scalar field redefinition such that $Z(\phi)$=1. However, we keep 3 independent functions $F(\phi)$, $Z(\phi)$ and $V(\phi)$ here in order to reuse the definition of the equations of motion in the rest of the thesis.

[(5)] In the presence of nontrivial topology in space, such contributions may be physically relevant for some symmetries, e.g. the supersymmetry, leading to quantization rules on some parameters at the quantum level [Govaerts08].

while the Klein-Gordon equation derives from the variation of the scalar field,

$$2\,Z(\phi)\Box\phi + \frac{\partial F}{\partial \phi}\frac{R}{2\kappa} = -\frac{\partial Z}{\partial \phi}\left(\partial\phi\right)^2 + \frac{\partial V}{\partial \phi}. \tag{3.2.3}$$

Including the contribution of matter $S_M\left[\psi_{\rm M}; g_{\mu\nu}\right]$,

$$S_{\rm JF} = \int {\rm d}^4x\,\sqrt{-g}\,\left[\frac{F(\phi)}{2\kappa}R - Z(\phi)\left(\partial\phi\right)^2 - V\left(\phi\right)\right] + S_{\rm M}\left[\psi_{\rm M}; g_{\mu\nu}\right], \tag{3.2.4}$$

the modified Einstein equations read,

$$\begin{aligned}&\left(G_{\mu\nu} + g_{\mu\nu}\Box - \nabla_\mu\nabla_\nu\right)F\left(\phi\right) = \\ &\qquad \kappa\left\{T^{\rm (M)}_{\mu\nu} + Z(\phi)\left[2\,\partial_\mu\phi\,\partial_\nu\phi - g_{\mu\nu}\left(\partial\phi\right)^2\right] - g_{\mu\nu}V\left(\phi\right)\right\},\end{aligned} \tag{3.2.5}$$

with the stress-energy tensor defined by,

$$T^{\rm (M)}_{\mu\nu} = -\frac{2}{\sqrt{-g}}\frac{\delta S_{\rm M}}{\delta g_{\mu\nu}}. \tag{3.2.6}$$

The Klein-Gordon equation remains unchanged.

In the Jordan frame, the stress-energy tensor is conserved. Indeed, by computing ∇^μ[Eq. (3.2.5)] where $Z(\phi) = 1^{(4)}$ and using the second Bianchi identity, the left-hand side reads,

$$\begin{aligned} G_{\mu\nu}\frac{{\rm d}F}{{\rm d}\phi}\nabla^\mu\phi + \nabla_\nu\Box F - \Box\nabla_\nu F &= G_{\mu\nu}\frac{{\rm d}F}{{\rm d}\phi}\nabla^\mu\phi + \left[\nabla_\nu,\,\nabla_\alpha\right]\nabla^\alpha F, && (3.2.7)\\ &= \left(R_{\mu\nu} - \frac{1}{2}Rg_{\mu\nu}\right)\frac{{\rm d}F}{{\rm d}\phi}\nabla^\mu\phi \\ &\qquad -R_{\alpha\nu}\nabla^\alpha\phi\frac{{\rm d}F}{{\rm d}\phi}, && (3.2.8)\\ &= -\frac{R}{2}\frac{{\rm d}F}{{\rm d}\phi}\nabla_\nu\phi. && (3.2.9)\end{aligned}$$

Between the first and the second equality, we used the relation for the commutator $[\cdot,\,\cdot]$ of two covariant derivatives (see e.g.[Carroll04]),

$$\left[\nabla_\mu,\,\nabla_\nu\right]V^\rho = R^\rho_{\sigma\mu\nu}V^\sigma, \tag{3.2.10}$$

with V^ρ a vector field ($[\nabla_\mu,\,\nabla_\nu]\phi = 0$), assuming a vanishing torsion. The right-hand side reads,

$$\begin{aligned}&\kappa\left[\nabla^\mu T^{\rm (M)}_{\mu\nu} + 2\Box\phi\nabla_\nu\phi + 2\nabla^\mu\phi\nabla_\mu\nabla_\nu\phi - 2\nabla^\alpha\phi\nabla_\nu\nabla_\alpha\phi - \frac{{\rm d}V}{{\rm d}\phi}\nabla_\nu\phi\right] \\ &\qquad = \kappa\left[\nabla^\mu T^{\rm (M)}_{\mu\nu} + \left(2\Box\phi - \frac{{\rm d}V}{{\rm d}\phi}\right)\nabla_\nu\phi\right], && (3.2.11)\\ &\qquad = \kappa\left[\nabla^\mu T^{\rm (M)}_{\mu\nu} - \frac{{\rm d}F}{{\rm d}\phi}\frac{R}{2\kappa}\nabla_\nu\phi\right], && (3.2.12)\end{aligned}$$

using the Klein-Gordon equation (3.2.3). Comparing Eqs. (3.2.9) and (3.2.12) we conclude,

$$\nabla^\mu T^{\rm (M)}_{\mu\nu} = 0. \tag{3.2.13}$$

3.2.2 The Einstein frame

Starting from the action in the Jordan frame (3.2.4) where the function $Z(\phi)$ has been absorbed into the kinetic term,

$$S = \frac{1}{2\kappa}\int \mathrm{d}^4x\,\sqrt{-g}\,\left[F(\phi)R - g^{\mu\nu}\partial_\mu\phi\partial_\nu\phi - V(\phi)\right] + S_{\mathrm{M}}\left[\psi_{\mathrm{M}}; g_{\mu\nu}\right], \quad (3.2.14)$$

it is possible to rewrite it in such a way that it looks like GR by performing a conformal transformation,

$$g_{\mu\nu} \longrightarrow \tilde{g}_{\mu\nu} = \Omega^2(\phi)\, g_{\mu\nu} \qquad \Rightarrow \qquad \left\{ \begin{array}{l} \sqrt{-\tilde{g}} = \Omega^4\sqrt{-g} \\ \tilde{g}^{\mu\nu} = \Omega^{-2} g^{\mu\nu}, \end{array} \right. \quad (3.2.15)$$

with the conformal factor,

$$\Omega^2(\phi) = F(\phi). \quad (3.2.16)$$

The conformal transformation of the Ricci scalar reads (see e.g. [Carroll04]),

$$R = \Omega^2\tilde{R} + 6\,\tilde{g}^{\alpha\beta}\Omega\left(\tilde{\nabla}_\alpha\tilde{\nabla}_\beta\Omega\right) - 12\,\tilde{g}^{\alpha\beta}\left(\tilde{\nabla}_\alpha\Omega\right)\left(\tilde{\nabla}_\beta\Omega\right). \quad (3.2.17)$$

The action (3.2.14) transforms then as,

$$\begin{aligned} S_{\mathrm{EF}} = \frac{1}{2\kappa}\int \mathrm{d}^4\tilde{x}\,\sqrt{-\tilde{g}}\,\Big[\tilde{R} &+ 6F^{-1/2}\tilde{g}^{\alpha\beta}\left(\tilde{\nabla}_\alpha\tilde{\nabla}_\beta F^{1/2}\right) \\ &-12F^{-1}\tilde{g}^{\alpha\beta}\tilde{\nabla}_\alpha F^{1/2}\tilde{\nabla}_\beta F^{1/2} - F^{-1}\tilde{g}^{\alpha\beta}\partial_\alpha\phi\partial_\beta\phi - U\Big] \\ &+S_{\mathrm{M}}\left[\psi_{\mathrm{M}}; g_{\mu\nu} = A^2\tilde{g}_{\mu\nu}\right], \end{aligned} \quad (3.2.18)$$

with

$$U \equiv F^{-2}V(\phi) \qquad \text{and} \qquad A \equiv \Omega^{-1}(\phi). \quad (3.2.19)$$

By computing,

$$\tilde{\nabla}_\alpha F^{1/2} = \frac{1}{2F^{1/2}}\frac{\mathrm{d}F}{\mathrm{d}\phi}\tilde{\nabla}_\alpha\phi, \quad (3.2.20)$$

$$\tilde{\nabla}_\alpha\tilde{\nabla}_\beta F^{1/2} = \frac{1}{2F^{1/2}}\left[\tilde{\nabla}_\alpha\tilde{\nabla}_\beta\phi\frac{\mathrm{d}F}{\mathrm{d}\phi} + \frac{\mathrm{d}^2F}{\mathrm{d}\phi^2}\partial_\alpha\phi\partial_\beta\phi - \frac{1}{2F}\left(\frac{\mathrm{d}F}{\mathrm{d}\phi}\right)^2\partial_\alpha\phi\partial_\beta\phi\right], \quad (3.2.21)$$

and by integrating by parts,

$$\frac{3}{F}\frac{\mathrm{d}F}{\mathrm{d}\phi}\tilde{\Box}\phi = \frac{3}{F}\left[\frac{1}{F}\left(\frac{\mathrm{d}F}{\mathrm{d}\phi}\right)^2 - \frac{\mathrm{d}^2F}{\mathrm{d}\phi^2}\right]\left(\tilde{\partial}\phi\right)^2, \quad (3.2.22)$$

the action (3.2.18) is finally formulated in the Einstein frame,

$$\begin{aligned} S_{\mathrm{EF}} = \frac{1}{2\kappa}\int \mathrm{d}^4\tilde{x}\,\sqrt{-\tilde{g}}\,\left[\tilde{R} - 2\left(\tilde{\partial}\sigma\right)^2 - U(\sigma)\right] \\ +S_{\mathrm{M}}\left[\psi_{\mathrm{M}}; g_{\mu\nu} = A^2(\sigma)\,\tilde{g}_{\mu\nu}\right], \end{aligned} \quad (3.2.23)$$

where the tildes denote Einstein frame quantities and σ is defined by,

$$\left(\frac{\tilde{\partial}\sigma}{\tilde{\partial}\phi}\right)^2 = \frac{3}{4}\left(\frac{\partial \ln F}{\partial \phi}\right)^2 + \frac{1}{2F}. \tag{3.2.24}$$

In the Einstein frame, the action (3.2.23) looks like the EH one with a minimally coupled scalar field σ, the coupling of the scalar field to matter $A(\sigma)$ appearing in $S_{\rm M}$. The modified Einstein equations then read (see Eq. (3.2.2)),

$$\tilde{G}_{\mu\nu} = \kappa \tilde{T}^{(\rm M)}_{\mu\nu} + 2\,\tilde{\partial}_\mu\sigma\,\tilde{\partial}_\nu\sigma - \tilde{g}_{\mu\nu}\left[\left(\tilde{\partial}\sigma\right)^2 + \frac{U\,(\sigma)}{2}\right], \tag{3.2.25}$$

the stress-energy tensor in the Einstein frame being defined as,

$$\tilde{T}^{(\rm M)}_{\mu\nu} = -\frac{2}{\sqrt{-\tilde{g}}}\frac{\delta S_{\rm M}}{\delta \tilde{g}_{\mu\nu}}. \tag{3.2.26}$$

The Klein-Gordon equation yields,

$$\tilde{\Box}\sigma = \frac{1}{4}\frac{\partial U}{\partial \sigma} - \frac{\kappa}{2}\alpha(\sigma)\,\tilde{T}^{(\rm M)}, \tag{3.2.27}$$

with α, the nonminimal coupling function,

$$\alpha(\sigma) = \frac{\mathrm{d}\ln A}{\mathrm{d}\sigma}, \tag{3.2.28}$$

and $\tilde{T}^{(\rm M)}$, the trace of $\tilde{T}^{(\rm M)}_{\mu\nu}$.

Because of the nonminimal coupling in $S_{\rm M}$, the stress-energy tensor in the Einstein frame $\tilde{T}^{(\rm M)}_{\mu\nu} \equiv A^4 T^{(\rm M)}_{\mu\nu}$ is not conserved. Indeed, we can show it explicitly by applying the Bianchi identity to Eq. (3.2.25),

$$\begin{aligned}
\tilde{\nabla}^\mu \tilde{T}^{(\rm M)}_{\mu\nu} &= \frac{1}{\kappa}\Bigg[-2\left(\tilde{\Box}\sigma\tilde{\partial}_\nu\sigma + \tilde{\partial}_\beta\sigma\tilde{\nabla}^\beta\tilde{\nabla}_\nu\sigma\right) \\
&\qquad + g_{\mu\nu}\left(2\tilde{\partial}_\beta\sigma\tilde{\nabla}^\mu\tilde{\nabla}^\beta\sigma + \frac{1}{2}\frac{\partial U}{\partial\sigma}\tilde{\partial}^\mu\sigma\right)\Bigg], &(3.2.29)\\
&= \frac{1}{\kappa}\Bigg\{-2\left[\tilde{\partial}_\nu\sigma\left(\frac{1}{4}\frac{\partial U}{\partial\sigma} - \frac{\kappa}{2}\alpha(\sigma)\,\tilde{T}^{(\rm M)}\right) + \tilde{\partial}_\beta\sigma\tilde{\nabla}^\beta\tilde{\nabla}_\nu\sigma\right] \\
&\qquad + 2\tilde{\partial}_\beta\sigma\tilde{\nabla}_\nu\tilde{\nabla}^\beta\sigma + \frac{1}{2}\frac{\partial U}{\partial\sigma}\tilde{\partial}_\nu\sigma\Bigg\}, &(3.2.30)\\
&= \alpha\tilde{T}^{(\rm M)}\tilde{\partial}_\nu\sigma, &(3.2.31)
\end{aligned}$$

using the Klein-Gordon equation (3.2.27) for the second equality and $[\nabla_\mu,\,\nabla_\nu]\sigma = 0$ for the third one.

3.2.3 Discussion about the frames

In this section, we briefly discuss the equivalence between the two formulations of STT. As we will see, the phenomenology predicted by STT does not depend on the frame. This is a mere change of variables [Esposito-Farèse06].

In the Jordan frame, the effective gravitational coupling defined as,

$$G_{\rm eff}\left(x^{\mu}\right) = \frac{G}{F\left(\phi\right)}, \tag{3.2.32}$$

with $G = m_{\rm pl}^{-2}$ the bare gravitational coupling that is the parameter appearing in the action, is varying in spacetime. On the other hand, matter is minimally coupled to gravity such that the definition of the lengths and times measured by rods and clocks, which are made of matter, does not depend on the scalar field [Esposito-Farèse06].

In the Einstein frame, the kinetic terms for the metric and the scalar fields are separated whereas the matter is directly coupled to the scalar field via the coupling function $A(\phi)$. As a result, the units system has to be re-calibrated since the rods and clocks are made of matter [Larena07]. On the other hand the effective coupling is not varying $\tilde{G}_{\rm eff} = G$.

In physics, observables are defined by dimensionless quantities. Indeed, such quantities do not depend on the spacetime coordinates $\{x^{\mu}\}$ nor on a unit system. Observables are frame-invariant since diffeomorphism-invariance is preserved in STT. As an example, let us consider the inertial mass $m_{\rm i}$ and define the corresponding observable,

$$\frac{m_{\rm i}}{m_{\rm pl}} = m_{\rm i}\sqrt{G_{\rm eff}}. \tag{3.2.33}$$

In order to compute $m_{\rm i}$, we consider the action for a point-particle starting with the Jordan frame,

$$\begin{aligned}
S_{\rm pp} &= -\int m_{\rm i}{\rm d}s, && (3.2.34)\\
&= -\int m_{\rm i}\sqrt{-g_{\mu\nu}{\rm d}x^{\mu}{\rm d}x^{\nu}}, && (3.2.35)\\
&= -\int m_{\rm i}A(\phi)\sqrt{-\tilde{g}_{\mu\nu}{\rm d}x^{\mu}{\rm d}x^{\nu}}, && (3.2.36)\\
&= -\int \underbrace{m_{\rm i}A(\phi)}_{\equiv\tilde{m}_{\rm i}(\phi)}{\rm d}\tilde{s} && (3.2.37)
\end{aligned}$$

where we used Eq. (3.2.15) with $A(\phi) = \Omega^{-1}(\phi)$, the tilde denoting quantities expressed in the Einstein frame. As a result, the inertial mass measured in the Einstein frame $\tilde{m}_{\rm i}(\phi)$ is found to vary in spacetime, even for laboratory-size, non self-gravitating objects [Esposito-Farèse06]. Therefore, the ratio of inertial mass in the Jordan and the Einstein frames is varying,

$$\frac{m_{\rm i}(\phi)}{\tilde{m}_{\rm i}(\phi)} = A^{-1}(\phi), \tag{3.2.38}$$

whereas the ratio of two inertial masses labeled by the subscript 1 and 2 does not depend on the frame,

$$\frac{\tilde{m}_{\mathrm{i},1}(\phi)}{\tilde{m}_{\mathrm{i},2}(\phi)} = \frac{A(\phi)m_{\mathrm{i},1}}{A(\phi)m_{\mathrm{i},2}} = \frac{m_{\mathrm{i},1}}{m_{\mathrm{i},2}}, \tag{3.2.39}$$

provided that the matter fields are universally coupled to the scalar field, i.e. $A(\phi)$ does not depend on the matter species. This question is further discussed in Sec. 3.2.4.3.

Moreover, using Eqs. (3.2.32) and (3.2.37), the measure of the observable $m_{\mathrm{i}}\sqrt{G_{\mathrm{eff}}}$ (3.2.33) does not depend on the frame,

$$\frac{m_{\mathrm{i}}\sqrt{G_{\mathrm{eff}}}}{\tilde{m}_{\mathrm{i}}\sqrt{\tilde{G}_{\mathrm{eff}}}} = \frac{m_{\mathrm{i}}\sqrt{\frac{G}{F(\phi)}}}{m_{\mathrm{i}}A(\phi)\sqrt{G}} = \frac{m_{\mathrm{i}}A(\phi)\sqrt{G}}{m_{\mathrm{i}}A(\phi)\sqrt{G}} = 1, \tag{3.2.40}$$

since $F(\phi) = \Omega^2(\phi) = A^{-2}(\phi)$ (see Eqs. (3.2.16) and (3.2.19)). In conclusion, there is an equivalence between the variation of the inertial mass in the Einstein frame and the variation of G_{eff} in the Jordan frame.

The calculations of other observables have been widely discussed in the literature (see e.g. [Flanagan04] and references therein), for instance in cosmology [Hees12a, Chiba13]. It shows that observables, i.e. dimensionless quantities, like the redshift, are frame-invariant while dimensional ones like the Hubble parameter are not [Chiba13].

In conclusion, the computation of observables gives the same result in both frames. In the Jordan frame, they are obtained as in GR but solving the equations of motion is trickier since the limit to GR is not obvious (in fact it is even singular, see Sec. 3.2.4.1 for the example of the Brans-Dicke theory). In the Einstein frame, computation of observables requires to take into account the rescaling of the metric and of the units system, because of the direct coupling of the scalar field to matter $A(\phi)$. However, in the Einstein frame, the equations of motion are written as in GR.

3.2.4 The equivalence principles

In the STT model formulated by Brans and Dicke in 1961, the scalar field involved in addition to the metric, is related to the Newton's constant G_{N}. Brans and Dicke were motivated by the Mach's principle as stated in Sec. 1.1[(6)]. Indeed, according to the Mach principle, the inertial mass of an object is related to its acceleration with respect to the local distribution of matter in the Universe. The dimensionless mass ratio $m_{\mathrm{i}}\sqrt{G_{\mathrm{eff}}}$ (see Sec. 3.2.3) should then depend upon the matter distribution in the Universe, considering a variation in spacetime of the inertial mass m_{i} or of the effective gravitational coupling G_{eff}.

[(6)] Brans and Dicke were also inspired from the Dirac's Large Number Hypothesis, $1/G_{\mathrm{N}} \propto M/R$ with M the mass of the Universe and R the Hubble radius. If M/R varies with time then G_{N} does [Brans08].

This is the reason why Brans and Dicke questioned the constancy of the gravitational "constant" (or equivalently of the inertial masses) and assumed that it could be a function of the matter distribution of the Universe. In order to formulate this statement mathematically, the gravitational constant has to be promoted as a scalar field, such that the SEP is violated. In more sophisticated STT, the WEP can be also violated.

3.2.4.1 The Brans-Dicke theory

Brans and Dicke initially considered the action [Brans61],

$$S = \frac{1}{2\kappa}\int \mathrm{d}^4x\,\sqrt{-g}\,\left[\Phi R - \frac{\omega}{\Phi}\left(\partial\Phi\right)^2\right] + S_{\mathrm{M}}\left[\Psi_{\mathrm{M}}; g_{\mu\nu}\right], \tag{3.2.41}$$

where Φ is the dimensionless scalar field and ω, a constant parameter.

The equations of motion for the Brans-Dicke theory, that is the modified Einstein equations, the Klein-Gordon equation and the conservation of $T^{(\mathrm{M})}_{\mu\nu}$ are given by (see Sec. 3.2.1 with $F(\Phi) = \Phi$, $Z(\Phi) = 2\kappa\omega/\Phi$ and $V(\Phi) = 0$ for the calculations),

$$\begin{aligned}
\Phi G_{\mu\nu} &= \kappa T^{(\mathrm{M})}_{\mu\nu} + \nabla_\mu\nabla_\nu\Phi - g_{\mu\nu}\Box\Phi \\
&\quad + \frac{\omega}{\Phi}\left[\nabla_\mu\Phi\nabla_\nu\Phi - \frac{1}{2}g_{\mu\nu}(\partial\Phi)^2\right], && (3.2.42)\\
\Box\Phi &= \frac{\kappa}{(2\omega+3)}T^{(\mathrm{M})}, && (3.2.43)\\
\nabla^\mu T^{(\mathrm{M})}_{\mu\nu} &= 0. && (3.2.44)
\end{aligned}$$

GR is recovered by imposing $\omega \longrightarrow \infty$, which means that STT is indistinguishable from GR if ω becomes unnaturally large. Indeed, in the limit where $\omega \longrightarrow \infty$, the Klein-Gordon equation reads $\Box\Phi = 0$, i.e. the scalar field is no more coupled to matter and GR is recovered (see also Eq. (B.0.16) for a second proof that GR is recovered when $\omega \longrightarrow \infty$).

3.2.4.2 The Local Position Invariance II: Varying fundamental constants

The LPI ensures that the measure of the observables does not depend on the spacetime position in GR. However, if the fundamental constants, either in GR or in SM, vary in spacetime, then measure of the observables would also vary in space and in time.

The fundamental constants of a physical theory are defined as any parameter that cannot be explained by this theory [Uzan11]. On the contrary, the other constants can be expressed in terms of the fundamental ones. In Sec. 2.1.2, we have already mentioned that the constancy of the speed of light has been questioned within the framework of Lorentz violation. Actually the constancy of the fundamental constants is tightly linked to the violation of the equivalence principles: in the particular case of G_{N} only the SEP is violated since it is related to the gravitational interaction only while for other constants like c, both

SEP and WEP are in general violated [Uzan11]. It has been widely explored along the last decades (see [Uzan11] for a review) for several fundamental constants, in particular $G_{\rm N}$, c and the fine-structure constant for electromagnetism $\alpha_{\rm EM}$.

A fundamental constant has by definition no dynamical equation which predicts its evolution. In order to implement the variation of fundamental "constants" mathematically in a consistent way, fundamental "constants" have to be promoted as dynamical scalar fields at the level of the action such that equations of motion for the scalar field, can be derived from a variational principle. At the end of the day, some constants will depend on the value of the scalar fields and a set of new fundamental constants must be defined.

In the case of Brans-Dicke theory (3.2.41), the effective gravitational "constant" $G_{\rm eff}$[(7)] is,

$$G_{\rm eff}\left(x^\mu\right) = \frac{G}{\Phi\left(x^\mu\right)}, \tag{3.2.45}$$

and its distribution in spacetime is determined by the Klein-Gordon equation (3.2.43). Both time and spatial variations of $G_{\rm eff}$ are then predicted, depending on the spacetime symmetry (for instance only variations in space are predicted in a static spacetime). $G_{\rm eff}$ has been measured at different redshifts, constraining its variation in time and, for some cases like for the CMB last scattering surface, also in space. Among the phenomenons probing the variation of the gravitational effective coupling $G_{\rm eff}$, we point out the Solar system tests, the stellar physics and cosmology, particularly at the BBN and the CMB last scattering surface (see [Uzan11] and references therein for experimental bounds).

However, we have to keep in mind that $G_{\rm eff}$ does not correspond to the gravitational constant as measured by torsion balance or Cavendish experiments which requires further computations (see e.g. [Uzan11]). Indeed, the effective Newton's constant is computed by expanding the conformal factor $A(\phi) = F^{-1/2}(\phi)$ in the weak-field approximation. In App. B, the Newton's constant as measured by Cavendish experiment $G_{\rm Cav}$ for the Brans-Dicke theory is obtained (B.0.16) and reads,

$$G_{\rm Cav} = \frac{2G}{\Phi_0}\frac{\omega+2}{2\omega+3}, \tag{3.2.46}$$

with Φ_0 the asymptotic value of Φ, far away from the gravitational source.

3.2.4.3 The equivalence principles revisited

In the 1960s, Dicke noticed that only the WEP had been tested through experiments of the UFF involving weakly self-gravitating bodies. The case of strongly gravitating bodies like stars where the gravitational binding energy contributes largely to the total mass, had never been studied. The Brans-Dicke theory (3.2.41) predicts violation of the SEP while the WEP is not violated.

(7) In Chaps. 4, 5 and 6, we will use $G_{\rm N}$ rather than G for the bare gravitational constant. However, we must keep in mind that it is a misuse of language.

In the Brans-Dicke theory, the scalar field Φ is nonminimally coupled to gravity in such a way that it introduces a variation of the effective gravitational "constant" only. Indeed, matter fields are universally coupled to the metric $g_{\mu\nu}$. It results that there exists a reference frame locally where the gravitational effects are vanishing for all matter species such that the SR laws applies. However, in the case of strongly gravitating objects, the gravitational binding energy which is affected by the variation of the gravitational strength, contributes largely to the inertial mass, the SEP being violated.

This variation of the gravitational mass $m_{\rm g}$ due to the scalar field was further formalized by Nordtvedt [Will08],

$$m_{\rm g} = m_{\rm i} + \eta \frac{E_{\rm b}}{c^2}, \tag{3.2.47}$$

with $E_{\rm b}$ the Newtonian gravitational binding energy [Nordtvedt68a, Nordtvedt68b, Nordtvedt68c]. The best constraint has been obtained by the Lunar Laser Ranging experiment, $|\eta| < (4.4 \pm 4.5) \times 10^{-4}$ [Williams09]. The **Nordtvedt effect** affects also the weakly gravitating bodies, but it cannot be detected experimentally, the sensitivity of the experimental set-up being far too low.

Considering now general STT formulated in the Einstein frame as introduced in Sec. 3.2.2, violations of the WEP and the SEP may arise depending on the way matter fields $\psi_{\rm M}$ are coupled to the gravitational fields in $\mathcal{L}_{\rm M}\left[\psi_{\rm M},\, g^{\mu\nu},\, \phi\right]$. In the case of a conformal coupling to matter $A(\phi)$ which is universal for all matter fields (see Eq. (3.2.23)), only the SEP is violated since the effect of the gravitational field is vanishing locally (see the discussion above about the Brans-Dicke theory). However, if the metric does not couple universally to matter fields, i.e. $g_{\mu\nu} = A^{(i)}(\phi)\tilde{g}_{\mu\nu}$, the superscript (i) denoting different matter species, for instance photons and electrons, then the WEP is also violated. Indeed, it is not possible to find out a reference frame locally where the gravitational effects are vanishing for all the matter species at once.

One example of such STT is the Abnormally Weighting Hypothesis (AWE) [Alimi08] where three different geometries are assumed, describing gravitation ($g_{\mu\nu}$), the matter of the SM ($A^2(\varphi)_{\rm M} g_{\mu\nu}$) and the matter-energy content in the dark sector ($A^2(\varphi)_{\rm AWE}\, g_{\mu\nu}$),

$$\begin{aligned} S = \frac{1}{2\kappa}\int {\rm d}^4x\sqrt{-g}\,(R - 2\,g^{\mu\nu}\partial_\mu\varphi\partial_\nu\varphi) \\ + S_{\rm M}\left[\psi_{\rm M},\, A^2_{\rm M}(\varphi)\, g_{\mu\nu}\right] + S_{\rm AWE}\left[\psi_{\rm AWE},\, A^2_{\rm AWE}(\varphi)\, g_{\mu\nu}\right]. \end{aligned} \tag{3.2.48}$$

In general, the SEP is violated provided that the modified gravity model exhibits two different geometries in a single model, one of them describing gravitation and the other, the geometry in which matter plays out its dynamics [Bekenstein93]. In order to predict a violation of the WEP, different geometries describe the matter dynamics like for AWE. The conformal transformation between two geometries is the easiest. However, more sophisticated

transformations exist like the disformal one [Bekenstein93],

$$g_{\mu\nu} = A(\phi,\ X)\tilde{g}_{\mu\nu} + B(\phi,\ X)\partial_\mu\phi\,\partial_\nu\phi, \tag{3.2.49}$$

where the disformal functions A and B depend on the scalar field ϕ and the metric $\tilde{g}^{\mu\nu}$ via the kinetic term $X = \tilde{g}^{\mu\nu}\partial_\mu\phi\partial_\nu\phi$. The disformal transformation between two geometries may lead to violations of the SEP or the WEP depending on the functions A and B.

In summary, GR satisfies both the WEP and the SEP, and thus predicts no violation of the UFF, the LPI nor the LLI. In STT, the SEP is violated whereas the WEP can be violated, depending on the way matter fields are coupled to the scalar field. In this last case, the UFF is violated too. The LLI is usually satisfied in STT since, even if the asymptotic value of the scalar field is varying depending of the location of the frame (the LPI is violated), the metric and the scalar fields are Lorentz invariant asymptotically[8] For more involved modified gravity models invoking vector, tensor or prior geometry (see Tab. 3.1), both LPI and LLI are generally not satisfied.

3.2.5 Current status of scalar-tensor theories from the observations

In this section we report the current observational constraints on general STT. Indeed, the Brans-Dicke theory passes the PPN constraints only for very large values of the ω parameter (see Sec. 3.2.5.1), such that it is now disfavored. In the last decades, the phenomenology predicted by more general STT, in particular in the presence of a potential, has been extensively explored. Today, the STT are also devoted to provide alternative to BHs or to model accelerated expansion of the Universe (either in the early or in the late-time Universe). In order to be viable, they must pass Solar System constraints.

3.2.5.1 The PPN parameters

The PPN parameters (see Sec. 2.2 for a general introduction) enable one to constrain the Brans-Dicke theory in the Solar System. The calculations of the parameters are reported in App. B for the Brans-Dicke theory (3.2.41) with $\omega = \omega(\Phi)$. They read,

$$\boxed{|\gamma_{\rm PPN} - 1| = \frac{1}{\omega + 2}, \qquad \beta_{\rm PPN} - 1 = \frac{1}{(2\omega+3)^2(2\omega+4)}\frac{{\rm d}\omega}{{\rm d}\Phi},} \tag{3.2.50}$$

the lower bound on the Brans-Dicke parameter ω yielding $\omega \gtrsim 4.3 \times 10^4$ according to Eqs. (2.2.14). It results that the Brans-Dicke is indistinguishable from GR in the Solar system.

[8] The LLI can be violated in STT in a particular case. If the asymptotic value of the scalar field is varying on cosmological time, for instance because of a de Sitter background, then variations of the rate of the scalar field (and thus of the effective gravitational coupling) are generated. As a result, the local physics may depend on the velocity of the reference frame [Will08].

In principle, the PPN parameters do not allow one to constrain general STT in the presence of a potential. However, as we will see in the rest of this thesis, PPN parameters are used provided that the potential can be considered as higher order terms in the Einstein equations, as the cosmological constant in GR. In order to test STT in the presence of a potential, the fifth force formalism has been developed.

3.2.5.2 Fifth force formalism

By analogy with particle physics, low mass scalar field coupled to gravity could mediate a fifth force of Yukawa-type. Such an interaction implies a deviation from the Newtonian gravitational potential $V(r)$ in $1/r$ in the weak-field regime (see [Fischbach98] for a review). The fifth force formalism enables to parametrize the deviation of Yukawa type,

$$V(r) = -G_{\rm N}\frac{m_1 m_2}{r}\left(1+\alpha \mathrm{e}^{-r/\lambda}\right), \tag{3.2.51}$$

with α, the dimensionless strength of interaction parameter and λ, the length scale [Adelberger03]. The wide variety of scales where gravity can be tested is characterized as a function of λ and α. The remaining viable space parameters is constrained by various experiments depending on the probed scale of interaction [Adelberger02, Upadhye12a, Kapner07], as reported on Fig. 3.2. Actually, the detection of a fifth force would correspond to a violation of the UFF in the particular case where a low mass particle would be responsible for the deviation.

3.2.5.3 Strong field regime: spontaneous scalarization and particlelike solutions

If STT beyond the Brans-Dicke theory pass Solar System constraints, then the question arises if they are able to pass strong field regime bounds. Following [Damour93a] it is convenient to consider the Einstein frame (see [Salgado98] for an analysis in the Jordan frame) with the coupling function $A(\varphi)$ (see Eq. (3.2.23)) parametrized as,

$$\ln A(\varphi) \simeq \ln A(\varphi_0) + \alpha_0(\varphi-\varphi_0) + \frac{1}{2}\beta_0(\varphi-\varphi_0)^2 + ..., \tag{3.2.52}$$

with φ_0 the background value of the scalar field imposed by the cosmological evolution which is usually assumed to be zero. α_0 and β_0 are related to the PPN parameters (see e.g. [Damour93a]). In particular, GR predicts $\alpha_0 = \beta_0 = 0$ while the Brans-Dicke theory $\alpha_0^2 = (2\omega_{\rm BD}+3)^{-1}$ and $\beta_0 = 0$. Considering the PPN parameters today gives $\alpha_0^2 < 10^{-5}$ [Freire12] while β_0 is poorly constrained. It results that the scalar field must be close to the minimum of the coupling function $\mathrm{d}A/\mathrm{d}\varphi \simeq 0$, i.e. the GR attractor.

Considering now strong field experiments, NSs appear to be the most promising candidates for confronting STT with observations, in particular

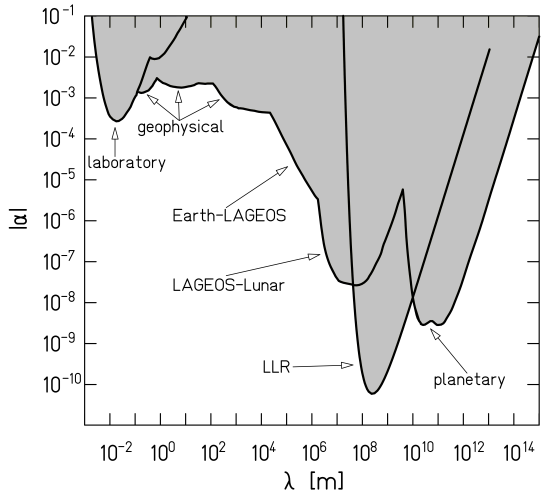

Figure 3.2: Current bounds on fifth force depending on the length of interaction λ (for $\lambda > 1$ cm) and its strength α. Regions excluded at 95% C.L. are shaded. Reprinted from [Adelberger03].

compact binaries. Indeed, most of STT admit the same BH solutions as in GR, the no-hair theorem applying to a large class of modified gravity theories [Sotiriou12], whereas the dynamics of BHs can differ in some particular cases (see e.g. [Berti15, Silva15] and references therein).

In the 1990s, Damour and Esposito-Farèse [Damour93a, Damour96] found a non-perturbative effect (see Sec. 2.3.5), named **spontaneous scalarization** such that the deviation from GR can be of the order one for NSs for parameters passing the Solar System tests. For stars with a baryonic mass above the critical value $m_{\rm bar}^{cr}$, the GR solution is less favored energetically than the solution with $\varphi \neq 0$ since the ADM mass (2.3.10) (assuming the baryonic matter and the scalar field contributions to $T_{\mu\nu}$) is smaller for the solution with $\varphi \neq 0$. Spontaneous scalarization is usually parametrized by the **scalar charge** $\alpha_{\rm s}$ given by the asymptotic behavior of the scalar field,

$$\varphi = \varphi_0 + \frac{G\alpha_{\rm s}}{r}, \tag{3.2.53}$$

with G the bare gravitational constant.

Spontaneous scalarization has been dubbed by analogy with the spontaneous magnetization in ferromagnets below the Curie temperature [Damour96]. The theory predicts that spontaneous scalarization cannot occur for $\beta_0 \gtrsim -4.35$ assuming spherically symmetric NSs [Damour93a]. The best bounds on β_0 have been obtained using compact binary observations (see Sec. 2.3.5) and show that STT are forbidden if $\beta_0 < -5$ whatever α_0

[Freire12, Wex14], such that β_0 is tightly constrained by compact binary observations. However, the effect of spontaneous scalarization in anisotropic NSs is found to increase when the tangential pressure is larger than the radial one [Silva15]. Finally, the mass-radius diagram of stars (see Sec. 2.3.5) is significantly affected by spontaneous scalarization [Berti15].

Particlelike solutions are another example of non-perturbative effect arising in the strong field regime. Those solutions are globally regular (i.e. they exhibit no singularity), asymptotically flat (Minkowski spacetime is recovered at spatial infinity) and are of finite energy. In the best case scenario, they are also stable under perturbations. Particlelike solutions allow to regularize singular solutions appearing in spherical symmetry, for instance BH.

As an example, boson stars are particlelike solutions appearing in the framework of GR. They are compact objects made of a self-gravitating massive complex scalar field [Ruffini69, Colpi86]. Assuming static and spherically symmetric spacetime with the complex scalar field minimally coupled to gravity, there exists a continuous family of particlelike solutions for the scalar field depending on their potential parameters. Boson stars are BHs mimickers whereas the prediction in terms of accretion disk or emission of GWs are different (see [Schunck03, Liebling12] for reviews).

A second particlelike solution was discovered by Bartnik and Mc Kinnon when the $\mathrm{SU}(2)$ Yang-Mills theory is coupled to gravity. Whereas there exists no particlelike solution for gravity nor for the Yangs-Mills theory in spherical symmetry, the gauge field solutions in spherically symmetric spacetime are particlelike [Bartnik88]. However, those solutions were found to be unstable with respect to small spherically symmetric perturbations (see [Volkov99] and references therein).

3.2.5.4 Cosmology: inflation and late-time cosmic acceleration

In order to build viable models for inflation and current cosmic acceleration, a potential term modeling the self-interaction of the scalar field is introduced in STT,

$$S = \int \mathrm{d}^4x\,\sqrt{-g}\,\left[F(\phi)R - Z(\phi)\,(\partial\phi)^2 - V\,(\phi)\right] + S_{\mathrm{M}}\left[g_{\mu\nu},\,\Psi_{\mathrm{M}}\right]. \quad (3.2.54)$$

If the STT is justified by the explanation of the late-time cosmic acceleration, it generally calls on a screening mechanism (see Sec. 3.1.3) in order to pass the Solar System constraints while mediating long range effect in cosmology. STT also allow to build viable inflationary models, among them the Starobinsky model (see Fig. 2.3). This is a particular example of $f(R)$ models (3.1.3),

$$S = \int \mathrm{d}^4x\sqrt{-g}\left(R + \frac{R^2}{6M^2}\right), \quad (3.2.55)$$

which is equivalent to a STT in the presence of a potential (see Sec. 5.2.2).

3.3 Beyond scalar-tensor theories: Horndeski gravity

In 1974, Horndeski generalized the Lovelock theorem to models where the metric $g_{\mu\nu}$ has a scalar counterpart for describing gravity, imposing that the equations of motion are up to second order [Horndeski74]. On the other hand, the Galileon theory was proposed in 2008 [Nicolis09] (while it was actually discovered in 1992 by [Fairlie92, Fairlie11]),

$$S_\pi = S_{\rm EH} + \int {\rm d}^4x\sqrt{-g}\sum_{i=1}^{5} c_i\mathcal{L}_\pi^{(i)} + S_{\rm M}\left[\psi_{\rm M};\ g_{\mu\nu}\right], \tag{3.3.1}$$

with,

$$\mathcal{L}_1 = \pi, \tag{3.3.2}$$

$$\mathcal{L}_2 = \left(\nabla\pi\right)^2, \tag{3.3.3}$$

$$\mathcal{L}_3 = \Box\pi\left(\nabla\pi\right)^2, \tag{3.3.4}$$

$$\mathcal{L}_4 = \left(\Box\pi\right)^2\left(\pi_{;\mu}\,\pi^{;\mu}\right) - 2\left(\Box\pi\right)\left(\pi_{;\mu}\,\pi^{;\mu\nu}\,\pi_{;\nu}\right) - \left(\pi_{;\mu\nu}\,\pi^{;\mu\nu}\right)\left(\pi_{;\rho}\,\pi^{;\rho}\right) + 2\left(\pi_{;\mu}\pi^{;\mu\nu}\,\pi_{;\nu\rho}\,\pi^{;\rho}\right), \tag{3.3.5}$$

$$\mathcal{L}_5 = \left(\Box\pi\right)^3\left(\pi_{;\mu}\,\pi^{;\mu}\right) - 3\left(\Box\pi\right)^2\left(\pi_{;\mu}\,\pi^{;\mu\nu}\,\pi_{;\nu}\right) - 3\left(\Box\pi\right)\left(\pi_{;\mu\nu}\,\pi^{;\mu\nu}\right)\left(\pi_{;\rho}\,\pi^{;\rho}\right) + 6\left(\Box\pi\right)\left(\pi_{;\mu}\pi^{;\mu\nu}\,\pi_{;\nu\rho}\,\pi^{;\rho}\right) + 2\left(\pi_{;\mu}{}^{\nu}\,\pi_{;\nu}{}^{\rho}\,\pi_{;\rho}{}^{\mu}\right)\left(\pi_{;\lambda}\,\pi^{;\lambda}\right) + 3\left(\pi_{;\mu\nu}\,\pi^{;\mu\nu}\right)\left(\pi_{;\rho}\,\pi^{;\rho\lambda}\,\pi_{;\lambda}\right) - 6\left(\pi_{;\mu}\,\pi^{;\mu\nu}\,\pi_{;\nu\rho}\,\pi^{;\rho\lambda}\,\pi_{;\lambda}\right), \tag{3.3.6}$$

the semi-colon denoting a covariant derivative. This model is an effective theory in a four-dimensional Minkowski background with second-order equations of motion and thus provides the well-defined modifications of gravity in the low energy limit. Various modified gravity models are particular cases of the Galileon effective theory, among them the DGP model [Dvali00] and the Lovelock gravity [Van Acoleyen11] (see also [deRham12]). The resulting theory is dubbed Galileon because of the Galilean shift symmetry,

$$\partial_\mu\pi \longrightarrow \partial_\mu\pi + b_\mu \qquad \text{and} \qquad \pi \longrightarrow \pi + c + b_\mu x^\mu, \tag{3.3.7}$$

with c and b_μ arbitrary constant and vector field respectively, in flat spacetime.

In order to study the predictions of the Galileon theory in a curved spacetime, the covariant version of the Galileon theory, i.e. the most general theory where a scalar field is coupled to gravity with at most second order equations of motion, was formulated [Deffayet09a, Deffayet09b, Kobayashi11],

$$\mathcal{L} = \sum_{i=2}^{5}\mathcal{L}_i, \tag{3.3.8}$$

with,

$$\mathcal{L}_2 = K(\phi, X), \tag{3.3.9}$$

$$\mathcal{L}_3 = -G_3(\phi, X)\Box\phi, \tag{3.3.10}$$

where K and G_3 are generic functions of ϕ and $X \equiv -\partial_\mu\phi\partial^\mu\phi/2$. Higher-order Galileons read,

$$\mathcal{L}_4 = G_4(\phi, X)R + G_{4X}\left[(\Box\phi)^2 - (\nabla_\mu\nabla_\nu\phi)^2\right], \quad (3.3.11)$$

$$\mathcal{L}_5 = G_5(\phi, X)G_{\mu\nu}\nabla^\mu\nabla^\nu\phi - \frac{G_{5X}}{6}\left[(\Box\phi)^3 - 3(\Box\phi)(\nabla_\mu\nabla_\nu\phi)^2 + 2(\nabla_\mu\nabla_\nu\phi)^3\right], \quad (3.3.12)$$

where $(\nabla_\mu\nabla_\nu\phi)^2 = \nabla_\mu\nabla_\nu\phi\nabla^\mu\nabla^\nu\phi$, $(\nabla_\mu\nabla_\nu\phi)^3 = \nabla_\mu\nabla_\nu\phi\nabla^\nu\nabla^\lambda\phi\nabla_\lambda\nabla^\mu\phi$, and $G_{iX} = \partial G_i/\partial X$. It appears that the covariant Galileon model is equivalent to the Horndeski model [Kobayashi11].

Besides the usual STT and the $f(R)$ models, Horndeski gravity also includes all the nonminimal derivative couplings of the scalar field to gravity like k-mouflage (see Sec. 3.1.3) [Deffayet09b, Deffayet11, Deffayet09a]. The EH action is also included by construction in the covariant version of the Galileon model. If equations of motion of more than second-order are allowed provided that they avoid the Ostrogradsky instability (see Sec. 1.3.4), then the class of well-posed models is extended and is referred to as the beyond Horndeski theory [Zumalacárregui14, Gleyzes15].

Since the additional degree of freedom is scalar, it generally preserves the LLI (see the discussion in Sec. 3.2.4.3) as well as the diffeomorphism-invariance. In some sense, Horndeski gravity is thus the minimal extension of GR since only the LPI is violated (see also Tab. 3.1).

Because of the non-linearities appearing in the scalar field kinetic term, the Horndeski models may exhibit the Vainshtein screening mechanism (see Sec. 3.1.3). The Vainshtein mechanism makes possible to build viable cosmological models, for the late-time acceleration and inflation, with sufficiently small effects at local scales to evade Solar System constraints. In addition, inflationary phase can be generated by the non-linearities appearing in the kinetic term of the scalar field without the introduction of a potential term for the scalar field.

As a result, the Galileon model (or equivalently Horndeski gravity) has opened the way to new models for cosmology [Chow09, Charmousis12a, Kobayashi11, Tsujikawa12] (see also Chap. 6).

3.4 Summary of the thesis

In the rest of this thesis, some modified gravity models are studied from the phenomenological point of view (assuming that there are well-posed) at different scales: in the lab, in the Solar System, around compact objects and at cosmological scales.

In Sec. 3.1.3 screening mechanisms have been introduced, among them the chameleon model. This is an example of STT, usually written in the Einstein frame (3.2.23). Due to the explicit coupling of the scalar field to matter $A(\phi)$,

the chameleon acquires an effective mass (see Sec. 3.1.3) varying as a function of the density. In relatively high density environment like in the Solar System or inside stars, the chameleon has a large effective mass such that it mediates a short-ranged fifth force (see the length of interaction introduced in Sec. 3.2.5.2) while in sparse environment, its effective mass is small, so that the chameleon is able to mediate long-ranged fifth force, that is the current cosmic acceleration.

Since its formulation by Khoury and Weltman [Khoury04a, Khoury04b], the chameleon model has been widely studied from the phenomenological point of view. Depending on the parameters of the potential and the non-minimal coupling function, the chameleon model can reproduce the current cosmic acceleration while it passes the current constraints in the Solar System. However, a part of this parameter space remains unconstrained. In Chap. 4 we focus on a lab experiment which appears to be the most promising probe of the chameleon model today. In 2012, Burrage, Copeland and Hinds proposed an atom interferometry experiment where the atom interferometer is placed inside a vacuum chamber in the presence of a test mass [Burrage15]. While the test mass is screened, the atoms are not, due to their small size and mass. They are thus sensitive to the chameleon field and the measure of interference fringes enable one to measure the additional acceleration due to the chameleon field.

The experiment has been performed at Berkeley in 2015 [Hamilton15]. Analytical forecasts have been provided [Hamilton15, Burrage15], relying on restrictive assumptions like negligible effects of the vacuum chamber wall. In this thesis we provide the full numerical solutions of the Klein-Gordon equation for a spherical vacuum chamber. This numerical method allows one to refine the analytical constraints and to analyze the effects of the chamber geometry.

In Chap. 5, we study a second STT where the scalar field is identified to the **Brout-Englert-Higgs field**[(9)]. Since its discovery in 2012 [Aad12, Chatrchyan12], the Higgs field is the first elementary scalar particle ever detected such that the existence of elementary scalar fields is not hypothetical anymore. The Higgs field has a crucial role in the SM because it is responsible to the mass generation of elementary particles relying on the spontaneous symmetry breaking of the SM gauge symmetry. Whereas SM is a quantum theory, the spontaneous symmetry breaking is a classical mechanism and could possibly be related to cosmology.

The question thus arises if the Higgs field could play a role in cosmology, for instance during inflation. In 2008, Bezrukov and Shaposhnikov highlighted that the Higgs field could be the inflaton, provided that it is non-minimally coupled to gravity [Bezrukov09b]. This model is still favored by Planck+Keck+BICEP2 data (see the Starobinsky model[(10)] in Fig. 2.3).

In this thesis, we focus on the predictions of Higgs inflation around com-

[(9)] In the following of this thesis, we will rather refer to the Higgs field.

[(10)] The Higgs inflation is equivalent to the Starobinsky model as highlighted in Sec. 5.2.2.

pact objects. Because of the nonminimal coupling, the distribution of the Higgs field in spherically symmetric spacetime is expected to be non-trivial, possibly leading to deviations from GR predictions. Moreover, variations of the Higgs vev could induce modifications in the nuclear processes inside neutron stars. Those questions are discussed in Chap. 5 and highlights the existence of a novel particlelike solution (see Sec. 3.2.5.3) for STT like the Higgs inflation.

In Chap. 6, we focus on a more sophisticated model, the Fab Four dubbed in reference to the four general Lagrangians appearing in Horndeski gravity (see Sec. 3.3) which may escape the Weinberg no-go theorem in order to solve the cosmological constant problem (see Sec. 2.4.4). We study the phenomenology predicted by two of the four Lagrangians for inflation, in the Solar System and around compact objects. The Fab Two are found to be able to reproduce the inflationary phase without any potential, because of the nonminimal derivative coupling between the scalar field counterpart to the metric and the Einstein tensor, depending on the nonminimal coupling parameter. The Fab Two model predicts that compact objects are spontaneously scalarized (see Sec. 3.2.5.3). Eventually some observables in the Solar System are computed numerically since the PPN parameters do not allow one to derive any constraint on the Fab Two model due to the presence of the nonminimal derivative coupling.

Part II

Combined constraints on modified gravity

Chapter 4

Probing the chameleon model with atom-interferometry

based on

S. Schlögel, S. Clesse, A. Füzfa,
Probing Modified Gravity with Atom Interferometry: a Numerical Approach,
Phys. Rev. D 93, 104036 (2016)

In this chapter we focus on the chameleon model which exhibits the eponymous screening mechanism introduced in Sec. 3.1.3. In sparse environment the chameleon behaves as a free field, allowing for the cosmic acceleration whereas in dense environment, it becomes massive, therefore possibly passing the Solar System constraints. After a brief introduction of the chameleon models, we review the current bounds on its parameter space, the constraints coming from the cosmological and astrophysical observations as well as from experiments. Then we focus on an atom-interferometry experiment recently proposed by [Burrage15]. We refine the constraints derived in [Burrage15, Hamilton15] providing numerical profiles of the chameleon field and of the induced acceleration on atoms. We establish that the near future atom-interferometry experiments could be able to rule out the chameleon parameter space up to the Planck scale.

4.1 The chameleon models

Chameleon models have been first proposed by Khoury and Weltman [Khoury04b, Khoury04a]. They are generally formulated in the Einstein frame

(see Sec. 3.2.2),

$$S = \int \mathrm{d}^4x\sqrt{-g}\left[\frac{R}{2\kappa} - \frac{1}{2}\left(\partial\phi\right)^2 - V(\phi)\right] + S_{\mathrm{M}}\left[\psi_{\mathrm{M}}; \tilde{g}_{\mu\nu} = A^2\left(\phi\right) g_{\mu\nu}\right], \quad (4.1.1)$$

the tilde denoting Jordan frame quantities in this chapter. Chameleon models were initially justified by the fact that quintessence is able to model cosmic acceleration (see Sec. 2.4.4) provided that the coupling of the scalar field to matter is extremely small in order to pass local tests of gravity. Similarly to tracking quintessence the typical chameleon potential is of the runaway type, that is a monotically decreasing function satisfying the tracker condition defined by,

$$\frac{V_{,\phi\phi}V}{V_{,\phi}^2} > 1, \quad (4.1.2)$$

and diverging at some finite value of $\phi = \phi_*$ (in the following $\phi_* = 0$). Other potential functions have been proposed (see e.g. [Gubser04, Mota11]). Contrary to quintessence models, the chameleon field exhibits a coupling to matter possibly strong,

$$A(\phi) = \exp\frac{\beta\phi}{M_{\mathrm{pl}}} \simeq \left(1 + \frac{\beta\phi}{M_{\mathrm{pl}}}\right), \quad (4.1.3)$$

where β can be of order unity (or even larger in the strongly coupled case [Mota06, Mota07]), the chameleon field being then allowed to pass local tests of gravity.

The effective dynamics is driven by the effective potential V_{eff} defined by,

$$\Box\phi \equiv \frac{\mathrm{d}V_{\mathrm{eff}}}{\mathrm{d}\phi}, \qquad \frac{\mathrm{d}V_{\mathrm{eff}}}{\mathrm{d}\phi} = \frac{\mathrm{d}V}{\mathrm{d}\phi} - T\frac{\mathrm{d}\ln A}{\mathrm{d}\phi}, \quad (4.1.4)$$

where T is the trace of the stress-energy tensor in the Einstein frame $T_{\mu\nu}$, which is related to its Jordan frame counterpart $\tilde{T}$ by,

$$T = A^4(\phi)\tilde{T}. \quad (4.1.5)$$

Assuming a perfect fluid the energy density ρ and the pressure p in the Einstein frame read [Damour93b],

$$\rho = A^4\left(\phi\right)\tilde{\rho}, \quad (4.1.6)$$

$$p = A^4\left(\phi\right)\tilde{p}. \quad (4.1.7)$$

In the rest of this chapter we will consider the Jordan frame energy tensor only since $\tilde{\nabla}_\mu\tilde{T}^{\mu\nu} = 0$ and the tilde are dropped.

Provided $\beta > 0$, the effective potential has a minimum $\phi_{\min}$ and an effective mass $m_{\min}^2 \equiv \mathrm{d}^2V_{\mathrm{eff}}/\mathrm{d}\phi^2\big|_{\phi=\phi_{\min}}$ (or equivalently the Compton wavelength $\lambda_{\mathrm{C}} = m_{\min}^{-1}$) which depend on ρ (see Figs. 4.1 and 4.2): in dense (sparse)

environment, $\phi_{\rm min}$ (denoted $\phi_{\rm c}$ in the figures) is small (large) while $m_{\rm min}$ is large (small). It results that in dense environment, the chameleon is decaying rapidly since its Compton wavelength is small while it mediates long range force in sparse environment. This is the reason why this screening mechanism has been named the chameleon (see Sec. 3.1.3).

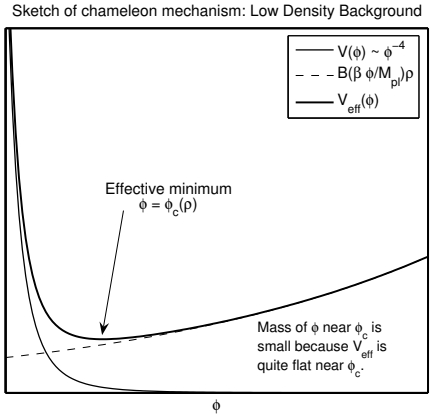

Figure 4.1: Effective potential, given by the runaway potential and the coupling to matter according to Eq. (4.1.4) for the chameleon field in sparse environment. The effective chameleon mass is small since $V_{\rm eff}$ is shallow around its minimum, allowing the chameleon to drive the current cosmic acceleration. Reprinted from [Mota07].

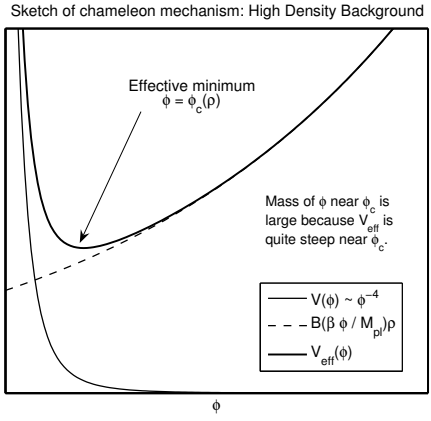

Figure 4.2: Effective potential, given by the runaway potential and the coupling to matter according to Eq. (4.1.4) for the chameleon field in dense environment. The effective chameleon mass is large since $V_{\rm eff}$ is steep around its minimum, allowing the chameleon to pass local tests of gravity, for instance in the Solar system. Reprinted from [Mota07].

4.1.1 The original chameleon model

Originally Khoury and Weltman considered the model for the Ratra-Peebles potential and the exponential coupling function,

$$V(\phi) = \frac{\Lambda^{4+\alpha}}{\phi^{\alpha}}, \qquad A(\phi) = \mathrm{e}^{\frac{\phi}{M}}, \tag{4.1.8}$$

with

$$M = \frac{M_{\rm pl}}{\beta}. \tag{4.1.9}$$

Assuming $A(\phi) \simeq 1$ and $\alpha > 0$, the minimum of the effective potential as well as the effective mass are respectively given by,

$$\left.\frac{\mathrm{d}V_{\rm eff}}{\mathrm{d}\phi}\right|_{\phi=\phi_{\rm min}} = 0 = -\frac{\alpha\Lambda^{\alpha+4}}{\phi_{\rm min}^{\alpha+4}} + \frac{\rho}{M} \quad \Rightarrow \quad \phi_{\rm min} = \left(\frac{\alpha\Lambda^{\alpha+4}M}{\rho}\right)^{\frac{1}{\alpha+1}}, \tag{4.1.10}$$

$$m_{\rm min}^2 = \left.\frac{\mathrm{d}^2V_{\rm eff}}{\mathrm{d}\phi^2}\right|_{\phi=\phi_{\rm min}} = \alpha(1+\alpha)\frac{\Lambda^{\alpha+4}}{\phi_{\rm min}^{\alpha+2}}$$

$$\Rightarrow \quad m_{\rm min}^2 = \alpha(1+\alpha)\Lambda^{4+\alpha}\left(\frac{\rho}{\alpha M\Lambda^{4+\alpha}}\right)^{\frac{2+\alpha}{1+\alpha}}. \tag{4.1.11}$$

We first derive the order of magnitude required for the parameters in order to explain the current cosmic acceleration. Following [Zhang16], we only consider the condition on the cosmological parameters today,

$$\left.\frac{\rho_{\Lambda,0}}{\rho_{\rm m,0}}\right|_{\rm obs} = 2.15. \tag{4.1.12}$$

Assuming that the chameleon field is at the minimum of its effective potential today[(1)], thus running a cosmological constant, yields,

$$\rho_{\Lambda,0} = V\left[\phi_{\rm min}\left(\rho_\infty\right)\right] = \frac{\Lambda^{\alpha+4}}{\phi_{\rm min}^{\alpha}} = \frac{\rho_\infty\phi_\infty}{\alpha M}, \tag{4.1.13}$$

where the subscript ∞ refers to background values with $\phi_\infty = \phi_{\rm min}(\rho_\infty)$ and ρ_∞ being either the cosmological matter density identified to $\rho_{\rm m,0} \sim 10^{-47}\ \mathrm{GeV}^4$ either the galactic background density $\rho_{\rm gal} \sim 10^5 \times \rho_{\rm m,0}$. Assuming $\rho_\infty = \rho_{\rm m,0}$ we obtain,

$$\frac{\rho_{\Lambda,0}}{\rho_{\rm m,0}} = \frac{\phi_\infty}{\alpha M} = \frac{1}{\alpha M}\left(\frac{\alpha M\Lambda^{\alpha+4}}{\rho_{\rm m,0}}\right)^{\frac{1}{\alpha+1}}. \tag{4.1.14}$$

[(1)] In their original paper [Brax04] Brax et al. showed that the chameleon exhibits an attractor behavior such as it remains very close to the minimum of its effective potential all along the cosmic history, the model being mainly insensitive to the scalar field initial conditions. Background cosmological constraints are then fulfilled provided that the chameleon has already settled to its minimum by the onset of BBN, $\phi_{\rm BBN} \lesssim 0.1\beta^{-1}M_{\rm pl}$, ensuring small mass variations. This results have been extended for large couplings by [Mota07]. Numerical computations allowed to establish that the chameleon model exhibits an attractor mechanism. While it is very efficient in the early Universe, where the effective potential is narrow since the density is high, it can be not strong enough at late time, especially for small β values. The attractor can be reached for a large span of initial conditions.

It is possible to rewrite this equation in order to find out an explicit relation between α and Λ using Eq. (4.1.9),

$$\Lambda^{\frac{\alpha+4}{\alpha+1}} = \rho_{\Lambda,0}\left(\rho_{\mathrm{m},0}\right)^{-\frac{\alpha}{\alpha+1}}\left(\alpha M\right)^{\frac{\alpha}{\alpha+1}}, \tag{4.1.15}$$

$$\log\Lambda = \frac{1}{\alpha+4}\left[(\alpha+1)\log\rho_{\Lambda,0} - \alpha\log\rho_{\mathrm{m},0} + \alpha\log\left(\frac{\alpha m_{\mathrm{pl}}}{\sqrt{8\pi}\beta}\right)\right], \tag{4.1.16}$$

$$= \frac{1}{\alpha+4}\left[\log\rho_{\Lambda,0} + \alpha\log m_{\mathrm{pl}} + \alpha\log\left(\frac{\rho_{\Lambda,0}}{\rho_{\mathrm{m},0}}\frac{\alpha}{\sqrt{8\pi}\beta}\right)\right], \tag{4.1.17}$$

the last term of the last equality being negligible for $\beta \sim 1$ and $\alpha \sim 1$. In this case, the equation reduces to,

$$\log\frac{\Lambda}{1\ \mathrm{GeV}} \approx \frac{19\alpha - 47}{4+\alpha}, \tag{4.1.18}$$

corresponding to the relation for quintessence as found by [Schimd07]. In summary the original chameleon model is able to reproduce the cosmic acceleration provided that Eq. (4.1.14) is fulfilled or equivalently the potential parameters obey to Eq. (4.1.18). Notice that Hees and Füzfa analyzed the likelihood of SN Ia data and obtained the same results [Hees12a]: the relation $\Lambda - \alpha$ (4.1.18) is not weakly affected by the nonminimal coupling even if the latter contributes non-negligibly to the luminosity distance D_{L} measurement where $D_{\mathrm{L}} \simeq z/H(v/c \ll 1)$ with z the redshift and H the Hubble parameter.

However, the original chameleon model is not able to pass the local tests of gravity for the corresponding parameters [Hees12a, Zhang16], as revealed by the computations of the PPN parameters. The Brans-Dicke formulas are not useful here since the potential cannot be neglected in the Klein-Gordon equation (even if the potential is negligible in the Einstein equations assuming that it contributes to higher order terms as for the cosmological constant in GR). As for the Brans-Dicke theory (see App. B), the Klein-Gordon equation must first be solved. Following [Hees12a], the numerical simulations are in good agreement with the analytical solutions for ϕ outside the Sun whereas deviations arise inside the Sun. Since the PPN parameters require the solution for the scalar field outside the Sun only, the analytical treatment of the solution is valid (see also App. C.1 for the analytical calculations). Then, it is possible to derive the PN expansion for the metric in the Einstein frame as for the Brans-Dicke theory (see App. B). In order to obtain the PPN parameters, the metric must be transformed in the Jordan frame by a conformal rescaling (see Sec. 3.2.2). We report the reader to [Zhang16] for the detailed calculations.

Eventually, the PPN parameters for the original chameleon read [Zhang16],

$$\gamma_{\mathrm{PPN}} - 1 = -\frac{2\phi_\infty}{M\Phi}, \tag{4.1.19}$$

$$\beta_{\mathrm{PPN}} - 1 = -\frac{3}{4(\alpha+1)\Phi}\left(\frac{\phi_\infty}{M_{\mathrm{pl}}}\right)^2, \tag{4.1.20}$$

where the gravitational potential $\Phi \simeq 2.12 \times 10^{-6}$ for the Sun. The constraints on $\gamma_{\rm PPN}$ are much more powerful than on $\beta_{\rm PPN}$ since,

$$|\beta_{\rm PPN} - 1| = \frac{3\Phi}{16\,(\alpha+1)} \left(\frac{M}{M_{\rm pl}}\right)^2 (\gamma_{\rm PPN} - 1)^2 \ll |\gamma_{\rm PPN} - 1|\,. \tag{4.1.21}$$

Indeed for $M \lesssim M_{\rm pl}$ and $\alpha \sim \mathcal{O}(1)$, $|\beta_{\rm PPN} - 1| \sim 10^{-16}$, thus far below the current constraints on $\beta_{\rm PPN}$ (see Sec. 2.2.2). Thus we focus on $\gamma_{\rm PPN}$ constraints from Cassini probe given by Eq. (2.2.14) yielding,

$$\frac{\phi_\infty}{M} = \left(\frac{\alpha \Lambda^{\alpha+4}}{\rho_\infty M^\alpha}\right)^{\frac{1}{\alpha+1}} \lesssim 2.4 \times 10^{-11}. \tag{4.1.22}$$

Combining the condition for the cosmic acceleration (4.1.14) and the $\gamma_{\rm PPN}$ (4.1.22), we obtain for $\alpha \sim 1$,

$$\frac{\rho_{\Lambda,0}}{\rho_{\rm m,0}} \lesssim 2.4 \times 10^{-11}, \tag{4.1.23}$$

which is incompatible with the cosmological observations, the original chameleon model being thus ruled out.

4.1.2 The exponential chameleon

In order to pass the local tests of gravity in the Solar System while explaining the current cosmic acceleration, we must rather assume the exponential potential[(2)],

$$V(\phi) = \Lambda^4 \exp\left(\frac{\Lambda^\alpha}{\phi^\alpha}\right) \simeq \Lambda^4 \left(1 + \frac{\Lambda^\alpha}{\phi^\alpha}\right). \tag{4.1.24}$$

The Klein-Gordon equation is exactly the same, the previous PPN analysis being thus still valid, while the cosmological constraint on the exponential chameleon differs from the original one due to the additional constant in the potential. Indeed, the minimum of the potential now reads,

$$\rho_{\Lambda,0} = V\left[\phi_{\rm min}\left(\rho_\infty\right)\right] = \Lambda^4 + \frac{\rho_\infty \phi_\infty}{\alpha M}, \tag{4.1.25}$$

where the second term in the right-hand side is negligible since,

$$\frac{\rho_{\Lambda,0}}{\rho_{\rm m,0}} = 2.15 = \frac{\Lambda^4}{\rho_{\rm m,0}} + \underbrace{\frac{\phi_\infty(\rho_{\rm m,0})}{\alpha M}}_{\lesssim 2.4\times 10^{-11}}, \tag{4.1.26}$$

by using (4.1.12) and (4.1.22), for $\alpha \sim 1$ and $\rho_\infty = \rho_{\rm m,0}$. It results that, for the exponential chameleon,

$$\Lambda = \rho_{\Lambda,0}^{1/4} \simeq 2\ {\rm meV}, \tag{4.1.27}$$

[(2)] Following Brax et al. [Brax04], the choice of this potential function is justified by two sufficient conditions: the potential is of runaway form and it diverges at some finite value, for instance $\phi = 0$. In addition the potential is flat and of order unity for the current value of the scalar field, ensuring the late-time cosmic acceleration.

in order to explain the current cosmic acceleration. The PPN parameters (4.1.22) allow one to further constrain the parameter space $\alpha - \mathrm{M}$,

$$\log\left(\frac{\alpha\Lambda^{\alpha+4}}{M^{\alpha}\rho_{\infty}}\right) \lesssim -10.6\,(\alpha+1), \tag{4.1.28}$$

$$\alpha\,(\log M - \log\Lambda - 10.6) - \log\alpha \gtrsim 10.6 - \log\frac{\rho_{\infty}}{\rho_{\Lambda,0}}. \tag{4.1.29}$$

The viable parameter space $\alpha - M$ is plotted in Fig. 4.4 for $\Lambda = 2.4$ meV and $\rho_{\infty} = \rho_{\mathrm{m},0}$ (the choice $\rho_{\infty} = \rho_{\mathrm{gal}}$ is more conservative). The combination of the constraints on PPN parameters and background cosmology enables one to rule out the exponential chameleon model for small α values, the constraint being more stringent for large β values. As we will see in the following additional tests on the exponential chameleon model are much more stringent than those coming from the Solar System observations today.

Further observables signatures for the chameleon model have been investigated (see [Joyce15] for a review of modified gravity models, among them the chameleon). Since the chameleon couples to the trace of $T_{\mu\nu}$ no significant effect is expected during the radiation era, provided that the chameleon is not coupled to photons[(3)]. Moreover, the range of its interaction is always much smaller than the horizon scale so no super-horizon effect is expected [Brax06].

Chameleon field should leave imprints during the structure formation in the matter era, especially when the coupling to matter β is large. The growth of matter fluctuations has been studied in a serie of papers, in the linear regime [Brax06, Gannouji10, Mota11, Hojjati16] and in the non-linear one (see [Brax13b] and references therein). It was found that first halos to form in chameleon cosmology are significantly more concentrated than according to the $\Lambda-$CDM concordance picture and matter collapses earlier to form structure [Brax06], the linear approximation thus fails at larger scale than for the $\Lambda-$CDM model. The main effects appear in the non-linear scales where the density contrast of matter is found to increase anomalously [Brax13b], the matter power spectrum being altered. The deviations are $\lesssim 10\%$ in the non-linear part of the power spectrum, which is hard to detect today. The ob-

[(3)]Further generalizations of the chameleon model were proposed, notably introducing a coupling function $A_{\gamma}^{2}(\phi)$ of the chameleon to photons,

$$S = \int \mathrm{d}^4x\sqrt{-g}\left[\frac{R}{2\kappa} - \frac{1}{2}\left(\partial\phi\right)^2 - V(\phi) - \frac{1}{4}A_{\gamma}^{2}(\phi)F^{\mu\nu}F_{\mu\nu}\right] + S_{\mathrm{M}}\left[\psi_{\mathrm{M}}; \tilde{g}_{\mu\nu} = A^2\left(\phi\right)g_{\mu\nu}\right], \tag{4.1.30}$$

with $F_{\mu\nu}$ the Faraday tensor, leading to a variation of the fine-structure constant [Brax07a].

Assuming a coupling of the chameleon field to photons (β_{γ}) enables one to test the chameleon models with other experimental setup. Several experiments have put constraints on β_{γ} for a given β (for different α). Among them, CHameleon Afterglow SEarch-GammeV [Steffen10] and Axion DM eXperiment [Rybka10] where the chameleon is tested using a laser beam in a vacuum chamber and in a microwave cavity respectively thanks to an intense magnetic field in both cases, and, more recently by CERN Axion Telescope, a telescope which detects soft X-ray coming from the Sun and possibly produced by the chameleon field [Anastassopoulos15]. Those constraints read $\beta_{\gamma} \lesssim 10^{11}$ for the range $1 < \beta \lesssim 10^{6}$ (Λ being of the order of the cosmological constant), a result being mostly independent of α [Anastassopoulos15].

servations of LSS, for instance by the Euclid satellite, should enable one to improve the current constraints on the chameleon model in the near future [Amendola16].

4.2 Current constraints on chameleon

In this section, we briefly discuss to what extent the exponential chameleon model is viable today in terms of those three parameters, that is the potential ($\alpha,\ \Lambda$) and nonminimal coupling (M or equivalently $\beta = M_{\rm pl}/M$) parameters. The parameter M is found to be poorly constrained because of the presence of the potential while, as we have already seen in the previous section $\Lambda \sim 1$ meV in order to account for the current cosmic expansion. The current best bounds are represented in Figs. 4.3 and 4.4. We consider the parameter ranges 10^{-2} meV $< \Lambda < 10^{2}$ meV, $1 < \alpha < 10$ and $10^{-15}\ M_{\rm pl} < M < M_{\rm pl}$.

In addition to the PPN constraints, stringent constraints on the chameleon parameter space arise from the experimental tests in labs (or in space) and from astrophysical tests of gravity. As a reminder, the larger values of β (or small values of M) the more efficient is the chameleon mechanism. For relatively small values of β, the chameleon field tends to behave like a non-chameleonic field, i.e. quintessence. On the contrary, for large values of β, the Compton wavelength of the chameleon field $\lambda_{\rm C}$ becomes so small in the presence of massive objects that the range of the fifth force interaction becomes smaller than the size of the objects. It results that the fifth force seems to be sourced by the thin shell of matter at the surface of the objects only [Amendola13]. This is the so-called thin-shell regime where the screening mechanism occurs. The precise boundary between screened (i. e. the thin shell regime) and unscreened objects is determined by the depth of the gravitational potential Φ (which is related to the density). Assuming spherically symmetric spacetime, the thin-shell parameter ϵ enables one to quantify the thin-shell effect,

$$\epsilon \equiv \frac{\phi_\infty - \phi_{\rm c}}{M_{\rm pl}\Phi}, \tag{4.2.1}$$

with $\phi_{\rm c}$ the central value of the sourcing object. The screening mechanism is efficient for $\epsilon \ll 1$.

4.2.1 Constraints from astrophysics

Following [Khoury04a], all the objects with a sufficiently large compactness, e.g. galaxies like the Milky Way ($s = 10^{-6}$), must be screened in order to pass observational tests. However, screened and unscreened objects do not fall at the same rate, leading to a possible violation of the UFF [Hui09]. The fact that an object is screened or not depends on its density and on its the environment as well as on β. Indeed, an object can be either self-screened either screened due to the environment (for instance, a dwarf galaxy ($s = 10^{-7} - 10^{-8}$) can be

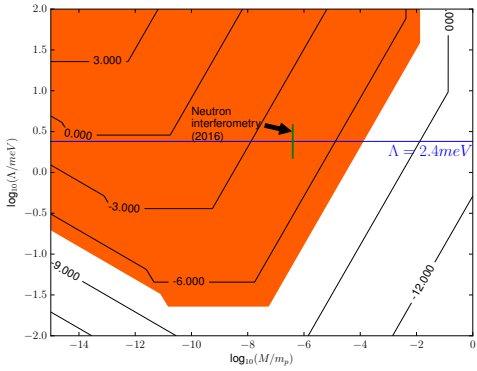

Figure 4.3: Exclusion contours for the chameleon parameters M and Λ ($\alpha = 1$ being fixed) for atom interferometry (in orange) and neutron interferometry (on the left of the green line), the blue line referring to the cosmological constant $\Lambda = 2.4$ meV. The contour lines refer to the logarithm of the normalized chameleon acceleration a_ϕ/g, the current constraint being given by Eq. (4.3.2) with $a_\phi/g \sim 10^{-7}$.

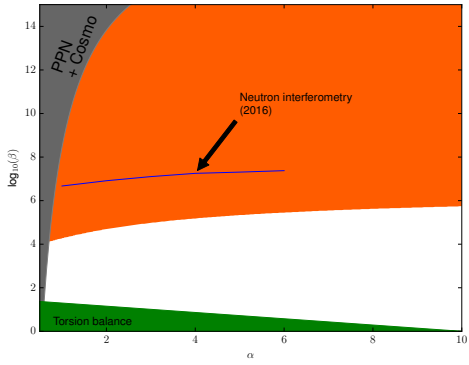

Figure 4.4: Exclusion contours for the chameleon parameters α and β ($\Lambda = 2.4$ meV being fixed) for atom interferometry (in orange), combined constraint from PPN parameters and background cosmology (in grey), torsion balance experiment (in green); and neutron interferometry (upper the blue line).

screened by the local group). Depending on the local environment in the Universe, for instance cosmic voids or above the cosmic mean, dwarf galaxies are thus less or more easily screened respectively since relatively dense environment can be more easily self-screened. In addition, when the matter is weakly coupled to the scalar field, i. e. for small β, the screening mechanism is less efficient and the UFF is satisfied while if the coupling is strong, i. e. for large β, violations can be detectable. Several observations have been proposed fol-

lowing this idea. As long as no deviation from GR is detected for less and less compact objects, they have to be unscreened, giving rise to constraint on the β parameter.

Some authors studied the effect of the chameleon field inside stars. The chameleon field is found to leave possible imprints in the mass-radius relationship of both NSs and white dwarfs (see also Sec. 2.3.5) by [Mota07]. Because of the nonminimal coupling, variations of $G_{\rm N}$ arise, potentially inside the star itself. Since $G_{\rm eff}$ is larger in unscreened environment, unscreened stars are subjected to a stronger gravitational force, which means that they are brighter and hotter while more ephemeral [Davis12, Chang11] compared to screened stars which have (almost) the same properties as predicted by GR [Davis12] (at the same mass) [Sakstein14]. Following [Chang11], the stellar evolution of red giants stars is modified, especially their color and luminosity, since the core of those stars ($s \gtrsim 5 \times 10^{-6}$ [Davis12]) is screened while the envelope is not[(4)]. In unscreened galaxies (neither self-screened nor screened by their environment) partially screened red giants stars are found to be hotter than completely screened ones at the same luminosity. This effect is potentially measurable since, looking at Hertzsprung–Russell diagram, that is the classification of stars as a function of their surface temperature and luminosity, there exists a tip in the red giant branch. The chameleon field affects the pattern of this tip, offering a unique signature for modified gravity.

Actually this effect has been found to apply also to the structure of the main sequence stars in the Hertzsprung–Russell diagram by [Davis12]. In unscreened galaxies (that is dwarf galaxies in cosmic voids), only partially screened stars, which are more luminous and ephemeral than screened ones, can considerably enhance the total galactic luminosity. However, it is difficult to disentangle the chameleon effect to other ones, like the metallicity of the stars. Therefore Davis et al. [Davis12] proposed to measure the systematic offsets in luminosity between screened dwarf galaxies in clusters and unscreened galaxies in voids.

Best bounds using stars have been obtained by comparing distance measurements inferred by the Cepheids and red giant stars observations [Jain13]. Since some stars are used as standard candles (at low redshift), a modification of their properties implies a change of distance measurement. In [Jain13] authors focused on two specific stages of the giant stars evolution, that is the tip of the red-giant branch and the Cepheids. The key idea is to compare distances inferred using Cepheids and red giants which would agree only in the screened galaxies. As mentioned above the tip is shifted while the period-luminosity relation for Cepheids is also modified (Cepheids pulsate at shorter period at fixed luminosity), both effects adding up to each other [Jain13]. No deviation has been found up to now, putting strong bounds on the chameleon parameter space [Sakstein14]. It results that the only possibly unscreened astrophysical objects in the Universe are isolated gas clouds, the smallest dwarf galaxies and very massive post main sequence stars [Sakstein14].

[(4)]The density of the core is roughly $10^{13}\times$ that in the mantle in red giant stars [Casoli00].

The current constraints are represented in Fig. 4.5 for two dimensionless parameters: α which defines the strength of the fifth force interaction outside the thin-shell radius S (see Eq. (C.1.22) for a mathematical definition),

$$G_{\rm eff} = G_{\rm N}\left[1+\alpha\left(1-\frac{M(r)}{M(S)}\right)\right], \tag{4.2.2}$$

with $M(r)$ the mass enclosed into the radius r; and χ_0 the self-screening parameter which defines if an object is completely screened,

$$\chi_0 < \Phi = \frac{G_{\rm N}M}{\mathcal{R}}. \tag{4.2.3}$$

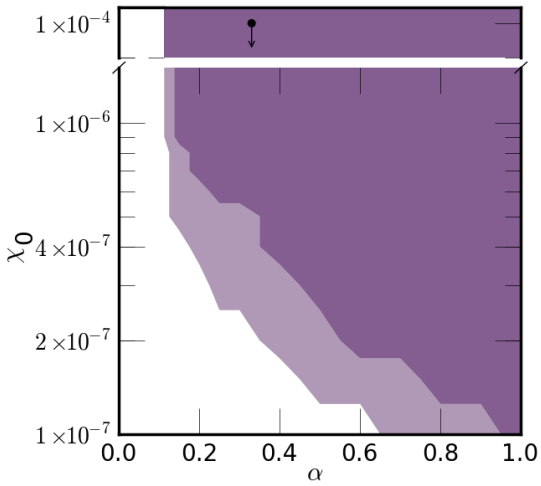

Figure 4.5: Constraints on the chameleon model using stars as a function of the parameters α and χ_0. The light and dark shaded regions show the regions excluded with 68% and 95% C.L. respectively. The black arrow indicates the previous constraint coming from galaxy cluster statistic [Schmidt09]. Reprinted from [Sakstein14].

4.2.2 Experimental tests of chameleon models

Since the formulation of the chameleon theory [Khoury04b, Khoury04a], fifth force searches have been found to constrain the chameleon parameter space. In order to compute predictions of the chameleon model, the scalar field profile has to be determined by solving the Klein-Gordon equation (4.1.4). Assuming the spherical symmetry in a Minkowski background $g_{\mu\nu} \simeq \eta_{\mu\nu}$[(5)], an approximation that is valid if the Newtonian gravitational potential is small

[(5)] More symmetries have been considered in [Mota07] for instance.

everywhere and if the backreaction due to the density on ϕ remains small [Khoury04a], the Klein-Gordon equation reads (4.1.4),

$$\phi'' + \frac{2}{r}\phi' = \frac{\mathrm{d}V_{\rm eff}}{\mathrm{d}\phi}, \qquad \frac{\mathrm{d}V_{\rm eff}}{\mathrm{d}\phi} = \frac{\mathrm{d}V}{\mathrm{d}\phi} + \tilde{\rho}A^3\frac{\mathrm{d}A}{\mathrm{d}\phi}, \tag{4.2.4}$$

the prime denoting a radial coordinate derivative. Since the relativistic effects are negligible in lab experiments, metric potentials arising in static and spherically symmetric spacetime (see $\nu(r)$ and $\lambda(r)$ in Eq. (2.3.1)) and pressure are assumed to be negligible. The radial profile of the chameleon field $\phi(r)$ can be solved either analytically (see App. C.1) or numerically (see Sec. 4.4 for an example of such numerical method) provided two boundary conditions[(6)],

$$\phi'(r=0) = 0, \tag{4.2.5}$$

$$\phi(r \longrightarrow \infty) = \phi_{\rm min}(\rho_\infty), \tag{4.2.6}$$

the chameleon field being settled to its attractor that is the minimum of its effective potential, at spatial infinity.

The fifth force mediated by the chameleon then reads,

$$\mathbf{F}_\phi = -\frac{m_{\rm test}}{M}\nabla\phi \qquad \Rightarrow \qquad \mathbf{a}_\phi \equiv \frac{\mathbf{F}_\phi}{m_{\rm test}} = -\frac{1}{M}\nabla\phi, \tag{4.2.7}$$

where $m_{\rm test}$ is the mass of the test particle and a_ϕ the acceleration induced by the chameleon. If the scalar field is weakly coupled to matter, the scalar field profile varies like $a_\phi \propto 1/(r^2M^2)$ outside the source mass (see Eq. (C.1.14) for the analytical formula) whereas $a_\phi \propto 1/(r^2M)$ in the strongly coupled case (see Eq. (C.1.23) for the analytical formula). Computing the ϕ profile allows to compare the fifth force mediated by the chameleon to the experimental bounds on the strength of the fifth force α and its length of interaction λ (see Eq. (3.2.51) where $\mathbf{F}_\phi \equiv -\nabla V$ for the definition of the parameters α and λ). At fixed length of interaction, roughly $\lambda \sim 10$ cm - 1 m for lab experiments, the strength of interaction α is constrained [Khoury04a] (see Fig. 3.2).

Fifth force test between two macroscopic objects like the Eöt-Wash experiment using torsion pendulum [Kapner07, Upadhye12b] gave rise to lower bound $|\alpha| < 1$ up to $\lambda = 56$ μm at 95 % C.L., enabling to rule out a part of the parameter space [Adelberger07, Upadhye12a] for $\beta \sim 1$. The experimental bounds obtained by Upadhye [Upadhye12a] with a torsion pendulum are reported in Fig. 4.4. Casimir forces experiment has been also used in order to test the fifth force by measuring the chameleon pressure between two parallel plates in the presence of a medium, e.g. a gas between the plates, affecting the chameleon field [Brax07b, Brax10]. However, the separation between the two plates have to be relatively large, around 10 μm so that the electrostatic potential is not uniform between the plates. The experiment is thus not straightforward and the total force between the two plates is rather measured as a function of the gas density inside the cavity [Brax10].

[(6)] To be more precise it is necessary to take into account the Yukawa suppression of the fifth force, the second border condition being rather given by Eq. (4.4.2).

However, such experiments testing fifth force between two macroscopic objects are not able to probe $\beta \gg 1$. In order to probe the extremely strongly coupled chameleons the fifth force searches between a macroscopic body and a microscopic one, e.g. cold neutrons, appear to be powerful [Brax11b, Brax13c, Jenke14]. In this case, only the macroscopic body is screened while the cold neutrons may have no thin shell. In the first experiment, ultracold neutrons are bouncing above a mirror. Considering bouncing of the order of mm, neutrons exhibit quantum behavior, their energy levels being discrete, and appear to be unscreened [Brax11b]. The chameleon introduces a shift in the quantum gravitational potential, possibly detected by neutron bouncing experiment [Brax11b]. While fifth force searches between two macroscopic bodies give rise to upper bound on β, neutron experiments to lower bounds. The current experimental constraint for $\Lambda \sim 2.4 \times 10^{-12}$ GeV are [Jenke14],

$$\beta < 5.8 \times 10^8 \qquad \text{for} \qquad -2 \leq \alpha \leq 2 \quad (95\,\%\ \text{C.L.}). \tag{4.2.8}$$

A second set-up has been proposed using neutron interferometry [Brax13c, Li16]. Their experimental constraints are even more stringent. They are reported in Tab. 4.1 and represented in Figs. 4.4 and 4.3.

Many other experimental tests of the chameleons have been proposed so far [Ivanov13, Brax11a, Shih74, Shih75, Anderson88, Sukenik93, Baumgärtner10, Harber05, Kasevich91, Cronin09, Harber05]. Some of them were realized in space where the ambient density is weaker, the thin shell being thus easier to reach [Joyce15, Khoury04a, Elder16]. The list of experiments presented in this section is not exhaustive, though leaving a part of the parameter space unconstrained.

In the rest of this chapter, we will focus on one lab experiment based on atom interferometry, proposed by Burrage et al. [Burrage15] in 2014 and realized by [Hamilton15] in 2015. This experiment offers the best bounds on the chameleon parameter space from now, as reported in Figs. 4.3 and 4.4. Like the neutrons, individual atoms are sufficiently small to let the scalar field unscreened even if their nuclei are dense. Cold atom interferometry experiments were developed recently for measuring the Newton's constant $G_{\rm N} = 6.67 \times 10^{-11}\ \mathrm{m^3\ kg^{-1}\ s^{-2}}$ with very good accuracy [Fixler07, Lamporesi08], the statistical uncertainty being given by $\pm 0.011 \times 10^{-11}\ \mathrm{m^3\ kg^{-1}\ s^{-2}}$ while the systematic uncertainty $\pm 0.003 \times 10^{-11}\ \mathrm{m^3\ kg^{-1}\ s^{-2}}$ [Lamporesi08]. Using laser-cooled atoms in a vacuum tube, the acceleration of the atoms due to the presence of a source mass was measured outside the tube. From the knowledge of the mass distribution of the source mass, $G_{\rm N}$ was determined according to the Newtonian gravitational force.

The experimental setup proposed by Burrage et al. [Burrage15] is based on similar atom interferometry experiments while the source mass is now inside the vacuum chamber. It consists in measuring the additional acceleration on individual atoms, due to the scalar field gradient induced by the presence of a source mass at the center of the chamber (see also Sec. 4.3). Forecasts provided

α	1	2	3	4	5	6
$\beta_{\rm lim} \times 10^6$	4.7	8.2	12.7	17.9	20.4	23.8

Table 4.1: Experimental bounds obtained using neutron interferometry. $\beta_{\rm lim}$ corresponds to the upper bounds on β at $95\ \%$ C.L. [Li16].

in [Burrage15] and the first experimental results obtained by [Hamilton15], highlight the fact that most of the remaining part of the chameleon parameter space corresponds to the case where the chameleon field is weakly coupled to matter, i.e. for $M/m_{\rm pl} \sim 1$ (see Figs. 4.3 and 4.4).

In the rest of this chapter, we will provide numerical simulations for the chameleon profile and acceleration measured by the Berkeley experiment. The experimental setup is briefly reviewed in Sec. 4.3 and the numerical strategy is detailed in Sec. 4.4. Numerical results are presented in Sec. 4.5 for the thin shell regime (we report the reader to [Schlögel16] for a discussion about the weak field regime) where they are compared to analytical results reviewed in App. C.1. We finally discuss our results and draw some conclusions and perspectives in Sec. 4.6.

4.3 Experimental setup of the Berkeley experiment

In the last decade, the chameleon model has been tested thanks to cosmological and astrophysical observations, as well as lab experiments, using neutron and atom interferometry. As we can see in Figs. 4.3 and 4.4, the atom interferometry experiment performed in Berkeley provides the most stringent constraints on the parameter space of the chameleon model today, for large β or small M. Those results were obtained by measuring the acceleration induced by the chameleon field on cesium-133 atoms inside a ultra-high vacuum chamber in the presence of a source mass. We will here explain in more detail this experimental setup [Hamilton15].

According to quantum mechanics cesium-133 atoms exhibit matter-wave properties in a Fabry-Perot cavity. When an atom absorbs/emits a photon, it recoils with a momentum $p = \hbar k$, with k the wave number of the absorbed/emitted photon. So, one can reproduce the equivalent of a Mach-Zehnder interferometer represented in Fig. 4.6 for cold atoms with three light pulses using counter-propagating laser beams. Atoms are initially prepared in a hyperfine state $F = 3$ and stored in a 2 dimensional magneto-optical trap. A first light pulse splits the matter-wave packet in two hyperfine states $F = 3$ and $F = 4$ (see the beamsplitter (1) in Fig. 4.6) and gives an impulse of $\hbar k_{\rm eff}$ to the atoms. The effective wave number $k_{\rm eff}$ depends on the two counterpropagating beam wave numbers. The probability of hyperfine transition can be controlled by the intensity and duration of both laser beams. The second pulse reverses the relative motion of the beams like the mirror of Mach-Zehnder interferometer (see the mirrors (2) and $(2')$ in Fig. 4.6) and the third pulse acts

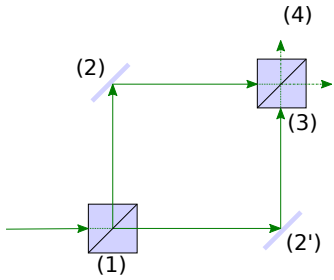

Figure 4.6: Illustration of the Mach-Zehnder interferometer. The incident beam goes through the beamsplitter (1). The two resultant beams are reflected on mirrors (2) and (2') and are recombined by the beamsplitter (3). A detector measures the fringes of interference in (4).

like a beam splitter which allows overlap of partial matter wave packets (see the beamsplitter (3) in Fig. 4.6). Because of the recoil of the atoms, the phase difference between the two arms of the interferometer $\Delta\phi$ is a function of the acceleration a of atoms,

$$\Delta\phi = k_{\rm eff} a T^2, \tag{4.3.1}$$

where $T \sim 10\,\mathrm{ms}$ in general, is the time interval between two pulses. To alleviate some systematics effects, counterpropagating laser beams are reversed and the aluminum sphere can be positioned in two places: a *near* and a *far* positions (the source mass surface is respectively located 8.8 mm and 3 cm far from the atoms), which allows to disentangle the contribution from chameleon force to Earth's gravity. One measurement consists thus of four interference fringes, corresponding to reversed counterpropagating laser beams and both positions of the source mass. Using this setup, the acceleration induced by the chameleon has been excluded up to

$$a_{\rm exp} < 5.5\,\mu\mathrm{m/s^2} \quad \Leftrightarrow \quad \frac{a_{\rm exp}}{g} < 5\times10^{-7} \qquad \text{at } 95\%\text{ C.L.}, \tag{4.3.2}$$

with g the Earth's acceleration of free fall. As a comparison, the Newtonian gravitational attraction due to the source mass is $a_{\rm N}/g(r = 8.8\ \mathrm{mm}) = (G_{\rm N} m_{\rm A}/r^2)/g\big|_{r=8.8\ \mathrm{mm}} = 2.25\times10^{-10}$ at the position where the acceleration of the atoms is measured. Since it is more than two orders of magnitude below the current experimental sensitivity, the gravitational acceleration due to the source mass is neglected.

The experimental setup proposed in [Burrage15] is similar, except that they plan to use cooled rubidium atoms launched in a small fountain located 1 cm far from the source mass. Our numerical simulations can be easily adapted for such a configuration. Details of the considered experimental setup are reported in Table 4.2. The size and density of the central mass, the geometry of the chamber and the vacuum density are those of [Hamilton15, Burrage15]. In addition we consider the thickness and density of the vacuum chamber

$R_{\rm A}$	Radius of the source mass	$1{\rm cm}/5.1\times10^{13}{\rm GeV}^{-1}$
L	Radius of the chamber	$10{\rm cm}/5.1\times10^{14}{\rm GeV}^{-1}$
$R_{\rm w}$	Wall thickness	$1{\rm cm}/5.1\times10^{13}{\rm GeV}^{-1}$
$m_{\rm A}$	Test mass	$11.3{\rm g}\ /6.7\times10^{24}{\rm GeV}$
$\rho_{\rm A}$	Test mass density	$1.2\times10^{-17}{\rm GeV}^4$
$\rho_{\rm w}$	Wall density	$3.5\times10^{-17}{\rm GeV}^4$
$\rho_{\rm v}$	Vacuum density	$5.0\times10^{-35}{\rm GeV}^4$
$\rho_{\rm atm}$	Air density ($P_{\rm atm}$)	$5.2\times10^{-21}{\rm GeV}^4$

Table 4.2: Fiducial experimental parameters, corresponding to the setup of [Hamilton15] .

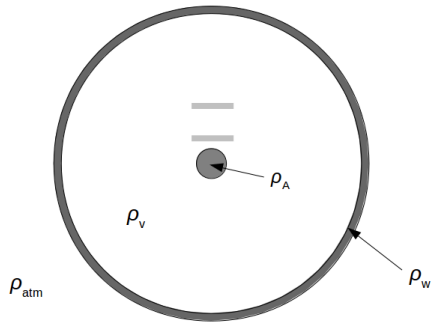

Figure 4.7: Outline of the atom-interferometry experiment, simulated by a four-region model including the source mass, the vacuum chamber, its wall and the exterior environment. In light gray, the *near* and *far* positions where the acceleration on atoms is measured (note that we consider a fixed source mass to keep spherical symmetry whereas in the real experimental setup the source mass is moved [Hamilton15]) .

wall, as well as the exterior density. In Fig.4.7, we draw the experimental setup considered in our numerical simulations. The four regions are labeled by their densities: (1) the source mass made of aluminum (ρ_A), (2) the vacuum where the acceleration due to the chameleon is measured ($\rho_{\rm v}$), (3) the wall of the chamber ($\rho_{\rm w}$) made of stainless steel, (4) the exterior of the chamber, mostly filled by air at atmospheric pressure ($\rho_{\rm atm}$).

4.4 Numerical strategy

Analytical approaches have been considered so far [Burrage15, Hamilton15], which are valid under some theoretical assumptions like static approxima-

tion[7], Minkowski background spacetime, the linearization of the solution (see also [Mota07] for a discussion), the coupling function $A(\phi) \sim 1$, and experimental ones like negligible chamber wall effects. Numerical methods enable to (in)validate those assumptions and to refine analytical results, by including the effects due to the experimental setup, like the thickness and the density of the wall as well as the exterior environment. In the future, numerical results will be also helpful to study more realistic situations where the vacuum chamber is not exactly spherical or cylindrical (see e.g. [Elder16]).

We consider two methods for solving the KG equation (4.2.4): a singular and multipoint boundary value problem (BVP) solver with unknown parameter and a non-linear BVP solver implementing up to sixth order a mono-implicit Runge-Kutta method with an adaptative mesh refinement, working in `quad` precision[8]. In the latter case, the density in the four regions was made continuous by considering arctan profiles with negligible widths. The requirement of the `quad` precision in order to solve the Klein-Gordon equation reveals the strongly fine-tuned nature of chameleon physics.

We take the minimal assumption which states that the scalar field is settled to its attractor at spatial infinity, i.e. $\phi_\infty = \phi_{\rm min}(\rho_{\rm atm})$ as [Hamilton15]. Then, the asymptotic scalar field profile is obtained by linearizing the KG equation up to first order around spatial infinity,

$$\phi'' + \frac{2}{r}\phi' = \mathcal{M}^2 \left(\phi - \phi_\infty\right), \tag{4.4.1}$$

with $\mathcal{M}^2 = \mathrm{d}^2 V_{\rm eff}/\mathrm{d}\phi^2\big|_{\phi=\phi_\infty}$, which admits the Yukawa profile solution ($\mathcal{M}^2 > 0$)

$$\phi = \phi_\infty + \frac{\mathcal{C}\mathrm{e}^{-\mathcal{M}r}}{r}, \tag{4.4.2}$$

with $\mathcal{C}$ the constant of integration. Since the KG equation is of second order and the parameter $\mathcal{C}$ is to be determined, three boundary conditions are needed. They are provided by the regularity condition on the scalar field derivative at the origin $\phi'(r = 0) = 0$ and by the asymptotic behavior of ϕ and ϕ' given by Eq.(4.4.2) at the end of the integration interval. For the multipoint BVP method, the continuity of ϕ and ϕ' are imposed at the interfaces of each region (6 conditions) while the profile is guaranteed to be continuous for arctan profiles of density. The density and size of each region are reported in Table 4.2. The two numerical methods have been checked to be in agreement with each other. Their applicability to the various regimes and their limitations in the deep thin-shell regime will be discussed in Sec. 4.5. We already point out that this numerical method enables one to properly account for the effect of neighboring matter on the chameleon fields and can be easily generalized to other experiments, possibly more sensitive (in the limit of spherical symmetry).

[7] A numerical method for studying screening mechanisms in cosmology beyond the quasistatic approximation has been proposed in [Llinares13].

[8] For this purpose we have used the Matlab function `bvp4c` which deals with singular BVP's and a modified version of the `mirkdc` BVP solver with adaptative mesh in Fortran.

4.5 Four-region model: numerical results

As we can see in Figs. 4.3 and 4.4, the atom interferometry experiment enables to probe the chameleon models for relatively small M (or large β), i.e. in the thin shell regime or the so-called strongly perturbing regime (see App. C.1 for the mathematical definition). In this regime, the chameleon field is screened in the source mass. On the contrary, the chameleon is unscreened inside the source mass is the so-called weak field regime. The analytical solutions in those two limit cases are reported in App. C.1. As we will see, the numerical treatment allows one also to probe the transitory regime between the weakly and strongly perturbed cases in addition to refine analytical constraints.

Since the original chameleon model has been already ruled out by the combined constraints on cosmological and PPN parameters [Hees12a], we will mainly focus on the exponential chameleon. We report thus the reader to our paper [Schlögel16] for the complete numerical results, in particular in the weak-field regime.

However, probing the deep thin-shell regime, i.e. for very small values of M, is very challenging numerically because the problem becomes stiff, the chameleon physics being strongly fine-tuned. Up to some point, it is nevertheless possible to track the solution and to check the validity of the analytical estimations, typically using mesh refinement methods. Since the original model is easier to probe we briefly discuss our results in the thin-shell regime.

4.5.1 The original model

The numerical scalar field and acceleration profiles for several values of M considering the original chameleon model are represented in solid lines in Figs. 4.8a and 4.8b, the dashed lines corresponding to the analytical calculations reported in App. C.1. The shaded region indicate the upper bound on the acceleration (4.3.2), the atom interferometry being thus able to rule out the original chameleon model in the strong field regime. This result is in agreement with the analytical analysis (see the Case (3) in App. C.1).

As expected from Eq. (4.1.10) given that $\rho_{\rm A} \lesssim \rho_{\rm w}$ with similar source mass radius and wall thickness, when lowering M, the field reaches first the potential minimum $\phi_{\rm min}(\rho_{\rm w})$ inside the wall, and then $\phi_{\rm min}(\rho_{\rm A})$ within the source mass, over a very thin radius. Analytical results appear to be in good agreement with the numerical ones, especially close to the source mass where a_ϕ is measured whereas important deviations are found close to the wall. In particular, one observes that the field roughly reaches the amplitude of the central value of the scalar field in the absence of the source mass $\phi_{\rm bg}$ given by Eq. (C.1.24) inside the vacuum chamber, which validates the analytical calculation of [Burrage15] (see App. C.1 for the details). In the vicinity of the chamber wall, however, the acceleration changes its sign and becomes negative, with a comparable magnitude with the acceleration close to the source mass. This effect could be helpful experimentally to discriminate between a signal of

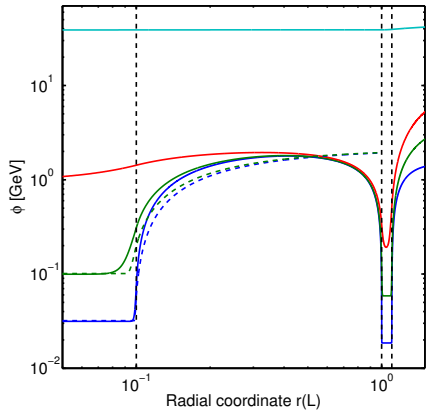

(a) Scalar field profile ϕ.

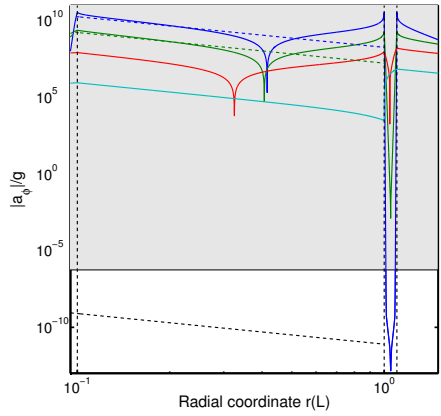

(b) Acceleration profile $|a_\phi|/g$. The numerical profile for the four-region model shows that from the middle of the chamber to the wall, the acceleration becomes negative and increases in magnitude. The Newtonian gravitational attraction due to the test mass is plotted in black dashed line.

Figure 4.8: Numerical results (solid lines) and analytical approximation (dashed lines) for the original model, in the *strongly perturbing* (thin shell) regime, for $\Lambda = 2.6 \times 10^{-6}$ GeV and values of the coupling M listed in Table 4.3. Differences between the two-region and four-region models are non-negligible inside the chamber, especially in the vicinity of the wall. Vertical lines mark out the four regions (source mass, chamber, wall and exterior).

Color	M [GeV]	a_ϕ/g (*near*)	a_ϕ/g (*far*)
Original chameleon, *thin-shell*: Figs. 4.8a, 4.8b			
Blue	10^8	5.8×10^9	1.4×10^8
Green	10^9	5.2×10^8	5.7×10^6
Red	10^{10}	1.9×10^7	-4.4×10^6
Light blue	10^{11}	2.5×10^5	5.5×10^4
Exponential chameleon, *thin-shell*: Figs. 4.10a, 4.10b			
Blue	10^{14}	5.2×10^{-7}	1.5×10^{-8}
Green	10^{15}	5.2×10^{-8}	1.5×10^{-9}
Red	10^{16}	5.2×10^{-9}	1.5×10^{-10}
Light blue	10^{17}	5.2×10^{-10}	1.5×10^{-11}
Purple	10^{18}	5.3×10^{-11}	2.4×10^{-12}
Beige	10^{19}	4.6×10^{-12}	6.8×10^{-14}

Table 4.3: Properties of the numerical scalar field and acceleration profiles for the two models in the different regimes.

modified gravity and systematic errors, by performing measurements of the acceleration at several key positions of the chamber.

4.5.2 The exponential model

For the exponential model and the considered experimental set-up, it has been impossible to track numerically the thin-shell regime up to the point where the acceleration would have been large enough to be observed in laboratory experiments. Nevertheless, the field and acceleration profiles are represented in Figs. 4.9a and 4.9b, for $M = 10^{17}\mathrm{GeV}$ and increasing values of ρ_w and ρ_A. The attractor field values within the source mass and the wall are reached progressively and the field variations at the borders between the four regions become more steep, as expected given that $(R_{\mathrm{A,w}} - S_{\mathrm{A,w}})/R_{\mathrm{A,w}} \propto M\rho_{\mathrm{A,w}}^{-1}R_{\mathrm{A,w}}^{-2}$ (see Eq. (C.1.22)). In the case $M = 10^{17}\mathrm{GeV}$, the attractor is reached inside the source mass for $\rho_\mathrm{A} \simeq 5 \times 10^{-20}\mathrm{GeV}^4$, i.e. about 1000 times lower than the aluminum density, whereas inside the wall, it is reached for $\rho_\mathrm{w} \simeq 7.5 \times 10^{-20}\mathrm{GeV}^4$. This slight difference is explained by the fact that the central source mass has a diameter two times larger than the wall thickness.

Inside the vacuum chamber, the analytical estimation is roughly recovered in the first half of the chamber. Once in the thin-shell regime, one can also observe that the field and acceleration profiles inside the chamber are independent of the wall and mass densities, except at their immediate vicinity. Therefore, in the deep thin-shell regime, the scalar field and acceleration both at the *near* and *far* positions of the interferometer do not depend on the source mass and wall densities and sizes, neither on the exterior environment. In order to obtain the numerical solution inside the chamber, down to low values of M, one can therefore use the trick to set the wall and mass densities high

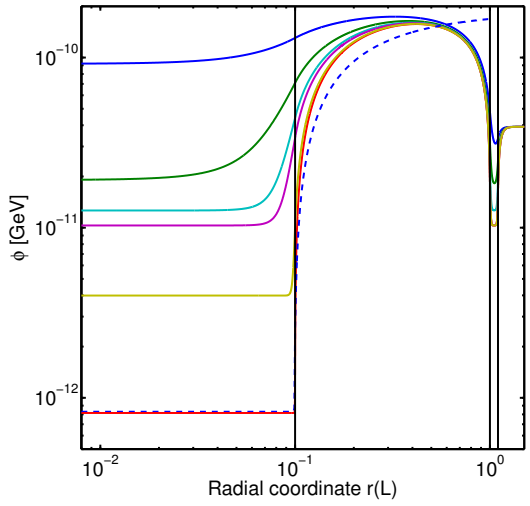

(a) Scalar field profile ϕ.

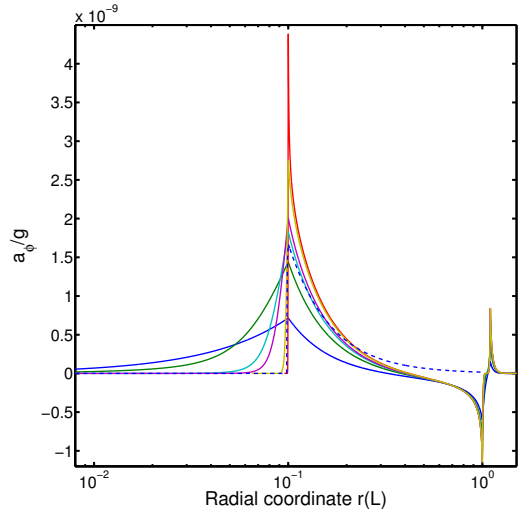

(b) Acceleration profile $|a_\phi|/g$.

Figure 4.9: Numerical results (solid lines) and analytical approximation (dashed line) for the exponential model, for various $\rho_{\rm A}$ and $\rho_{\rm w}$ reported in Tab. 4.4, $M = 10^{17}$ GeV being fixed.

Color	$\rho_{\rm A}$ $\left[\mathrm{GeV}^4\right]$	$\rho_{\rm w}$ $\left[\mathrm{GeV}^4\right]$
Blue	1.0×10^{-20}	1.0×10^{-20}
Green	2.5×10^{-20}	2.5×10^{-20}
Light blue	5.0×10^{-20}	5.0×10^{-20}
Purple	7.5×10^{-20}	7.5×10^{-20}
Beige	5.0×10^{-19}	7.5×10^{-20}
Red	1.2×10^{-17}	7.5×10^{-20}

Table 4.4: Densities inside the source mass $\rho_{\rm A}$ and the wall $\rho_{\rm w}$ for the numerical scalar field and acceleration profiles of Figs. 4.9a and 4.9b.

enough to be in the thin-shell regime but low enough for the field profile to be numerically tractable through the borders of the four regions. As an example, for $M = 10^{17}$ GeV, the numerical solution is tractable for the real source mass density whereas the wall density has been adapted ($\rho_{\rm w} = 7.5 \times 10^{-20}$ GeV^4 instead of 3.5×10^{-17} GeV^4) (see the red curves in Figs. 4.9a and 4.9b).

The field and acceleration profiles have been calculated numerically and compared to the analytical results, for several values of M and $\Lambda \simeq 2.4$ meV. These are represented in Figs. 4.10a and 4.10b. As expected the profiles have the same behavior as for the original model (see Figs. 4.8a and 4.8b). Close to the source mass, one recovers the analytical estimation but one can nevertheless notice differences higher than 20%.

Close to the wall, the acceleration becomes negative, and its amplitude reaches values comparable to the acceleration at a position close to the source mass, which is a potentially measurable prediction that could be useful to discriminate between experimental systematic effects and an acceleration induced by the presence of some scalar field.

In conclusion, we find that the atom-interferometry experiment of [Hamilton15] has already excluded values of the coupling parameter $M \lesssim 10^{14}$ GeV at 95% C.L.[(9)]. Moreover, if the experimental sensitivity could be reduced down to $a_\phi/g \sim 10^{-11}$ (as it is claimed to be feasible in [Burrage15]), the model would be probed nearly up to the Planck scale. Finally, note that the typical field values reached inside the chamber are too low to induce large deviations from $A(\phi) \simeq 1$, which implies that our results are roughly independent of the power-law index α.

4.5.3 Chamber geometry effects

The numerical method developed in this chapter takes into account the effects of the chamber geometry, in the limit where the vacuum chamber is spherical. Exploring various chamber size and wall density, we propose to consider the possibility to realize the same atom interferometry experiment in a vacuum

[(9)] In [Elder16] they found $M < 2.3 \times 10^{-5}\ M_{\rm pl}$.

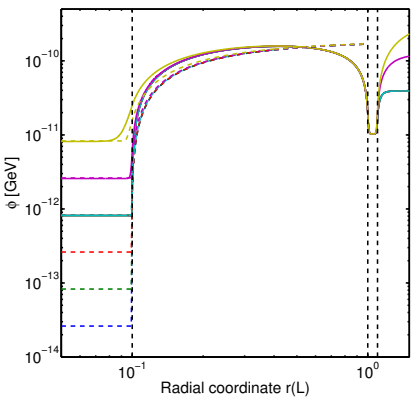

(a) Scalar field profile ϕ. Noticeable deviations from the analytical estimation are observed inside the chamber, due to the wall effects.

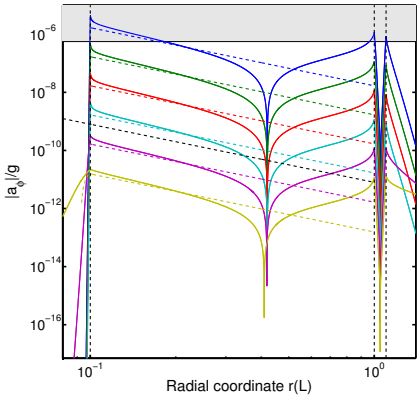

(b) Acceleration profile $|a_\phi|/g$. Strong discrepancies are observed between the four-region (numerical) and the two-region (analytical) models in the vicinity of the wall. The Newtonian gravitational attraction due to the test mass is plotted in black dashed line.

Figure 4.10: Numerical results (solid lines) and analytical approximation (dashed lines) for the exponential model, in the *strongly perturbing* (thin shell) regime, for $\Lambda = 2.4 \times 10^{-12}$ GeV and values of the coupling M listed in Table 4.3. The source mass, wall and exterior densities have been adapted for making the profile numerically tractable, with no effect inside the vacuum chamber (apart in the immediate vicinity of the borders), as explained in Sec. 4.5.2. The ratios M/ρ were kept constant (with the same value as for the red curve of Fig. 4.9a), which fixes the thin-shell radius, apart for $M = 10^{18}$GeV (purple) and $M = 10^{19}$GeV (beige) for which only the wall density was adapted. Vertical lines mark out the four regions (source mass, chamber, wall and exterior).

room in order to make the test of M values up to the Planck scale possible in the near future. The largest vacuum rooms have a radius larger than $R = 10$ m and their walls made of concrete are sufficiently large such that the field reaches its attractor inside the walls. One can thus neglect the exterior of the chamber (see Sec. 4.5). The vacuum room can sustain a vacuum around 10^{-6} Torr (we assume $\rho_{\rm v} = 5 \times 10^{-31}{\rm GeV}^4$), low enough to prevent $\phi_{\rm bg}$ to reach its effective potential minimum in vacuum.

Numerical field and acceleration profiles are reported in Figs. 4.11a and 4.11b respectively. Assuming as before $\rho_{\rm A} = 1.2 \times 10^{-17}$ GeV^4, it results that a source mass of 1 cm radius only enables to probe the regime where the field does not reach $\phi_{\rm A}$ inside the source mass (see dashed green lines on Figs. 4.11a and 4.11b), the acceleration being thus poorly constrained. However, provided that the source mass radius is larger (e.g. $R_{\rm A} = 3.3$ cm), the strongly perturbing regime is reached and the acceleration is large enough to be measurable in the near future for M of the order of $m_{\rm pl}$. As a result, for $M = m_{\rm pl}$, $|a_\phi|/g = 2.4 \times 10^{-10}$ at 8.8 mm from the surface of the source mass (the previously called *near* position in Sec. 4.3) while $|a_\phi|/g = 5.7 \times 10^{-10}$ for $M = 0.1\ m_{\rm pl}$. In comparison, the source mass of 1 cm gives rise to $|a_\phi|/g = 1.7 \times 10^{-11}$ for $M = m_{\rm pl}$.

Similarly to what was obtained in Secs. 4.5.1 and 4.5.2, the thin shell regime cannot be tracked numerically if the wall density is of the order of the concrete $\rho \sim 10^{-17}$ GeV^4. But one can safely consider lower values of $\rho_{\rm w}$ (see Fig. 4.11a) without any significant change of the results inside the vacuum room.

4.6 Conclusion

The chameleon screening mechanism is able to suppress the fifth force induced by a scalar field in locally dense environment, while allowing the scalar field to be responsible for the current cosmic acceleration on large astrophysical scales and thus to affect significantly the LSS formation. Since chameleon models have not been already ruled out for their entire parameter space, they are still viable candidates for explaining the current cosmic acceleration. By the way, they will be tested by future cosmology-dedicated experiments, such as Euclid [Amendola13, Amendola16] or the next generation of giant radio-telescopes dedicated to 21 cm cosmology [Brax13a]. Chameleon theories are also well constrained by local tests of gravity in the Solar System, in the galaxy, as well as in laboratory. Recently it has been proposed to use an atom-interferometry experiment to constrain chameleon models with an unprecedented accuracy by probing the acceleration induced by the presence of the scalar field on cold atoms. The experiment is realized inside a vacuum chamber in order to reduce the screening effect, and a central mass is used to source some field gradient. Forecasts were calculated in [Burrage15] and a first experimental setup was built and used to establish new constraints on the chameleon model [Hamilton15]. However, the calculations of the field

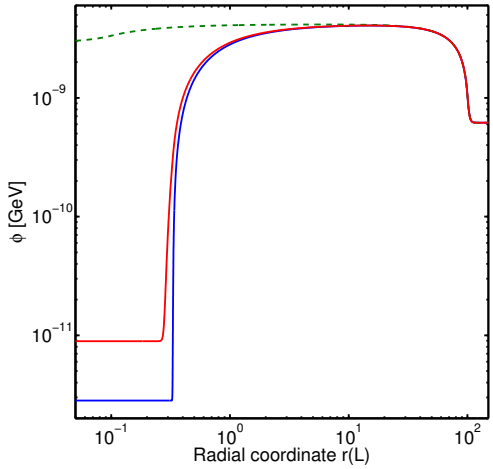

(a) Scalar field profile ϕ.

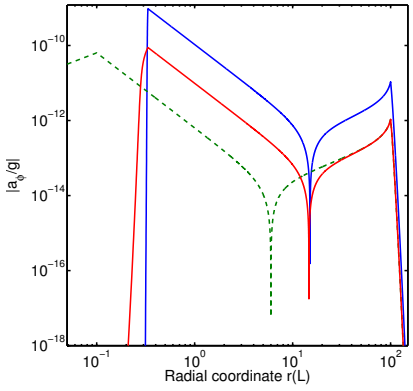

(b) Acceleration profile $|a_\phi|/g$.

Figure 4.11: Numerical profiles for a vacuum room ($L = 10$ m). The green dashed curve is obtained for a test mass of $R_{\rm A}$ =1 cm with $M = m_{\rm p}$ ($\rho_{\rm w} = 2.5\times10^{-21}\,{\rm GeV}^4$) while the blue and the red ones are obtained for $R_{\rm A} = 3.3$ cm with $M = 0.1 \times m_{\rm p}$ ($\rho_{\rm w} = 2.5 \times 10^{-22}\,{\rm GeV}^4$) and $M = m_{\rm p}$ ($\rho_{\rm w} = 2.5 \times 10^{-21}\,{\rm GeV}^4$) respectively. We only consider a three regions model, neglecting the effect of the exterior of the vacuum room (see discussion in Sec. 4.5).

and acceleration profiles rely on several approximations, and until now had not fully considered the effects of the vacuum chamber wall and of the exterior environment.

The purpose of this work was to refine and eventually validate previous calculations, by using a numerical approach consisting in solving the Klein-Gordon equation in the static and spherically symmetric case for a four-region model representing the central source mass, the vacuum chamber, its wall, and the exterior environment. Three boundary conditions are imposed: the field must be regular at the origin and reach the minimum of the effective potential with a Yukawa profile, at large distance in the exterior environment. Our method allows one to probe the transition between the regime where the central source mass only weakly perturbs the field configuration, and the thin-shell regime where the field inside the central mass and inside the chamber wall reaches the minimum of the effective potential over a very small distance. Two typical chameleon potentials were considered, in inverse power-laws and allowing varying powers, as well as a standard exponential form for the coupling function.

In the weakly perturbing regime, it is found that the chamber wall enhances significantly the scalar field inside the vacuum chamber and reduces the induced acceleration, by up to one order of magnitude compared to previous analytical estimations and with a maximal effect close to the wall (see [Schlögel16] for details).

Going to the thin-shell regime, for our fiducial experimental setup, the field reaches the attractor inside the chamber wall and the exterior environment becomes thus irrelevant. However, for reasonable value of the induced acceleration, the field inside the vacuum chamber does not reach the minimum of the effective potential and is instead related to the size of the chamber, as first noticed in [Burrage15]. Our analysis refines the field and acceleration profiles in the chamber and highlights noticeable deviations from the analytical estimation, which is nevertheless roughly recovered close to the central source mass. Close to the chamber wall, the acceleration becomes negative, with a magnitude similar to the one close to the central mass. We argue that this prediction could be useful to distinguish between systematic effects and fifth-force effects which should be *maximal and opposite close to the central mass and to the wall*, and should vanish roughly at the middle distance between the source mass and the wall.

Refined constraints have been derived on the coupling parameter M from the atom-interferometry experiment of [Hamilton15]. For the chameleon potential $V(\phi) = \Lambda^{4+\alpha}/\phi^{\alpha}$ and a coupling function $A(\phi) = \exp(\phi/M)$, one finds $M \gtrsim 7 \times 10^{16}$ GeV, independently of the power-law. For the bare potential $V(\phi) = \Lambda^4(1+\Lambda/\phi)$, we find that $M \gtrsim 10^{14}$ GeV. We have also confirmed that a future experiment reducing its sensitivity down to $a \sim 10^{-10}\mathrm{m/s^2}$ would be able to rule out most of the parameter space of the latter model, nearly up to the Planck scale.

Finally, we have proposed to realize a similar atom-interferometry exper-

iment inside a vacuum room. The density inside such rooms is low enough for the field profile and the induced acceleration to depend only on the size of the room. If the room radius is larger than about 10 meters, we find that the chameleon model could be probed up to the Planck scale. Nevertheless, further work is needed to implement realistic non-spherical geometries of the room (or of the vacuum chamber).

We conclude that numerical results will be helpful in the future in order to establish accurate bounds on various modified gravity models. In particular, the effects of the vacuum chamber wall and its exterior environment cannot be neglected. Our numerical method is easily extendable to study other forms of the field potential and other modified gravity models requiring a screening mechanism, such as the symmetron, dilaton and f(R) models. Finally, it can be easily adapted to other experiments.

We point out that relaxation numerical methods have also been developed for modeling the same experiment. We developed a code based on [Ringeval05] and Elder et al. also proposed a relaxation method on a uniform grid [Elder16]. The advantage of this numerical method is its adaptability to various geometry (whereas the mesh refinement method is based on the spherical symmetry) requiring to solve partial differential equations rather than ordinary differential equations. Both results are compatible. In addition Elder et al. propose a space-based experiment in order to prolong the time spent by the atoms near the source mass [Elder16]. The acceleration at 2 mm far from the source mass is then of the same order of magnitude as on the Earth,

$$a_\phi = 2.7 \times 10^{-3} \frac{M_{\rm pl}}{M} \mu{\rm m/s}^2, \tag{4.6.1}$$

with a longer interaction time between the source mass and the atoms. Following [Elder16], such a set-up would in principle be sensitive to the entire parameter space $M \lesssim M_{\rm pl}$, the same order of magnitude as that probed in a vacuum room.

Even more recently a novel experiment has been proposed using atom-interferometry where atoms are trapped between two parallel plates with different densities but the same total mass [Burrage16]. Such a set-up enables to subtract the gravitational background because, even if the field profile for the gravitational profile is symmetric, the chameleon field profile is not. This experimental setup could also probe the chameleon fifth force for smaller β (larger M) than the Berkeley one.

Chapter 5

The Higgs monopoles

based on

A. Füzfa, M. Rinaldi, S. Schlögel,
Particlelike distributions of the Higgs field nonminimally coupled to gravity
Phys. Rev. Lett. 111, 121103 (2013)

and

S. Schlögel, M. Rinaldi, F. Staelens, A. Füzfa,
Particlelike solutions in modified gravity: the Higgs monopole
Phys. Rev. D90: 044056 (2014)

In this chapter, we first discuss the possible relation between the Higgs field and gravity. Then we focus on the Higgs inflation model where the Higgs field is responsible at once for inflation and the elementary particle mass generation through the $SU(2)\times U(1)$ spontaneous symmetry breaking at electroweak scale. Because of the nonminimal coupling appearing in Higgs inflation, this model predicts nontrivial distribution of the Higgs field around compact object rather than the Higgs field settled to its vev everywhere. The underlying deviations from GR could rule out Higgs inflation, for instance if it does not fulfill Solar System constraints. We will see that Higgs inflation is indistinguishable from GR in the Solar System and around astrophysical compact objects, even if the distribution of the Higgs field is non trivial. Moreover, we will highlight the existence of a novel amplification mechanism of the Higgs field at the center of compact objects due to the combined effect of the nonminimal coupling and the Higgs potential.

5.1 Higgs field and gravity

A fundamental question still open today is the nature and the origin of the mass. In particle physics, gauge bosons and fermions have to be massless in order to preserve gauge invariance. In particular, the W and Z gauge bosons mediating the weak interactions appear to be massive since the weak interactions are short-range. In the SM, the Higgs field is responsible for the mass generation of elementary particles[(1)]. The most general potential which is renormalizable and gauge invariant under the electroweak symmetry $SU(2)_{\rm L} \times U(1)_{\rm Y}$ where L refers to the left chirality and Y to the hypercharge, is,

$$V(\mathcal{H}^\dagger\mathcal{H}) = \mu^2\mathcal{H}^\dagger\mathcal{H} + \lambda\left(\mathcal{H}^\dagger\mathcal{H}\right)^2, \tag{5.1.1}$$

with $\mathcal{H}$ the Higgs $SU(2)$ isospin doublet parametrized by,

$$\mathcal{H} = \begin{pmatrix} H^+ \\ H^0 \end{pmatrix} = \frac{1}{\sqrt{2}}\begin{pmatrix} H_1 + iH_2 \\ H_3 + iH_4 \end{pmatrix}, \tag{5.1.2}$$

μ the mass and λ the self-interaction parameters. Before the symmetry breaking arising in the early Universe, all elementary particles were massless and the local gauge invariance of the electroweak model was preserved. By allowing $\mu^2 < 0$, there is an infinite number of vacua connected together through the residual $U(1)$ symmetry such that the symmetry $SU(2)_{\rm L} \times U(1)_{\rm Y}$ is spontaneously broken while $U(1)_{\rm EM}$ remains invariant. By fixing the gauge to the unitary one ($H_1 = H_2 = H_4 = 0$), the complex Higgs doublet reduces to,

$$\mathcal{H} = \frac{1}{\sqrt{2}}\begin{pmatrix} 0 \\ v + H(x) \end{pmatrix}, \tag{5.1.3}$$

and the potential (5.1.1) reads,

$$V(H) = \frac{\lambda_{\rm sm}}{4}\left(H^2 - v^2\right)^2, \tag{5.1.4}$$

with $v = \sqrt{-\mu^2/\lambda_{\rm sm}}$ the Higgs vev and $\lambda_{\rm sm}$ the SM Higgs field self-interaction parameter. When the Higgs field is settled to its vev, elementary particles start to behave as they would have acquired a mass because of their coupling to the Higgs field, W and Z gauge bosons via covariant derivatives (the photon remains massless since $U(1)_{\rm EM}$ is unbroken), and fermions, through the Yukawa coupling. Since their masses are proportional to the vev, they depend on the local value of the scalar field.

This is not dissimilar to the Brans-Dicke theory (see Sec. 3.2) where the scalar field Φ is responsible for the variation of $G_{\rm N}$ over spacetime [Kaiser07]. In the late 1970s, Zee [Zee79, Zee80] and Smolin [Smolin79] proposed (independently) that a spontaneous symmetry breaking could be incorporated into

[(1)] Note that QCD interactions provide the additional mass arising from bounded microscopic states.

the theory of gravity. In [Zee79], Zee studied the action now referred to as induced gravity[2],

$$S = \int \mathrm{d}^4x\sqrt{-g}\left[\frac{\epsilon\phi^2}{2}R - \frac{1}{2}(\partial\phi)^2 + V(\phi)\right] + S_{\mathrm{M}}\left[\psi_{\mathrm{M}}; g_{\mu\nu}\right], \tag{5.1.5}$$

where ϕ is a Higgs-like real scalar field responsible for the relevant symmetry group breaking[3], $\epsilon \lesssim 1$ denotes a dimensionless nonminimal coupling and V the Mexican-hat potential,

$$V(\phi) = \frac{\lambda}{4}\left(\phi^2 - v^2\right)^2, \tag{5.1.6}$$

which ensures that $|\phi_{\min}| = v$. After the spontaneous symmetry breaking, the scalar field is anchored to its minimum and it generates the Newton's gravitational constant,

$$G_{\mathrm{N}} = \frac{1}{8\pi\epsilon v^2}. \tag{5.1.7}$$

The only dimensional constant G_{N} becomes dynamical and its weakness is explained provided that $v \sim m_{\mathrm{pl}}$. Assuming that ϕ is rigorously equal to the vev, no deviation from GR would be noticeable and the model passes all observational constraints. However, if $\mathrm{d}^2V/\mathrm{d}\phi^2 \neq 0$, then the scalar field acquires a mass and it can affect the dynamics. The Zee's theory looks like the Brans-Dicke one, excepted for the self-interaction term $V(\phi)$ which is precisely responsible for the symmetry breaking, and both SM and GR emerge as low-energy effective theories.

Zee noticed also that a similar theory invoking symmetry breaking with several scalar fields could explain the horizon problem [Zee80] by a weakening of G_{N} in the early Universe. One year later, Guth proposed the first inflationary model with a scalar field modelled on the Higgs one [Guth81]. In addition, since Linde's work about chaotic inflation [Linde83], we know that the Higgs field cannot lead to a viable inflationary model if the Higgs field is minimally coupled to gravity[4].

Induced gravity (5.1.5) has been studied a lot in the framework of cosmology, notably for inflation (see e.g. [Fakir90, Kaiser95]), considering λ and ϵ as free parameters. In such models, the scalar field (not yet identified to the Higgs field) is settled to its vev at the end of inflation in order to get the EH action with G_{N} fixed according to (5.1.7). Actually, if the SM Higgs field is considered as the inflaton in the framework of induced gravity, its mass is far too large to solve the horizon and flatness problems [Cervantes-Cota95]. In order to show this result explicitly, let us start from the induced gravity Lagrangian with the SM Higgs field,

$$L = \sqrt{-g}\left[\frac{\epsilon}{2}\mathcal{H}^\dagger\mathcal{H}R - \frac{1}{2}D_\mu\mathcal{H}^\dagger D^\mu\mathcal{H} - V\left(\mathcal{H}^\dagger\mathcal{H}\right) + \mathcal{L}_{\mathrm{SM}}\right], \tag{5.1.8}$$

[2] Induced gravity was first proposed by Sakharov in 1967 [Sakharov68].

[3] Zee considered the breaking of SU(5) to $SU(3) \times SU(2) \times U(1)$.

[4] No interaction between gauge bosons and inflaton is assumed in chaotic inflation. We will see that this assumption remains in Higgs inflation even if it is questionable.

where $D_\mu \mathcal{H}$ is the covariant derivative of $\mathcal{H}$ for the internal gauge group $SU(3)_{\rm C} \times SU(2)_{\rm L} \times U(1)_{\rm Y}$, the subscript C denoting the color quantum number. $\mathcal{L}_{\rm SM}$ contains the fermionic and massless bosonic fields of the SM, included the Yukawa coupling. Eq. (5.1.7) where v is the Higgs vev then yields to $\epsilon \sim 10^{40}$, highlighting the huge difference between the Planck scale and the vev. In order to get a viable inflationary scenario in terms of the scalar and tensor density perturbations amplitude, the Higgs mass must be very large, $m_{\rm H} \gg G_{\rm F}^{-1/2} \sim 300$ GeV, $G_{\rm F}$ being the Fermi constant, in disagreement with the observations, $m_{\rm H} = 125$ GeV [Olive14]. Moreover, the Higgs field decouples from bosonic and fermionic masses after the symmetry breaking, interacting mostly via gravity [Cervantes-Cota95]. In conclusion, this model is able to predict viable inflation but is inconsistent with high energy physics.

Since its discovery at the Large Hadron Collider (LHC) in 2012 [Chatrchyan12, Aad12], the Higgs boson has been the first elementary scalar field ever detected in nature (even though it could still be composite [Georgi84]). However, several questions remain today like the origin of the spontaneous symmetry breaking of the electroweak interaction during the cosmological history, the (classical) stabilization mechanism of the vev (which cannot vary significantly since it would change the strength of the nuclear interactions) as well as the hierarchy problem between $m_{\rm H}$ and $m_{\rm pl}$ mentioned above. Recently a novel scenario has been proposed where $m_{\rm H}$ depends on the value of an additional scalar field, the relaxion [Graham15]. This model solves the hierarchy problem since in the early Universe, the Higgs field is naturally large and then decreases gradually to zero. It becomes then unstable and as a result is fixed to its current value through the spontaneous symmetry breaking. On the other hand, the relaxion gives rise to inflation. Maybe LHC experiments will allow to reveal a part of the history by discovering the signature of a new particle. Anyway the Higgs sector is probed today by high-energy physics and cosmology at once.

5.2 Higgs inflation

In 2007, Bezrukov and Shaposhnikov proposed that the SM Higgs boson could be the inflaton provided that it is nonminimally coupled to gravity [Bezrukov08]. In this section, we briefly expose their model and review their results for inflation.

5.2.1 The model

In Higgs inflation, the SM Higgs boson is responsible for the elementary particles mass generation and inflation at once, provided that it is nonminimally coupled to gravity,

$$\mathcal{L}_{\rm tot} = \mathcal{L}_{\rm SM} - \frac{M_{\rm pl}^2}{2}\left(1 + \xi \mathcal{H}^\dagger \mathcal{H}\right) R, \tag{5.2.1}$$

with $\mathcal{L}_{\rm SM}$ the Lagrangian density of the SM, including the Higgs sector, ξ the nonminimal coupling parameter and $\mathcal{H}$ the SM Higgs doublet [GeV]. The shape of the nonminimal coupling function differs from the one of induced gravity (assuming the SM Higgs potential) such that Higgs inflation is able to predict a viable inflation scenario while preserving high energy physics as we will see in the following.

By fixing the SU(2) gauge to the unitary one,

$$\mathcal{H} = \frac{1}{\sqrt{2}} \begin{pmatrix} 0 \\ v + H(x) \end{pmatrix}, \tag{5.2.2}$$

the action for Higgs inflation becomes,

$$S_{\rm HI,\,JF} = \int \mathrm{d}^4x\sqrt{-g}\left[F(h)\frac{R}{2\,\kappa} - \frac{M_{\rm pl}^2}{2}\left(\partial h\right)^2 - V(h)\right], \tag{5.2.3}$$

with the Higgs field normalized as $H = M_{\rm pl}\, h$. The potential $V(H)$ is assumed to be the SM Mexican-hat,

$$V(h) = \frac{\lambda_{\rm sm} M_{\rm pl}^4}{4}\left(h^2 - \frac{v^2}{M_{\rm pl}^2}\right)^2, \tag{5.2.4}$$

with SM parameters $\lambda_{\rm sm} \sim 0.1$ [Olive14] and $v = 246$ GeV, and the nonminimal coupling function reads,

$$F(h) = 1 + \xi h^2. \tag{5.2.5}$$

The form of this coupling function is further justified by invoking the (semi-classical) renormalization of the energy momentum tensor associated to the scalar field on a curved background, which needs terms like H^2R in the Lagrangian [Callan70].

By applying the usual conformal transformation [Wald84],

$$\tilde{g}_{\mu\nu} = \Omega^2\, g_{\mu\nu} \qquad \text{with} \qquad \Omega^2 = 1 + \xi h^2, \tag{5.2.6}$$

$$\tilde{R} = \Omega^{-2}\, R - 6\Omega^{-3} g^{\alpha\beta}\nabla_\alpha\nabla_\beta\Omega, \tag{5.2.7}$$

it is possible to write the action 5.2.3 in the Einstein frame,

$$S_{\rm HI,\,EF} = \int \mathrm{d}^4x\sqrt{-\tilde{g}}\left[\frac{\tilde{R}}{2\,\kappa} - \frac{M_{\rm pl}^2}{2}\tilde{g}^{\mu\nu}\tilde{\partial}^\mu\chi\tilde{\partial}_\nu\chi - U\left(\chi\right)\right], \tag{5.2.8}$$

with χ the dimensionless scalar field defined by,

$$\frac{\mathrm{d}\chi}{\mathrm{d}h} = \sqrt{\frac{\Omega^2 + 6\xi^2h^2}{\Omega^4}}, \tag{5.2.9}$$

and U the potential in the Einstein frame,

$$U(\chi) = \Omega^{-4}\, V[h(\chi)]. \tag{5.2.10}$$

We can discuss the low energy and the high energy limits in the Einstein frame:

- $\xi h^2 \ll 1 \Rightarrow \Omega \simeq 1$: In this case, the Jordan and the Einstein frames are equivalent since $h \simeq \chi$ and $U(\chi) \simeq V(h)$, so that the Higgs field appears to be minimally coupled to gravity in the Jordan frame, giving rise to no inflationary phase. The SM model is thus preserved at low energy scales.

- $\xi h^2 \gg 1 \Rightarrow \Omega^2 \simeq \xi h^2$: In this limit, the Higgs inflation looks like induced gravity in the Jordan frame, leading to an inflationary phase. The implicit equation for χ (5.2.9) reduces to,

$$\frac{\mathrm{d}\chi}{\mathrm{d}h} = \frac{\sqrt{6}}{h}, \tag{5.2.11}$$

the integration yielding,

$$h = \mathcal{C} \exp\left(\frac{\chi}{\sqrt{6}}\right), \tag{5.2.12}$$

with $\mathcal{C}$ the integration constant. Similarly to the induced gravity scenario, the Higgs vev is determined by,

$$1 = \frac{\xi v^2}{M_{\rm pl}^2} \qquad \Rightarrow \qquad v = \frac{M_{\rm p}}{\sqrt{\xi}}, \tag{5.2.13}$$

leading to [Kaiser95],

$$H = \frac{M_{\rm p}}{\sqrt{\xi}} \exp\left(\frac{\chi}{\sqrt{6}}\right). \tag{5.2.14}$$

The potential in the Einstein frame then reads,

$$\begin{aligned} U(\chi) &= \frac{\lambda_{\rm sm} M_{\rm pl}^4}{4\xi^2}\left(1 - \frac{v^2}{H^2}\right)^2, & (5.2.15)\\ &= \frac{\lambda_{\rm sm} M_{\rm pl}^4}{4\xi^2}\left[1 - \exp\left(-\frac{2\chi}{\sqrt{6}}\right)\right]^2. & (5.2.16) \end{aligned}$$

Because of the flatness of $U(\chi)$ for large field χ values, it results that slow-roll inflation is efficient.

5.2.2 Equivalence between the Starobinsky model and the Higgs inflation

The Planck results for inflationary models depicted in Fig. 2.3 reveal that the Starobinsky model given by,

$$S = \frac{1}{2\kappa}\int \mathrm{d}^4x\sqrt{-g}f(R), \tag{5.2.17}$$

with,

$$f(R) = R + \frac{R^2}{6M^2}, \tag{5.2.18}$$

M being an energy scale, and the Higgs inflation are equivalent in terms of $n_{\rm s}$ and r. The equations of motion for the Starobinsky model are of second order. Indeed, $f(R)$ theories avoid the Ostrogradsky instability (see Sec. 1.3.4) provided that $\mathrm{d}^2 f/\mathrm{d}R^2 = 1/(3M^2) \neq 0$[5] (see e.g. [De Felice10]). In this section the equivalence between both models is explicitly shown [Whitt84].

The Legendre transform of $f(R)$ to another function of an auxiliary field $V(\Phi)$,

$$V(\Phi) = \Phi R(\Phi) - f\left[R(\Phi)\right], \tag{5.2.19}$$

enables one to rewrite the Starobinsky model as a STT in the Jordan frame in the absence of any kinetic term. Indeed, by defining,

$$\Phi = \frac{\mathrm{d}f}{\mathrm{d}R} = 1 + \frac{R}{3M^2}, \tag{5.2.20}$$

the potential function reads,

$$\begin{aligned} V(\Phi) &= 3M^2\Phi\left(\Phi-1\right) - 3M^2\left(\Phi-1\right) - \frac{3}{2}\left(\Phi-1\right)^2, & (5.2.21)\\ &= \frac{3M^2}{2}\left(\Phi-1\right)^2, & (5.2.22) \end{aligned}$$

and the action (5.2.18) becomes,

$$\begin{aligned} S &= \frac{1}{2\kappa}\int \mathrm{d}^4x\sqrt{-g}\left[\Phi R(\Phi) - V(\Phi)\right], & (5.2.23)\\ &= \frac{1}{2\kappa}\int \mathrm{d}^4x\sqrt{-g}\left[\Phi R - \frac{3M^2}{2}\left(\Phi-1\right)^2\right]. & (5.2.24) \end{aligned}$$

The Starobinsky model corresponds thus to a STT in the Jordan frame in the absence of a kinetic term for the scalar field Φ.

$f(R)$ theory can also be expressed in the Einstein frame by performing the conformal transformation (3.2.17) with $\Omega = \sqrt{\Phi}$ (see also Sec. 3.2.2), which requires to compute,

$$\begin{aligned} \tilde{\nabla}_\alpha\sqrt{\Phi} &= \frac{1}{2\sqrt{\Phi}}\tilde{\nabla}_\alpha\Phi, & (5.2.25)\\ \tilde{\nabla}_\alpha\tilde{\nabla}_\beta\sqrt{\Phi} &= \frac{1}{2\sqrt{\Phi}}\left(-\frac{1}{2\Phi}\tilde{\nabla}_\alpha\Phi\tilde{\nabla}_\beta\Phi + \tilde{\nabla}_\alpha\tilde{\nabla}_\beta\Phi\right), & (5.2.26) \end{aligned}$$

hence, the Ricci scalar eventually transforms as (see Eq. (3.2.17)),

$$R = \Phi\tilde{R} + 3\tilde{\Box}\Phi - \frac{9}{2}\frac{\left(\tilde{\nabla}\Phi\right)^2}{\Phi}. \tag{5.2.27}$$

[5] Actually in order to ensure the stability of FLRW solutions, we must rather impose $\mathrm{d}^2 f/\mathrm{d}R^2 > 0$ [Capozziello06].

Using Eqs. (3.2.15), it results that the action (5.2.23) becomes,

$$S = \frac{1}{2\kappa}\int \mathrm{d}^4x\sqrt{-\tilde{g}}\Phi^{-2}\left[\Phi^2\tilde{R} + 3\Phi\tilde{\Box}\Phi - \frac{9}{2}\left(\tilde{\nabla}\Phi\right)^2 - V(\Phi)\right], \quad (5.2.28)$$

$$= \frac{1}{2\kappa}\int \mathrm{d}^4x\sqrt{-\tilde{g}}\left[\tilde{R} + 3\frac{\tilde{\Box}\Phi}{\Phi} - \frac{9}{2}\left(\frac{\tilde{\nabla}\Phi}{\Phi}\right)^2 - \frac{V(\Phi)}{\Phi^2}\right]. \quad (5.2.29)$$

Integrating the second term by parts,

$$\frac{\tilde{\Box}\Phi}{\Phi} = -\tilde{\nabla}_\alpha\left(\frac{1}{\Phi}\right)\tilde{\nabla}^\alpha\Phi = \left(\frac{\tilde{\nabla}\Phi}{\Phi}\right)^2, \quad (5.2.30)$$

the action yields,

$$S = \frac{1}{2\kappa}\int \mathrm{d}^4x\sqrt{-\tilde{g}}\left[\tilde{R} - \frac{3}{2}\left(\frac{\tilde{\nabla}\Phi}{\Phi}\right)^2 - \frac{V(\Phi)}{\Phi^2}\right]. \quad (5.2.31)$$

Eventually, by rescaling of the scalar field,

$$\varphi = \sqrt{\frac{3}{2}}\ln\Phi \qquad \Rightarrow \qquad \Phi = \mathrm{e}^{\sqrt{2/3}\varphi}, \quad (5.2.32)$$

the potential yields (see Eq. (5.2.22)),

$$V(\varphi) = \frac{3M^2}{2}\left(\mathrm{e}^{\sqrt{\frac{2}{3}}\varphi} - 1\right)^2. \quad (5.2.33)$$

Hence, the action in the Einstein frame for the Starobinsky model reads,

$$S_{\mathrm{S,\,EF}} = \frac{1}{2\kappa}\int \mathrm{d}^4x\sqrt{-\tilde{g}}\left[\tilde{R} - \tilde{\nabla}_\mu\varphi\tilde{\nabla}^\mu\varphi - \frac{3M^2}{2}\left(1 - \mathrm{e}^{-\sqrt{\frac{2}{3}}\varphi}\right)^2\right]. \quad (5.2.34)$$

in agreement with the Higgs inflation (5.2.16),

$$S = \int \mathrm{d}^4x\sqrt{-\tilde{g}}\left[\frac{\tilde{R}}{2\kappa} - \frac{M_{\mathrm{pl}}^2}{2}\tilde{\nabla}_\mu\varphi\tilde{\nabla}^\mu\varphi - \frac{3M^2M_{\mathrm{pl}}^2}{4}\left(1 - \mathrm{e}^{-\sqrt{\frac{2}{3}}\varphi}\right)^2\right], \quad (5.2.35)$$

in the limit $\xi h^2 \gg 1$ provided that $\chi = \varphi$ (see Eq. (5.2.16)) and,

$$M^2 = \frac{\lambda_{\mathrm{sm}}M_{\mathrm{pl}}^2}{3\xi^2}. \quad (5.2.36)$$

Another way to show the equivalence between the Starobinsky model and the Higgs inflation in the large field limit ($H \gg v$) consists of starting from the Higgs inflation in the Jordan frame (5.2.3) assuming the slow-roll conditions at the action level, $(\partial H)^2/2 \ll V(H)$ [Kehagias14]. Starting from Eq. (5.2.3), the Euler-Lagrange equation for the scalar field yields ($h \neq 0$),

$$\frac{1}{\sqrt{-g}}\frac{\partial S_{\mathrm{HI,\,JF}}}{\partial h} = 0 \qquad \Leftrightarrow \qquad h^2 = \frac{\xi R}{\lambda_{\mathrm{sm}}M_{\mathrm{pl}}^2}. \quad (5.2.37)$$

By replacing h into Eq. (5.2.3),

$$S = \frac{1}{2\kappa}\int \mathrm{d}^4x\sqrt{-g}\left(R + \frac{\xi^2 R^2}{2M_{\rm pl}^2\lambda_{\rm sm}}\right), \tag{5.2.38}$$

the Higgs inflation and the Starobinsky model are thus equivalent if Eq. (5.2.36) holds.

In summary, both models are equivalent for large Higgs field values ($\xi h^2 \gg 1$), that is during the inflationary phase only, and at leading order. Radiative corrections as well as the reheating temperature predicted by both models differ [Bezrukov12] (see also Sec. 5.2.4). However, Planck results do not enable one to distinguish both models.

5.2.3 Constraints from inflation

In order to confront the Higgs inflation with the Planck observations, the slow-roll analysis in the large field limit ($\xi h^2 \gg 1$) allows to compute the spectral index $n_{\rm s}$ and the tensor-to-scalar ratio r (see also Sec. 2.4.5). Computing the first and second derivatives of Eq. (5.2.16) and using Eq. (5.2.14), the slow-roll parameters read,

$$\epsilon_{\rm V} \equiv \frac{1}{2}\left(\frac{\mathrm{d}U/\mathrm{d}\chi}{U}\right)^2 \simeq \frac{4}{3\xi^2 h^4}, \tag{5.2.39}$$

$$\eta_{\rm V} \equiv \frac{\mathrm{d}^2U/\mathrm{d}\chi^2}{U} \simeq -\frac{4}{3\xi h^2}. \tag{5.2.40}$$

Slow-roll inflation ends when $\epsilon_{\rm V} \simeq 1$ or equivalently, for the Higgs field value, $h_{\rm end}^4 \simeq 4/(3\xi^2)$. The number of e-folds (2.4.22) from the onset $t_{\rm i}$ to the end of inflation $t_{\rm end}$ is then given by,

$$N(t) \equiv \int_{t_{\rm i}}^{t_{\rm end}} H(t)\mathrm{d}t = \int_{\chi_{\rm i}}^{\chi_{\rm end}} H(\chi)\frac{\mathrm{d}\chi}{\dot\chi}. \tag{5.2.41}$$

In the slow-roll conditions (2.4.23) and (2.4.24), the Friedmann and the Klein-Gordon Eqs. (2.4.16), (2.4.19) and (2.4.18) reduce to[(6)],

$$H(\chi) = \sqrt{\frac{U}{3M_{\rm pl}^2}}, \qquad \dot\chi = -\frac{1}{\sqrt{3}M_{\rm pl}}\frac{U_\chi}{\sqrt{U}}, \tag{5.2.42}$$

where the subscript χ denotes a derivative with respect to χ. Using the definition of $\epsilon_{\rm V}$ (5.2.39), the number of e-folds is then given by,

$$N(\chi) = -\int_{\chi_{\rm i}}^{\chi_{\rm end}} \frac{U}{U_\chi}\mathrm{d}\chi = -\int_{\chi_{\rm i}}^{\chi_{\rm end}} \frac{1}{\sqrt{2\epsilon_{\rm V}}}\mathrm{d}\chi, \tag{5.2.43}$$

[(6)] Note that the slow-roll conditions are given for U rather than V since the Einstein frame looks like GR.

which finally reads in terms of the Higgs field h using (5.2.11) and (5.2.39),

$$N(h) = -\int_{h_\mathrm{i}}^{h_\mathrm{end}} \frac{1}{\sqrt{2\epsilon_\mathrm{V}}}\frac{\mathrm{d}\chi}{\mathrm{d}h}\mathrm{d}h = \frac{3\xi}{4}\left(h_\mathrm{i}^2 - h_\mathrm{end}^2\right). \tag{5.2.44}$$

Using the definition of h_end, h_i^2 yields,

$$h_\mathrm{i}^2 = \frac{4}{3\xi}N + \frac{2}{\sqrt{3}\xi}, \tag{5.2.45}$$

the slow-roll parameters at the onset of inflation reading then approximately,

$$\epsilon_\mathrm{V}(N) \simeq \frac{12}{(4N+3)^2}, \tag{5.2.46}$$

$$\eta_\mathrm{V}(N) \simeq -\frac{4}{4N+3}. \tag{5.2.47}$$

The scalar spectral index n_s and the tensor-to-scalar ratio r for $N = 60$ corresponding to the pivot scale $k_* = 0.002/$ Mpc then follow from Eqs. (2.4.33),

$$n_\mathrm{s} \simeq 0.97, \tag{5.2.48}$$

$$r \simeq 0.0033. \tag{5.2.49}$$

Those results are represented on Fig. 2.3 in agreement with the Starobinsky model as expected.

Preheating and reheating were analyzed in detail by [Garcia-Bellido09], Higgs inflation offering the advantage that the couplings between the Higgs field and the other fields of the SM sector are known thanks to particle accelerator experiments, which is not the case for other inflationary models. The dependence of the Higgs inflation predictions on the reheating temperature at which inflation ends has been analyzed numerically by [Martin14b]. The spectral index is found to in good agreement with the data while the contribution of gravity waves is small, whatever reheating temperature in the range $[10^{-2} - 10^{14}]$ GeV.

Eventually, the parameter ξ is constrained thanks to the normalization of the CMB power spectrum Eq. (2.4.32) for the pivot scale $k = k_*$ yielding,

$$\mathcal{P}_\zeta(k = k_*) \simeq \frac{H_*^2}{\pi M_\mathrm{pl}^2 \epsilon_{\mathrm{V},*}} \simeq \frac{U_*}{3\pi M_\mathrm{pl}^4 \epsilon_{\mathrm{V},*}}, \tag{5.2.50}$$

where the asterisk denotes a quantity evaluated at the pivot scale k_* and the Friedmann equation (2.4.16) in the slow-roll approximation (2.4.23) has been used. According to the COBE satellite measurements $\mathcal{P}_\zeta(k = k_*) = A_\mathrm{s}/(2\pi^2) \sim 10^{-10}$ [Lyth99]. Using the expression for ϵ_V (5.2.39) for $h_* \equiv h_\mathrm{COBE}$, the definition of U (5.2.10) in the large field limit ($\Omega^2 \simeq \xi h^2$) and the expression (5.2.44) for N_COBE corresponding to $k = k_*$ gives,

$$\frac{U_*}{\epsilon_*} \simeq \frac{3\lambda_\mathrm{sm} M_\mathrm{pl}^4}{16} h_\mathrm{COBE}^4, \tag{5.2.51}$$

$$\simeq \frac{\lambda_\mathrm{sm} M_\mathrm{pl}^4}{3\xi^2} N_\mathrm{COBE}^2. \tag{5.2.52}$$

By definition of the normalization of the CMB power spectrum (5.2.50) $U_*/\epsilon_* \sim 3\pi 10^{-10} M_{\rm pl}^4 \sim (0.027 M_{\rm pl})^4$, yielding,

$$\xi \simeq \sqrt{\frac{\lambda_{\rm sm}}{3}} \frac{N_{\rm COBE}}{(0.027)^2} \simeq 49,000\sqrt{\lambda_{\rm sm}} \simeq 10^4 - 10^5, \tag{5.2.53}$$

since $N_{\rm COBE} \simeq 62$ and $\lambda_{\rm sm} \sim 0.1$.

5.2.4 High energy physics and extensions of the Higgs inflation

Higgs inflation appears to be favored by latest cosmological observations provided the nonminimal coupling $\xi \sim 10^4 - 10^5$. However, such a model involves quantum corrections (somewhat flawed by the non-renormalizable character of GR), either from quantum gravity or from loop corrections of the SM fields (among them the Higgs field itself) [Bezrukov08]. The crucial point is the flatness of the effective potential in the Einstein frame for large χ which must be preserved. The one-loop and two-loop corrections have been studied assuming that the SM is valid up to the Planck scale [Bezrukov09b, Bezrukov09a] (see also [Martin14b]). Following [Bezrukov09a] it results that the SM Higgs inflation is viable for Higgs mass values $m_{\rm H} \in [126,\ 194]$ GeV depending on the mass of the top quark and the coupling constant of strong interactions $\alpha_{\rm s}$. Their analysis is nevertheless controversial (see e.g. [Barvinsky08, De Simone09] where $m_{\rm H} \sim 120 - 135$ GeV in the latter) notably because the Jordan and the Einstein frames are equivalent at tree level only [Steinwachs12]. The slow-roll analysis of the radiatively corrected Higgs inflation depending on the potential parameter responsible for the radiative corrections (and on the reheating temperature) has been presented in [Martin14b]. They found that, in agreement with [Barvinsky08], radiatively corrected Higgs inflation model appears to be disfavored when cosmological and particle physics data are taken into account altogether.

Moreover, some authors argued that Higgs inflation is an effective theory valid up to the scale $\Lambda_0 = m_{\rm pl}/\xi$ only, below the Higgs field value during the slow-roll inflation, $H \gg m_{\rm pl}/\sqrt{\xi}$, since above Λ_0 the Higgs field becomes strongly coupled to the Ricci scalar [Barbon09] (see Sec. (3.1.2)). A similar result was derived by [Burgess09] where it is shown that the semiclassical treatment of Higgs inflation is correct for energy scale, $m_{\rm pl}/\xi \gg \Lambda_0 \gg \sqrt{\lambda_{\rm sm}} m_{\rm pl}/\xi$. Otherwise unitarity at the quantum level could be lost for processes like the graviton-Higgs and Higgs-Higgs scattering (in flat space). This means that above the ultra-violet cutoff Λ_0 the SM should be replaced by a more fundamental theory. In [Bezrukov11] authors claimed that the cutoff scale depends to the background value of the Higgs field leading to the validity of the semiclassical treatment during inflation where $\Lambda_0 \sim m_{\rm pl}$. Moreover, the effect of the couplings to fermions does not spoil this result while those to gauge bosons lead to a slightly lower cutoff.

In order to avoid the loss of unitarity some modifications of the Higgs inflation have been proposed, either via additional interactions due to the term with covariant derivatives of the Higgs doublet in the action [Lerner10] or by including additional scalar field like the dilaton [Garcia-Bellido11, Bezrukov13] which can lead to the late-time accelerating phase. In addition a model involving a nonminimal derivative coupling of the Higgs field to gravity has been proposed [Germani10b, Germani10a],

$$S = \int \mathrm{d}^4x\sqrt{-g}\left[\frac{R}{2\kappa} - \frac{1}{2}\left(g_{\mu\nu} - w^2 G_{\mu\nu}\right)\partial^\mu H \partial^\nu H - \frac{\lambda}{4}H^4\right], \qquad (5.2.54)$$

with w^2 a coupling constant in $[\mathrm{GeV}^{-2}]$. This model also preserves unitarity and leads to viable inflation if w is around the geometric mean of the electroweak and the Planck scale [Germani10a]. In Chap. 6 we will come back on this nonminimal coupling function.

5.3 Particlelike distributions of the Higgs Field nonminimally coupled to gravity

Since the nonminimal coupling ξ for a viable inflation model is very large (see Sec. 5.2), of the order of 10^4, it naturally raises concerns about static configurations: how a such strongly coupled Higgs field reacts in the presence of gravitationally bound matter? What does the vacuum look like in the vicinity of a compact object? Since the works of Damour and Esposito-Farèse [Damour93a], we know that a non-minimally coupled scalar field can give rise to spontaneous scalarization in compact objects (see Sec. 3.2.5.3). In this section, we will show that all spherically symmetric distributions of matter carry a classical Higgs charge, whose magnitude depends on their mass, their compactness, and the strength of ξ. However, contrary to spontaneous scalarization, only one particlelike distribution of the Higgs field, that is globally regular and asymptotically flat distribution with finite energy, does exist. This solution is characterized by the radius and baryonic energy density of the compact object as well as the nonminimal coupling. Finally we highlight the existence of a mechanism of resonant amplification of the Higgs field inside the so-called Higgs monopoles that comes into play for large nonminimal coupling. This mechanism might degenerate into divergences of the Higgs field that reveal the existence of forbidden combinations of radius and baryonic energy density.

5.3.1 The Model

We start from the same action as for the Higgs inflation (5.2.3), including the matter part of the action,

$$\mathcal{L} = \sqrt{g}\left[\frac{F(H)}{2\kappa}R - \frac{1}{2}\left(\partial H\right)^2 - V(H)\right] + \mathcal{L}_{\mathrm{M}}\left[g_{\mu\nu}; \Psi_{\mathrm{M}}\right], \qquad (5.3.1)$$

where $H = m_{\rm pl} h$ is the Higgs scalar field in the unitary gauge[7]. The potential V is given by Eq. (5.2.4) with the usual SM model parameters[8] and the nonminimal coupling function by Eq. (5.2.5). As reminded in Sec. 5.2, this model yields a successful inflation provided ξ is large, of the order 10^4 [Bezrukov08]. We will consider only positive values of ξ to avoid the possibility that the effective reduced Planck mass (that can be identified with $(m_{\rm pl}^2 + \xi H^2)^{1/2}$) becomes imaginary during its dynamical evolution.

A similar Lagrangian for compact objects was already considered by [Salgado98], where, however, the potential was neglected. As we will see below, this is an important difference as the presence of the Higgs potential prevents the solution from converging smoothly to GR. In other words, the solution $H = 0$ does not yield the Schwarzschild solution but, rather, a de Sitter black hole with a cosmological constant proportional to v^4.

It should also be kept in mind that the Higgs field is in general a complex doublet and, here, it is reduced to a single real component by choosing the unitary gauge [Bezrukov08]. However, the other components, also known as Goldstone bosons, can have physical effects, especially at high energy, when renormalizability imposes a different gauge choice (e.g. the so-called R_ξ-gauges, see for example [Peskin95]). In cosmology, the effects of the Goldstone boson in a toy $U(1)$ model was investigated by [Rinaldi14, Rinaldi15b]. In the context of compact object, some results can be found in [vanderBij87] although the potential is not of the Higgs type.

The equations of motion obtained from the Lagrangian (5.3.1) by variation with respect to the metric read,

$$\left(1 + \frac{\xi}{m_{\rm pl}^2} H^2\right) G_{\mu\nu} = \kappa \left[T_{\mu\nu}^{(H)} + T_{\mu\nu}^{(\xi)} + T_{\mu\nu}^{(\rm M)}\right], \tag{5.3.2}$$

where,

$$T_{\mu\nu}^{(H)} \;=\; \partial_\mu H \partial_\nu H - g_{\mu\nu}\left[\frac{1}{2}\left(\partial H\right)^2 + V\left(H\right)\right], \tag{5.3.3}$$

is the part of the stress-energy tensor associated to the Higgs field, and,

$$T_{\mu\nu}^{(\xi)} = -\frac{\xi}{4\pi}\left[g_{\mu\nu}\nabla^\lambda\left(H\nabla_\lambda H\right) - \nabla_\mu\left(H\nabla_\nu H\right)\right], \tag{5.3.4}$$

is the stress-energy tensor induced by the nonminimal coupling ξ. Finally, the stress-energy tensor of the baryonic matter fields $T_{\mu\nu}^{(\rm M)}$ is given by Eq. (1.2.8) that we assume to have the form of a perfect fluid given by Eq. (2.2.2) with the specific energy density $\Pi = 0$. We point out that we do not introduce any coupling between the Higgs field and baryonic matter.

[7] Notice that the gauge symmetry does not appear explicitly in the Lagrangian (5.3.1). Following [Bezrukov08] the effect of gauge bosons is neglected according to chaotic inflation scenario.

[8] We use the SM values for the parameters of the potential $\lambda_{\rm sm}$ and v. However, it would be interesting to study this theory as a generic STT to see in which range these parameters are compatible with the current observations.

Here, we adopt the splitting of the energy momentum tensor proposed in [Salgado98] as each part will give distinct contributions, as we will see in Sec. 5.3.4. The set of equations of motion is completed by the Klein-Gordon equation,

$$\Box H + \frac{\xi H R}{8\pi} = \frac{\mathrm{d}V}{\mathrm{d}H}, \tag{5.3.5}$$

from which we can understand in a qualitative way the main characteristics of the solution, as we show in the next section.

5.3.2 Effective dynamics

Our first goal is to assess whether spherically symmetric and asymptotically flat solutions to the equations of motion exist. The term in the Klein-Gordon equation (5.3.5) that tells us if this is possible, is the one proportional to $\xi H R$. For a start, it is clear that the trivial function $H(r) = 0$ is always a solution of Eq. (5.3.5) even with $\xi \neq 0$ and in the presence of matter, i.e. when $R \neq 0$. If we consider a static and spherically symmetric spacetime in the Schwarzschild coordinates, described by the metric (2.3.1), we see from (5.3.1) that, for $H = 0$ and in the absence of matter, we obtain a de Sitter black hole solution since $V(H = 0) = \lambda_{\mathrm{sm}} v^4/4$. Therefore, this solution is not asymptotically flat and has infinite energy. In the absence of nonminimal coupling ($\xi = 0$), the only asymptotically flat solution of finite energy, namely $H = \pm v$, leads to the usual Schwarzschild metric (with or without internal matter). On the other hand, with a nonminimal coupling and in the absence of matter, there are no-hair theorems that force the solution to be the Schwarzschild one, i.e. again $H(r) = \pm v$ everywhere [Sotiriou12]. Therefore, the only non-trivial case is the one with nonminimal coupling and nonvanishing baryonic matter density, which, as we will show, has indeed finite energy and is asymptotically flat unless $H = \pm v$ is a global solution.

To examine in detail the dynamics, we rewrite the Klein-Gordon equation (5.3.5) as,

$$\Box H = -\frac{\mathrm{d}V_{\mathrm{eff}}}{\mathrm{d}H}, \tag{5.3.6}$$

where,

$$V_{\mathrm{eff}} = -V + \frac{\xi H^2 R}{16\pi} + \mathcal{C}, \tag{5.3.7}$$

$\mathcal{C}$ being a constant of integration. Note that the form of the effective potential in a time-dependent inflationary background has the opposite sign with respect to the one in a static and spherically symmetric background. In fact, if the metric has the flat FLRW form given by (2.4.1) with $k = 0$, the scalar field rolls down (in time) into the potential well since the Klein-Gordon equation has the form,

$$\frac{\mathrm{d}^2 H}{\mathrm{d}t^2} + \frac{3}{a}\frac{\mathrm{d}a}{\mathrm{d}t}\frac{\mathrm{d}H}{\mathrm{d}t} = \frac{\mathrm{d}V_{\mathrm{eff}}}{\mathrm{d}H}. \tag{5.3.8}$$

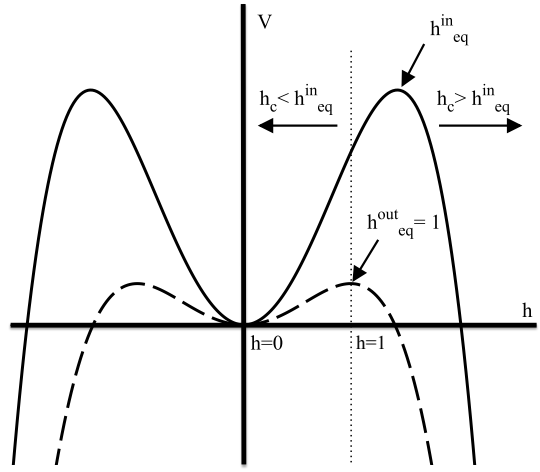

Figure 5.1: Qualitative plot of the potential inside (solid line) and outside (dashed line) the body. The effective potential corresponds to the Higgs one outside the body while the local maxima (see $h^{\rm in}_{\rm eq}$ with $H = m_{\rm pl} v h$) are displaced from the vev inside the body.

On the other hand, with the static and spherically symmetric metric (2.3.1) the Klein-Gordon equation becomes,

$$H'' - H'\left(\lambda' - \nu' - \frac{2}{r}\right) \equiv -\frac{{\rm d}V_{\rm eff}}{{\rm d}H}, \qquad (5.3.9)$$
$$= \left[-\frac{\xi R}{8\pi} + \lambda_{\rm sm}(H^2 - v^2)\right] H,$$

where the prime denotes a derivative with respect to the radial coordinate r. For minimal coupling $\xi = 0$, while $H = \pm v$ ($H = 0$) corresponds to local minima (maximum) in the cosmological case, it corresponds to local maxima (minimum) in the spherical symmetric static configuration. In addition, for nonminimal coupling, $H = 0$ is a stable equilibrium point while $H = v$ is an unstable one. In order to fully characterize the stability of these points in the nonminimal coupling case, it is necessary to compute R.

For simplicity, a top-hat distribution is assumed of baryonic matter from now on, namely,

$$\rho(r) = \begin{cases} \rho_0 & 0 < r < \mathcal{R}, \\ 0 & r > \mathcal{R}, \end{cases} \qquad (5.3.10)$$

where $\mathcal{R}$ is the radius of the spherical body. In this case, the effective potential shows a sharp transition between the interior and the exterior of the body. Indeed, if $\xi \neq 0$, the second term in the right-hand side of Eq. (5.3.7) comes

into play and we can show that the Ricci scalar satisfies the inequality,

$$R(r < \mathcal{R}) \gg R(r > \mathcal{R}). \tag{5.3.11}$$

The reason is that, inside the body, the Higgs field turns out to be almost constant, as shown in Sec. 5.3.4. Therefore, all the derivatives in the trace of the stress-energy tensor vanish and the only consistent contribution to R comes from the potential, as one can easily check by calculating the trace of Eq. (5.3.2). If the Higgs field is not too much displaced from its vev inside the body, the greatest contribution to the curvature then comes from the baryonic matter, provided the density is sufficiently large. Outside the body, the Higgs field drops very rapidly towards its vev and R vanishes at large r to match the Schwarzschild solution $R = 0$ everywhere. For practical purposes, this means that we can approximate R, inside the body, as there was no Higgs field but just matter. To show this property a bit more rigorously, it is sufficient to calculate the trace of Eq. (5.3.2) and recall that, at the center of the body, we must have $\mathrm{d}H/\mathrm{d}r = 0$ according to the regularity conditions. Therefore, near the center of the body, the trace of the Einstein equations is approximate by,

$$\left(1 + \frac{\xi H^2}{m_{\rm pl}^2}\right) R \simeq -\kappa \left(2V + T^{(\rm M)} - \frac{3\xi}{4\pi} H \Box H\right). \tag{5.3.12}$$

In addition, for energies much lower than the Planck scale, $H \lll m_{\rm pl}$, all the terms like $\xi H^2/m_{\rm pl}^2$ can be safely neglected, even when $\xi \sim 10^4$. Finally by also using the Klein-Gordon equation (5.3.5), Eq. (5.3.12) can be accurately approximated by,

$$\begin{aligned} \frac{1}{v^2}\left(R + \kappa T^{(\rm M)}\right) &= -\frac{\kappa}{v^2}\left(2V - \frac{3\xi H}{4\pi}\frac{\mathrm{d}V}{\mathrm{d}H}\right), \\ &= -\frac{4\pi\lambda v^2}{m_{\rm pl}^2}\left(\frac{H^2}{v^2} - 1\right)\left[\frac{H^2}{v^2}\left(1 - \frac{3\xi}{2\pi}\right) - 1\right]. \end{aligned} \tag{5.3.13}$$

Now, since $(v/m_{\rm pl})^2 \sim 10^{-34}$, we need a very large ratio H/v to yield a non-negligible right hand side, even for ξ of the order of 10^4. Therefore, unless we consider planckian energies for the Higgs field, the left hand side of the above equation is negligibly small, at least near the center of the body. This means that, inside the body, the Einstein equations are indistinguishable from the standard GR equation $R = -\kappa T^{(\rm M)}$. In the App. D, the validity of this approximation is established numerically, so it can be used to investigate the particlelike solutions for a very large range of parameters.

Let us now study the equilibrium points of $V_{\rm eff}$. Outside the body, where $T^{(\rm M)} = 0$, the scalar curvature is almost vanishing $R \simeq 0$. Therefore, $\mathrm{d}V_{\rm eff}/\mathrm{d}H$ vanishes at,

$$\frac{H_{\rm eq}^{\rm out}}{v} = 0, \pm 1. \tag{5.3.14}$$

Inside the body, where $R \simeq -\kappa T^{(\rm M)}$,

$$\frac{H_{\rm eq}^{\rm in}}{v} = 0, \pm\sqrt{1 + \frac{R\xi}{8\pi\lambda_{\rm sm} v^2}}, \tag{5.3.15}$$

and the crucial role of a nonvanishing ξ becomes evident.

The solutions that we are looking for, must interpolate between the value of the Higgs field at the center of the body $H_{\rm c}$ and at the spatial infinity $H_\infty = \pm v$. Furthermore, since H' must vanish at the origin, H rolls down into the effective potential from rest. Suppose that $|H_{\rm c}|$ is greater than the nonzero value of $|H_{\rm eq}^{\rm in}|$ (see the solid line curve in Fig. 5.1). Then, the Higgs field will roll outwards increasing boundlessly its value without any possibility of reaching an equilibrium point outside the body (see the dashed line curve in Fig. 5.1), leading to infinite energy configurations. On the contrary, if $|H_{\rm c}|$ is smaller than the nonzero value of $|H_{\rm eq}^{\rm in}|$, the Higgs field rolls down inward, towards the equilibrium at $H_\infty = 0$, see Fig. 5.1, a solution of infinite energy too. By requiring a Higgs distribution which is globally regular and an asymptotically flat metric, only one initial value $H_{\rm c}$ converges to the vev at spatial infinity, i.e. $|H_{\rm eq}^{\rm out}|$, for a given nonminimal coupling ξ as well as energy density ρ and radius $\mathcal{R}$ of the body (or equivalently its compactness s and baryonic mass m). All the other trajectories lead to either an asymptotically de Sitter solution or to a divergent Higgs field at infinity. These particular solutions, with finite energy and asymptotically flat geometry, are dubbed *Higgs monopoles* since they behave like isolated SM scalar charges. Numerical solutions will be obtained with a specifically designed shooting method in the following sections.

5.3.3 Analytic properties

Before exploring the numerical solutions to the equations of motion, it is worth investigating their analytical properties in order to obtain information able to target more efficiently the numerical analysis. For this section, it is more convenient to write the Lagrangian (5.3.1) in the standard Brans-Dicke form,

$$\mathcal{L}_{\rm BD} = \frac{\sqrt{-g}}{2\kappa}\left[\phi R - \frac{\omega}{\phi}(\partial\phi)^2 - \bar{V}(\phi)\right] + \mathcal{L}_{\rm M}. \tag{5.3.16}$$

where

$$\phi = 1 + \frac{\xi H^2}{m_{\rm pl}^2}, \quad \omega(\phi) = \frac{2\pi\phi}{\xi(\phi-1)}, \tag{5.3.17}$$

and

$$\bar{V}(\phi) = \frac{\kappa\lambda_{\rm sm}}{2}\left[\frac{8\pi}{\xi\kappa}(\phi-1) - v^2\right]^2. \tag{5.3.18}$$

The Einstein equations now read,

$$\begin{aligned} R_{\mu\nu} - \frac{1}{2}g_{\mu\nu}R &= \frac{1}{\phi}\nabla_\mu\nabla_\nu\phi + \frac{\omega}{\phi^2}\nabla_\mu\phi\nabla_\nu\phi \\ &- \frac{1}{\phi}\left[\Box\phi + \frac{\omega}{2\phi}(\partial\phi)^2 + \frac{\bar{V}}{2}\right]g_{\mu\nu} + \frac{\kappa}{\phi}T_{\mu\nu}, \end{aligned} \tag{5.3.19}$$

where $T^{\nu}_{\mu} = \mathrm{diag}(-\rho, p, p, p)$ is the energy momentum tensor of the fluid. Using the trace of this equation, the Klein-Gordon equation (5.3.5) becomes,

$$(2\omega+3)\Box\phi + \frac{\mathrm{d}\omega}{\mathrm{d}\phi}(\partial\phi)^2 - \phi\frac{\mathrm{d}\bar{V}}{\mathrm{d}\phi} + 2\bar{V} = \kappa T. \tag{5.3.20}$$

With the metric (2.3.1), the $tt-$ and $rr-$components of the Einstein equations are, respectively,

$$\lambda'\left(\frac{2}{r}+\frac{\phi'}{\phi}\right) - \frac{\kappa\rho}{\phi}\mathrm{e}^{2\lambda} + \frac{1}{r^2}\left(\mathrm{e}^{2\lambda}-1\right) - \frac{\phi''}{\phi} - \frac{2\phi'}{r\phi} - \frac{\bar{V}\mathrm{e}^{2\lambda}}{2\phi} - \frac{\omega}{2}\left(\frac{\phi'}{\phi}\right)^2 = 0, \tag{5.3.21}$$

$$\nu'\left(\frac{2}{r}+\frac{\phi'}{\phi}\right) - \frac{\kappa p}{\phi}\,\mathrm{e}^{2\lambda} - \frac{1}{r^2}\left(\mathrm{e}^{2\lambda}-1\right) + \frac{2\phi'}{r\phi} + \frac{\bar{V}\mathrm{e}^{2\lambda}}{2\phi} - \frac{\omega}{2}\left(\frac{\phi'}{\phi}\right)^2 = 0, \tag{5.3.22}$$

while the angular component is,

$$\nu'' + (\nu')^2 + \nu'\left(\frac{1}{r}+\frac{\phi'}{\phi}\right) - \lambda'\left(\nu'+\frac{1}{r}+\frac{\phi'}{\phi}\right) + \frac{\phi''}{\phi} + \frac{\phi'}{r\phi} + \frac{\omega}{2}\left(\frac{\phi'}{\phi}\right)^2 + \frac{\mathrm{e}^{2\lambda}}{\phi}\left(\frac{\bar{V}}{2} - \kappa p\right) = 0. \tag{5.3.23}$$

Finally, the Klein-Gordon equation becomes,

$$(2\omega+3)\left(\phi'' + \phi'\nu' - \phi'\lambda' + \frac{2}{r}\phi'\right) + (\phi')^2\frac{\mathrm{d}\omega}{\mathrm{d}\phi} + \mathrm{e}^{2\lambda}\left(2\bar{V} - \phi\frac{\mathrm{d}\bar{V}}{\mathrm{d}\phi}\right) + \kappa\mathrm{e}^{2\lambda}(\rho - 3p) = 0. \tag{5.3.24}$$

To these we must add the TOV equation (2.3.6) obtained by the usual Bianchi identities. The total energy momentum tensor is identified with the right hand side of Eq. (5.3.19). Therefore, the total energy density, given by $\rho_{\mathrm{tot}} = -T^0_{\mathrm{tot}\ 0}$, reads,

$$\rho_{\mathrm{tot}} = \mathrm{e}^{-2\lambda}\left(\frac{\phi''}{\phi} - \frac{\phi'\lambda'}{\phi} + \frac{2\phi'}{r\phi} + \frac{\omega\phi'^2}{2\phi^2}\right) + \frac{\bar{V}}{2\phi} + \frac{\kappa\rho}{\phi}. \tag{5.3.25}$$

As mentioned in the previous section, if ϕ (and hence, H) varies very slowly with r, the energy density is dominated by the baryonic matter. This is certainly true near the center, as there $\phi'(r=0)=0$ is imposed, as required by symmetry arguments. As a consequence, all the derivatives are negligible and we are left with,

$$\rho_{\mathrm{tot}} \simeq \frac{\bar{V}_{\mathrm{c}}}{2\phi_{\mathrm{c}}} + \frac{\kappa\rho}{\phi_{\mathrm{c}}}, \tag{5.3.26}$$

where a subscript "c" indicates the value of a quantity at the center of the body. If $\bar{V}_c$ is not too large, that is the Higgs field is not displaced too much from its vev, then the energy density can be taken as the one of GR, as already mentioned in Sec. 5.3.2.

Now, consider the Klein-Gordon equation (5.3.24) and suppose that there exists a point $\bar{r}$ such that $\phi'(\bar{r}) = 0$. Suppose also that the energy density is constant inside the body, $\rho = E$. It follows that, at that point,

$$\bar{\phi}'' = \frac{\mathrm{e}^{2\bar{\lambda}}}{(2\bar{\omega}+3)}\left[\frac{64\pi^2\lambda_{\rm sm}\phi_v(\bar{\phi}-\phi_v)}{\kappa\xi^2} - \kappa(E-3\bar{p})\right], \tag{5.3.27}$$

where the bar denotes quantities calculated at $\bar{r}$ and $\phi_v = 1 + \xi\kappa v^2/(8\pi)$ is the vev of ϕ. Outside the body, where $p = E = 0$ everywhere and $\mathrm{e}^{2\lambda}$ is positive definite, we have two cases:

- $\bar{\phi}'' > 0$, i.e. a local minimum, which implies that $\bar{\phi} > \phi_v$,
- $\bar{\phi}'' < 0$, i.e. a local maximum, which implies that $\bar{\phi} < \phi_v$.

This shows that if there is a local maximum or a local minimum for ϕ at a point outside the body, then the field cannot converge to its vev ϕ_v at infinity. This is possible only if ϕ is a monotone and decreasing function of r (or if $\phi = \phi_v$ everywhere). As we will see further, this property allows to approximate the Higgs field outside the body with a Yukawa function and an associated scalar charge (see Eq. (3.2.53) for a general definition). This is no longer true inside the body, as $E - 3\bar{p} > 0$ and the displacement of ϕ from its vev can be compensated by contributions from the energy density and the pressure. Thus, we can have both minima and maxima of the field inside the body. In other words, ϕ can oscillate only inside the body. The monopole solution that is reported in App. C.1, illustrates this analytical property.

Let us look at the equations of motion in the absence of matter, i.e. with $\rho = p = 0$. From the Klein-Gordon equation (5.3.24), we see that, in this case, asymptotic flatness (namely $\lambda' = \nu' = \phi' \simeq 0$ for large r) is consistent with $\phi(r \to \infty) = \phi_v \approx 1$ (since $\kappa\xi v^2 \ll 1$) only if,

$$2V(\phi_\infty) - \phi_\infty \left.\frac{\mathrm{d}V}{\mathrm{d}\phi}\right|_{\phi=\phi_\infty} = 0. \tag{5.3.28}$$

As discussed in [Sotiriou12], this implies that the only asymptotically flat solution to the equations of motion is the one that coincides with GR, namely the Schwarzschild metric with constant scalar field.

5.3.3.1 Classical energy

In STT, it is customary to calculate the binding energy of the system and compare it to the GR value in order to see if a solution is energetically favored. The binding energy (see also Sec. 2.3.4) is defined by the difference between

the baryonic energy (the energy of the baryons if they were dispersed) and the ADM energy $E_{\rm bin} = E_{\rm bar} - E_{\rm ADM}$. The baryonic energy is defined by,

$$E_{\rm bar} \equiv \int_{\rm V} {\rm d}^3x\sqrt{^{(3)}g}T^0_{0,({\rm M})}, \tag{5.3.29}$$

$$= \int_{\rm V} {\rm d}^3x\sqrt{^{(3)}g}\, n(r)m_{\rm b}, \tag{5.3.30}$$

$$= \frac{4\pi}{\phi}\int_0^{\mathcal{R}} {\rm d}r\, r^2\rho(r){\rm e}^{\lambda(r)}, \tag{5.3.31}$$

where $n(r)$ is the density number, $m_{\rm b}$ is the average mass of a baryon, $\rho(r)$ is the density profile and $\sqrt{^{(3)}g}$ is the proper volume measure. The ADM energy is defined as (see also Eq. (2.3.10)),

$$E_{\rm ADM} \equiv \int_{\rm V} {\rm d}^3x\sqrt{^{(3)}g}\left[T^0_{0,({\rm M})} + T^0_{0,({\rm H})}\right], \tag{5.3.32}$$

$$= -4\pi\int_0^{\infty} {\rm d}r\, r^2\rho_{\rm tot}, \tag{5.3.33}$$

where $\rho_{\rm tot}$ is the total energy density, including the scalar field contributions. In our case, it is given by Eq. (5.3.25). In general, when the potential is such that the scalar field vanishes at its minimum, there are always two types of solutions. The first has a vanishing scalar field everywhere and coincides with standard GR solutions. In the absence of matter and angular momentum, this solution is the Schwarzschild metric. The second solution has a varying scalar field and it approaches the Schwarzschild solution only at spatial infinity. In that case, the compact object carries a scalar charge whose effects are asymptotically vanishing [Damour93a, Salgado98]. The important point is that the two families of solution are smoothly connected and this allows to compare the binding energy of the two configurations and to determine the stable one, or at least the one that minimizes the energy[(9)]. In our case, however, this comparison is meaningless since the monopole solution cannot smoothly reduce to the Schwarzschild one because of the nonminimal coupling. In fact, the monopole is the unique solution (for a given energy density and radius) with finite energy. All other solutions have either a diverging or vanishing scalar field H at spatial infinity, as highlighted in Sec.5.3.2. In the first case, the potential term diverges so $E_{\rm ADM}$ is infinite. In the second case, if $H \to 0$ then $\phi \to (2\kappa)^{-1}$ so the term r^2V/ϕ diverges, yielding again an infinite ADM energy [(10)].

5.3.3.2 The TOV equation

We now find an approximate formula for the pressure as a function of the energy density and the value of the scalar field at the center $\phi_{\rm c}$, in analogy

[(9)]The stability under small perturbations of the metric is a different and much more complicated issue that will not be considered in this work.

[(10)]For a correct calculation of the mass associated to a de Sitter black hole see Ref. [Gibbons77].

with the usual TOV equation (see also Sec. 2.3.4). To do so, it is sufficient to expand and solve the equations of motion around $r = 0$. It should be kept in mind that, for the monopoles, the value of $\phi_{\rm c}$ (or, equivalently, of $\bar{V}(r = 0)$) is not arbitrary. As we explained in the previous sections, the value of $\phi_{\rm c}$ for a given mass and body radius is determined by the condition that $\phi = \phi_v$ at spatial infinity and, therefore, cannot be fixed by a local expansion. This is the reason why the best we can do, analytically, is to find the central pressure $p_{\rm c} = p(r = 0)$ as a function of $\phi_{\rm c}$. As before, we assume that $\rho = E = \text{const}$. At the center, owing to spherical symmetry, the scalar field can be approximated by $\phi \simeq \phi_{\rm c} + \phi_2 r^2$ so that we can solve the tt-component of the Einstein equations and find,

$$\mathrm{e}^{2\lambda(r)} = \left[1 - \frac{2m(r)}{r}\right]^{-1}, \tag{5.3.34}$$

where

$$m(r) \simeq \frac{\left(2\kappa E + \bar{V}_{\rm c}\right) r^3}{12\phi_{\rm c}}, \tag{5.3.35}$$

with $\bar{V}_{\rm c} = \bar{V}(\phi_{\rm c})$. This result can be inserted in the rr-component of the Einstein equations, which, together with the usual TOV equation (2.3.6), gives the modified TOV equation,

$$\frac{\mathrm{d}p(r)}{\mathrm{d}r} \simeq -\frac{\left[p(r) + E\right]\left[\kappa E + 3\kappa p(r) - \bar{V}_{\rm c}\right]\, r}{6\phi_{\rm c} - \left(2\kappa E + \bar{V}_{\rm c}\right) r^2}, \tag{5.3.36}$$

that can be solved by separation of variables with the boundary condition that $p = 0$ at $r = \mathcal{R}$. The result reads,

$$p(r) = \frac{E(\kappa E - \bar{V}_{\rm c})\left(\sqrt{1 - 2m/r} - \sqrt{1 - 2m\mathcal{R}^2/r^3}\right)}{3\kappa E\sqrt{1 - 2m\mathcal{R}^2/r^3} - (\kappa E - \bar{V}_{\rm c})\sqrt{1 - 2m/r}}, \tag{5.3.37}$$

where m is the function (5.3.35). This equation reproduces the relativistic expression in the limit $\bar{V}_{\rm c} \to 0$. At the center of the body we have,

$$p_{\rm c} = \frac{E(\kappa E - \bar{V}_{\rm c})\left[1 - \sqrt{1 - 2m(\mathcal{R})/\mathcal{R}}\right]}{3\kappa E\sqrt{1 - 2m(\mathcal{R})/\mathcal{R}} - \kappa E + \bar{V}_{\rm c}}, \tag{5.3.38}$$

where $m(\mathcal{R})$ is the mass function (5.3.35) calculated at $r = \mathcal{R}$. As for the ordinary relativistic stars, there is a maximum value of the energy density, at which the pressure diverges, given by

$$E_{\rm max} = \frac{12\phi_{\rm c} - \bar{V}_{\rm c}\mathcal{R}^2}{2\kappa\mathcal{R}^2}. \tag{5.3.39}$$

However, in contrast with the GR case, there exists also a critical value of the energy density, below which the pressure becomes negative, that is

$$E_{\rm min} = \frac{\bar{V}_{\rm c}}{\kappa} = \frac{\lambda_{\rm sm}}{2}\left[\frac{8\pi}{\xi\kappa}(\phi_{\rm c}-1)-v^2\right]^2, \qquad (5.3.40)$$
$$= \frac{\lambda_{\rm sm}}{2}\left(H_{\rm c}^2-v^2\right)^2.$$

The interpretation is that the Higgs field potential contributes with a negative pressure at the center of the body, at least in the linearized regime considered in this section. When this approximation is no longer valid, we need to resort to numerical tools to calculate the central pressure and verify in which part of the parameter space it is negative and an eventual threat to the stability of the spherical body.

5.3.3.3 Discussion about astrophysical compact objects

In App. B, the PPN formalism (see also Sec. 2.2) for the Brans-Dicke theory is reviewed. It leads straightforwardly to the PPN analysis for the Higgs monopoles, which tells us the amount of deviations from GR outside a body of the size of the Sun. However, because of the presence of the potential, PPN parameters only give upper bounds. According to the PPN prescriptions, we assume that far outside the Sun, the Higgs field is close to its vacuum value so that $V \simeq 0$ and the Newton's constant coincides with its bare value. The PPN parameters follow immediately from Eqs. (B.0.25) and (B.0.62) [Damour92],

$$\gamma_{\rm PPN} = \frac{\omega+1}{\omega+2}, \qquad \beta_{\rm PPN}-1 = \frac{1}{(2\omega+3)^2(2\omega+4)}\frac{{\rm d}\omega}{{\rm d}\phi}. \qquad (5.3.41)$$

When $\phi \to \phi_v, \omega(\phi=\phi_v) \simeq 2\pi m_{\rm pl}^2/(\xi^2 v^2) \simeq 1.5\times 10^{26}$ and $({\rm d}\omega/{\rm d}\phi)(\phi=\phi_v) \simeq -(2\pi/\xi^3)(m_{\rm pl}^4/v^4) \simeq -3\times 10^{55}(-2.2\times 10^{-20})$ for $\xi = 10^4$ according to Higgs inflation. It results that the PPN parameters $\beta_{\rm PPN}-1=\gamma_{\rm PPN}-1=0$ with a precision far larger than the current observational constraints. Moreover, these are upper bounds since the Higgs field is massive ($V \neq 0$) and thus decays as a Yukawa function outside the matter distribution at a much faster rate than $1/r$ (typical in the case of a vanishing scalar potential, [Damour92]). The scalar charge is thus almost completely screened over a distance of a few Schwarzschild radii.

Following the discussion in Sec. 5.3.2, the equilibrium point of the effective potential inside the compact object (5.3.15) gives an upper bound on the central value of the Higgs field $H_{\rm c}$, $|H(r)| \leq |H_{\rm c}| \leq |H_{\rm eq}^{\rm in}| \; \forall \; r \geq 0$. Inside the matter distribution, the Ricci scalar is found to be nearly constant and well approximated by $R \approx R(r=\mathcal{R}) = 3s^3/r_{\rm s}^2$ where s is the compactness of the compact object and $r_{\rm s} = 8\pi\rho_0/(3m_{\rm pl}^2)\mathcal{R}^3$ is its standard Schwarzschild radius[(11)] (see Eq. (5.3.48) in the next section). This allows one to give the order

[(11)] The physical Schwarzschild radius should take into account also the contribution of the Higgs

of magnitude of $H_{\rm eq}^{\rm in}$,

$$H_{\rm eq}^{\rm in} - v \simeq \frac{3s^3\xi}{16\pi r_{\rm s}^2 \lambda_{\rm sm} v}. \tag{5.3.42}$$

Considering the Sun ($s = 10^{-6}$ and $m \sim 10^{30}$ kg) and viable nonminimal parameter for Higgs inflation ($\xi = 10^4$) yields,

$$H_{\rm eq}^{\rm in} - v \sim 10^{-58} v, \tag{5.3.43}$$

such that no observable effect can be detected. The effect of the Higgs field in the Sun ($s = 10^{-6}$ and $m \sim 10^{30}$ kg) remains smaller than $H_{\rm eq}^{\rm in} - v \ll 10^{-2} v$ provided that $\xi < 10^{58}$. Therefore, we can conclude that deviations from GR around astrophysical objects like the Sun are outstandingly small, provided that the nonminimal coupling parameter ξ is not extremely large.

Considering NSs ($s = 0.2$ and $m \sim 10^{30}$ kg), the variation of the Higgs field cannot be larger than,

$$H_{\rm eq}^{\rm in} - v \sim 10^{-41} v, \tag{5.3.44}$$

for $\xi = 10^4$. For example, if $\xi = 10^4$ we find that $H_{\rm c}/v < 1.01$ for a mass $m > 3 \times 10^{10}$ kg with $s = 0.2$ and $H_{\rm c}/v < 1.01$ for a compactness of $s < 10^{-5}$ and a mass of 10^4 kg. We conclude that no effect is measurable in astrophysical compact objects.

5.3.4 Numerical results

After discussing the dynamics of the model and some generic analytical results, we now study numerically the properties of the solutions. We report the reader to App. D for the complete set of equations of motion, the system of units and the numerical methods that we used. In the previous sections, we have shown that the metric components inside the compact object are almost the same as in GR when we choose the SM values for the parameters of the potential. Therefore, we follow a simplified procedure, which consists in using the GR solution (with the top-hat matter distribution (5.3.10)) for the metric components and focus solely on the non-trivial dynamics of the Higgs field. We provide for a proof of this approximation in App. D through the comparison between this approach and the numerical integration of the unaltered system of equations of motion. With these assumptions, the problem essentially reduces to solving the Klein-Gordon equation,

$$h_{uu} + h_u \left(\nu_u - \lambda_u + \frac{2}{u} \right) = {\rm e}^{2\lambda} \left(-\frac{R\xi h}{8\pi} + \frac{r_{\rm s}^2}{m_{\rm pl}^2 \tilde{v}^2} \frac{{\rm d}V}{{\rm d}h} \right), \tag{5.3.45}$$

where $h = H/(m_{\rm pl}\tilde{v})$, $\tilde{v} = v/m_{\rm pl}$ being the dimensionless vev, and a subscript u denotes a derivative with respect to $u = r/r_{\rm s}$. The metric fields and the

field. Here, we define it instead as a scale of the theory, uniquely determined by the baryonic mass of the monopole as in GR.

scalar curvature are approximated by the interior and exterior Schwarzschild metric, and read respectively,

$$\mathrm{e}^{2\nu}(u) = \begin{cases} \frac{3}{2}\sqrt{1-s} - \frac{1}{2}\sqrt{1-s^3u^2}, & 0 < u < s^{-1}, \\ 1 - u^{-1}, & u \geq s^{-1}, \end{cases} \tag{5.3.46}$$

$$\mathrm{e}^{-2\lambda}(u) = \begin{cases} 1 - s^3u^2, & 0 < u < s^{-1}, \\ 1 - u^{-1}, & u \geq s^{-1}, \end{cases} \tag{5.3.47}$$

$$R(u) = \begin{cases} -\frac{6s^3}{r_{\mathrm{s}}^2}\left(\frac{2\sqrt{1-s^3u^2}-3\sqrt{1-s}}{3\sqrt{1-s}-\sqrt{1-s^3u^2}}\right), & 0 < u < s^{-1}, \\ 0, & u \geq s^{-1}, \end{cases} \tag{5.3.48}$$

Regularity at the origin requires that $h_u|_{u=0} = 0$ leaving $h_{\mathrm{c}} = h(u = 0)$ as the only initial condition for Eq. (5.3.45).

In Fig. 5.2 we plot the numerical solutions of Eq. (5.3.45) for different values of the initial condition $h_{\mathrm{c}} = h(u = 0)$. We see that, for fixed mass and compactness, there exists only one value for the initial condition $h_{\mathrm{c}} = h_0$ that yields a solution that tends to $h = 1$ at spatial infinity (marked by a thicker line). This solution corresponds to the non-trivial, asymptotically flat, and spherically symmetric distribution of the Higgs field, dubbed "Higgs monopole" in [Füzfa13, Schlögel14]. For slightly different initial conditions $h_{\mathrm{c}} \neq h_0$, the field either diverges (if $h_{\mathrm{c}} > h_0$) or tends to zero after some damped oscillations (if $h_{\mathrm{c}} < h_0$). This result confirms the analytic treatment of Sec. 5.3.2.

For each choice of mass m, compactness s, and coupling strength ξ, there exists only one solution of the kind depicted in Fig. 5.2. Its form varies a lot in function of the parameters, as we show in Fig. 5.3 where we plotted several solutions, corresponding to the parametrization listed in Tab. 5.1. We notice that the value of the Higgs field at the center of the monopole can be lower than the vev for typically large compactness s. For small or moderate compactness, the central value of the Higgs field is generically larger than the vev.

Such behavior can be easily understood by considering the upper bound for $|h_{\mathrm{c}}|$ introduced in section 5.3.2 and discussed in Sec. 5.3.3.3. If we work in GeV units, it is expressed as,

$$h_{\mathrm{eq}}^{\mathrm{in}} = 0, \pm\sqrt{1 + \frac{R\xi}{8\pi\lambda_{\mathrm{sm}}\tilde{v}^2}} = 0, \pm\sqrt{1 + \frac{R\xi}{8\pi m_{\mathrm{H}}^2}}, \tag{5.3.49}$$

where m_{H} is the mass of the Higgs field. Since R depends on the radial coordinate (see Eq. (5.3.48)) so does the effective potential. In order to show that

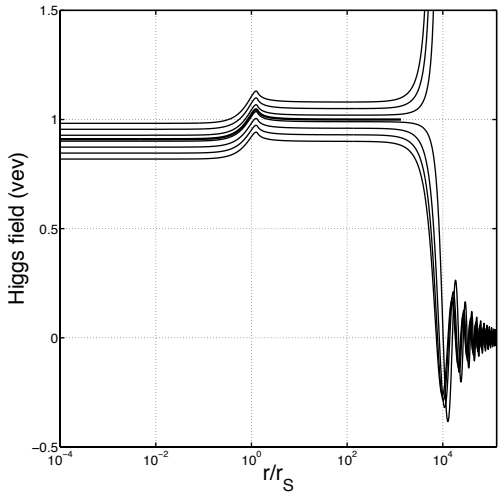

Figure 5.2: Numerical solutions of Eq. (5.3.45) with varying initial conditions $h_{\rm c} = h(r/r_{\rm s} = 0)$ for $\xi = 10$, $m = 10^6$ kg, and $s = 0.75$. The thicker line represents the unique solution that converges to $h = 1$ at large r/r_s.

we may have $|h_{\rm c}| < 1$, we approximate R in Eq. (5.3.49) by its spatial average,

$$\langle R\rangle = \frac{\int R(u)\sqrt{g}\,\mathrm{d}^3x}{\int \sqrt{g}\,\mathrm{d}^3x} = \frac{\int_0^{1/s} R(u)u\,\mathrm{e}^{\lambda}\mathrm{d}u}{\int_0^{1/s} u\,\mathrm{e}^{\lambda}\mathrm{d}u}. \tag{5.3.50}$$

In Fig. 5.4 we plot the value of $\langle R\rangle$ in function of the compactness. We see that, for $s \gtrsim 0.72$, $\langle R\rangle$ becomes negative so that $h_{\rm eq}^{\rm in} < 1$, which implies $|h_{\rm c}| < 1$. This happens, for instance, for the monopole represented by the curve B in Fig. 5.3. In this plot we also notice that, for large ξ, oscillations are present only inside the compact body (see monopoles A and C), confirming the analytical results found in Sec. 5.3.3.

Finally, we point out that the central value of the Higgs field can be significantly larger than the vev (see e.g. the monopole D). We will see below that there is a novel amplification mechanism that explains these large values. The numerical relation between the mass of the monopole and the value of $h_{\rm c}$ is depicted in Fig. 5.5 for a fixed compactness $s = 0.2$ and a nonminimal coupling parameter $\xi = 60$. The plot shows an interpolation between two asymptotic values at small and large masses. For large masses, the value of $h_{\rm c}$ is bounded from above by $h_{\rm eq}^{\rm in}$ in Eq. (5.3.49) which converges to $h_{\rm eq}^{\rm in} = 1$ for $m \approx 10^9$ kg (with $s = 0.2$ and $\xi = 60$). At small masses, the central value $h_{\rm c}$ is independent of the mass because the Higgs potential contributes very little to the effective potential inside the matter distribution (see also Fig. 5.7).

In Fig. 5.6 we show that this behavior is present also for large compact-

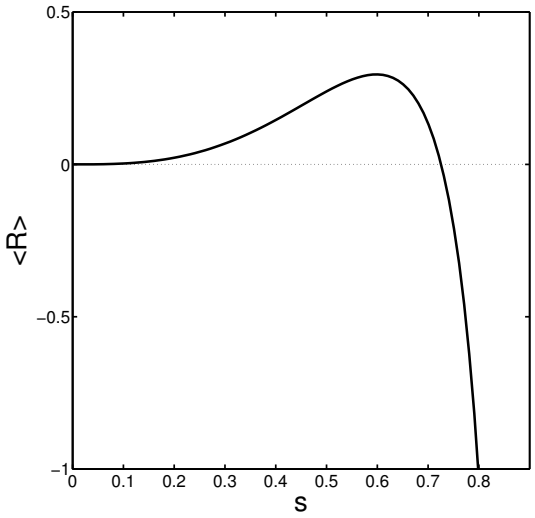

Figure 5.4: Plot of $\langle R \rangle$ as a function of the compactness in the interval $[0, \mathcal{R}]$.

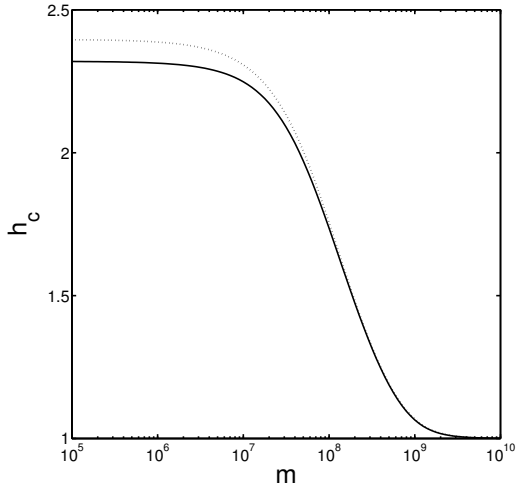

Figure 5.5: Plot of h_c as a function of the mass for $s = 0.2$ and $\xi = 60$. The solid line is the result of the numerical analysis, the dotted one is obtained with the analytical approximation described in Sec. 5.3.5.

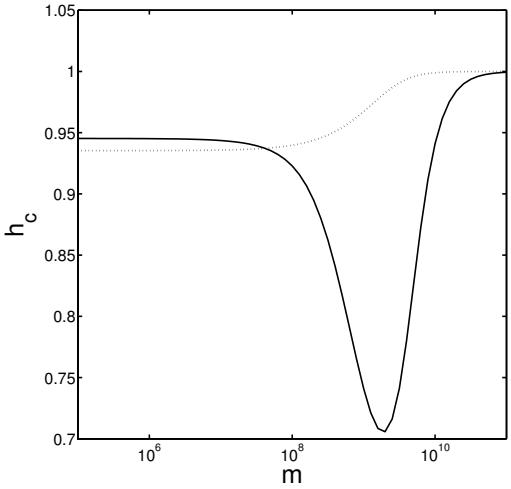

Figure 5.6: Plot of $h_{\rm c}$ in function of the mass for $s = 0.73$ and $\xi = 60$. The solid line is the result of the numerical analysis while the dotted one is obtained with the analytical approximation described in Sec. 5.3.5. We see that the analytical approximation does not work well with large s.

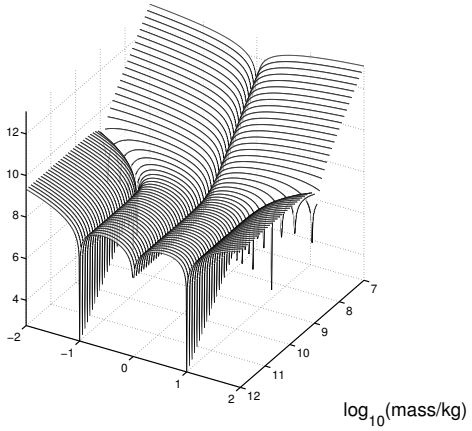

Figure 5.7: Derivative of the effective potential $V_{\rm eff}$ of Eq. (5.3.7) as a function of the mass of the monopole for fixed nonminimal coupling and compactness ($\xi = 60$ and $s = 0.5$).

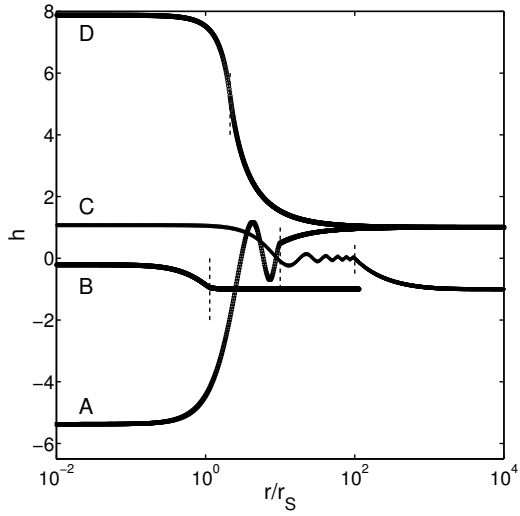

Figure 5.3: Plots of the Higgs field with the parameters listed in Tab. 5.1. The vertical dashed lines mark the radius of the body for each monopole.

	h_c	ξ	m	s
F	0.91	10	10^6 kg	0.75
A	- 5.37	10^4	10^3 kg	0.1
B	- 0.21	10	10^6 kg	0.88
C	1.077	10^6	10^6 kg	0.01
D	7.88	60	10^4 kg	0.47

Table 5.1: Properties of the Higgs monopoles plotted in Fig. 5.2 (curve F) and Fig. 5.3 (curves A,B,C,D).

ness ($s = 0.73$), which yields $|h_c| < 1$, as seen above. In Fig. 5.7 we represent the derivative of the effective potential $V_{\rm eff}$ given in Eq. (5.3.7) inside the matter distribution as a function of the mass of the monopole for fixed ξ and s. Local maxima and minima, where $\mathrm{d}V_{\rm eff}/\mathrm{d}h = 0$, are marked by the peaks appearing on the plot. We see that $h = 0$ is always a minimum while there are two maxima at $h_{\rm eq}^{\rm in}$ (see Eq.(5.3.49)), whose value converges to one for large masses. From the expression of the effective potential (5.3.7) (with averaged Ricci scalar),

$$V_{\rm eff} = -V + \frac{\xi H^2 \langle R \rangle}{16\pi}, \tag{5.3.51}$$

and the behavior of $\langle R \rangle$ (see Fig. 5.4) we deduce that the term $\xi H^2 \langle R \rangle/(16\pi)$ is dominant for small masses and becomes negligible compared to the Higgs

potential for large masses. Thus, for small masses, the field behaves inside the matter distribution as if there was no potential, in a way similar to that in spontaneous scalarization [Damour93a, Salgado98] where the field inside the body is almost constant. This explains why a plateau appears for small masses in Figs. 5.5 and 5.6. However, outside the body $R \approx 0$ and the Higgs potential can no longer be neglected compared to the nonminimal coupling term. As a result, the Higgs field decreases faster than in [Damour93a, Salgado98] because of the quartic potential.

What fixes the central value $h_{\rm c}$ of the monopoles is a non-linear phenomenon of classical resonance. In Fig. 5.8 we show an example, where $h_{\rm c}$ increases around a specific value of the compactness. For small values of s, $h_{\rm c}$ is close to one and the monopole distribution is pretty close to the homogeneous GR solution $h(r) = 1$. We find that, for astrophysical objects like the Sun, the combination of low compactness and large mass makes the Higgs field extremely close to its vev everywhere, yielding negligible deviations from GR. This is in line with the PPN analysis presented in Sec. 5.3.3.3. On the other hand, we have seen that, for $s > 0.7$, $|h_{\rm c}|$ is smaller than one, since $\langle R \rangle$ is negative. Between these two extreme cases, there exists a specific value of s that maximizes $h_{\rm c}$. This is a new result due to the combined action of the nonminimal coupling and the field potential. In fact, it is absent if the potential vanishes as in [Salgado98].

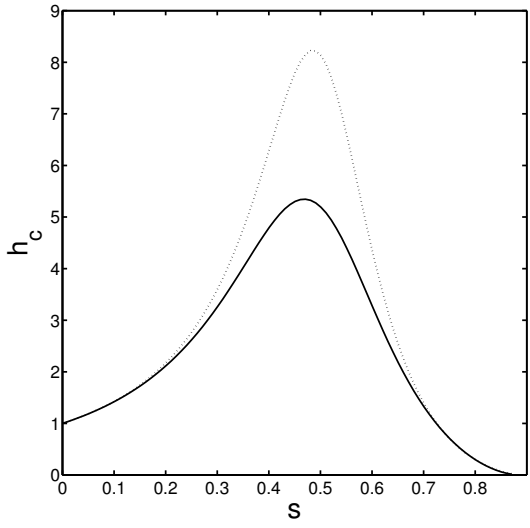

Figure 5.8: The plot of $h_{\rm c}$ shows a peak at some value of s and for fixed ξ. In the case plotted here (solid line) we choose $m = 100$ kg and $\xi = 55$. The dotted line is obtained with the analytical approximation described in Sec. 5.3.5.

5.3.5 Amplification mechanism

In this section, we present an analytical model of the scalar field resonant amplification found numerically in the previous section. As before, we consider the Klein-Gordon equation (5.3.45) in dimensionless units and we suppose that the metric fields λ and ν are the ones given by GR. The combination of Eqs. (5.3.46) and (5.3.47) gives,

$$\nu_u - \lambda_u + \frac{2}{u} = \begin{cases} -\frac{uR}{6(1-s^3u^2)} + \frac{2}{u} & 0 < u < 1/s, \\ \frac{2u-1}{u(u-1)} \approx \frac{2}{u-1} & u > 1/s, \end{cases} \tag{5.3.52}$$

where the top (bottom) line corresponds to the internal (external) solution.

We now expand $\mathrm{d}V/\mathrm{d}h$ around $h = h_*$, where $h_* = 1$ outside and $h_* = h_\mathrm{c}$ inside the body. The function to be expanded has the form,

$$f(h) = \alpha h \left(h^2 - 1\right), \tag{5.3.53}$$

where $\alpha = 2\lambda_\mathrm{sm} r_\mathrm{s}^2 m_\mathrm{pl}^2 \tilde{v}^2$, thus, up to the first order,

$$f(h) \approx \alpha \left[h_* \left(h_*^2 - 1\right) + \left(3h_*^2 - 1\right)(h - h_*)\right]. \tag{5.3.54}$$

We now examine more carefully the external and internal solutions of the Klein-Gordon equation.

5.3.5.1 External solution

For the external solution, we can assume that $u \gg 1$, $R \simeq 0$ (like for the numerical treatment), $\nu_u - \lambda_u + \frac{2}{u} \simeq \frac{2}{u}$, and $\mathrm{e}^{2\lambda} \sim 1$ and the Higgs field is essentially driven by the quartic potential with extrema at $h \simeq \pm 1$ since the Higgs field settles to its vev at large distance. After the expansion, upon the change of variables $h = Y/u$ and $Z = Y - u$, Eq. (5.3.45) can be written as,

$$Z_{uu} = \alpha Z, \tag{5.3.55}$$

which has the general solution,

$$h_\mathrm{ext} = \frac{\mathcal{C}_1}{u}\mathrm{e}^{\sqrt{\alpha}u} + \frac{\mathcal{C}_2}{u}\mathrm{e}^{-\sqrt{\alpha}u} + 1, \tag{5.3.56}$$

for arbitrary constant $\mathcal{C}_1$ and $\mathcal{C}_2$. The requirement $\lim_{u\to\infty} h = 1$ yields $\mathcal{C}_1 = 0$, so we find the Yukawa distribution for the Higgs field outside the compact object given by,

$$h_\mathrm{ext} = \frac{Q}{u}\mathrm{e}^{-u/L} + 1. \tag{5.3.57}$$

The parameters $Q = \mathcal{C}_2$ and $L = 1/\sqrt{\alpha}$ can be identified as the scalar charge and the characteristic length respectively, which further justifies the term "monopole" used to name these solutions. To fix $\mathcal{C}_2$, we will use the continuity condition of the Higgs field at the boundary of the compact object given by $h_\mathrm{ext}(1/s) = h_\mathrm{int}(1/s)$. In addition, the continuity condition of the derivative, $h'_\mathrm{ext}(1/s) = h'_\mathrm{int}(1/s)$, will lead to an implicit equation for h_c.

5.3.5.2 Internal solution

We now derive the analytical Higgs field profile for the internal region. We make the same assumption as before for the terms involving ν and λ, excepted $u \simeq 0$ and $R \sim \langle R \rangle \neq 0$. We now expand $f(h)$ around $h_* = h_{\rm c}$ and change the variables according to $h = Y/u$ as well as,

$$Z = Y + \frac{B(h_{\rm c})}{A(h_{\rm c})} u, \tag{5.3.58}$$

where

$$A(h_{\rm c}) = \frac{\alpha}{2}\left(3h_{\rm c}^2 - 1\right) - \frac{\langle R \rangle \xi}{8\pi}, \tag{5.3.59}$$

$$B(h_{\rm c}) = -\alpha h_{\rm c}^3. \tag{5.3.60}$$

We then obtain the differential equation,

$$Z_{uu} = A\left(h_{\rm c}\right) Z, \tag{5.3.61}$$

for which it is sufficient to discuss the solution for $A\left(h_{\rm c}\right) < 0$, the positive case being basically the same. The case $A\left(h_{\rm c}\right) = 0$ is not considered as it corresponds to a fine-tuning of the parameters. The solution reads,

$$h_{\rm int} = \frac{\mathcal{D}_1}{u} {\rm e}^{\sqrt{A}u} + \frac{\mathcal{D}_2}{u} {\rm e}^{-\sqrt{A}u} - \frac{B}{A}, \tag{5.3.62}$$

where $\mathcal{D}_1$ and $\mathcal{D}_2$ are constants of integration. The condition of regularity of the Higgs field at the origin, $h_{\rm int}(u = 0) = h_{\rm c}$ implies that $\mathcal{D}_1 = -\mathcal{D}_2$. In addition, the limit $u \to 0$ enables to fix $\mathcal{D}_1$,

$$\mathcal{D}_1 = \frac{1}{\sqrt{|A|}}\left(h_{\rm c} + \frac{B}{A}\right), \tag{5.3.63}$$

so, the linearized expression for the Higgs field inside the compact object is given by,

$$h_{\rm int} = \frac{\mathcal{D}_1}{u} \sin\left(\sqrt{|A|}u\right) - \frac{B}{A}. \tag{5.3.64}$$

As mentioned above, the conditions of continuity of the Higgs field and its derivative allow to fix $\mathcal{C}_2$ and to derive an implicit equation for determining $h_{\rm c}$. Indeed, by imposing $h_{\rm ext}\left(1/s\right) = h_{\rm int}\left(1/s\right)$, we find that,

$$\mathcal{C}_2 = \frac{1}{s} {\rm e}^{\frac{\sqrt{\alpha}}{s}} \left[\mathcal{D}_1 s \sin\left(\frac{\sqrt{|A|}}{s}\right) - \frac{B}{A} - 1\right], \tag{5.3.65}$$

while the regularity condition $h'_{\rm ext}\left(1/s\right) = h'_{\rm int}\left(1/s\right)$ yields the implicit equation,

$$\left(h_{\rm c} + \frac{B}{A}\right)\left[\sqrt{\frac{\alpha}{|A|}} \sin\left(\frac{\sqrt{|A|}}{s}\right) + \cos\left(\frac{\sqrt{|A|}}{s}\right)\right] = \left(1 + \frac{B}{A}\right)\left(1 + \frac{\sqrt{\alpha}}{s}\right). \tag{5.3.66}$$

The solution for the case $A(h_c) > 0$ can be found by replacing the sine and cosine by hyperbolic sine and hyperbolic cosine. However, the condition $A(h_c) < 0$ is necessary for the resonant amplification. The expression (5.3.66) greatly simplifies when α is small as for macroscopic bodies [12]. In fact, since $B/A \simeq 0$ when α is negligible, the implicit equation for h_c (5.3.66) reduces to,

$$h_c = \left| \cos \sqrt{\frac{\xi \langle R \rangle}{8\pi s^2}} \right|^{-1}, \tag{5.3.67}$$

where the absolute value is necessary when the positive h_c branch is chosen. In this approximation, the central value of the Higgs field h_c has periodic divergences corresponding to certain values of s, ξ and m. E.g. for asteroids, the compactness is very small ($s \sim 10^{-12}$) and one finds that $h_c = 1$ to great accuracy. Notice that, for small s, the condition $A < 0$ is no longer true and $\cos$ to $\cosh$ must be switched, which yields, however, the same result. We thus confirm the results obtained in the previous section: for small values of the compactness, the central value of the Higgs field h_c is very close to the Higgs vev. For larger values of the compactness, the approximate formula (5.3.67) shows that, for a given m and ξ, h_c has peaks corresponding to critical values of s. These are the resonances that we have also seen numerically. The number of peaks depends on the nonminimal coupling ξ as we will see on the next section. Note that the condition $A(h_c) < 0$ is favored by a large nonminimal coupling (see Eq. (5.3.59)), and so the approximate equation (5.3.67), is even more accurate in the large s regime. As we will see in the next section, there exists a critical value of ξ for which one peak splits into two separate peaks. Another interesting limit is $\sqrt{A}/s \ll 1$. In this case, the formula reduces to,

$$\left(h_c + \frac{B}{A}\right)\left(1 + \frac{\sqrt{\alpha}}{s}\right) \simeq \left(1 + \frac{B}{A}\right)\left(1 + \frac{\sqrt{\alpha}}{s}\right), \tag{5.3.68}$$

which implies that $h_c \sim 1$. The regime $A/s^2 \sim 0$ corresponds to,

$$r_s = \frac{16\pi\lambda v^2 \mathcal{R}^3}{3\xi}, \tag{5.3.69}$$

where $\mathcal{R}$ is the radius of the compact object (assuming $\langle R \rangle \approx 3s^3/r_s^2$). This relation can be written again as $s\xi \simeq (10^{18}\mathcal{R})^2$ with $\mathcal{R}$ expressed in meters. It is then obvious that this regime is totally unphysical unless ξ is very large [13].

5.3.5.3 Analysis of the parameter space

As we saw in Sec. 5.3.4, Figs. 5.5, 5.6, and 5.8, the value of h_c as a function of the parameters can be qualitatively reproduced thanks to the analytical model presented in last section. There are some discrepancies (see for instance Fig.

[12] As an example, for an object of the mass range of an asteroid ($M \simeq 10^7$), $\alpha \simeq 10^{-25}$.
[13] A very large ξ is not excluded by LHC experiments, see [Atkins13].

5.6 for large compactness) but the analytical model expressed by Eq. (5.3.66) is sufficient to understand the amplification mechanism. For example, in Fig. 5.8 we see a good agreement between our analytical model and the full solution for the position of the resonance, although there is an overestimation of its amplitude, up to a factor two.

In the rest of this section, we will use the analytical model to explore the parameter space of the monopole, given by mass, compactness, and nonminimal coupling. Once these are fixed, the central value of the Higgs field is uniquely determined by the implicit equation (5.3.66).

In Fig. 5.9 we show how the resonance in $h_{\rm c}$ evolves as a function of the compactness and of the nonminimal coupling. As ξ increases, the peak grows and sharpens. The question is then how large the resonance can be. It seems that there exists a critical value of $\xi = \xi_{\rm cr}$ above which $h_{\rm c}$ diverges. This is illustrated in Fig. 5.10 where we plotted $h_{\rm c}$ for both $\xi < \xi_{\rm cr}$ and $\xi = \xi_{\rm cr}$. The two vertical asymptotes in $h_{\rm c}$ appear when the nonminimal coupling becomes larger than $\xi = \xi_{\rm cr}$ and they correspond to a phase transition, in which $h_{\rm c}$ switches sign. We recall in fact that there are two branches corresponding to $v = \pm 246$ GeV. Even though we chose v to be the positive root, there is still the possibility that $h(r)$ jumps to the negative branch, which is a perfectly valid mathematical solution of the Klein-Gordon equation [(14)].

This also implies that, when the nonminimal coupling is larger than $\xi_{\rm cr}$, there can be forbidden values for s (or, equivalently, for $\mathcal{R}$) in the parameter space. As an example, we plot in Fig. 5.11 $h_{\rm c}$ in function of the compactness for $m = 10^2$ kg and $\xi = 10^4$, which corresponds to the value predicted by Higgs inflation [Bezrukov08, Bezrukov11, Bezrukov09b]. We see that there are multiple divergences, also for relatively small values of s. However, this does not prevent the nonminimal coupling parameter to be arbitrarily large since $\xi_{\rm cr}$ basically depends on the mass of the monopole.

On Fig. 5.12, $h_{\rm c}$ is plotted in function of m and s for three values of ξ. We see that $h_{\rm c}$ generically settles to its vev, $h_{\rm c} = 1$ for small compactness and large mass. For sufficiently large ξ, the peaks appear for small masses (see Fig. 5.12c) and tend to $h_{\rm c} = 1$ at large m values. The peaks sharpen as ξ increases, until $h_{\rm c}$ eventually diverge at some $\xi_{\rm cr}$. In the small mass regime the Higgs potential is much smaller than the coupling term, which is proportional to ξ, see Eq. (5.3.51). In the large mass regime, however, the upper bound imposed by Eq. (5.3.49) becomes closer and closer to one. These two competing effects explain qualitatively the presence of the peaks in the small mass region rather than in the large mass one, provided the compactness s is not too small, otherwise $\langle R \rangle$ is too small and always smaller than the Higgs potential. In such a case, scalar amplification is negligible, no matter the monopole mass.

In summary, for large values of the nonminimal coupling, monopoles with small masses cannot exist for certain values of the compactness for which the

[(14)] This problem could be avoided by considering a Higgs multiplet with an Abelian $U(1)$ symmetry. The amplitude and the phase of the Higgs field would be under a much better analytical and numerical control.

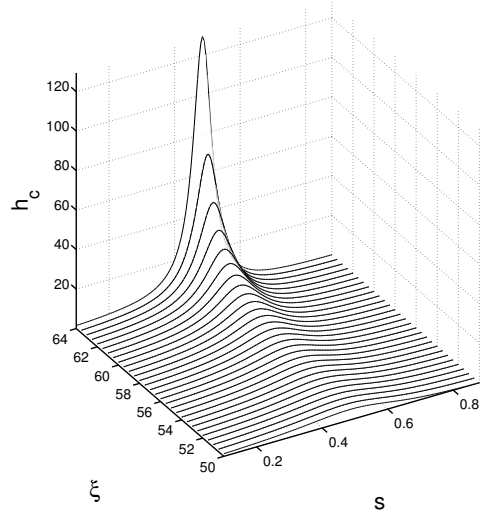

Figure 5.9: Plot of $h_{\rm c}$ in function of s and ξ as given by the implicit relation (5.3.66) for a fixed mass $m = 10^3{\rm kg}$. We see that the peak sharpens for increasing ξ.

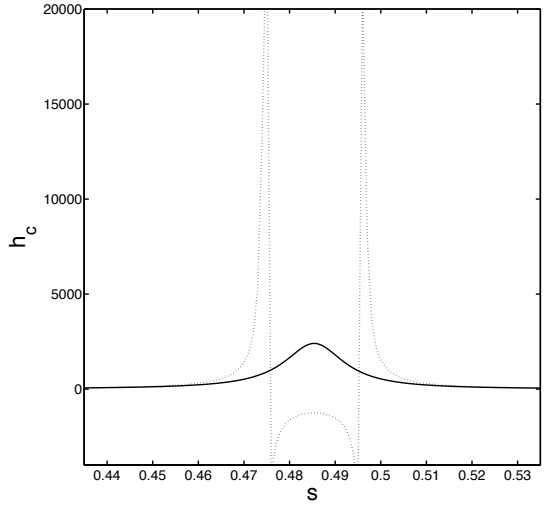

Figure 5.10: Plot of $h_{\rm c}$ given by the implicit Eq. (5.3.66) in function of the compactness for $\xi = 64.6$ (solid line) and $\xi = 64.7$ (dashed line). The monopole mass is fixed at $m = 10^3{\rm kg}$.

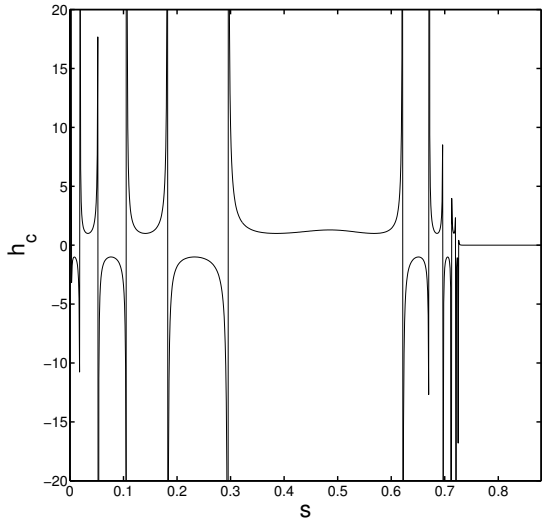

Figure 5.11: Plot of h_c in function of s for $\xi = 10^4$ and $m = 10^2\mathrm{kg}$ obtained from the expression (5.3.66).

Higgs field at the center of the body diverges. On the opposite, large mass monopoles always exist but the scalar amplification is much smaller.

5.4 Conclusion and perspectives

The Higgs monopole is inspired by Higgs inflation, where the coupling strength $\xi \gtrsim 10^4$ in order to get a viable inflationary model. Such a large coupling could imply a strong deviation from GR, possibly in conflict with astrophysical observations. We show that the deviations are so small ($h_c - 1 < 10^{-58}$ for the Sun and 10^{-41} for typical neutron stars parameters) that there are not far below the observational sensitivity today. This is due to the hierarchy between the vev and the Planck scale, which remains unexplained.

However, the main result of [Füzfa13, Schlögel14] is the existence of particlelike solutions that are asymptotically flat and have finite classical energy and that cannot smoothly reduce to GR as they only exist because of the violation of the equivalence principle. The Higgs inflation predicts deviations from the Higgs vev inside any compact objects, the Schwarzschild solution being never recovered. Nevertheless, since the deviations from the Higgs vev depends on the compactness and the baryonic mass of the compact object, the Higgs monopoles solution is indistinguishable from the Schwarzschild one in the case of physical objects. Whereas other particlelike solutions exist only in the context of exact and unbroken gauge symmetry, as in the Einstein-Yang-

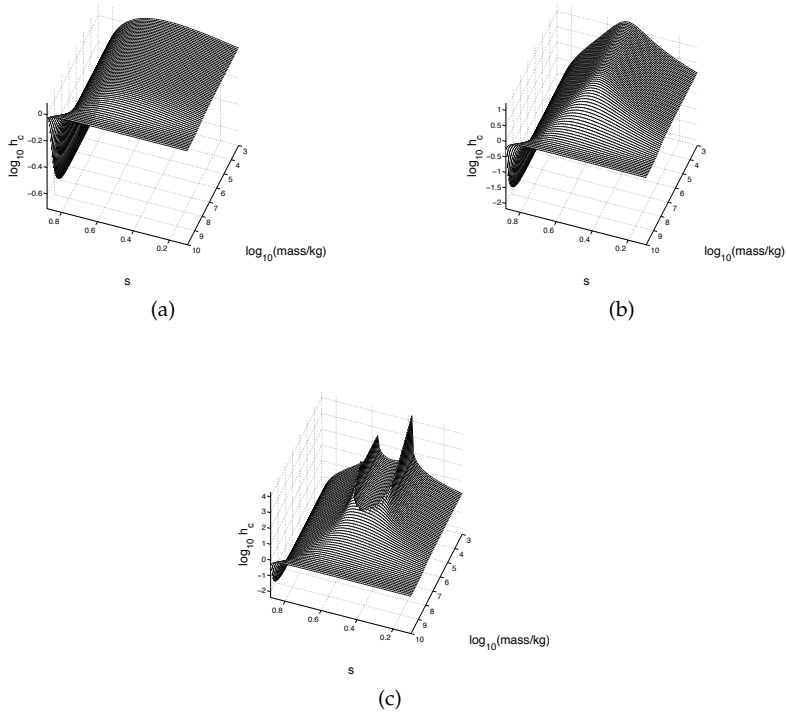

Figure 5.12: Plot of h_c (obtained with the analytical approximation) in function of the mass of the monopole and its compactness for $\xi = 10, 60, 70$ (for Figs. 5.12a, 5.12b, 5.12c respectively).

Mills system [Bartnik88], the Higgs monopole solution is compatible with spontaneously broken gauge symmetry at the price of a nonminimal coupling to gravity.

In particular, we have found a new non-linear mechanism of resonant amplification that is not present in the models with vanishing potentials studied so far since spontaneous scalarization has been studied for relatively small nonminimal coupling (see e.g. [Salgado98]). We explored this amplification mechanism numerically and found an analytical approximation that shows that, in the large coupling regime, there are forbidden combinations of radius and baryonic density, at which the value of the Higgs field at the center of the spherical body tends to diverge. As for spontaneous scalarization, the amplification mechanism found here is a general feature that can be applied to cases with different parameters and/or potential shapes.

In principle, the shift in the Higgs expectation value inside the compact object leads to a change in the mass of the W and Z bosons that, in turn, has an impact on the mass of decay products, decay rates and so on. In the case at hand, however, we have seen that the shift in objects like neutron stars is negligible. Larger effects are possible only in ranges of mass and density that are very unphysical, as shown in Tab. 5.1. Therefore, in realistic compact objects we do not expect any observable modification. Similarly, in the case of a Yukawa coupling to fermions we do not expect any dramatic effect for the same reasons. Technically, the addition of a Yukawa coupling to fermions would introduce in the Klein-Gordon equation new terms (one for each fermion) proportional to H, which will compete in the dynamics with the non-minimal coupling term ξR, see Eq. (5.3.5). However, for realistic objects, this contribution will be much larger than the gravitational one so we do not expect significant deviations from the case with ordinary EoS. We point out that this is a very different situation as in previous models, like [Salgado98], where the amount of spontaneous scalarization was much larger. In our case, the presence of Higgs potential in the action effectively prevents fundamental interactions to change inside compact objects.

From the quantum field theory point of view, a r-dependent vacuum leads to a non-local effective action whose effect are very small in the regime of small curvature considered here but might be important in the primordial Universe or in strong field configurations [Gorbar04].

We remark that the top-hat profile (5.3.10) is a simplifying hypothesis that saves some computational effort. Introducing a different profile, and a specific equation of state, would be more realistic but no substantial changes are expected in our results. This claim is supported by some previous work (e.g. [Salgado98, Damour96]) and by some numerical tests that we performed by smoothing out the step function.

About the stability of our solutions, we point out that any change of the value of the Higgs field at the center of the body leads to a change in the geometry of the spacetime at infinity: while particlelike solutions are asymptotically flat, any other solution is asymptotically de Sitter, as discussed in

Sec. 5.3.2. In a realistic scenario of a spherical collapse in an asymptotically flat spacetime we expect that the Higgs monopoles are the only solutions and are stable. A formal proof of this statement would require the study of perturbations around the (numerical) monopole solution (see e.g. [Volkov99]) and goes beyond the scope of this thesis, although it is a very interesting question.

In Higgs inflation, these monopoles could form and if they are not washed out by the exponential expansion, they could constitute a candidate for DM, with a mass range similar to the one of primordial BHs below the evaporation limit [(15)]. However, as they also interact through their Higgs external field, the phenomenology is expected to be distinct from the one of BHs. We also point out that there exists an intriguing possibility that the formation of these monopoles is related to the semiclassical instability found in [Lima10] and discussed in terms of spontaneous scalarization in[(16)] [Pani11]. Although for astrophysical bodies we do not expect that this instability plays a significant role, as the scalarization is negligible, it could be crucial for the formation of inflationary remnants.

There are several aspects that deserve further analysis. For instance, we assumed that the characteristic parameters are the ones of the SM (in particular the coupling $\lambda_{\rm sm}$ and the vev v, see Eq. (5.2.4)). As a result, the deviations from GR are negligible. It would be interesting to find to what extent these parameters can vary without violations of the current observational constraints.

Moreover, we believe that also the symmetry structure of the Higgs field and its influence on the solutions should be studied, relaxing the assumption of the unitary gauge which appears to be restrictive. Indeed, the Higgs field should be treated as a complex multiplet with $SU(2)$ gauge symmetry rather than as a real scalar singlet. Imposing the unitary gauge is possible only if the expansion of the Lagrangian around a classical, time-independent vacuum state. In the case of a nonminimal coupling to gravity, the classical vacuum state is time-dependent since $H = v$ is not a solution anymore. In the case of a complex multiplet, the Higgs multiplet drives rather a multifield inflation due to the presence of Goldstone components [Greenwood13], such models being in agreement with current observations from Planck [Kaiser14]. Moreover, Goldstone bosons might also play a role at low energy where they lead to an acceleration of the expansion rate due to the displacement of the Higgs field from its vev (either in the Abelian and non-Abelian cases) [Rinaldi14], even in the absence of the nonminimal coupling [Rinaldi15b] and if the effect of the coupling of the Higgs field to gauge bosons is taken into account [Rinaldi15a]. Eventually, the Higgs vacuum state has been found to be metastable that is temporarily stable on cosmological time scales, assuming that the SM is valid up to the Planck scale, this result strongly depending on the measure of the top quark mass and the Higgs mass [Degrassi12, Bednyakov15]. The implications of the metastability of the electrovacuum state should be also investigated for

[(15)] Roughly, for $h(r = \mathcal{R}) \approx 1.1v$ we have $m < 10^{11}$ kg.

[(16)] Note, however, that the stability analysis presented in [Pani11] cannot be applied to our model because the GR solution does not coexist with the monopole.

compact objects and when the Higgs field is nonminimally coupled to gravity.

Static spherically-symmetric solution for non-Abelian Higgs field have also been studied by [Brihaye15] for self-gravitating system assuming a non-minimal coupling of the Higgs to gravity. They show that the monopole and the sphaleron solutions [Volkov99, vanderBij00], that is classical and non-perturbative solutions of Einstein-Yang-Mills-Higgs theory, remain in the presence of the nonminimal coupling.

The effect of the Yukawa coupling has not been studied yet in this context. It would imply either to build an effective action for matter fields where the Yukawa coupling to fermions is explicit (and possibly the QCD contribution for the energy density too [Shifman78]) either to write a field theory where the gauge invariance is explicit and the coupling of the Higgs to fermions is introduced through spinors fields [Boehmer07].

In relation to this, we also recall that there exist exact solutions for Abelian and non-Abelian configuration in Minkowski space called Q-balls [Lee89, Coleman85, Theisen86]. In the baryonic massless limit, but with the gauge symmetry restored, Higgs monopoles could be generalized to describe gauged Q-balls in curved space. This direction remains to be explored as it might lead to discover solutions with physical properties that are compatible with DM. If not, it would nevertheless be interesting to see if these solutions are excluded by precise Solar System tests.

Chapter 6

Fab Four: When John and George play inflation and gravitation

based on

J.-P. Bruneton, M. Rinaldi, A. Kanfon, A. Hees, S. Schlögel, A. Füzfa,
Fab Four:
When John and George play gravitation and cosmology
Advances in Astronomy, Volume 2012 (2012) 430694

In the last two chapters, two STT "à la Brans-Dicke" in the presence of a potential have been studied. We now turn to a more sophisticated model, that is a subclass of the generalized Galileon model dubbed the "Fab Four" in reference to the Beatles, introduced in Sec. 3.3. In particular, we focus on the "John" Lagrangian which exhibits a nonminimal derivative coupling between the scalar field and the Einstein tensor. This model is referred to as "purely kinetic gravity" since no potential is invoked in order to predict inflation and/or dark energy.

First the phenomenology of inflation predicted by this model is analyzed in terms of number of e-folds as well as the no-ghost and causality conditions. Since a kinetically driven inflationary phase requires highly transplanckian values for the initial field velocity, which basically rule out the model, the considerations are extended to a more general model including a coupling of the scalar field to the Ricci scalar, or "George" in the Fab Four terminology. We then study the John plus George model, establishing how far inflation is viable (for background cosmology), provided that the no-ghost and causality conditions are satisfied. Finally, the deviations from GR around compact objects

predicted by George and John are studied and the Solar System constraints are derived.

6.1 The Fab Four model

The Fab Four is a subclass of Horndeski gravity [Horndeski74] (see also Sec. 3.3) justified by cosmological considerations, assuming FLRW background. More precisely the Fab Four model contains the four Lagrangians able to alleviate the cosmological constant problem, assuming that the WEP is not violated. In the Fab Four scenario, even if the vacuum energy density $\rho_{\rm vac}$ is large at all time during the Universe history, the vacuum energy is "screened" by the scalar field such that the cosmic expansion is not accelerated [Copeland12]. As a result, the vacuum energy does not affect significantly the evolution of the scale factor and the inflation/radiation/matter dominated evolution could be recovered for some combination of the Fab Four Lagrangians. The cosmological constant problem might be solved since the vacuum energy $\rho_{\rm vac}$ is allowed to have a much larger value than the cosmological constant one ρ_Λ. This solution evades the Weinberg no-go theorem (see Sec. 2.4.4) by breaking the Poincaré invariance in the scalar sector [Charmousis12a].

The resulting theory reads[(1)],

$$\mathcal{L}_{\rm john} = V_{\rm john}(\phi)G^{\mu\nu}\nabla_\mu\phi\nabla_\nu\phi, \tag{6.1.1}$$

$$\mathcal{L}_{\rm paul} = V_{\rm paul}(\phi)P^{\mu\nu\alpha\beta}\nabla_\mu\phi\nabla_\alpha\phi\nabla_\nu\nabla_\beta\phi, \tag{6.1.2}$$

$$\mathcal{L}_{\rm george} = V_{\rm george}(\phi)R, \tag{6.1.3}$$

$$\mathcal{L}_{\rm ringo} = V_{\rm ringo}(\phi)\mathcal{G}, \tag{6.1.4}$$

where $V(\phi)$'s are arbitrary potential functions, $\varepsilon_{\mu\nu\alpha\beta}$ is the Levi-Civita tensor and $P^{\mu\nu\alpha\beta} = -\frac{1}{4}\varepsilon^{\mu\nu\lambda\sigma}\ R_{\lambda\sigma\gamma\delta}\ \varepsilon^{\alpha\beta\gamma\delta}$ is the double dual of the Riemann tensor. GR is recovered considering George only with $V_{\rm george}$ =const and the Brans-Dicke model is recovered when $V_{\rm george}$ $\neq$const with the parameter $\omega(\phi) = 0$.

The covariant Galileons might pass local tests of gravity thanks to the non-linearities appearing in the kinetic term of the scalar field. This theory thus relies on the Vainshtein screening mechanism (see Sec. 3.1.3 for a definition) in order to be possibly allowed to reproduce inflation and/or the late-time cosmic acceleration while passing the local tests of gravity. Therefore, considering the Fab Four Lagrangians, the Vainshtein mechanism is expected to work for the John and/or Paul Lagrangian(s).

In the following we focus first on the John Lagrangian[(2)] and analyze what are the viable inflationary solutions. As we will see, the John Lagrangian is

[(1)] The Fab Four Lagrangians also appear in the Kaluza-Klein reduction of Lovelock gravity[Van Acoleyen11].

[(2)] George and Ringo must not be considered in isolation for theoretical and phenomenological reasons respectively [Charmousis12b]. In addition, only John and Paul might exhibit the Vainshtein screening mechanism.

not able to play alone gravitation in a static and spherically symmetric spacetime: its solution is trivial since it is the Schwarzschild one. In the rest of the chapter, we thus study the combination of George and John. The George Lagrangian is reminiscent of the Brans-Dicke theory (with the parameter $\omega = 0$) or GR ($V_{\rm george} = {\rm cst}$) such that the phenomenology should allow for minimal modifications of gravity.

6.2 The John Lagrangian

In order to study the phenomenology predicted by John, we start from the John Lagrangian (6.1.1) where the potential reduces to a constant $V_{\rm john}(\phi) = {\rm cst}$, combined with the EH action with a minimally scalar field,

$$S = \int {\rm d}^4x\,\sqrt{-g}\left[\frac{R}{2\kappa} - \frac{1}{2}\left(g^{\mu\nu} + \kappa\gamma G^{\mu\nu}\right)\partial_\mu\phi\partial_\nu\phi\right] + S_{\rm M}[\psi_{\rm M};\, g_{\mu\nu}], \quad (6.2.1)$$

where γ is a dimensionless parameter whereas ϕ has the dimension of a mass in natural units. This action is a special case of the generalized Galileon one presented in [Kobayashi11] (see Eqs. (3.3.9)-(3.3.12)), where $K(X) = X, G_3 = 0, G_4 = 1/(2\kappa), G_5 = \kappa\gamma\phi/2, G_{4X} = 0, G_{5X} = 0$.

The modified Einstein equations are then given by (see App. E.1 for the detailed computations) [Sushkov09],

$$G_{\mu\nu} = \kappa\left[T^{(\rm M)}_{\mu\nu} + T^{(\phi)}_{\mu\nu} + \kappa\gamma\Theta_{\mu\nu}\right], \quad (6.2.2)$$

with,

$$\begin{aligned}\Theta_{\mu\nu} &= -\frac{1}{2}R\,\phi_\mu\phi_\nu + 2\,\phi_{(\mu}R_{\nu)\alpha}\,\phi^\alpha - \frac{1}{2}G_{\mu\nu}\left(\nabla\phi\right)^2 + R_{\mu\alpha\nu\beta}\phi^\alpha\phi^\beta + \phi_{\alpha\mu}\phi^\alpha_{\ \nu} \\ &\quad -\phi_{\mu\nu}\Box\phi + \frac{g_{\mu\nu}}{2}\left[-\phi^{\alpha\beta}\phi_{\alpha\beta} + \left(\Box\phi\right)^2 - 2\,\phi^\alpha\phi^\beta\,R_{\alpha\beta}\right], \quad (6.2.3)\\ T^{(\phi)}_{\mu\nu} &= \partial_\mu\phi\partial_\nu\phi - \frac{1}{2}g_{\mu\nu}\left(\partial\phi\right)^2, \quad (6.2.4)\end{aligned}$$

while the Klein-Gordon equation reads,

$$\left(g_{\mu\nu} + \kappa\gamma G_{\mu\nu}\right)\nabla^\mu\nabla^\nu\phi = 0. \quad (6.2.5)$$

6.2.1 Inflation with John

As it was realized in [Sushkov09], this model allows for a quasi de Sitter inflation with a graceful exit without the need for any specific scalar potential. Inflation is essentially driven by the non-standard kinetic term of the scalar field and it crucially depends on the initial high velocity of the field, as we will shortly see. Although, in principle, the inflationary solutions begin at $t = -\infty$ such that this theory does not suffer from Big Bang singularity (see [Sushkov09]), we will consider the action as an effective model only valid from

few Planck times after an unknown transplanckian phase. Our first concern is to establish whether the model accommodates an inflationary phase together with reasonable assumptions for the initial conditions at that time. This section thus completes the analysis found in [Sushkov09] by providing the number of e-folds as a function of the free parameters of the theory. The equations of motion derived from Eq. (6.2.1) considering the metric ansatz (2.4.1),

$$\mathrm{d}s^2 = -\mathrm{d}t^2 + \mathrm{e}^{2\alpha(t)}\mathrm{d}\mathbf{x}^2, \tag{6.2.6}$$

read in the absence of matter,

$$3\dot{\alpha}^2 = \frac{\kappa\dot{\phi}^2}{2}\left(1 - 9\kappa\gamma\dot{\alpha}^2\right), \tag{6.2.7a}$$

$$2\ddot{\alpha} + 3\dot{\alpha}^2 = -\frac{\kappa\dot{\phi}^2}{2}\left[1 + \kappa\gamma\left(3\dot{\alpha}^2 + 2\ddot{\alpha} + 4\dot{\alpha}\ddot{\phi}\dot{\phi}^{-1}\right)\right], \tag{6.2.7b}$$

$$\frac{1}{a^3}\frac{\mathrm{d}}{\mathrm{d}t}\left[a^3\dot{\phi}\left(1 - 3\kappa\gamma\dot{\alpha}^2\right)\right] = 0, \tag{6.2.7c}$$

with $\alpha = \ln a$, a being the scale factor, and $\dot{\alpha} = H$, H being the Hubble parameter. In order to solve the equations of motion numerically (see Sec. 6.2.3 for the numerical results), the system is partially decoupled isolating the second order derivatives $\ddot{\alpha}$ and $\ddot{\phi}$,

$$\ddot{\alpha} = \frac{\left(3\kappa\gamma\dot{\alpha}^2 - 1\right)}{2}\frac{3\dot{\alpha}^2 + \frac{\kappa\dot{\phi}^2}{2}\left(1 - 9\kappa\gamma\dot{\alpha}^2\right)}{1 - 3\gamma\kappa\dot{\alpha}^2 + \frac{\kappa^2\gamma\dot{\phi}^2}{2}\left(1 + 9\kappa\gamma\dot{\alpha}^2\right)}, \tag{6.2.8a}$$

$$\ddot{\phi} = \frac{-3\dot{\alpha}\dot{\phi}\left(1 + \kappa^2\gamma\dot{\phi}^2\right)}{1 - 3\gamma\kappa\dot{\alpha}^2 + \frac{\kappa^2\gamma\dot{\phi}^2}{2}\left(1 + 9\kappa\gamma\dot{\alpha}^2\right)}. \tag{6.2.8b}$$

This system can be solved as an initial value problem (IVP) by fixing the initial conditions $\alpha_\mathrm{i},\ \dot{\alpha}_\mathrm{i},\ \phi_\mathrm{i},\ \dot{\phi}_\mathrm{i}$.

The effective EoS for the scalar field can be obtained from its stress-energy tensor or, more simply, by comparing the equations of motion (6.2.7a) and (6.2.7b) directly to the standard Friedmann equations (2.4.16) and (2.4.17) ($V = 0$):

1. From Eqs. (6.2.7a) and $H^2 \equiv \dot{\alpha}^2 = (\kappa/3)\rho_\phi$ (2.4.16), the energy density of the scalar field reads,

$$\dot{\alpha}^2\left(1 + \frac{3}{2}\kappa^2\gamma\dot{\phi}^2\right) = \frac{\kappa\dot{\phi}^2}{6}, \tag{6.2.9}$$

$$\dot{\alpha}^2 = \frac{\kappa\dot{\phi}^2}{3(2 + 3\kappa^2\gamma\dot{\phi}^2)} \qquad \longrightarrow \qquad \rho_\phi = \frac{\dot{\phi}^2}{(2+3\kappa^2\gamma\dot{\phi}^2)}, \tag{6.2.10}$$

2. The EoS of the scalar field is identified by comparing the standard Friedmann equation $\ddot{\alpha} + \dot{\alpha}^2 = -(\kappa/6)\rho_\phi(1 + 3w_\phi)$ (2.4.17) with the modified

one (6.2.7b). After some algebra, we obtain,

$$w_\phi = \frac{\left(2 + 3\kappa^2\gamma\dot{\phi}^2\right)\left(1 - \kappa^2\gamma\dot{\phi}^2\right)}{2 + 3\kappa^2\gamma\dot{\phi}^2 + 3\kappa^4\gamma^2\dot{\phi}^4}. \tag{6.2.11}$$

The EoS of the scalar field w_ϕ is plotted in Fig. 6.1 for $\gamma = +1$ and $\gamma = -1$. For both signs of γ, the EoS tends to -1 in the high energy limit ($\kappa|\dot{\phi}| \gg 1$), so that a large initial velocity for the scalar field will result in a quasi de Sitter phase. However, only the case of positive γ can lead to inflation. Indeed, $\dot{\alpha}$ in Eq. (6.2.10) needs to be positive since the Hubble parameter is a real number. Thus, $\gamma < 0$ implies that $\kappa\left|\dot{\phi}\right| < \sqrt{-2/3\gamma}$, which, in turn, means that $w_\phi > 0$ always ($1 - \kappa^2\gamma\dot{\phi}^2 > 0$ always). Therefore, the scalar field cannot even start when $w_\phi < 0$ if $\gamma < 0$. As a result, accelerated phases driven by a scalar field in this model require $\gamma > 0$.

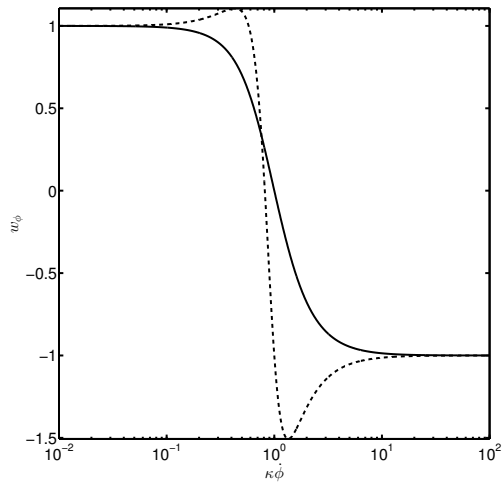

Figure 6.1: EoS of the scalar field w_ϕ as a function of its velocity defined by the dimensionless variable $\kappa\dot{\phi}$ for $\gamma = 1$ (solid line) and $\gamma = -1$ (dashed line). In the high energy limit ($\kappa\dot{\phi} \gg 1$), the EoS results in a de Sitter phase (the EoS can even be phantom-like $w_\phi < -1$ for $\gamma < 0$) where it is of stiff matter in the low energy limit ($\kappa\dot{\phi} \ll 1$). However, the inflationary phase is viable for $\gamma > 0$ only.

Therefore, we focus on the case where γ is positive. In that case, we can show that the sign of $\ddot{\phi}$ is always negative (see Eq. (23) in [Sushkov09] for instance). Hence, the velocity of the field decreases with time and w_ϕ is driven towards $w_\phi = +1$. Assuming that inflation ends at the instant t_{end}, at which $w_\phi = -1/3$ (the condition $\ddot{a} > 0$ is no more satisfied), $\kappa\gamma\dot{\phi}$ is initially large and

leads to the inflationary phase. One may derive an analytical (approximate) solution for the scale factor $a(t) = \mathrm{e}^{\alpha(t)}$ and the scalar field at early times in this regime ($\kappa\gamma\dot{\phi}^2 \gg 1$), considering first Eq. (6.2.10),

$$H = \dot{\alpha} \simeq \frac{1}{3\sqrt{\kappa\gamma}}. \tag{6.2.12}$$

Integration yields the approximate scale factor,

$$a(t) \simeq a_{\rm i} \exp\left(\frac{t - t_{\rm i}}{3\sqrt{\kappa\gamma}}\right), \tag{6.2.13}$$

where the subscript i denotes the initial condition. Inserting Eq. (6.2.12) into Eq. (6.2.8b), and expanding according to $\kappa^2\dot{\phi}^2 \gg 1$, gives $\ddot{\phi}/\dot{\phi} \simeq -1/\sqrt{\kappa\gamma}$ and, after integration, yields,

$$\dot{\phi}(t) \simeq \dot{\phi}_{\rm i} \exp\left(-\frac{t - t_{\rm i}}{\sqrt{\kappa\gamma}}\right). \tag{6.2.14}$$

Assuming that $w_\phi(t_{\rm end}) = -1/3$ and defining $\zeta_{\rm end} \equiv \kappa^2\gamma\dot{\phi}^2_{\rm end} > 0$ with $\phi_{\rm end} = \phi(t_{\rm end})$, Eq. (6.2.11) yields,

$$w_\phi(t_{\rm end}) = \frac{(2 + 3\zeta_{\rm end})(1 - \zeta_{\rm end})}{2 + 3\zeta_{\rm end} + 3\zeta^2_{\rm end}} = -\frac{1}{3}, \tag{6.2.15}$$

whose solution reads,

$$\zeta_{\rm end} = \frac{1}{6}\left(3 + \sqrt{57}\right) \approx 1.76, \tag{6.2.16}$$

since only the positive solution verifies $\gamma > 0$. Then Eq. (6.2.14) reduces to,

$$\kappa^2\gamma\dot{\phi}^2_{\rm i} \exp\left[-\frac{2(t_{\rm end} - t_{\rm i})}{\sqrt{\kappa\gamma}}\right] \simeq \zeta_{\rm end}, \tag{6.2.17}$$

leading to,

$$t_{\rm end} - t_{\rm i} = \frac{\sqrt{\kappa\gamma}}{2} \ln\left(\frac{\kappa^2\gamma\dot{\phi}^2_{\rm i}}{\zeta_{\rm end}}\right). \tag{6.2.18}$$

Inserting this expression into Eq. (6.2.13) yields,

$$\frac{a_{\rm end}}{a_{\rm i}} \simeq \left(\frac{\kappa^2\gamma\dot{\phi}^2_{\rm i}}{\zeta_{\rm end}}\right)^{\frac{1}{6}}. \tag{6.2.19}$$

Imposing that inflation lasts for a number of e-folds $N = \ln(a_{\rm end}/a_{\rm i})$ larger than 60, we obtain,

$$\dot{\phi}_{\rm i}^{\,2} \gtrsim \frac{\zeta_{\rm end}}{\kappa^2\gamma} \exp(360), \tag{6.2.20}$$

which is the crucial condition for a successful (purely kinetic-driven) inflationary phase. We see that it involves a rather unusual very large pure number.

The Eq. (6.2.12) is also relevant in order to discuss naturalness[3], as it fixes the Hubble parameter at the beginning of the inflationary phase $H_{\rm i} \simeq 1/(3\sqrt{\kappa\gamma})$. Therefore, Eq. (6.2.20) might be rewritten as,

$$\kappa \frac{\dot{\phi}_{\rm i}^{\,2}}{H_{\rm i}^2} \gtrsim 9\,\zeta_{\rm end}\exp(360) \sim 10^{157}. \tag{6.2.21}$$

It follows that the "natural" initial conditions $H_{\rm i} = \mathcal{O}(1) \sim M_{\rm pl}$ and $\dot{\phi}_{\rm i} = \mathcal{O}(1) \sim M_{\rm pl}^2$ in Planckian units are not allowed. On the contrary, a natural value for the initial expansion $H_{\rm i} = M_{\rm pl}$ (and thus $\gamma \approx 0.11$) requires an extremely high transplanckian value for the initial velocity of the field $\dot{\phi}_{\rm i} \gtrsim 10^{78} M_{\rm pl}^2$.

It is not even possible to obtain a Planckian value for the initial velocity in this model. Indeed, assuming $\dot{\phi}_{\rm i} \sim M_{\rm pl}^2$, the initial Hubble parameter will be smaller than the one today, $H_0 \simeq 2.1\,h\ \times 10^{-42}$ GeV $\sim 10^{-61} M_{\rm pl}$. This implies that in such an inflationary scenario, $H_{\rm i}^{-1} \sim \sqrt{\kappa\gamma}$ must be less than the Hubble radius today H_0^{-1} whereas the inflation predicts a huge expansion of the Universe.

6.2.2 Theoretical constraints

In this section, we investigate if there exist metric backgrounds for which the propagation of the scalar field becomes pathological, that is non hyperbolic, and thus possibly non causal (see also Sec. 1.3.1), or carrying negative energy degrees of freedom, i.e. ghosts (see also Sec. 3.1.2)). In the following, the cosmological background is assumed to be flat (6.2.6) and we explore the conditions for the theory to be well-defined, for both scalar and tensor metric perturbations.

Conditions for the avoidance of ghosts in scalar, vector and tensor perturbations of the metric have been derived in full generality in a very wide class of Galileon models by [De Felice12]. Let us first introduce the reduced dimensionless variables,

$$x(t) = \kappa\dot{\phi}, \tag{6.2.22}$$

$$y(t) = \sqrt{\kappa}\dot{\alpha}. \tag{6.2.23}$$

The no-ghost conditions $Q_{\rm S,\,T} > 0$ where the subscripts S and T are for scalar and tensor metric perturbations, are given by Eqs. (23)–(25) in [De Felice12] while the conditions for the avoidance of Laplacian instabilities $c^2_{\rm S,\,T} \geq 0$ are given by Eqs. (27)–(28) in [De Felice12]. Those conditions reduce to rather simple algebraic constraints in our case, after the necessary manipulation using

[3] This argument about naturalness is questionable since the scale at which the Fab Four model breaks down might differ from the GR one.

the equations of motion (6.2.7) and (6.2.8),

$$Q_{\rm T} > 0 \qquad \Leftrightarrow \qquad 1 + \frac{\gamma x^2}{2} > 0, \tag{6.2.24a}$$

$$c_{\rm T}^2 \geq 0 \qquad \Leftrightarrow \qquad 1 - \frac{\gamma x^2}{2} \geq 0, \tag{6.2.24b}$$

for the tensor metric perturbations, and,

$$Q_{\rm S} > 0 \quad \Leftrightarrow \quad \frac{4 + 6\gamma x^2 + 6\gamma^2 x^4}{2 + 3\gamma x^2} > 0, \tag{6.2.25a}$$

$$c_{\rm S}^2 \geq 0 \quad \Leftrightarrow \quad \frac{12 + 36\gamma x^2 + 19\gamma^2 x^4 - 12\gamma^3 x^6 - 3\gamma^4 x^8}{2 + 3\gamma x^2 + 3\gamma^2 x^4} \geq 0, \tag{6.2.25b}$$

for the scalar metric perturbations.

This whole set of equations is difficult to reduce algebraically because of the last one. However, one might easily plot the four functions of x defined above, and one typically finds that both positive and negative values for γ are allowed on a given range $|x| < \xi_\gamma$, where typically ξ_γ behaves as $\mathcal{O}\left(1/\sqrt{|\gamma|}\right)$, see the Figs. 6.2a and 6.2b for $\gamma = 1$ and $\gamma = -1$. Hence, large (transplanckian) values for $|x|$ are only allowed for small $|\gamma| \ll 1$. This means that the space for possible velocities of the field $x = \kappa\dot{\phi}$ needs to be typically subplanckian, unless γ is vanishingly small. This will be linked to the results found earlier, where transplanckian initial velocity were required for a successful inflation, leading to negative squared speeds $c_{\rm S}^2$ and $c_{\rm T}^2$ in that epoch. This is further discussed in Sec. 6.2.3.

Meanwhile, we note that the claim made in the literature (see e.g. [Tsujikawa12, Germani10b, Germani11]) according to which only the subclass $\gamma < 0$ is a ghost-free theory is wrong (at least in the background considered here). Notice that the scalar field is well-defined although being a phantom, i.e. $w_\phi < -1$, in a certain regime (in the case $\gamma < 0$) (see Fig. 6.1), a situation reminiscent of the one discussed in [Creminelli10]. However, as shown previously, the Friedmann equations actually prevent the scalar field from entering this regime.

6.2.3 Numerical results

In this section, the cosmological evolution predicted by the John model is quickly discussed, for both positive and negative γ. The equations of motion (6.2.8) were solved by numerical integration as an IVP. The initial conditions for the scalar field velocity were fixed to $\kappa\dot{\phi}_{\rm i} = 10$ for $\gamma = 1$, and $\kappa\dot{\phi}_{\rm i} = 0.1$ for $\gamma = -1$ in order to satisfy the condition $|x_{\rm i}| = 0.1 < 1.4$ required by the stability conditions (see Fig. 6.2a). In Fig. 6.3, the evolution of the EoS w_ϕ as well as the acceleration parameter,

$$q = +\frac{\ddot{a}a}{\dot{a}^2}, \tag{6.2.26}$$

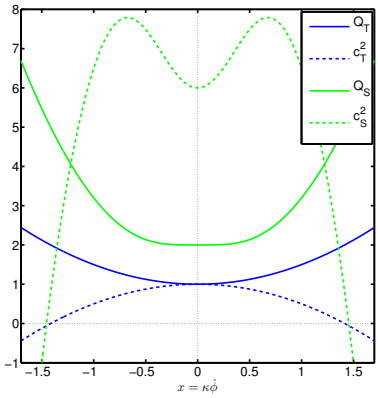

(a) The field velocity must be $|x| < 1.4$ for $\gamma = 1$.

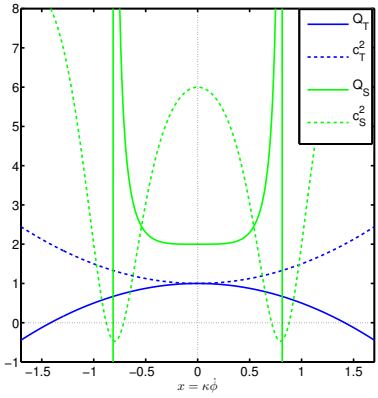

(b) The field velocity must be $|x| < 0.7$ for $\gamma = -1$.

Figure 6.2: Analysis of the causal behavior for and the metric (scalar and tensor) perturbations as a function of the scalar field velocity $x = \kappa\dot{\phi}$. In order to avoid ghost and Laplacian instabilities, $Q_{\rm S}$, $Q_{\rm T}$ and $c_{\rm S}^2$, $c_{\rm T}^2$ must be positive. Allowed values for the field velocity are typically $|x| < \xi_\gamma \sim \mathcal{O}(\gamma^{-1/2})$ in order to preserve causality.

are represented depending on the scale factor. The evolution of the conditions to avoid ghost $Q_{\mathrm{S,\,T}} > 0$ and Laplacian instabilities $c^2_{\mathrm{S,\,T}} \geq 0$ are also shown. As discussed before, the negative γ case leads only to a decelerating Universe: the phantom regime is not an acceptable initial condition (as it entails an imaginary Hubble parameter), and neither can be reached. Only a positive γ leads to an accelerated phase of the expansion, and to an inflationary phase in the early Universe, a drawback being the presence of non-causal behavior for the scalar and tensor perturbations of the metric.

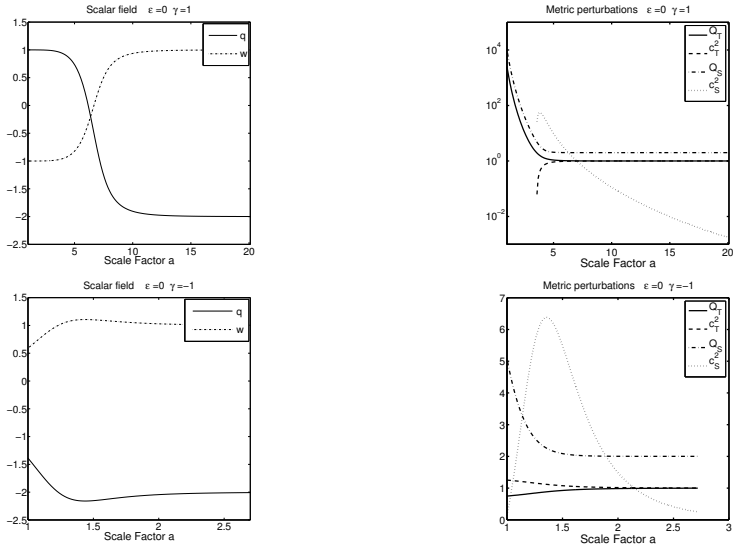

Figure 6.3: Cosmological evolution of $q, Q_{\mathrm{S}}, c^2_{\mathrm{S}}, Q_{\mathrm{T}}, c^2_{\mathrm{T}}$ as a function of the scale factor. (Top): This model leads to an accelerating expansion ($q > 0$). However, the large initial velocity of the scalar field drives the speed of both scalar and tensor metric perturbations to imaginary values ($c^2_{\mathrm{S}} < 0$ and $c^2_{\mathrm{T}} < 0$, the corresponding curves terminate since the scale of the y axis is logarithmic), thus signaling a breakdown of hyperbolicity for metric perturbations. (Bottom): The field starts with an EoS $w_\phi \sim 0.5$ and the Universe only decelerates ($q < 0$). This model with $\gamma < 0$ is well-behaved but does not accommodate inflation.

6.2.4 Discussion

We have established that kinetically driven inflation in the Galileon theory involving the simplest coupling to the Einstein tensor, that is the John Lagrangian, is not viable. It requires unnatural transplanckian values for the initial velocity of the field, which, in turn, implies various instabilities.

This model has anyway another serious drawback. In the absence of any

direct coupling to the Ricci scalar, there is no reason why the scalar field should be generated at all since there is no source term in the Klein-Gordon equation (6.2.5) (even in the presence of a cosmological matter fluid). In other words, $\phi = 0$ is always a solution in this class of models, whatever the matter content is.

This statement is further justified by considering the prediction of the John Lagrangian (6.2.1) at local scales, in a static and spherically symmetric spacetime. Using the metric ansatz (2.3.1), the Klein-Gordon equation yields,

$$\kappa\gamma\, r^2 \mathrm{e}^{-2\,\lambda}\left(3\,\frac{\nu'\phi'}{r^2} - 6\,\frac{\phi'\nu'\lambda'}{r} + 2\,\frac{\nu'^2\phi'}{r} - 3\,\frac{\phi'\lambda'}{r^2} + 2\,\frac{\phi''\nu'}{r} + 2\,\frac{\phi'\nu''}{r} + \frac{\phi''}{r^2}\right) + r^2\left[\phi'' + \phi'\left(\nu' + \frac{2}{r} - \lambda'\right)\right] + \kappa\gamma\left(\phi'\lambda' - \nu'\phi' - \phi''\right) = 0, \tag{6.2.27}$$

the prime denoting derivative with respect to the radial coordinate. By imposing the regularity condition at the origin $\phi'(r = 0) = 0$, the solution of the Klein-Gordon equation is trivial,

$$\phi'' = 0 \qquad \Rightarrow \qquad \phi' = \mathrm{cst} = 0 \qquad \forall\, r. \tag{6.2.28}$$

Imposing that the solution is asymptotically flat at spatial infinity, i.e. $\phi(r \longrightarrow \infty) = 0$, the solution for a relativistic star is the GR one, i.e. the Schwarzschild solution ($\phi = 0\,\forall r$), even in the presence of matter.

To conclude, the model considered so far is trivial in the sense that it cannot be different than GR, except if one imposes non-vanishing initial conditions for the scalar field at early times. In order to obtain non-trivial solutions, we consider the combination of the John and the George Lagrangians, the latter introducing a direct coupling to the Ricci scalar, $V_{\mathrm{george}}(\phi)R$ (6.1.3).

6.3 The John and George Lagrangian

We now consider the extended model given by,

$$S = \int \mathrm{d}^4x\sqrt{-g}\left[\frac{R}{2\kappa}\left(1 + \epsilon\sqrt{\kappa}\phi\right) - \frac{1}{2}\left(g^{\mu\nu} + \kappa\gamma G^{\mu\nu}\right)\partial_\mu\phi\partial_\nu\phi\right] + S_{\mathrm{M}}[\psi_{\mathrm{M}};\, g_{\mu\nu}], \tag{6.3.1}$$

where the nonminimal coupling function is fixed to $V_{\mathrm{george}}(\phi) = 1 + \epsilon\sqrt{\kappa}\phi$ from now on, and ϵ is a dimensionless, free parameter. The modified Einstein equations then read (see Sec. 3.2.1 and App. E.1 for the calculations of the equations of motion),

$$G_{\mu\nu}\left(1 + \epsilon\sqrt{\kappa}\phi\right) + \epsilon\sqrt{\kappa}\left(g_{\mu\nu}\Box\phi - \nabla_\mu\nabla_\nu\phi\right) = \kappa\left(T^{(\phi)}_{\mu\nu} + \kappa\gamma\Theta_{\mu\nu}\right), \tag{6.3.2}$$

with $T^{(\phi)}_{\mu\nu}$ and $\Theta_{\mu\nu}$ defined in Eqs. (6.2.3), while the Klein-Gordon equation reads,

$$\left(g_{\mu\nu} + \kappa\gamma G_{\mu\nu}\right)\nabla^\mu\nabla^\nu\phi + \frac{\epsilon R}{2\sqrt{\kappa}} = 0. \tag{6.3.3}$$

Notice that one can argue that the effective gravitational constant $G_{\rm eff} = G/(1+\epsilon\sqrt{\kappa}\phi)$ might easily become negative in this model, meaning that the action chosen here shall trivially lead to dynamical pathologies for $\epsilon\phi$ sufficiently large and negative[(4)].

Such an argument would call in favor of defining a better coupling function $V_{\rm george}(\phi)$. However, this would be a misleading conclusion here, since the John term introduces a derivative coupling between the metric and the scalar field, thus impacting the propagation of the metric and scalar degrees of freedom. Therefore, only the entire set of stability conditions for both the scalar and the metric perturbations (i.e. positivity of the squared velocities $c_{\rm S}^2 \geq 0$ and $c_{\rm T}^2 \geq 0$) can decide which regions of the configuration space are well-behaved. The results are presented in the following sections assuming a cosmological background, based on the conditions derived in App. E.3. In this light, the function $V_{\rm george}(\phi)$ chosen above is just one of the simplest that we can choose, and might furthermore be understood as retaining only the first term in a series expansion of a more general function $V_{\rm george}(\phi) = {\rm e}^{\epsilon\sqrt{\kappa}\phi}$.

The cosmological evolution predicted by John and George is typically a function of four parameters: the initial value of the field $\phi_{\rm i}$, its velocity $\dot{\phi}_{\rm i}$, as well as the two dimensionless parameters γ and ϵ. It goes beyond the scope of this thesis to provide a comprehensive study of this parameter space. However, the numerical results presented in the next section, highlight some essential features in the case where John and George are playing cosmology together. As for the case where John plays alone, the cosmological evolution is studied in terms of w_ϕ and q for particular combination of the parameters γ and ϵ. The conditions for causality and for energy positivity are analyzed, depending on the signs of γ and ϵ.

6.3.1 Cosmological behavior

The equations of motion in a flat, empty Universe, derived from Eq. (6.3.1) are given in App. E.2 (see Eqs. (E.2.1)-(E.2.3)). The analysis of the no-ghost and causality conditions to this more general framework is reported in App. E.3 while the derivation of the scalar field EoS is given in App. E.2.

The numerical results are the following. The case $\epsilon = 1$ and $\gamma = 1$ is pretty similar to the case John alone ($\gamma > 0$), see Figs. 6.4a and 6.4b. Inflation thus

[(4)] In fact, what matters in the case $\gamma = 0$, is that the scalar field propagates positive energy in the Einstein frame. Performing a conformal transformation, this is equivalent to the usual Brans-Dicke condition $2\omega + 3 > 0$, where $\omega = \epsilon^{-2}(1+\epsilon\sqrt{\kappa}\phi)$ here. Then, our model with $\gamma = 0$ would indeed be pathological if $\phi \leq -[3/(2\epsilon^2)+1]/(\epsilon\sqrt{\kappa})$. However, there are new terms in the equations of motion for the scalar field due to the presence of the John terms, which invalidate such a conclusion in the general case $\gamma \neq 0$.

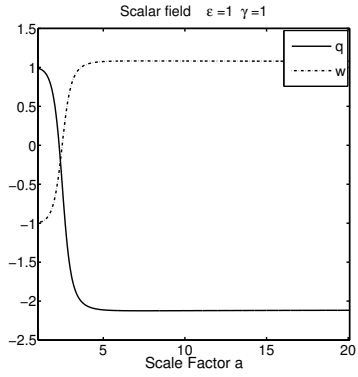

(a) We observe the same transition from inflation to stiff matter for the scalar field.

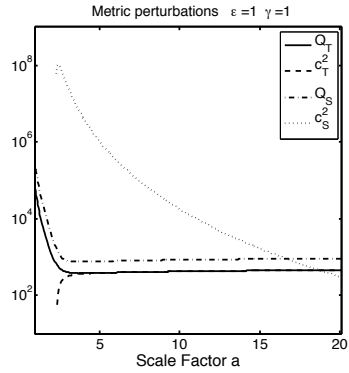

(b) The "sound" speeds of scalar and tensor metric perturbations are negative in the early Universe.

Figure 6.4: Evolution of q, w_ϕ (on the left) as well as $Q_{\rm S}$, $Q_{\rm T}$ and $c_{\rm S}^2, c_{\rm T}^2$ (on the right), as a function of the scale factor a, assuming the initial conditions $\dot{\phi}_{\rm i} = 100$ and $\phi_{\rm i} = 1$.

occurs in the case $\epsilon > 0$ and $\gamma > 0$, but the acausal behavior still shows up in the very early Universe. The number of e-folds is a function of the two initial conditions for the field and its velocity, as well as of the dimensionless parameters ϵ and γ. A further analysis would determine whether the addition of the George term helps in solving the naturalness problem encountered with John alone in Sec. 6.2.

The case $\epsilon = -1$, $\gamma = 1$ is pathological since $c_{\rm T}^2 < 0$ and w_ϕ becomes imaginary as seen on Fig. 6.5. Actually this theory leads to a double inflation scenario (see the acceleration parameter): the Universe transits from one de Sitter phase to another one, and experiences in between a super-acceleration phase.

Finally, the case with negative γ is similar to the John alone model ($\gamma < 0$): the theory is well-defined, ghost free and causal, but fails to exhibit any acceleration, see Fig. 6.5.

6.3.2 Compact objects

In the last two sections, we explore the phenomenology predicted by the John and George Lagrangians around compact objects and, in particular, in the Solar System. As we will see, the tests of GR in the Solar System put severe constraints on the parameter space of the model.

In order to study the Fab Two model around compact objects, the full system of equations of motion for a static and spherically symmetric spacetime (E.4.1)–(E.4.4) reported in App. E.4, is solved numerically inside and outside the compact object, using a boundary value problem. Inside the compact ob-

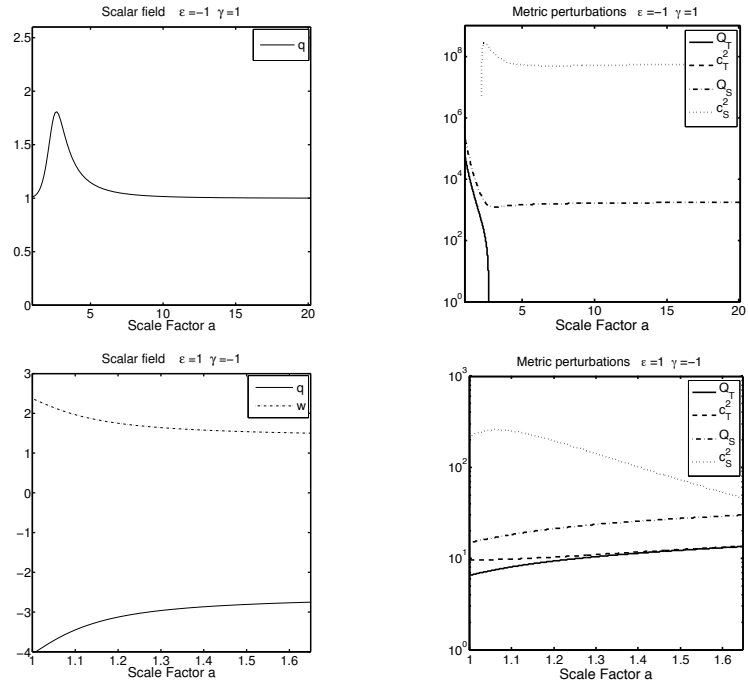

Figure 6.5: Cosmological evolution of $q, w_\phi, Q_{\rm S}, c_{\rm S}^2, Q_{\rm T}, c_{\rm T}^2$ with the scale factor. (Top): In the case $\epsilon = -1$ and $\gamma = 1$, a "double inflation" scenario is predicted, i.e. q comes twice close to 1. This model is pathological in many respects: w_ϕ is imaginary (consequently it is not plotted), $c_{\rm T}^2 < 0$ (the y axis is logarithmic such that it is not represented), and there are periods for which $c_{\rm S}^2 < 0$ and $Q_{\rm T} < 0$ (see top right). (Bottom): In the case $\epsilon = 1$ and $\gamma = -1$, the model is well behaved but the expansion is not accelerated as in the John alone model. The universe is actually in a super-stiff regime, and hence, in a highly decelerating phase.

ject, the TOV equation (2.3.6) characterizes the pressure profile. For the sake of simplicity, we assume a top-hat profile $\rho = \rho_0 \ \forall\, r < \mathcal{R}$, $\mathcal{R}$ being the radius of the compact object, and a perfect fluid (2.2.2) inside the compact object. Three of the four Einstein equations as well as the TOV equation are integrated numerically, the fourth Einstein equation serving to validate the numerical results[(5)]. The boundary conditions corresponding to the dynamical variables read,

$$\nu(0) = 0, \qquad \nu'(0) = 0, \qquad \lambda(0) = 0, \tag{6.3.4}$$

$$\phi(0) = \phi_{\rm c}, \qquad \phi'(0) = 0, \qquad \frac{p}{\rho_0}(\mathcal{R}) = 0, \tag{6.3.5}$$

[(5)]One of the Einstein equations is redundant to the others because of the Bianchi identities.

the conditions at the origin being justified by the same arguments as in App. D. The value of the scalar field at the center of the compact object $\phi_{\rm c}$ is the only remaining unknown and is determined by a shooting method, imposing that the spacetime is asymptotically flat at spatial infinity, namely $\phi\left(r \longrightarrow r_{\rm max}\right) = 0$, $r_{\rm max}$ being the maximal value of the integration interval. Outside the compact object, the equations of motion are solved as an IVP, the initial conditions being given by the inner solution at $r = \mathcal{R}$.

Contrary to the case where John is playing alone, if George is included, deviations from GR arise. As an example, the pressure profile for a NS ($s = 0.3$) is plotted on Fig. 6.6 for $\epsilon = 1$ and $\gamma = 0$. Allowing $\gamma \neq 0$ affects negligibly the solution such that the Vainshtein mechanism possibly arising in the presence of John, seems to be not that efficient in order to hide the George's effect. Depending on the compactness, the pressure at the center of the NS is expected to be larger than GR ($s = 0.3$, see Fig. 6.6) or smaller ($s = 0.5$) if George plays alone ($\epsilon = 1$). The relative error $\left[p_{\rm c}(\epsilon = 1) - p_{\rm c}(GR)\right]/p_{\rm c}(GR) = 5 \times 10^{-3}$ (see Fig. 6.6) and -0.08 respectively.

A second physical quantity to be computed is the effective gravitational constant $G_{\rm eff}$ defined as,

$$G_{\rm eff} = \frac{G_{\rm N}}{1 + \epsilon\sqrt{\kappa}\phi(r)}, \tag{6.3.6}$$

which tells one to what extent the SEP is violated. Its profile for a NS ($s = 0.3$) is represented on Fig. 6.7 for $\epsilon = 1$ and various γ. As a result, the spontaneous scalarization arises for the George model as in other STT (see Sec. 3.2.5.3). Imposing that $\phi = 0$ at spatial infinity, variations of the gravitational constant are more than 5% at the center. The larger the John coupling is, the smaller the variation, while of the same order of magnitude. The spontaneous scalarization is further modelled by the scalar charge $\alpha_{\rm s}$ (3.2.53) given by,

$$\phi(r) = \phi_\infty + \alpha_{\rm s}\frac{r_{\rm s}}{r}. \tag{6.3.7}$$

The scalar charge is numerically determined by,

$$\alpha_{\rm s} = -\frac{\mathcal{R}^2\phi'(r = \mathcal{R})}{r_{\rm s}}, \tag{6.3.8}$$

and is plotted on Fig. 6.8 for $\epsilon = 1$ and $\gamma = 0,\ 1,\ 10$ assuming $s = 0.3$. We observe that the scalar charge does not vary significantly for values of $G_{\rm eff}$ deviating from $G_{\rm N}$ by a few percents, γ being fixed. However, γ has a non negligible influence. Depending on the compactness, $\alpha_{\rm s}$ increases ($s = 0.5$) or decreases ($s = 0.3$) for increasing γ. Further analysis would reveal if those values are compatible with the current NSs observations.

6.3.3 Solar system

The reader is reported to our paper [Bruneton12] for the detailed analysis of the John and George model using Solar System observables. The results obtained are briefly exposed in this section.

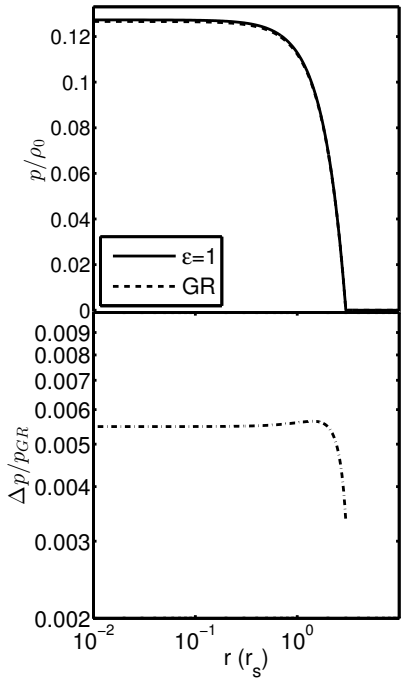

Figure 6.6: Pressure profile (in solid line) predicted by GR and the George model ($\epsilon = 1$) in a NS ($s = 0.3$). The relative error at the center of the star $[p_{\rm c}(\epsilon = 1) - p_{\rm c}(GR)]\,/p_{\rm c}(GR)$ (in dashed line) is found to be of the order of 5×10^{-3}. John has negligible influence on this result.

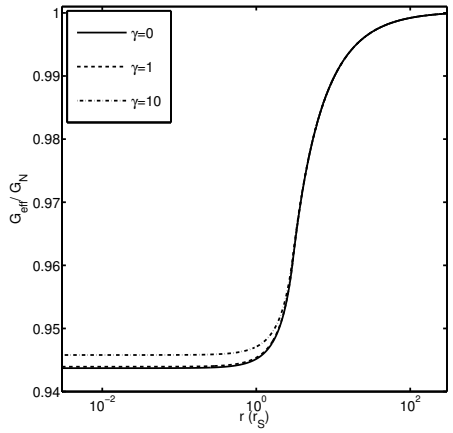

Figure 6.7: Profile of the variation of the gravitational constant $G_{\rm eff}$ for a NS ($s = 0.3$) with $\epsilon = 1$ and $\gamma = 0,\ 1,\ 10$. The variations at the center of the compact object are among 5%, a result which should be compared to the NSs physics.

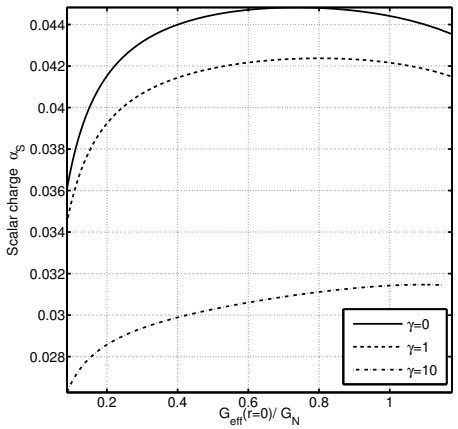

Figure 6.8: Plot of the scalar charge $\alpha_{\rm s}$ of the NS ($s = 0.3$) as a function of $G_{\rm eff}(r = 0)/G_{\rm N}$ for $\epsilon = 1$ and $\gamma = 0,\ 1,\ 10$. The variation of the scalar charge depending on the effective gravitational coupling is not large provided that the deviation of $G_{\rm eff}$ from $G_{\rm N}$ are about of few percents.

The Solar System constraints are usually derived using the isotropic coordinates, the line element of the metric reading,

$$\mathrm{d}s^2 = -A(r)^2\mathrm{d}t^2 + B(r)^2\left(\mathrm{d}r^2 + r^2\mathrm{d}\Omega^2\right), \tag{6.3.9}$$

A and B being the metric fields. The equations of motion for the John and George model in the isotropic gauge are reported in App. E.4. The post-Newtonian analysis requires first to expand the metric components $A(r)$, $B(r)$ as well as the scalar field $\varphi(r)$ in the equations of motion depending on the powers of $1/r$,

$$A^2(r) = 1 + \sum_{\mathrm{i}} a_{\mathrm{i}}/r^{\mathrm{i}}, \tag{6.3.10}$$

$$B^2(r) = 1 + \sum_{\mathrm{i}} b_{\mathrm{i}}/r^{\mathrm{i}}, \tag{6.3.11}$$

$$\varphi(r) = p_0 + \sum_{\mathrm{i}} p_{\mathrm{i}}/r^{\mathrm{i}}, \tag{6.3.12}$$

with $p_0 = \phi_\infty$ and $p_1 = \alpha_{\mathrm{s}} r_{\mathrm{s}}$. By inserting the field expansions (6.3.10-6.3.12) into the equations of motion reported in App. E.4, and equating the coefficients of corresponding powers of r, we find,

$$\begin{aligned} A^2 = {} & 1 - \frac{r_{\mathrm{s}}}{r} + \frac{r_{\mathrm{s}}^2}{2r^2} + \frac{\epsilon^2 p_1^2}{4M_{\mathrm{pl}}^2 z^2 r^2} + \frac{p_1 \epsilon r_{\mathrm{s}}^2}{24 M_{\mathrm{pl}} z r^3} \\ & - \frac{p_1^2 r_{\mathrm{s}}}{24 M_{\mathrm{pl}}^2 z r^3} + \frac{3}{4}\frac{\bar{\gamma}\epsilon^2}{M_{\mathrm{pl}}^4 z^2 r^4} - \frac{r_{\mathrm{s}}\bar{\gamma}}{8 M_{\mathrm{pl}}^4 z r^5}, \end{aligned} \tag{6.3.13a}$$

$$B^2 = 1 + \frac{r_{\mathrm{s}}}{r} - 2\frac{\epsilon p_1}{M_{\mathrm{pl}} z r} - \frac{p_1^2}{4M_{\mathrm{pl}}^2 z r^2} - \frac{\bar{\gamma}}{4M_{\mathrm{pl}}^4 z r^4}, \tag{6.3.13b}$$

where $z = 1 + \epsilon p_0/M_{\mathrm{pl}}$, and $\bar{\gamma} = \gamma p_1^2$. In the expansion above, we neglected higher order terms in r_{s}/r, ϵ, $p_1/(rM_{\mathrm{pl}})$ and $\bar{\gamma}/(rM_{\mathrm{pl}})$ (which means we suppose these terms to be smaller than 1). We recall that, in our conventions, γ and ϵ are dimensionless parameters. The asymptotic scalar field value $p_0 = \phi(r \to \infty)$ (in GeV) is a free parameter that can eventually be connected to the cosmological evolution of the scalar field since there is no additional scale in the theory in the absence of a potential term for the scalar field. Note that the dimensionless parameter p_1 can be related to the scalar charge of the central body derived numerically in Sec. 6.3.2.

In principle, we could identify the PPN parameters from the metric expansion (2.2.13),

$$\gamma_{\mathrm{PPN}} = -2\frac{\epsilon p_1}{z M_{\mathrm{pl}} r_{\mathrm{s}}}, \qquad \beta_{\mathrm{PPN}} = \frac{\epsilon^2 p_1^2}{2 z^2 M_{\mathrm{pl}}^2 r_{\mathrm{s}}^2}. \tag{6.3.14}$$

However, the terms $1/r^3$, $1/r^4$ and $1/r^5$ can be larger than the ones $1/r$, $1/r^2$ depending on the nonminimal coupling parameters ϵ and γ. As a result, the

PPN expansion is not relevant in order to test the Fab Four in the Solar System, which rather requires other tools for computing the observable effects from the metric. In our paper [Bruneton12], the anomalous perihelion shifts of the planets and radioscience observables, i.e. using the propagation of light rays in the Solar system [Hees12b] were computed. The four parameters of the John and George model which must be constrained, are $\bar{\gamma}/z$, $\bar{\gamma}\epsilon^2/z^2$, p_1^2/z and $p_1\epsilon/z$.

The secular perihelion precession rates were computed for the planets of the Solar System (excepted Uranus and Neptune) in [Bruneton12]. The most stringent constraints for the John and George model are obtained by the data from Mercury and read,

$$-3.12\times10^{31}\ \mathrm{m}^4 \quad < \frac{\bar{\gamma}}{M_{\rm pl}^4 z} < \quad 6.25\times10^{30}\ \mathrm{m}^4, \tag{6.3.15a}$$

$$-2.06\times10^{23}\ \mathrm{m}^4 \quad < \frac{\bar{\gamma}\epsilon^2}{M_{\rm pl}^4 z^2} < \quad 4.12\times10^{22}\ \mathrm{m}^4, \tag{6.3.15b}$$

$$-1.13\times10^{10}\ \mathrm{m}^2 \quad < \frac{p_1^2}{M_{\rm pl}^2 z} < \quad 2.26\times10^{9}\ \mathrm{m}^2, \tag{6.3.15c}$$

$$-5.16\times10^{-2}\ \mathrm{m} \quad < \frac{p_1\epsilon}{zM_{\rm pl}} < \quad 1.03\times10^{-2}\ \mathrm{m}. \tag{6.3.15d}$$

The constraints on the John and George Lagrangians were also computed using radioscience simulations (see [Bruneton12] for technical details). The Doppler effect, i.e. the ratio of frequencies between the emitted and the received signals, perturbing the propagation of light between the Earth and the Cassini spacecraft in orbit around Saturn has been measured with very good accuracy [Bertotti03]. Requiring the residuals, i.e. deviation between the John and George predictions and the observations, to be lower than the Cassini accuracy yields,

$$\left|\frac{\bar{\gamma}}{M_{\rm pl}^4 z}\right| = \left|\frac{\gamma p_1^2}{M_{\rm pl}^4(1+\frac{\epsilon p_0}{M_{\rm pl}})}\right| \quad < \quad 3.65\times10^{26}\ \mathrm{m}^4, \tag{6.3.16a}$$

$$\left|\frac{\bar{\gamma}\epsilon^2}{M_{\rm pl}^4 z^2}\right| = \left|\frac{\gamma p_1^2\epsilon^2}{M_{\rm pl}^4(1+\frac{\epsilon p_0}{M_{\rm pl}})^2}\right| \quad < \quad 1.15\times10^{26}\ \mathrm{m}^4, \tag{6.3.16b}$$

$$\left|\frac{p_1^2}{M_{\rm pl}^2 z}\right| = \left|\frac{p_1^2}{M_{\rm pl}^2(1+\frac{\epsilon p_0}{M_{\rm pl}})}\right| \quad < \quad 3.53\times10^{8}\ \mathrm{m}^2, \tag{6.3.16c}$$

$$\left|\frac{p_1\epsilon}{zM_{\rm pl}}\right| = \left|\frac{p_1\epsilon}{M_{\rm pl}(1+\frac{\epsilon p_0}{M_{\rm pl}})}\right| \quad < \quad 5.56\times10^{-2}\ \mathrm{m}. \tag{6.3.16d}$$

It should be noted that radioscience constraints are significantly better for $\bar{\gamma}/(M_{\rm pl}^4 z)$ and $p_1^2/(M_{\rm pl}^2 z)$ compared to the Mercury perihelion advance ones. On the other hand, the constraint from the Mercury perihelion advance on $\bar{\gamma}\epsilon^2/(M_{\rm pl}^4 z^2)$ is significantly better than the radioscience one, the constraint on $p_1\epsilon/(zM_{\rm pl})$ being of the same order of magnitude.

6.4 Conclusions

In this chapter, we explored the phenomenology associated to a subset of the Fab Four Lagrangians in cosmology, around compact objects and in the Solar System. The philosophy behind this preliminary work was that we cannot forget about Solar System constraints on the parameter space, even when we deal with inflationary solutions. In general, inflationary models rely upon the fact that the inflaton field decays, at some stage, into ordinary matter through some reheating mechanism. Therefore, the scalar-tensor nature of inflationary gravity is lost very soon in the evolution of the Universe. On the opposite, in the John and George models, the scalar field should live and show its effects until nowadays. Therefore, the parameter space determined by the constraints from cosmological observations must overlap with the one determined by Solar system tests. The Fab Four theory has many parameters with a very rich phenomenology and the entire parameter space must still be further studied. In this work, we restricted ourselves to the cases John and John plus George.

When John, i.e. a theory with a nonminimal derivative coupling between the scalar field and the Einstein tensor whose strength is parametrized by γ, plays inflation and gravitation:

- It was already known that the John Lagrangian admits inflationary solutions with a graceful exit without any ad hoc potential [Sushkov09].
- If the nonminimal derivative coupling parameter γ is positive, John drives an inflationary phase (the acceleration parameter is positive $q > 0$). However, very unnatural initial conditions are required. In particular, the field velocity, which is related to the energy density, must be huge compared to the Planck scale, rendering the theory no longer trustworthy. Moreover, the analysis of the scalar field and metric perturbations reveals that $\kappa\dot{\phi}_{\rm i} \lesssim 1/\sqrt{\gamma}$ in order to preserve causality such that γ must be very small.
- Negative values for γ are permitted in the sense that the scalar field and metric perturbations preserve causality. However, this model, while admitting a solution with accelerated expansion, does not allow for inflation since the Hubble parameter would become imaginary. It results that the EoS for the scalar field must be positive.
- Finally, the most serious problem comes from the fact that the model turns out to be trivial when one tries to solve the equations of motion inside a compact object. Indeed, we found that the only solution allowed by the regularity conditions is $\varphi = 0$ everywhere.

These facts have convinced us to extend the theory to include the term named George, which is nothing but a coupling between the scalar field and the Ricci scalar whose strength is parametrized by ϵ. When George and John are playing together:

- The numerical solutions of the equations of motion in cosmology (in the absence of stress-energy-momentum sources) highlight that the sign of the two coupling constants γ and ϵ must be positive in order to have an inflationary phase with graceful exit. However, a non-causal behavior of metric perturbations is expected in the very early Universe. The analysis of the naturalness of the initial conditions for inflation, i.e. the need for extreme initial conditions, is still an open question.

- By solving the Einstein equations for a static and spherically symmetric spacetime, we show that there are non-trivial solutions inside compact objects, like the Sun and NSs, provided that $\epsilon \neq 0$. The John's effect tends to lower the deviation from GR induced by George. However, the John's effect is negligible with respect to the George's one. The efficiency of the Vainshtein mechanism is thus questionable and requires a careful analysis of the complete parameter space.

- The variation of the gravitational coupling $G_{\rm eff}/G_{\rm N}$ due to George is up to 5% at the center of the NSs, the effect of the John being negligible.

- The George model predicts that NSs are spontaneously scalarized whereas the scalar charge only slightly depends on the deviation of $G_{\rm eff}$ from $G_{\rm N}$ at the center of the compact objects even for deviations of a few percents. Spontaneous scalarization is decreasing for increasing values of γ.

- In order to provide combined constraints with the tests of GR in the Solar System, a PN analysis of the theory was performed. It required to solve the Einstein equations in a static and spherically symmetric spacetime order by order by expanding the fields to large radial distance. The results still allow for a large parameter space, therefore future work is necessary in order to improve the constraints.

Systematic study of the Fab Four phenomenology is still to be investigated, in order to isolate which part of the parameter space is viable from the theoretical and phenomenological point of view. Besides these aspects, there are several issues that deserve further analysis:

- If the Fab Four model truly leads to inflation with a graceful exit, an alternative to the reheating mechanism is needed since the scalar field is not expected to decay in the early Universe.

- The question arises if the Fab Four can lead to late-time acceleration. This would include, at the background level, the study of tracking solutions with a convergence mechanism towards GR, if any (see e.g. [Copeland12]). The study of cosmological perturbations, in particular CMB spectra and LSS, might then further reduce the parameter space (see [De Felice12, Barreira13] and references therein).

- Astrophysical constraints for Horndeski gravity have been derived in the last few years. While no-hair theorems put severe constraints on the existence of BH solutions, there exists an exact static BH solution considering John provided that the action reads,

$$S = \int \mathrm{d}^4x \sqrt{-g} \left[\frac{R}{2\kappa} - \frac{\kappa\gamma}{2} G^{\mu\nu} \partial_\mu \phi \partial_\nu \phi \right], \tag{6.4.1}$$

  in the absence of the cosmological constant [Rinaldi12]. This result was further generalized [Babichev14].

- Finally, the existence of NSs has been verified in the static and slowly rotating regime (see [Cisterna16, Maselli16] and references therein). John appears to be the most interesting term (Paul does not give rise to viable stars [Maselli16]), the maximal NS mass $M_{\max}$ predicted by John being generally smaller than in GR. The limit of $M_{\max} = 2\,M_\odot$ (see Sec. 2.3.5) is reachable for specific EoS only. Provided that the action for gravitation is given by Eq. (6.4.1) (in the absence of the cosmological constant), cosmological and astrophysical configurations are found to be consistent with each other [Cisterna16].

Part III

Conclusion

Conclusion

GR has opened the way to precision cosmology. According to Einstein's theory of gravitation, the cosmological observations today converge towards the $\Lambda-$CDM concordance picture. However, cosmology requires understanding the nature of the matter-energy sources in the Universe. Within the $\Lambda-$CDM concordance picture, only baryonic matter and radiation which constitute 5% of the Universe's content, are described by the SM. While the question of the nature of DM has shifted to (astro-)particle physics today, the nature of the late-time cosmic acceleration is still debated. It could reveal the existence of new fields like DE, or modifications of GR at large scales.

The $\Lambda-$CDM concordance picture also suffers from the fine-tuning problem of the initial conditions in the early Universe. The current paradigm assumes an inflationary phase. The simplest models relying on the assumption of a single scalar field responsible for the huge accelerated expansion, are still favored today by the latest CMB observations. Again, the nature of this scalar field is still unknown.

In this thesis the assumption stating that late-time cosmic acceleration and inflation come from modifications of gravity, was investigated. In particular, we considered models where the Einstein metric field has a scalar field counterpart. However, as developed in Chap. 1, GR has a privileged status. Indeed, if the Schlögel-Füzfa conjecture applies, GR is the only theory of gravity in four spacetime dimensions which satisfies the SEP, i.e. the existence of a gravitational field cannot be detected locally whatever observations or experiments are undertaken (see Sec. 1.6).

Modifications of gravity are thus challenging, first from the theoretical point of view: modifications of gravity must be well-defined like GR. Further, modified gravity models have to be confronted with the observations: in cosmology, if those models are dedicated to late-time cosmic acceleration or inflation; with local tests of gravity, in the Solar System or in labs; and in astrophysics, looking at compact objects (black holes, gravitational waves and neutron stars). In Chap. 2, the tests of GR are reviewed and classified depending on the regime the tests investigate (strong or weak field, in the presence of sources or not, the sources being relativistic or not).

In the rest of this thesis we focused on three different modified gravity models: the chameleon model, the Higgs gravity and the Fab Four. Those

models appear to be well-posed, even if the chameleon model possibly suffers from strong coupling (see Sec. 3.1.2) and the Higgs gravity could suffer from a loss of unitarity (see Sec. 5.2.4). The predictions of these three models were studied at different scales: in the lab, in compact objects and in cosmology. For these cases, the equations of motion were solved numerically.

Laboratory experiment: the chameleon model

In Chap. 4, we focused on the chameleon model which has been extensively studied in the last decade. Initially, this model was built in order to reproduce the late-time cosmic acceleration. This model exhibits a screening mechanism due to the combined effect of the potential and the nonminimal coupling to gravity. It can pass the Solar System constraints provided that the potential is exponential and the value of the potential parameter Λ is of the same order of magnitude as the cosmological constant.

Recently, this model was tested with an unprecedented accuracy in the laboratory, using an atom interferometry experiment inside a vacuum chamber. Analytical forecasts were derived by [Burrage15, Hamilton15], assuming negligible chamber wall effects. The first experimental bounds were obtained in Berkeley [Hamilton15, Elder16]. In this thesis we provide numerical simulations for the Berkeley experiments. They lead to the following results:

- The numerical method we developed in this thesis allowed us to take the minimal assumption that the chameleon field settled to the minimum of its effective potential far away from the vacuum chamber. Moreover, the effects of the experimental set-up were taken into account using the limit of spherical symmetry, contrary to analytical calculations.

- In the strongly perturbing regime, the numerical method enabled validation and refinement of the analytical calculations close to the test mass where the acceleration induced by the chameleon field is measured. In addition, we highlighted that the acceleration becomes negative close to the wall, this effect being of the same order of magnitude as close to the test mass and thus possibly measurable.

- The effect of the size and the density of the test mass were analyzed. We found that a larger test mass gives rise to a larger induced acceleration. Moreover, the experimentalists in Berkeley now use a test mass made of tungsten rather than aluminum.

- The numerical method confirmed that the chameleon model would be ruled out up to the Planck scale if the induced acceleration is measured with about 3 orders of magnitude more sensitivity. This limit should be reachable in the near future. Indeed, the control of systematics will allow the experimentalists in Berkeley to improve the sensitivity of their experimental set-up. We also provided a forecast for probing the chameleon in

a very large vacuum chamber, i.e. vacuum room of 10 m radius, where the chameleon acceleration is found to be (almost) measurable for values of the nonminimal coupling parameter up to the Planck scale with the current experimental sensitivity.

- The numerical method developed in this thesis is easily adaptable to various experiments, in the limit of spherical symmetry, the general modeling of the experiment requires other numerical methods like relaxation.
- Eventually, the experimental set-up developed in Berkeley should also offer the opportunity to test other screening mechanisms like the symmetron, the dilaton and $f(R)$.

Such an experimental set-up reveals that stringent bounds on modified gravity can be obtained in the laboratory, at least for some particular models exhibiting screening mechanisms.

Compact objects: the Higgs gravity

The Higgs inflation appears to be a promising model today since it is still favored by the latest observations, among them the Planck satellite, provided that there is nonminimal coupling $\xi > 10^4$ [Ade15e]. The Higgs inflation predicts that the tensor-to-scalar ratio is very small $r \simeq 0.0033$ such that as long as r is not detected, for instance by the future space mission COrE+, this model will be favored.

In Chap. 5, the numerical solutions for the same STT were derived around compact objects, in the presence of baryonic matter. Indeed, no-hair theorems guarantee the Schwarzschild solution in the vacuum, i.e. for black holes. The solution that we derived numerically has the following characteristics:

- The distribution of the Higgs field around compact objects is particlelike. The Higgs field converges to the vev at spatial infinity. Its distribution is globally regular, i.e. there is no singularity, it is asymptotically flat (the spacetime is Minkowski at spatial infinity, the Higgs field being settled to its vev) and of finite energy. The Higgs field distribution is characterized by the nonminimal coupling as well as the baryonic mass and the compactness of the object.
- Contrary to the case of spontaneous scalarization (see Sec. 3.2.5.3) there is only one solution which always differs from that of GR, i.e. when the scalar field is minimally coupled to gravity. Indeed, in GR, there exist only unrealistic homogeneous distributions of the Higgs field around compact objects while Higgs inflation predicts non-trivial distributions of the Higgs field. Whatever the compact objects, the vev will be shifted to the center of the objects.

- However, no measurable deviations were found for astrophysical objects. At the center of the Sun, the variation of the Higgs field around its vev is less than 1% provided that the nonminimal coupling is $\xi < 10^{58}$, thus, far above the critical value for the inflation $\xi > 10^4$. Inside neutron stars, the variation of the Higgs field cannot be higher than $10^{-41}\times$ the vev, assuming $\xi = 10^4$. We concluded that this effect was not measurable, either with gravitational or nuclear physics experiments.

- Considering nonphysical values of the compactness and the mass, we highlighted the existence of a mechanism of amplification of the central value of the Higgs field in compact objects. This means that there exists a critical nonminimal coupling above which some compactnesses – or radii - of compact objects are forbidden, since the central value of the Higgs field diverges. This is due to the combined effects of the Higgs potential and the nonminimal coupling function.

- This amplification mechanism could possibly be generalized to other STT.

- The fact that divergence from the central values of the Higgs field appeared, is related to the assumption of the unitary gauge. Indeed, in Higgs inflation, they consider one real scalar field only rather than the Higgs doublet, the positive and negative asymptotic values of the vev no longer being equivalent. In a realistic model, the $\mathrm{SU}(2)$ gauge symmetry of the electroweak interaction should be included. It shows that the Higgs inflation model should rather be considered as a multifield model due to the presence of the Goldstone bosons [Greenwood13]. In that case, the Yukawa coupling between the Higgs field and elementary particles could be also considered in-side compact objects.

- Lastly, the question of the stability of this particlelike solution has not been investigated yet. The only argument in favor of this solution is that it is the only one with a finite energy. Indeed, if the scalar field is not settled to its vev at spatial infinity, the potential energy is non-vanishing and becomes infinite at large distances. Also, the question of the formation of the Higgs monopoles as a result of gravitational collapse is still open.

STT provide a framework to model the nonminimal coupling of the Higgs field to gravity. The realistic modeling of the nonminimally coupled Higgs field around compact objects, that is in agreement with the $\mathrm{SU}(2)$ gauge of the electroweak interactions, requires further investigation. It has already been studied for dark energy [Rinaldi15a]. However, in the presence of baryonic matter, the Yukawa coupling of the Higgs field to elementary particles should also be taken into account.

From inflation to compact objects: the Fab Four model

STT consist of a subclass of Horndeski gravity, i.e. the theory of gravity invoking a scalar field counterpart to the metric and leading to second order equations of motion.

In Chap. 6, we focused on the Fab Four model which belongs to the Horndeski gravity theory while not being a STT. More precisely we studied the phenomenology predicted by two of the four: John, a nonminimal derivative coupling between the scalar field and the Einstein tensor, and George, a nonminimal non-derivative coupling between the scalar field and the Ricci scalar. In particular, this model does not exhibit any potential term in the Lagrangian.

In this thesis, we explored the predictions of this model for inflation, in the Solar System and for compact objects:

- In the case where John plays alone, it can succeed in reproducing inflation provided that the non-minimal coupling parameter is positive. The number of e-folds generated during inflation is sufficient for solving the horizon and the flatness problems and this model predicts a graceful exit. However, the initial conditions, in particular the kinetic energy of the scalar field, were found to be super-Planckian.

- In compact objects, John only predicts trivial solutions: imposing regularity conditions at the center of the compact objects, the scalar field vanishes everywhere.

- In order to obtain a richer phenomenology, we included the George term. In that case, inflation exhibits a graceful exit provided that both nonminimal coupling parameters are positive. Considering that the Solar System constraints are obtained by radio-simulations, a large part of the parameter space appears to still be viable. When John and George play together, spontaneous scalarization arises around compact objects.

The work presented in Chap. 6 is prospective in the sense that a careful analysis of the parameter space of two of the Fab Four is missing, either in cosmology, in the Solar System or around compact objects. The analysis of two of the Fab Four around NSs has been presented [Cisterna16, Maselli16]. It has been found that John can predict the existence of NSs of the maximal mass observed today, i.e. $2\ M_\odot$, assuming a realistic equation of state. Finally, we only considered two of the Fab Four Lagrangians, the phenomenology predicted by Paul and Ringo being still unexplored.

Appendices

Appendix A

General covariance: a variational approach

In this appendix, the implications of active diffeomorphism invariance on the EH action are analyzed. As we will see, it results that the second Bianchi identity holds in GR assuming the Levi-Civita connection.

Infinitesimal active diffeomorphisms $\phi_{\Delta\lambda}$, with $\Delta\lambda$ the infinitesimal shift along the vector field ξ from the point $P = \{x^\mu\}$ to the point $\phi_{\Delta\lambda}(P) = \{y^\mu\}$ where $y^\mu = x^\mu + \xi^\mu \Delta\lambda$, are generated by the **Lie derivative** $\mathcal{L}_\xi$. Applied to a tensor field $\mathbf{T}$, this linear operator is defined as,

$$\mathcal{L}_\xi \mathbf{T} \equiv \lim_{\Delta\lambda \longrightarrow 0} \frac{\phi_{\Delta\lambda}\mathbf{T}(x) - \mathbf{T}(x)}{\Delta\lambda}. \tag{A.0.1}$$

The only tensor field appearing in the EH action is the metric $g_{\mu\nu}$. Its Lie derivative reads (up to first order),

$$\begin{aligned}
\mathcal{L}_\xi g_{\mu\nu}\, \Delta\lambda &= \bar{g}_{\mu\nu}(x) - g_{\mu\nu}(x), \\
&= g_{\alpha\beta}(x + \xi\Delta\lambda)\frac{\partial x^\alpha}{\partial \overline{x}^\mu}\frac{\partial x^\beta}{\partial \overline{x}^\nu} - g_{\mu\nu}(x), \\
&\simeq (g_{\alpha\beta} + \partial_\rho g_{\alpha\beta}\, \xi^\rho \Delta\lambda)\,(\delta^\alpha_\mu + \partial_\mu \xi^\alpha \Delta\lambda)(\delta^\beta_\nu + \partial_\nu \xi^\beta \Delta\lambda) - g_{\mu\nu}, \\
&\simeq [\xi^\alpha \partial_\alpha g_{\mu\nu}(x) + g_{\alpha\nu}(x)\partial_\mu \xi^\alpha + g_{\mu\alpha}(x)\partial_\nu \xi^\alpha]\, \Delta\lambda, \\
\mathcal{L}_\xi g_{\mu\nu} &\simeq \xi^\alpha \nabla_\alpha g_{\mu\nu} + g_{\alpha\nu}\nabla_\mu \xi^\alpha + g_{\mu\alpha}\nabla_\nu \xi^\alpha + T^\alpha_{\mu\beta} g_{\alpha\nu}\xi^\beta + T^\alpha_{\nu\beta} g_{\mu\alpha}\xi^\beta,
\end{aligned}$$

where $\bar{g}_{\mu\nu}(x) = \phi_{\Delta\lambda} g_{\mu\nu}(x)$ is the metric obtained by applying the infinitesimal active diffeomorphism to $g_{\mu\nu}(x)$, and $T^\alpha_{\nu\beta}$ is the torsion defined by Eq. (1.2.15). We also used,

$$\xi^\alpha \nabla_\alpha g_{\mu\nu} = \xi^\alpha \left(\partial_\alpha g_{\mu\nu} - \Gamma^\rho_{\alpha\mu} g_{\rho\nu} - \Gamma^\rho_{\alpha\nu} g_{\mu\rho}\right), \tag{A.0.2}$$

$$g_{\alpha\nu}\nabla_\mu \xi^\alpha = g_{\rho\nu}\left(\partial_\mu \xi^\rho + \Gamma^\rho_{\mu\alpha}\xi^\alpha\right). \tag{A.0.3}$$

Assuming the Levi-Civita connection, the Lie derivative of the metric tensor

reads[1],

$$\mathcal{L}_\xi g_{\mu\nu} = \nabla_\mu \xi_\nu + \nabla_\nu \xi_\mu. \tag{A.0.4}$$

The variation of the EH action (in the absence of the cosmological constant) under an infinitesimal active diffeomorphism, i.e. with $\delta g^{\mu\nu} = \mathcal{L}_\xi g^{\mu\nu}$ yields,

$$\begin{aligned} \delta S_{\rm EH} &= \frac{1}{2\kappa}\int \mathrm{d}^4x \left(R\,\delta\sqrt{-g} + \delta g^{\mu\nu}\sqrt{-g}\,R_{\mu\nu} + \sqrt{-g}\,g^{\mu\nu}\,\delta R_{\mu\nu}\right), \\ &= \frac{1}{2\kappa}\int \mathrm{d}^4x\sqrt{-g}\left(G_{\mu\nu}\,\delta g^{\mu\nu} + g^{\mu\nu}\,\delta R_{\mu\nu}\right), \end{aligned} \tag{A.0.5}$$

using Eq. (1.2.5). The last term of this equation is vanishing. Indeed, the variation of the Ricci tensor reads (see e.g. [Hobson06]),

$$\delta R_{\mu\nu} = \nabla_\rho \delta\Gamma^\rho_{\nu\mu} - \nabla_\nu \delta\Gamma^\rho_{\rho\mu}, \tag{A.0.6}$$

such that,

$$\begin{aligned} \int \mathrm{d}^4x\sqrt{-g}\,g^{\mu\nu}\,\delta R_{\mu\nu} &= \int \mathrm{d}^4x\,\sqrt{-g}\,g^{\mu\nu}\,\left(\nabla_\rho\delta\Gamma^\rho_{\nu\mu} - \nabla_\nu\delta\Gamma^\rho_{\rho\mu}\right), \\ &= \int \mathrm{d}^4x\,\sqrt{-g}\,\left[\nabla_\rho\left(g^{\mu\nu}\,\delta\Gamma^\rho_{\nu\mu}\right) - \left(\nabla_\rho g^{\mu\nu}\right)\,\delta\Gamma^\rho_{\nu\mu}\right] \\ &\quad - \int \mathrm{d}^4x\,\sqrt{-g}\,\left[\nabla_\nu\left(g^{\mu\nu}\,\delta\Gamma^\rho_{\rho\mu}\right) - \left(\nabla_\nu g^{\mu\nu}\right)\,\delta\Gamma^\rho_{\rho\mu}\right], \\ &= \int \mathrm{d}^4x\,\sqrt{-g}\,\left[\nabla_\rho\left(g^{\mu\nu}\,\delta\Gamma^\rho_{\nu\mu}\right) - \nabla_\nu\left(g^{\mu\nu}\,\delta\Gamma^\rho_{\rho\mu}\right)\right], \\ &= \int \mathrm{d}^4x\,\sqrt{-g}\,\nabla_\nu\left(g^{\mu\rho}\,\delta\Gamma^\nu_{\rho\mu} - g^{\mu\nu}\,\delta\Gamma^\rho_{\rho\mu}\right), \end{aligned}$$

assuming the Levi-Civita connection. Because of the total derivative, the covariant Gauss-Ostrogradsky theorem applies (see e.g. [Wald84] for a careful treatment of this term),

$$\int_{\mathcal{M}} \mathrm{d}^4x\sqrt{-g}\,(\nabla_\mu V^\mu) = \int_{\partial\mathcal{M}} \mathrm{d}^3y\sqrt{-\gamma}n_\mu V^\mu, \tag{A.0.7}$$

where $\mathcal{M}$ is the spacetime manifold and $\partial\mathcal{M}$ its 3 dimensional hypersurface border with $\gamma(y^\mu)$ the induced metric on the border and n_μ a unit vector normal to the border. Fixing the boundary conditions, it results that the contribution of $\delta R_{\mu\nu}$ in Eq. (A.0.5) vanishes,

$$\begin{aligned} \int \mathrm{d}^4x\sqrt{-g}g^{\mu\nu}\delta R_{\mu\nu} &= \int_{\partial\mathcal{M}} \mathrm{d}^3y\,\sqrt{-\gamma}\,n_\nu\left(g^{\mu\rho}\,\delta\Gamma^\nu_{\rho\mu} - g^{\mu\nu}\,\delta\Gamma^\rho_{\rho\mu}\right), \\ &= 0, \end{aligned}$$

and the variation of the EH action finally yields,

$$\delta S_{\rm EH} = \frac{1}{2\kappa}\int \mathrm{d}^4x\sqrt{-g}\,G_{\mu\nu}\,\delta g^{\mu\nu}. \tag{A.0.8}$$

[1] This equation reduces to the Killing equation when $\mathcal{L}_\xi g_{\mu\nu}$ is required to vanish, defining the Killing vectors is the direction of spacetime isometries.

Considering now that the variation of the metric $\delta g^{\mu\nu}$ is generated by the Lie derivative (A.0.2),

$$\delta g_{\mu\nu} = \mathcal{L}_\xi g_{\mu\nu} \simeq \nabla_\mu \xi_\nu + \nabla_\nu \xi_\mu, \tag{A.0.9}$$

and using Eq. (1.2.4), the variation of the EH action reads,

$$\begin{aligned}
\delta S_{\rm EH} &= -\frac{1}{\kappa}\int_{\mathcal{M}} \mathrm{d}^4x\sqrt{-g}\, G^{\mu\nu}\nabla_\mu \xi_\nu, && \text{(A.0.10)}\\
&= \frac{1}{\kappa}\left[\int_{\mathcal{M}} \mathrm{d}^4x\sqrt{-g}\,(\nabla_\mu G^{\mu\nu})\,\xi_\nu - \int_{\partial\mathcal{M}} \mathrm{d}^3\Sigma_\mu\sqrt{-g}\,(G^{\mu\nu}\xi_\nu)\right], && \text{(A.0.11)}\\
&\equiv 0. && \text{(A.0.12)}
\end{aligned}$$

assuming the Levi-Civita connection, using Eq. (1.2.4) and applying the Gauss-Ostrogradsky theorem (A.0.7). Since the vector field ξ^ν is arbitrary, it results that the second Bianchi identity is a consequence of the active diffeomorphism-invariance, assuming the Levi-Civita connection.

Appendix B

Application of the PPN formalism to the Brans-Dicke theory

The Brans-Dicke formalism leads straightforwardly to the PPN analysis for the Brans-Dicke theory or for any STT in the absence of a potential (see also Sec. 2.2). In this appendix, the Brans-Dicke formalism is briefly reviewed and the expressions for $\gamma_{\rm PPN}$ and $\beta_{\rm PPN}$ are derived.

The Lagrangian density in the standard generalized Brans-Dicke form reads[(1)],

$$\mathcal{L}_{\rm BD} = \frac{\sqrt{-g}}{2\kappa}\left[\Phi R - \frac{\omega(\Phi)}{\Phi}(\partial\Phi)^2 - \bar{V}(\Phi)\right] + \mathcal{L}_{\rm M}[\psi_{\rm M}; g_{\mu\nu}]. \qquad \text{(B.0.1)}$$

It is equivalent to Eq. (3.2.4) with $F(\phi) = \Phi$, $Z(\phi) = \omega(\Phi)/(2\kappa\Phi)$ and $\bar{V}(\phi) = V/(2\kappa)$. The modified Einstein equations now read (see Sec. 3.2.1),

$$\begin{aligned} R_{\mu\nu} - \frac{1}{2}g_{\mu\nu}R &= \frac{1}{\Phi}\nabla_\mu\nabla_\nu\Phi + \frac{\omega}{\Phi^2}\nabla_\mu\Phi\nabla_\nu\Phi \\ &\quad -\frac{1}{\Phi}\left[\Box\Phi + \frac{\omega}{2\Phi}(\partial\Phi)^2 + \frac{\bar{V}}{2}\right]g_{\mu\nu} + \frac{\kappa}{\Phi}T_{\mu\nu}, \end{aligned} \qquad \text{(B.0.2)}$$

where the stress-energy tensor is assumed to be a perfect fluid (2.2.2)[(2)]. The Ricci scalar then yields,

$$R = \frac{1}{\Phi}\left[-\kappa T + \frac{\omega(\Phi)}{\Phi}(\partial\Phi)^2 + 3\Box\Phi + 2\bar{V}(\Phi)\right]. \qquad \text{(B.0.3)}$$

[(1)]The original Brans-Dicke theory does not admit any potential and the function ω is independent of Φ [Brans61]. For the sake of generality, the potential is included here even if it does not appear in the derivation of the PPN parameters. The function $\omega(\Phi)$ is considered since it is relevant for the derivation of $\beta_{\rm PPN}$.

[(2)]In this appendix, we use the notation $T_{\mu\nu} \equiv T^{(\rm M)}_{\mu\nu}$

The Klein-Gordon equation follows from Eq. (3.2.3) which after replacing R according to Eq. (B.0.3) reads,

$$(2\omega+3)\Box\Phi+\frac{\mathrm{d}\omega}{\mathrm{d}\Phi}(\partial\Phi)^2-\Phi\frac{\mathrm{d}\bar{V}}{\mathrm{d}\Phi}+2\bar{V}=\kappa T, \tag{B.0.4}$$

and the modified Einstein equations becomes,

$$\begin{aligned}R_{\mu\nu}=\frac{8\pi G}{\Phi}\left(T_{\mu\nu}-\frac{\omega+1}{2\omega+3}Tg_{\mu\nu}\right)+\frac{\omega}{\Phi^2}\partial_\mu\Phi\partial_\nu\Phi+\frac{1}{\Phi}\nabla_\mu\nabla_\nu\Phi\\ -\frac{\omega_\Phi}{2\Phi}\frac{(\partial\Phi)^2}{3+2\omega}g_{\mu\nu}+\frac{1}{2\Phi\,(3+2\omega)}\left[\Phi\frac{\mathrm{d}\overline{V}}{\mathrm{d}\Phi}+\overline{V}(2\omega+1)\right]g_{\mu\nu},\end{aligned} \tag{B.0.5}$$

where the subscript Φ denotes a derivative with respect to Φ. As previously shown in Sec. 2.2, in order to compute γ_{PPN} and β_{PPN}, the modified Einstein equations must be solved up to $\mathcal{O}(2)$ or 1PN and $\mathcal{O}(4)$ or 2PN for g_{00}, up to $\mathcal{O}(3)$ or 1.5PN for g_{0i} and up to $\mathcal{O}(2)$ or 1PN for g_{ij}. The bookkeeping of the different quantities has already been introduced in Sec. 2.2 excepted for the scalar field which is expanded as,

$$\Phi\left(x^\mu\right)=\Phi_0+\zeta\left(x^\mu\right), \tag{B.0.6}$$

where Φ_0 is the constant background value and ζ is at least of order $\mathcal{O}(2)$. In the rest of this appendix, we assume $\overline{V}=0$ since the PPN derivation for STT is exact for vanishing potential only. The steps of the computations then follow:

1. Solution for the scalar field ζ up to $\mathcal{O}(2)$,

   The expansion of the Klein-Gordon equation (B.0.4) up to $\mathcal{O}(2)$ enables one to determine ζ as a function of the gravitational potential U (2.2.12). Indeed,

   $$\Box\Phi\equiv|g|^{-1/2}\partial_\mu(|g|^{1/2}\partial^\mu\Phi)\sim\nabla^2\Phi-\partial_0^2\Phi\sim\nabla^2\zeta+\mathcal{O}(4), \tag{B.0.7}$$

   where $g_{\mu\nu}=\eta_{\mu\nu}$, the derivative of the scalar field being at least of order $\mathcal{O}(2)$. Only the trace of $T_{\mu\nu}$ further contributes to $\mathcal{O}(2)$ and reads,

   $$T=g_{\mu\nu}T^{\mu\nu}=-\rho\left(1+3\frac{p}{\rho}\right)\simeq-\rho\left[1+\mathcal{O}(2)\right], \tag{B.0.8}$$

   according to the bookkeeping rules given by Eqs. (2.2.8). The Klein-Gordon equation (B.0.4) up to $\mathcal{O}(2)$ finally yields,

   $$\nabla^2\zeta^{(2)}=-\frac{8\pi G}{3+2\omega}\rho, \tag{B.0.9}$$

   the superscript denoting the order of the expansion. Replacing ρ according to the Poisson equation (1.2.10) with $U\equiv-\Phi/G$, the solution for ζ reads,

   $$\zeta^{(2)}-\zeta_0=\frac{2GU}{3+2\omega}. \tag{B.0.10}$$

   where ζ_0 is the constant of integration.

2. Solution for h_{00} up to $\mathcal{O}(2)$,

   Given the expansion of the Levi-Civita connection up to $\mathcal{O}(2)$,

$$\Gamma^{\lambda,\,(2)}_{\mu\nu} = \frac{1}{2}\eta^{\lambda\rho}\left(\partial_\mu h_{\rho\nu} + \partial_\nu h_{\mu\rho} - \partial_\rho h_{\mu\nu}\right), \tag{B.0.11}$$

   the expansion of the Ricci tensor up to $\mathcal{O}(2)$ reads[3] [Will93],

$$R^{(2)}_{\mu\nu} = \frac{1}{2}\left(-\Box h_{\mu\nu} - \partial_\mu\partial_\nu h + \partial_\alpha\partial_\mu h^\alpha_\nu + \partial_\nu\partial_\alpha h^\alpha_\mu\right), \tag{B.0.12}$$

   with $h = h^\mu_\mu$, hence,

$$R^{(2)}_{00} \simeq -\frac{1}{2}\nabla^2 h_{00} + \mathcal{O}(>2). \tag{B.0.13}$$

   The only additional terms up to order $\mathcal{O}(2)$ of the $00-$component of Eqs. (B.0.5) involve the stress-energy tensor, with $T^{(2)}_{00} = \rho$ and $T^{(2)} = -\rho$ (see Eq. (B.0.8)). The expansion up to $\mathcal{O}(2)$ thus yields,

$$-\frac{1}{2}\nabla^2 h_{00} = \frac{8\pi G\rho}{\Phi_0}\left(1 - \frac{\omega+1}{2\omega+3}\right) + \mathcal{O}(4). \tag{B.0.14}$$

   Given the Poisson equation (1.2.10), the solution for h_{00} up to $\mathcal{O}(2)$ is,

$$h^{(2)}_{00} = \frac{4G}{\Phi_0}\frac{\omega+2}{2\omega+3}U \equiv 2\bar{G}U, \tag{B.0.15}$$

   where we used Eq. (2.2.13), $\bar{G} \equiv G_{\rm Cav}$ (see Sec. 3.2.4.2) being the measured gravitational constant, for instance by Cavendish experiments, which differs from G in STT,

$$\boxed{\bar{G} = \frac{2G}{\Phi_0}\frac{\omega+2}{2\omega+3}} \tag{B.0.16}$$

   In the limit $\omega \longrightarrow \infty$, the measured gravitational constant is the Newton's constant,

$$\bar{G} = \frac{G}{\Phi_0} = G, \tag{B.0.17}$$

   assuming that Φ_0 corresponds to the value of Φ at large distance from the central body. Considering Eq. (B.0.16), the perturbation around the scalar field background Eq. (B.0.10) yields,

$$\frac{\zeta}{\Phi_0} = \frac{\bar{G}U}{\omega+2}, \tag{B.0.18}$$

   where ζ_0 has been absorbed in Φ_0.

[3] Notice that only the terms involving the derivative of the Christoffel symbols are relevant here contrary to order $\mathcal{O}(4)$.

3. Solution for h_{ij} up to $\mathcal{O}(2)$,

   The expansion of R_{ij} to order $\mathcal{O}(2)$ reads (see Eq. (B.0.12)),

$$R_{ij}^{(2)} = -\frac{1}{2}\left(\nabla^2 h_{ij} - \partial_i\partial_j h_{00} + \partial_i\partial_j h^k{}_k - 2\partial_k\partial_j h^k{}_i\right). \tag{B.0.19}$$

   Because of the diffeomorphism-invariance (see Sec. 1.3.3), four gauge conditions must be imposed to the modified Einstein equations for fixing the gauge. The **first three gauge conditions** are given by[4],

$$\partial_\mu h^\mu{}_i - \frac{1}{2}\partial_i h^\mu{}_\mu = \frac{1}{\Phi_0}\partial_i\zeta. \tag{B.0.20}$$

   The derivative with respect to spatial component of these conditions expanded up to $\mathcal{O}(2)$ then yields,

$$\partial_j\partial_k h^k{}_i - \frac{1}{2}\left(\partial_i\partial_j h^k{}_k - \partial_i\partial_j h_{00}\right) = \frac{1}{\Phi_0}\partial_i\partial_j\zeta, \tag{B.0.21}$$

   leading to,

$$R_{ij}^{(2)} = -\frac{1}{2}\nabla^2 h_{ij} + \frac{1}{\Phi_0}\partial_i\partial_j\zeta. \tag{B.0.22}$$

   Since T_{ij} is at least of $\mathcal{O}(4)$ according to Eq. (2.2.8), the only term up to $\mathcal{O}(2)$ involving the stress-energy tensor is the one involving T (see Eq. (B.0.8)). The $ij-$component of Eqs. (B.0.5) thus reads,

$$\nabla^2 h_{ij} = -\frac{16\pi G}{\Phi_0}\frac{\omega+1}{2\omega+3}\rho\delta_{ij}, \tag{B.0.23}$$

   which is solved using the Poisson equation (1.2.10) and Eq. (B.0.16) yielding,

$$h_{ij}^{(2)} = 2\,\frac{\omega+1}{\omega+2}\,\bar{G}\,U\,\delta_{ij} \equiv 2\,\gamma_{\rm PPN}\,\bar{G}\,U\,\delta_{ij}. \tag{B.0.24}$$

   According to the standard PPN metric expansion (2.2.13) the parameter $\gamma_{\rm PPN}$ for the Brans-Dicke theory is thus,

$$\boxed{\gamma_{\rm PPN} = \frac{\omega+1}{\omega+2}} \tag{B.0.25}$$

4. Solution for h_{0j} up to $\mathcal{O}(3)$,

   Since h_{0j} is at least of $\mathcal{O}(3)$, the expansion of R_{0j} up to $\mathcal{O}(3)$ reads (see also Eq. (B.0.12)),

$$R_{0j}^{(3)} = -\frac{1}{2}\left(\nabla^2 h_{0j} - \partial_j\partial_k h^k{}_0 + \partial_0\partial_j h^k{}_k - \partial_0\partial_k h^k{}_j\right). \tag{B.0.26}$$

[4] Note that this gauge condition is valid to all orders.

The **fourth gauge condition** is now useful[5],

$$\partial_\mu h^\mu_{\ 0} - \frac{1}{2}\partial_0 h^\mu_{\ \mu} + \frac{1}{2}\partial_0 h_{00} = \frac{1}{\Phi_0}\partial_0\zeta, \tag{B.0.27}$$

and yields up to order $\mathcal{O}(3)$,

$$\partial_i h^i_{\ 0} - \frac{1}{2}\partial_0 h^i_{\ i} = \frac{1}{\Phi_0}\partial_0\zeta. \tag{B.0.28}$$

Combining the four gauge conditions (∂_0 [Eq. (B.0.20)]$\times$ ∂_j [Eq. (B.0.27)]) up to order $\mathcal{O}(3)$ yields,

$$R^{(3)}_{0j} = -\frac{1}{2}\nabla^2 h_{0j} - \frac{1}{4}\partial_0\partial_j h^{(2)}_{00} + \frac{1}{\Phi_0}\partial_0\partial_j\zeta. \tag{B.0.29}$$

Since g_{0j} is at least of order $\mathcal{O}(3)$, the $0j-$component of the modified Einstein equations (B.0.5) reads to order $\mathcal{O}(3)$,

$$R^{(3)}_{0j} = \frac{8\pi G}{\Phi_0}\left[T^{(3)}_{0j} - \mathcal{O}(>3)\right] + \mathcal{O}(>3) + \frac{1}{\Phi_0}\partial_0\partial_j\zeta, \tag{B.0.30}$$

where $T^{(3)}_{0j} = -\rho v_j$ assuming a perfect fluid (2.2.2). Using Eq. (B.0.15) it finally leads to,

$$\nabla^2 h_{0j} = \frac{16\pi G}{\Phi_0}\rho v_j - \bar{G}\partial_0\partial_j U. \tag{B.0.31}$$

Defining two additional potentials, V_j and χ [Will93],

$$\nabla^2 V_j = -4\pi\rho v_j, \qquad \nabla^2\chi = -2U, \tag{B.0.32}$$

and using Eqs. (B.0.18) and (B.0.15), $h^{(3)}_{0j}$ reads,

$$h^{(3)}_{0j} = -\frac{4\omega+6}{\omega+2}\bar{G}V_j + \frac{1}{2}\bar{G}\partial_0\partial_j\chi. \tag{B.0.33}$$

5. Solution for h_{00} up to $\mathcal{O}(4)$

   The expansion of the Levi-Civita connection up to $\mathcal{O}(4)$ yields,

$$\Gamma^{\lambda,\,(4)}_{\mu\nu} = \frac{1}{2}\left(\partial_\mu h^\lambda_\nu + \partial_\nu h^\lambda_\mu - \partial^\lambda h_{\mu\nu}\right) + \frac{1}{2}h^{\lambda\rho}\left(\partial_\mu h_{\rho\nu} + \partial_\nu h_{\mu\rho} - \partial_\rho h_{\mu\nu}\right), \tag{B.0.34}$$

   the expansion of R_{00} up to $\mathcal{O}(4)$ thus reading [Will93],

$$\begin{aligned} R^{(4)}_{00} \;=\; & -\frac{1}{2}\nabla^2 h^{(4)}_{00} - \frac{1}{2}\left(\partial_0\partial_0 h^{j\ (2)}_{\ j} - 2\partial_0\partial_j h^{j\ (3)}_{\ 0}\right) - \frac{1}{4}\partial^i h^{(2)}_{00}\partial_i h^{(2)}_{00} \\ & + \frac{1}{2}\partial_j h^{(2)}_{00}\left(\partial^k h^{j\ (2)}_{\ k} - \frac{1}{2}\partial^j h^{k\ (2)}_{\ k}\right) + \frac{1}{2}h^{jk\ (2)}\partial_j\partial_k h^{(2)}_{00}. \end{aligned} \tag{B.0.35}$$

[5] Note that this fourth gauge condition cannot be compactified with the three first ones (B.0.20) in a covariant way.

Using the fourth gauge condition (B.0.27) and Eq. (B.0.18),

$$\partial_0\partial_i h_0^i - \frac{1}{2}\partial_0^2 h_k^k = \frac{1}{\Phi_0}\partial_0^2\zeta, \tag{B.0.36}$$

$$= \frac{\bar{G}}{\omega+2}\partial_0^2 U, \tag{B.0.37}$$

as well as the expressions for $h_{00}^{(2)}$ (B.0.15), $h_{ij}^{(2)}$ (B.0.24), and ζ (B.0.18), the expansion for $R_{00}^{(4)}$ finally reads,

$$R_{00}^{(4)} = -\frac{1}{2}\nabla^2 h_{00}^{(4)} + \frac{\bar{G}}{\omega+2}\partial_0^2 U - \bar{G}^2\frac{2\omega+3}{\omega+2}(\nabla U)^2 + 2\bar{G}^2\frac{\omega+1}{\omega+2}U\nabla^2 U. \tag{B.0.38}$$

The modified Einstein equations (B.0.5) expanded to $\mathcal{O}(4)$ then yield,

$$R_{00}^{(4)} = \frac{8\pi G}{\Phi_0+\zeta}\left[T_{00}^{(4)} - \frac{\omega+1}{2\omega+3}T^{(4)}g_{00}\right] + \mathcal{O}(6) + \frac{1}{\Phi_0}\nabla_0\partial_0\zeta - \frac{\omega_\Phi}{2\Phi}\frac{(\partial\Phi)^2}{3+2\omega}g_{00}, \tag{B.0.39}$$

We first focus on the term involving $T_{\mu\nu}$. In order to expand $T_{\mu\nu}$ up to $\mathcal{O}(4)$, the four-velocity given by,

$$g_{\mu\nu}u^\mu u^\nu = -1, \tag{B.0.40}$$

is expanded as,

$$u^0u^0 = -\frac{1+g_{ij}u^iu^j}{g_{00}}, \tag{B.0.41}$$

$$\simeq -\frac{1+v^2}{-1+2\bar{G}U}, \tag{B.0.42}$$

$$\simeq 1+2\bar{G}U+v^2+\mathcal{O}(4), \tag{B.0.43}$$

where $u^iu_i = v^2$. Thus, assuming a perfect fluid (2.2.2), the stress-energy tensor T_{ij} and its trace read up to $\mathcal{O}(4)$,

$$T_{00}^{(4)} = \rho(1+\Pi-2\bar{G}U+v^2), \tag{B.0.44}$$

$$T_{ij}^{(4)} = \rho(u_iu_j+\frac{p}{\rho}\delta_{ij}), \tag{B.0.45}$$

$$T^{(4)} = -\rho\left(1+\Pi-\frac{3p}{\rho}\right), \tag{B.0.46}$$

with Π the specific energy density (see Sec. 2.2.1). Moreover the multiplicative term Φ^{-1} needs to be expanded as,

$$\frac{1}{\Phi} \simeq \frac{1}{\Phi_0}\left[1-\frac{\zeta}{\Phi_0}+\mathcal{O}(4)\right]. \tag{B.0.47}$$

The first term of the right-hand side of Eq. (B.0.39) thus reads,

$$\frac{8\pi G}{\Phi_0+\zeta}\left[T^{(4)}_{00}-\frac{\omega+1}{2\omega+3}T^{(4)}g_{00}\right]=\frac{8\pi G\rho}{\Phi_0}\left(1-\frac{\zeta}{\Phi_0}\right)\times \left[1+\Pi-2\bar{G}U+v^2+\frac{\omega+1}{2\omega+3}\left(1+\Pi-\frac{3p}{\rho}\right)\left(-1+2\bar{G}U\right)\right]. \quad \text{(B.0.48)}$$

The second term in Eq. (B.0.39) to be expanded involves the second derivative $\nabla_0(\partial_0\zeta)$ that requires the expansion of the Levi-Civita connection (B.0.11). Since $\Gamma^0{}_{00}\partial_0\zeta > \mathcal{O}(4)$ the only relevant term is,

$$\Gamma^i{}_{00}=-\frac{1}{2}\partial^i h_{00}+\mathcal{O}(4)\simeq-\bar{G}\partial^i U, \quad \text{(B.0.49)}$$

hence,

$$\nabla_0(\partial_0\zeta)=(\partial_0^2-\Gamma^\mu{}_{00}\partial_\mu)\zeta=(\partial_0^2+\bar{G}\partial^i U\partial_i)\zeta. \quad \text{(B.0.50)}$$

In the case where $\omega=\omega(\Phi)$, the last term involving ω_Φ has also to be expanded,

$$\begin{aligned}-\frac{\omega_\Phi}{2\Phi}\frac{(\partial\Phi)^2}{2\omega+3}g_{00} &\simeq -\frac{\omega_\Phi}{2(2\omega+3)}\frac{1}{\Phi_0}\left(1-\frac{\zeta}{\Phi_0}\right)(-1+h^{(2)}_{00}) \\ &\quad\times\left[(-1+h^{(2)}_{00})(\partial^0\zeta)^2+(\delta_{ij}+h^{(2)}_{ij})\partial^i\zeta\partial^j\zeta\right], \\ &= \frac{\omega_\Phi\bar{G}^2\Phi_0}{2(2\omega+3)(\omega+2)^2}(\nabla U)^2+\mathcal{O}(6), \quad \text{(B.0.51)}\end{aligned}$$

where Eq. (B.0.18) has been used. Therefore, the 00-component of Eqs. (B.0.5) becomes up to order $\mathcal{O}(4)$,

$$\begin{aligned}-\frac{1}{2}\nabla^2 h^{(4)}_{00}+\frac{\bar{G}}{\omega+2}\partial_0^2U-\bar{G}^2\frac{2\omega+3}{\omega+2}(\nabla U)^2+2\bar{G}^2\frac{\omega+1}{\omega+2}U\nabla^2U = \\ 4\pi\bar{G}\rho\frac{2\omega+3}{\omega+2}\left(1-\frac{\bar{G}U}{\omega+2}\right)\times \\ \left[\left(1+\Pi-2\bar{G}U\right)\frac{\omega+2}{2\omega+3}+v^2+\frac{\omega+1}{2\omega+3}\frac{3p}{\rho}\right] \\ +\left(\partial_0^2+\bar{G}\partial^iU\partial_i\right)\frac{\bar{G}U}{\omega+2}+\frac{\omega_\Phi\bar{G}^2\Phi_0}{2(2\omega+3)(\omega+2)^2}(\nabla U)^2, \quad \text{(B.0.52)}\end{aligned}$$

where Φ_0 has been removed using Eqs. (B.0.16) and (B.0.18). For the term involving ω_Φ, we assume that Φ_0 corresponds to the value of Φ at large distance from the central body, where $\bar{G}\simeq G$. Therefore, from Eq. (B.0.16),

$$\Phi_0\simeq\frac{2\omega+4}{2\omega+3}. \quad \text{(B.0.53)}$$

After some algebra, we obtain,

$$\begin{aligned} -\frac{1}{2}\nabla^2 h_{00}^{(4)} &= 4\pi\bar{G}\rho\left[1+\Pi-\frac{2\omega+5}{\omega+2}\bar{G}U+\frac{2\omega+3}{\omega+2}v^2+\frac{3\omega+3}{\omega+2}\frac{p}{\rho}\right] \\ &\quad +2\bar{G}^2(\nabla U)^2-\frac{2\omega+2}{\omega+2}\bar{G}^2U\nabla^2U \\ &\quad +\left[\frac{\omega_\Phi}{(2\omega+3)^2(\omega+2)}\right]\bar{G}^2\left(\nabla U\right)^2. \end{aligned} \tag{B.0.54}$$

By using the identity,

$$2(\nabla U)^2=\nabla^2(U^2)-2U\nabla^2U, \tag{B.0.55}$$

in order to remove the terms proportional to $(\nabla U)^2$, and by defining four potentials in addition to the one given by Eq. (1.2.10),

$$\nabla^2\Phi_1=-4\pi\rho v^2, \qquad \nabla^2\Phi_2=-4\pi\rho U, \tag{B.0.56}$$

$$\nabla^2\Phi_3=-4\pi\rho\Pi, \qquad \nabla^2\Phi_4=-4\pi p, \tag{B.0.57}$$

one can solve the equation for $h_{00}^{(4)}$ (B.0.54) and find,

$$\begin{aligned} h_{00}^{(4)} &= 2\bar{G}U-2\left[1+\frac{\omega_\Phi}{(2\omega+3)^2(2\omega+4)}\right]\bar{G}^2U^2+\frac{6+4\omega}{2+\omega}\bar{G}\Phi_1 \\ &\quad +\left[\frac{2+4\omega}{2+\omega}+\frac{2\omega_\Phi}{(2\omega+3)^2(\omega+2)}\right]\bar{G}^2\Phi_2+2\bar{G}\Phi_3 \\ &\quad +\frac{6+6\omega}{2+\omega}\bar{G}\Phi_4. \end{aligned} \tag{B.0.58}$$

In the limit where $\omega\to\infty$ and $\omega_\Phi=0$, the GR result is recovered as expected [Will93],

$$h_{00}^{(4)}=2\bar{G}U-2\bar{G}^2U^2+4\bar{G}\Phi_1+4\bar{G}^2\Phi_2+2\bar{G}\Phi_3+6\bar{G}\Phi_4. \tag{B.0.59}$$

In the vacuum ($\Phi_1=\Phi_2=\Phi_3=\Phi_4=0$), the expansion becomes ($\omega_\Phi\neq0$),

$$g_{00}^{(4)}=-1+2\bar{G}U-2\left[1+\frac{\omega_\Phi}{(2\omega+3)^2(2\omega+4)}\right]\bar{G}^2U^2, \tag{B.0.60}$$

that must be compared to the standard PPN expansion (2.2.13),

$$g_{00}=-1+2\bar{G}U-2\beta_{\rm PPN}\bar{G}^2U^2+\mathcal{O}(6), \tag{B.0.61}$$

yielding,

$$\boxed{\beta_{\rm PPN}=1+\frac{\omega_\Phi}{(2\omega+3)^2(2\omega+4)}} \tag{B.0.62}$$

These results are consistent with [Nutku69, Ni72] reported by [Will93].

Appendix C

The chameleon model: an analytical approach

In this appendix we reproduce the main steps of [Burrage15] and derive analytically the chameleon field profile in the spherically symmetric and static Minkowski spacetime for a two-region model (the source mass and the vacuum chamber). For the sake of simplicity, we assume in this appendix that $\alpha = 1$. Those analytical calculations are compared to the numerical computations in Sec. 4.4 where the analytical analysis is found to be reliable close to the source mass where the induced acceleration is measured. In the second part of this appendix we use the acceleration profiles derived analytically in order to compute the viable parameter space for the Berkeley experiment, as represented in Figs. 4.3 and 4.4.

C.1 Four different regimes

Assuming $A(\phi) = \mathrm{e}^{\phi/M} \simeq 1$, the minimum of the effective potential and its effective mass around it are respectively given by (see Eqs. (4.1.10)–(4.1.11) with $\alpha = 1$),

$$\phi_{\rm min} = \left(\frac{\Lambda^5 M}{\rho}\right)^{1/2}, \qquad m_{\rm min} = \sqrt{2}\left(\frac{\rho^3}{\Lambda^5 M^3}\right)^{1/4}. \tag{C.1.1}$$

The case where the effect of $A(\phi)$ becomes important, is discussed in our paper [Schlögel16] for the original model. For a two-region model the density ρ is either the source mass density $\rho_{\rm A}$ or the density in the vacuum chamber $\rho_{\rm v}$.

Four different regimes can be identified, depending on whether the field reaches the effective potential minimum or not: (1) the field does not reach the minimum of the effective potential in any region, (2) the field reaches the minimum in the vacuum chamber but not in the source mass, (3) the field reaches the minimum in the source mass but not in the vacuum chamber,

(4) the field reaches the minimum both inside the test mass and the vacuum chamber. The Cases (1) and (2) were referred to as the *weakly perturbing regime* in [Burrage15], whereas the Cases (3) and (4) were referred to as *strongly perturbing*. Below we consider those four cases separately, as in [Hamilton15]. In principle, one should also distinguish between the cases where the field reaches $\phi_{\rm min}$ inside the chamber wall, or not. When lowering M, depending on the central mass density and size, on the chamber wall density and thickness, $\phi_{\rm min}$ can be reached first inside the central mass or inside the chamber walls. Nevertheless, for the considered experimental set-up, the wall and the central mass have similar densities and sizes, and so those two cases will not be distinguished in the following.

- Case (1): $\phi(r=0) \neq \phi_{\rm min}(\rho_A)$ and $\phi(R_A < r < L) \neq \phi_{\rm min}(\rho_{\rm v})$

  Within the source mass the field does not reach the attractor that is the minimum of the effective potential. Since $\rho_{\rm v} < \rho_{\rm atm} < \rho_{\rm A}$, the second term in the effective potential (4.2.4) dominates, $V_{\rm eff} \simeq \phi\rho_{\rm A}/M$. The Klein-Gordon equation inside the source mass then reads,

$$\phi'' + \frac{2}{r}\phi' = \frac{\rho_{\rm A}}{M}. \tag{C.1.2}$$

  By setting $\phi = Z/r$, the Klein-Gordon equation reads $Z'' = (\rho/M)r$, whose solution is given by,

$$Z = \frac{\rho_{\rm A}}{6M}r^3 + \mathcal{C}r + \mathcal{D}, \tag{C.1.3}$$

  with $\mathcal{C}$ and $\mathcal{D}$ the two constants of integration. Imposing that the field profile is regular at the origin, implies that $\mathcal{C} = 0$,

$$\phi = \mathcal{D} + \frac{m_{\rm A} r^2}{8\pi M R_{\rm A}^3}. \tag{C.1.4}$$

  The constant of integration $\mathcal{D}$ is fixed by matching ϕ and ϕ' to the field solution in the vacuum chamber at $r = R_A$. Inside the vacuum chamber the field does not reach the attractor value. Let us denote $\phi_{\rm bg}$ the value that the field would take at the center of the chamber in the absence of the source. Then one can consider a harmonic expansion of the potential,

$$V_{\rm eff}(\phi) \simeq V_{\rm eff}(\phi_{\rm bg}) + \frac{m_{\rm bg}^2}{2}(\phi - \phi_{\rm bg})^2\,, \tag{C.1.5}$$

  higher order terms being subdominant, the Klein-Gordon equation in the vacuum chamber then reading,

$$\phi'' + \frac{2}{r}\phi' = m_{\rm bg}^2\,(\phi - \phi_{\rm bg})\,. \tag{C.1.6}$$

  By setting $Y = \phi - \phi_{\rm bg}$ and $Y = Z/r$, the Klein-Gordon equation becomes,

$$Z'' = m_{\rm bg}^2 Z, \tag{C.1.7}$$

whose solution reads,

$$Z = \mathcal{A}\,\mathrm{e}^{|m_{\rm bg}|r} + \mathcal{B}\,\mathrm{e}^{-|m_{\rm bg}|r}, \tag{C.1.8}$$

with $\mathcal{A}$ and $\mathcal{B}$ the two constants of integration. Assuming that the field profile decays at spatial infinity implies that $\mathcal{A} = 0$, the scalar field profile thus yielding,

$$\phi(r) = \phi_{\rm bg} + \frac{\mathcal{B}}{r}\,\mathrm{e}^{-|m_{\rm bg}|r}\,. \tag{C.1.9}$$

Note that at $r = R_A$, one has $m_{\rm bg}R_A \ll 1$ for typical experimental parameters and thus $\phi(R_A) \simeq \phi_{\rm bg} + \mathcal{B}/R_A$.

By matching the solutions (C.1.4) and (C.1.9) at $r = R_{\rm A}$, we obtain,

$$\mathcal{B} = -\frac{1}{4\pi}\frac{m_{\rm A}}{M}\mathrm{e}^{m_{\rm bg}R_{\rm A}}\frac{1}{1+m_{\rm bg}R_{\rm A}} \simeq -\frac{1}{4\pi}\frac{m_{\rm A}}{M}, \tag{C.1.10}$$

$$\mathcal{D} = \phi_{\rm bg} - \frac{1}{8\pi R_{\rm A}}\frac{m_{\rm A}}{M} - \frac{1}{4\pi R_{\rm A}}\frac{m_{\rm A}}{M}\frac{1}{1+m_{\rm bg}R_{\rm A}}, \tag{C.1.11}$$

$$\simeq \phi_{\rm bg} - \frac{3}{8\pi R_{\rm A}}\frac{m_{\rm A}}{M}, \tag{C.1.12}$$

the second equality being obtained assuming $m_{\rm bg}R_{\rm A} \ll 1$. Eventually the field profile in the Case (1) reads,

$$\phi^{(1)}(r) = \phi_{\rm bg} - \frac{m_{\rm A}}{8\pi R_{\rm A}M} \times \left[\left(3 - \frac{r^2}{R_{\rm A}^2}\right)\Theta(R_{\rm A} - r) + \left(2\frac{R_{\rm A}}{r}\mathrm{e}^{-m_{\rm bg}r}\right)\Theta(r - R_{\rm A})\right], \tag{C.1.13}$$

where Θ is the Heaviside function. Therefore the effect of the source mass is to deepen the field profile, by a quantity $3m_{\rm A}/(8\pi R_{\rm A}M) \ll \phi_{\rm bg}$ at $r = 0$. By definition, the Case (1) is valid as long as $|\phi_{\rm bg} - \phi^{(1)}(r = 0)| \ll \phi_{\rm bg}$. Outside the source mass, the difference $|\phi_{\rm bg} - \phi|$ decreases like $\propto 1/r$ for realistic experimental configurations where the exponential decay factor can be neglected.

A subtlety arises in the evaluation of $\phi_{\rm bg}$, which in [Burrage15] was either the attractor in the vacuum or related to the chamber size[(1)], under the assumption that the scalar field reaches its attractor inside the vacuum chamber wall. This assumption is actually not valid in the Case (1) because $\rho_{\rm w} \sim \rho_{\rm A}$, and because the wall thickness is about the radius of the source mass. So in most of the parameter space corresponding to the

[(1)] $\rho_{\rm v}$ is much lower than the wall density $\rho_{\rm w}$ where the field was assumed to reach its attractor $\phi_{\rm min}\,(\rho_{\rm w})$. Thus the first term of $V_{\rm eff}$ in Eq. (C.1.5) dominates the Klein-Gordon equation inside the chamber, which can be solved to get $\phi_{\rm bg}$ as a function of the size of the vacuum chamber. However, behind this calculation is hidden the assumption that the field reaches $\phi_{\rm min}\,(\rho_{\rm w})$ in the wall, which is not valid in the Case (1) in most of the parameter space.

Case (1), the scalar field does not reach its attractor inside the wall. As a result, $\phi_{\rm bg}$ is better approximated by $\phi_{\rm min}(\rho_{\rm atm})$, as highlighted by our numerical results which take the effects of the chamber wall on the scalar field profile into account (see our paper [Schlögel16] for the comparison between analytical and numerical results). Even if the background field value has no effect on the acceleration itself, this result is important because it changes the region in the parameter space in which the Case (1) applies: it is extended to lower values of M, as developed thereafter.

The acceleration induced by the scalar field gradient inside the vacuum chamber is well approximated by,

$$a_\phi \approx \frac{m_{\rm A}}{4\pi M^2 r}\left(\frac{1}{r}+m_{\rm bg}\right). \tag{C.1.14}$$

Since $m_{\rm bg} r \ll 1$ for realistic laboratory experiments, the acceleration is independent of Λ and thus one can constrain directly the value of M. This is the reason why the power-law of the potential has no effect on the acceleration as long as $|A(\phi)-1| \ll 1$ (see [Schlögel16] for a discussion about the original chameleon model).

- Case (2): $\phi(0) \neq \phi_{\rm min}(\rho_A)$ and $\phi_{\rm bg} = \phi_{\rm min}(\rho_{\rm v})$

  When the size of the vacuum chamber is larger than the characteristic distance over which the field reaches its attractor, that is when,

$$L \gg \frac{1}{m_{\rm min}(\rho_{\rm v})} = \left(\frac{\Lambda^5 M^3}{4\rho_{\rm v}^3}\right)^{1/4}, \tag{C.1.15}$$

  the field profile is still governed by Eq. (C.1.13). However, the value of $\phi_{\rm bg}$ is now simply $\phi_{\rm min}(\rho_{\rm v})$. In the case of the original chameleon potential $V(\phi)=\Lambda^5/\phi$, one has $\Lambda \simeq 2.6\times10^{-6}$ GeV in order to reproduce the late-time cosmic acceleration. For typical vacuum densities and chamber sizes, e.g. those reported in Table 4.2, one finds that this regime would occur when $M \lesssim 10^{-6}$ GeV. This does not correspond anymore to the weakly perturbing regime requiring $\phi_{\rm bg} \gtrsim m_A/(4\pi R_A M)$, yielding $M \gtrsim 2\times10^9$ GeV in our fiducial experimental setup. In the case of the exponential potential $V(\phi)=\Lambda^4(1+\Lambda/\phi)$, $\Lambda \simeq 10^{-12}$ GeV is the cosmological constant. It results that the field in the chamber is expected to reach $\phi_{\rm min}(\rho_{\rm v})$ only if $M \lesssim 10^5$ GeV. This is far from the regime where the source mass perturbs only weakly the field, valid when $M \gtrsim 10^{20}$ GeV, i.e. in the super-Planckian regime.

- Case (3): $\phi(0) = \phi_{\rm min}(\rho_A)$ and $\phi(R_A < r < L) \neq \phi_{\rm min}(\rho_{\rm v})$

  In the Case (3) the field reaches $\phi_{\rm A} \equiv \phi_{\rm min}\left(\rho_{\rm A}\right)$ inside the source mass. One can define a radius S such that $\phi(S)=\phi_{\rm A}(1+\epsilon)$ with $0<\epsilon\ll1$, so that, for $r<S$,

$$\phi \simeq \phi_{\rm A}. \tag{C.1.16}$$

For $S < r < R_{\rm A}$, the density term dominates in $V_{\rm eff}$ and the solution of the linearized Klein-Gordon equation is given by Eq. (C.1.3) (with $\phi = Z/r$), the scalar field profile reading,

$$\phi = \mathcal{D} + \frac{\mathcal{C}}{r} + \frac{m_{\rm A} r^2}{8\pi M R_{\rm A}^3} \,, \tag{C.1.17}$$

which is the same as Eq. (C.1.4) but with a non-vanishing integration constant $\mathcal{C}$. Outside the test mass, the field still obeys Eq. (C.1.9). The constants of integration $\mathcal{C}$ and $\mathcal{D}$ are fixed by matching the solutions for ϕ and ϕ' given by Eqs. (C.1.16) and (C.1.17) at $r = S$, yielding,

$$\mathcal{C} = \frac{1}{4\pi}\frac{m_{\rm A}}{M}\frac{S^3}{R_{\rm A}^3}, \tag{C.1.18}$$

$$\mathcal{D} = \phi_{\rm A} - \frac{3}{8\pi}\frac{m_{\rm A}}{M}\frac{S^2}{R_{\rm A}^3}. \tag{C.1.19}$$

By matching the solutions for ϕ and ϕ' given by Eqs. (C.1.17) and (C.1.9) at $r = R_{\rm A}$, the last constant of integration $\mathcal{B}$ is given by,

$$\mathcal{B} = \frac{1}{4\pi}\frac{m_{\rm A}}{M}\left(\frac{S^3}{R_{\rm A}^3} - 1\right), \tag{C.1.20}$$

assuming $m_{\rm bg} R_{\rm A} \ll 1$. The resulting field profile in the Case (3) corresponding to the thin shell regime reads [Burrage15],

$$\phi^{(3)}(r) = \begin{cases} \phi_{\rm A} \,, & r < S, \\ \phi_{\rm A} + \frac{m_{\rm A}}{8\pi R_{\rm A}^3 M r}\left(r^3 - 3S^2 r + 2S^3\right) \,, & S < r < R_{\rm A}, \\ \phi_{\rm bg} - \frac{m_{\rm A}}{4\pi M r}{\rm e}^{-m_{\rm bg} r}\left(1 - \frac{S^3}{R_{\rm A}^3}\right) \,, & r > R_{\rm A}, \end{cases} \tag{C.1.21}$$

with the so-called thin-shell radius,

$$S \equiv R_{\rm A}\sqrt{1 - \frac{8\pi M R_{\rm A}\phi_{\rm bg}}{3m_{\rm A}}}, \tag{C.1.22}$$

being such that one has typically $(R_{\rm A} - S)/R_{\rm A} \ll 1$. The induced acceleration is well approximated ($m_{\rm bg} R_{\rm A} \ll 1$) by,

$$a_\phi \approx \frac{m_{\rm A}}{4\pi M^2 r^2}\left(1 - \frac{S^3}{R_{\rm A}^3}\right) \simeq \frac{R_{\rm A}\phi_{\rm bg}}{M r^2}, \tag{C.1.23}$$

and contrary to the Case (1), it is related to the value of $\phi_{\rm bg}$. If the wall is sufficiently large, then the field reaches $\phi_{\rm min}(\rho_{\rm w})$ and so the calculation of $\phi_{\rm bg}$ for a spherical chamber in [Burrage15] is valid,

$$\phi_{\rm bg} \simeq 0.69\left(\Lambda^5 L^2\right)^{1/3}. \tag{C.1.24}$$

Following [Hamilton15], $\phi_{\rm bg}$ is rather given by,

$$\phi_{\rm bg} = \aleph \left[\alpha\left(\alpha+1\right)\Lambda^{4+\alpha}\rho_{\rm v}\right]^{\frac{1}{\alpha+2}}, \tag{C.1.25}$$

with $\aleph = 1.6,\ 1.8$ if the vacuum chamber is assumed to be spherical or an infinite cylinder respectively. Compared to the Case (1), the induced acceleration (C.1.23) does not only depend on M but also on Λ and on the size of the vacuum chamber L (see Eq. (C.1.24)). When Λ is set to the cosmological constant and L to the fiducial value reported in Table 4.2, one finds that the Berkeley experiment [Hamilton15] constrains the coupling parameter down to $M \sim 10^{15}$ GeV. The above calculation does not involve the power-law index α (apart indirectly via $m_{\rm bg}$, but there is no effect in the limit $m_{\rm bg}r \ll 1$). Therefore it is expected that the predictions are independent of α, as long as $|A(\phi) - 1| \ll 1$.

Remark: In the strongly perturbing regime, the reliability of the theory is questionable. Indeed the quantum corrections, either in the matter or in the chameleon sector must remain small. Most of the parameter space reachable by the Berkeley experiment [Hamilton15] belongs to this regime. Following [Upadhye12c] the underlying instabilities are harmless and the classical analysis is reliable, keeping in mind that quantum corrections can become large at very small scales. However, since our aim consists of modeling how the environment can affect the analytical results derived for the classical field, we also provide numerical forecasts in the questionable strongly perturbing regime. Nevertheless we do not explore the deeply strongly perturbing regime but focus on the transition between the strongly and the weakly perturbing regimes, where the numerical computations allow one to follow the smooth evolution of the field and acceleration profiles whereas analytical assumptions break. Our computations show that the analytical estimations are recovered once in the strongly perturbing regime, and that they are quite reliable, at least classically. The underlying quantum aspects are not discussed in this thesis.

- Case (4): $\phi(0) = \phi_{\rm min}(\rho_A)$ and $\phi_{\rm bg} = \phi_{\rm min}(\rho_{\rm v})$

  In the Case (4) the field profile is governed by Eq. (C.1.21) since the field reaches the effective potential minimum at the center of the source mass. However, as long as the condition Eq. (C.1.15) is satisfied, $\phi_{\rm bg} = \phi_{\rm min}\left(\rho_{\rm v}\right)$. For the original chameleon potential $V(\phi) = \Lambda^5/\phi$, the Case (4) takes place when $M \lesssim 10^{-3}$ GeV, whereas for the exponential potential $V(\phi) = \Lambda^4(1 + \Lambda/\phi)$ one needs $M \lesssim 10$ GeV in order to reach the strongly perturbing regime inside the source mass. Therefore the Case (4) is irrelevant for values of Λ compatible with cosmology and realistic experimental configurations.

C.2 Parameter space

It is possible to understand the shape of the viable parameter space depicted on Fig. 4.3 in the light of the analytical computations. Following [Burrage15, Hamilton15], it is possible to rewrite the acceleration a_ϕ given by Eqs. (C.1.14) and (C.1.23) as,

$$a_\phi = \frac{2G_{\rm N}m_{\rm A}}{r^2}\lambda_{\rm at}\lambda_{\rm A}\left(\frac{M_{\rm pl}}{M}\right)^2 = \frac{8\pi G_{\rm N}\rho_{\rm A}}{3}\frac{R_{\rm A}^3}{r^2}\lambda_{\rm at}\lambda_{\rm A}\left(\frac{M_{\rm pl}}{M}\right)^2, \qquad \text{(C.2.1)}$$

with $G_{\rm N} = (8\pi M_{\rm pl}^2)^{-1}$, $m_{\rm A} = \rho_{\rm A}(4/3)\pi R_{\rm A}^3$ and,

$$\lambda_i \simeq \begin{cases} 1 & \rho_i r_i^2 < 3M\phi_{\rm bg}, \\ 1 - \frac{S_i^3}{r_i^3} & \rho_i r_i^2 > 3M\phi_{\rm bg}, \end{cases} \qquad \text{(C.2.2)}$$

corresponding to the weakly and strongly perturbing regimes respectively, the i subscript denoting the species under consideration (atoms or the source mass).

Four regimes are distinguishable in Fig. 4.3, depending on whether the source mass and/or the atoms are screened as well as on $\phi_{\rm bg} = \phi_{\rm min}(\rho_{\rm v})$ or given by Eq. (C.1.25). In Fig. 4.3, the acceleration is normalized with respect to the Earth's acceleration of free fall $g = G_{\rm N}M_\oplus/R_\oplus^2 = (4/3)\pi G_{\rm N}R_\oplus\rho_\oplus$, $M_\oplus$, $R_\oplus$ and $\rho_\oplus$ denoting the Earth mass, radius and density respectively. The normalized acceleration then reads,

$$\frac{a_\phi}{g} = \frac{2\rho_{\rm A}}{R_\oplus\rho_\oplus}\frac{R_{\rm A}^3}{r^2}\lambda_{\rm at}\lambda_{\rm A}\left(\frac{M_{\rm pl}}{M}\right)^2. \qquad \text{(C.2.3)}$$

For large values of M the source mass is unscreened (and a fortiori the atoms are), so $\lambda_{\rm at} = \lambda_{\rm A} = 1$, the normalized acceleration reading,

$$\frac{a_\phi}{g}^{\rm (i)} = 2\left(\frac{M_{\rm pl}}{M}\right)^2\frac{\rho_A R_{\rm A}^3}{r^2 R_\oplus\rho_\oplus}. \qquad \text{(C.2.4)}$$

This regime corresponds to the Case (1) in App. C.1 and is marked by the vertical line at the top right of Fig. 4.3. If the source mass strongly perturbs the chameleon field whereas the atoms remain unscreened then $\lambda_{\rm at} = 1$ while $\lambda_{\rm A} \simeq 3M\phi_{\rm bg}/(\rho_A R_{\rm A}^2)$ according to Eq. (C.1.22). This regime corresponds to the Case (3) in App. C.1 and the acceleration then yields (see Eq. (C.1.23)),

$$\frac{a_\phi}{g}^{\rm (ii)} = \frac{6M_{\rm pl}^2}{r^2R_\oplus\rho_\oplus}\frac{\phi_{\rm bg}\rho_A}{M}, \qquad \text{(C.2.5)}$$

$$= \frac{6M_{\rm pl}^2}{r^2R_\oplus\rho_\oplus}\frac{\rho_A}{M}\aleph\left[\alpha\left(\alpha+1\right)\Lambda^{4+\alpha}\rho_{\rm v}\right]^{\frac{1}{\alpha+2}}, \qquad \text{(C.2.6)}$$

with $\phi_{\rm bg}$ given by Eq. (C.1.25). In the previous section we implicitly assumed that the atoms remain unscreened, which is true only as long as $\rho_{\rm at}R_{\rm at} <$

$3M\phi_{\rm bg}$. Otherwise $\lambda_{\rm at} \simeq 3M\phi_{\rm bg}/(\rho_{\rm at}R_{\rm at}^2)$ and the acceleration becomes,

$$\frac{a_\phi}{g}^{\rm (iii)} = \frac{18M_{\rm pl}^2}{\rho_{\rm at}R_{\rm at}^2R_\oplus\rho_\oplus}\frac{R_{\rm A}}{r^2}\phi_{\rm bg}^2, \tag{C.2.7}$$

$$= \frac{18M_{\rm pl}^2}{\rho_{\rm at}R_{\rm at}^2R_\oplus\rho_\oplus}\frac{R_{\rm A}}{r^2}\aleph\left[\alpha\left(\alpha+1\right)\Lambda^{4+\alpha}\rho_{\rm v}\right]^{\frac{2}{\alpha+2}}. \tag{C.2.8}$$

In this case the acceleration is independent of M. If the vacuum chamber is larger than the Compton wavelength of the chameleon (see Eq. (C.1.15)), then the chameleon reaches its attractor inside the vacuum chamber such that $\phi_{\rm bg}$ is given by $\phi_{\rm min}\left(\rho_{\rm v}\right)$, yielding,

$$\frac{a_\phi}{g}^{\rm (iv)} = \frac{18M_{\rm pl}^2}{\rho_{\rm at}R_{\rm at}^2R_\oplus\rho_\oplus}\frac{R_{\rm A}}{r^2}\phi_{\rm bg}^2, \tag{C.2.9}$$

$$= \frac{18M_{\rm pl}^2}{\rho_{\rm at}R_{\rm at}^2R_\oplus\rho_\oplus}\frac{R_{\rm A}}{r^2}\left(\frac{\alpha\Lambda^{\alpha+4}M}{\rho_{\rm v}}\right)^{\frac{2}{\alpha+1}}. \tag{C.2.10}$$

In this latter case, a_ϕ depends on M (see on the bottom left of Fig. 4.3). This latter regime is not tractable by our numerical simulations, as discussed in Sec. 4.4. Notice also that atom interferometry is not able to test the strongly coupled chameleon ($M > m_{\rm pl}$).

Appendix D

Numerical methods for the Higgs monopoles

In Sec. 5.3.4 we present monopole solutions obtained by a simplified integration method, considering the Klein-Gordon equation only. To show that this method is accurate, here we present the results obtained by integrating the full set of equations of motion, namely the Klein-Gordon together with the Einstein equations (5.3.2). This result confirms that we can safely replace the metric inside the compact object by the standard GR metric as explained in Sec. 5.3.2.

D.1 Equations of motion

We first list the full set of equations to be solved. The explicit $tt-$, $\theta\theta-$ and $rr-$ components of the Einstein equations (5.3.2) are, respectively,

$$\nu'' + \nu'^2 - \lambda'\nu' + (\nu' - \lambda')\left(\frac{1}{r} + \frac{H'}{F}\frac{\mathrm{d}F}{\mathrm{d}H}\right) + \frac{1}{F}\frac{\mathrm{d}F}{\mathrm{d}H}\left(H'' + \frac{H'}{r}\right) + \frac{H'^2}{F}\left(\frac{\kappa}{2} + \frac{\mathrm{d}^2F}{\mathrm{d}H^2}\right) + \left(\kappa V - \frac{3p}{\mathfrak{R}^2\rho}\right)\frac{\mathrm{e}^{2\lambda}}{F} = 0, \quad \text{(D.1.1)}$$

$$\lambda'\left(\frac{2}{r} + \frac{H'}{F}\frac{\mathrm{d}F}{\mathrm{d}H}\right) - \frac{H''}{F}\frac{\mathrm{d}F}{\mathrm{d}H} - \frac{H'^2}{2F}\left(\kappa + 2\frac{\mathrm{d}^2F}{\mathrm{d}H^2}\right) - \frac{2H'}{rF}\frac{\mathrm{d}F}{\mathrm{d}H} - \frac{1}{r^2}\left(1 - \mathrm{e}^{2\lambda}\right) - \frac{\mathrm{e}^{2\lambda}}{F}\left(\kappa V + \frac{3}{\mathfrak{R}^2}\right) = 0, \quad \text{(D.1.2)}$$

$$\nu'\left(\frac{2}{r} + \frac{H'}{F}\frac{\mathrm{d}F}{\mathrm{d}H}\right) - \frac{\kappa H'^2}{2F} + \frac{1}{r^2}\left(1 - \mathrm{e}^{2\lambda}\right) + \frac{2H'}{rF}\frac{\mathrm{d}F}{\mathrm{d}H} - \frac{\mathrm{e}^{2\lambda}}{F}\left(\frac{3p}{\mathfrak{R}^2\rho} - \kappa V\right) = 0, \quad \text{(D.1.3)}$$

where the prime denotes a derivative with respect to r and $\mathfrak{R}^2 = \mathcal{R}^3/r_{\rm s}$, $r_{\rm s}$ being the standard Schwarzschild radius. We assume a top-hat density profile (5.3.10) so that $\mathfrak{R} = 3/(\kappa\rho_0)$. Finally, the Klein-Gordon equation reads,

$$H'' - H'\left(\lambda' - \nu' - \frac{2}{r}\right) + \mathrm{e}^{2\lambda}\left(\frac{R}{2\kappa}\frac{\mathrm{d}F}{\mathrm{d}H} - \frac{\mathrm{d}V}{\mathrm{d}H}\right) = 0, \tag{D.1.4}$$

where the Ricci scalar R is given by,

$$R = \frac{2}{r^2} - \mathrm{e}^{-2\lambda}\left(2\nu'' - 2\nu'\lambda' + \frac{4\nu'}{r} + \frac{2}{r^2} - \frac{4\lambda'}{r} + 2\nu'^2\right). \tag{D.1.5}$$

D.2 Dimensionless system

To implement the numerical integration we need to write the above equations in a convenient dimensionless units system. This step is actually crucial in order to extract significant numerical results because of the involved scales, like the Planck mass. We first rescale the Higgs field as,

$$H[\mathrm{GeV}] = m_{\rm pl}\tilde{v}h = m_{\rm pl}\tilde{v}\,(1+\chi)\,, \tag{D.2.1}$$

where h and $\tilde{v} = 246\ \mathrm{GeV}/m_{\rm pl}$ are dimensionless. The quantity χ characterizes the dimensionless displacement of the Higgs scalar field around its vev. We express the radial coordinate in term of $r_{\rm s}$,

$$u = \frac{r}{r_{\rm s}}, \tag{D.2.2}$$

and we remind that the Schwarzschild radius in Planck units is,

$$r_{\rm s}[\mathrm{GeV}^{-1}] = \frac{2m}{m_{\rm pl}^2} \times 5.61 \times 10^{26}[\mathrm{GeV\ kg}^{-1}], \tag{D.2.3}$$

where m is the baryonic mass of the monopole in [kg]. The numerical factor converts mass from [kg] to [GeV] in such a way that the units are consistent. We also define the dimensionless potential,

$$\mathbb{V} = V\frac{r_{\rm s}^2}{m_{\rm pl}^2}, \tag{D.2.4}$$

which becomes according to the definition (D.2.1),

$$\mathbb{V}\,(\chi) = \frac{\lambda_{\rm sm}}{4}m_{\rm pl}^2 r_{\rm s}^2\tilde{v}^4\chi^2\,(2+\chi)^2\,. \tag{D.2.5}$$

Finally, we define the dimensionless coupling function in an analogous way, as,

$$\mathbb{F}\,(\chi) = 1 + \xi\tilde{v}^2\,(1+\chi)^2\,. \tag{D.2.6}$$

D.3 Numerical integration method

There exist different ways to perform the numerical integration of the Eqs. (D.1.1)-(D.1.4). We choose to treat them like an IVP, by integrating from the center of the body. We first find the internal solution and then use it at the boundary of the compact object to fix the initial conditions for the external solution. We choose to solve the system of equations with respect to the variables λ, ν, h and p since $\rho = \rho_0$ is constant. In addition to the equations of motion, we must consider the TOV equation,

$$p_u = -\nu_u \left(p + \rho_0\right), \tag{D.3.1}$$

where a subscript u denotes a derivative with respect to u. In the top-hat profile approximation, this equation admits the exact solution,

$$\frac{p}{\rho_0} = \mathcal{C} e^{-\nu} - 1, \tag{D.3.2}$$

where $\mathcal{C}$ is a constant of integration to be fixed by the numerical shooting method. In order to find a guess for the shooting method, we use the standard GR expression for the pressure (2.3.14). This is a very good approximation since a small discrepancy between the GR solution and the numerical one is expected, as explained in Sec. 5.3.3. In our units, Eq. (D.3.2) becomes (see also Sec. 2.3.4),

$$\frac{p(u)}{\rho_0} = \left[\frac{\sqrt{1-s} - \sqrt{1-s^3u^2}}{\sqrt{1-s^3u^2} - 3\sqrt{1-s}}\right]. \tag{D.3.3}$$

Imposing the initial condition $\nu(u=0) = 0$ [(1)], $\mathcal{C}$ reads,

$$\mathcal{C} = \frac{p_{\rm c}}{\rho_0} + 1, \tag{D.3.4}$$

where $p_{\rm c} = p(u=0)$ is the pressure at the center. Then we optimize the value of $\mathcal{C}$ in such a way that it satisfies also the boundary condition for the pressure at the boundary $p(u = 1/s) = 0$. In addition, this method has the advantage that it allows to test the limit for the central pressure coming from GR (2.3.15),

$$p(u=0) \longrightarrow \infty \Leftrightarrow \mathcal{R} = \frac{9m}{4}. \tag{D.3.5}$$

It turns out that the difference between $\mathcal{C}$ in GR and in our model is so small that the two solutions are undistinguishable so this step can be safely neglected.

Therefore, we are left with the four equations Eqs. (D.1.1), (D.1.2), (D.1.3) and (D.1.4). Of these, we keep Eq. (D.1.3) as the Hamiltonian constraint and

[(1)] Note that $\nu(u=0) = 0$ is not a regularity condition, which is instead given by asymptotic flatness, namely $\nu\left(u \to \infty\right) = 0$. Since we solve an IVP, we prefer to fix $\nu(u=0) = 0$ and then shift the solution to $\nu(u) - \nu_{\rm end}$, without loss of generality.

we integrate the other three as an IVP. The initial conditions for λ, ν_u and h_u are obtained from the regularity conditions of the solution at the center of the Higgs monopole,

$$\lambda(0) = 0, \tag{D.3.6}$$

$$\nu_u(0) = 0, \tag{D.3.7}$$

$$h_u(0) = 0. \tag{D.3.8}$$

In addition, we need to choose a value for h_c to begin the integration. We know that this value is an irrational number that can be determined numerically with finite accuracy only. Thus, the basic idea of our algorithm consists of incrementing the value of h_c digit by digit for a given number of digits. We also have an indication that makes integration easier. Indeed, we saw in Sec. 5.3.2 that if h_c is larger than $h_\mathrm{eq}^\mathrm{in}$ (see Eq. (5.3.49)) then it never reaches the vev at spatial infinity. So, we can stop the integration as soon as $h > h_\mathrm{eq}^\mathrm{in}$ and reject the chosen value of h_c. Therefore, we begin by integrating from the approximate value of $h_\mathrm{eq}^\mathrm{in}$ (we recall that this value is calculated in the approximation that the internal solution is the same as GR) and if h becomes larger than $h_\mathrm{eq}^\mathrm{in}$ we stop the integration, we keep the previous digit and perform once again numerical integration with a value of h_c incremented by one less significant digit. Otherwise, namely when the Higgs field does not become higher than $h_\mathrm{eq}^\mathrm{in}$ and is trapped into the local minimum of the effective potential $h = 0$, we increment the same digit. With this algorithm, we are able to maximize the precision on h_c in the limit of the precision we impose or, in other words, we are able to push back the radial distance from the center of the body at which the scalar field is trapped into the local minimum of the effective potential $h = 0$.

We have also to take care of the "degeneracy" of the solution at spatial infinity. Indeed, the scalar field can tend to $\pm v$. So, when we perform numerical integration for different values of the parameters, we have to choose between the positive and the negative solution.

In order to check the validity of our numerical code, we plot in Fig. D.1 the Hamiltonian constraint for the same monopole solution as represented in Fig. 5.2 and obtained with the full numerical integration. Here, the Hamiltonian constraint is defined as the absolute value of the difference between ν_u coming from Eq. (D.1.3), where we replaced the values of all fields with the ones found numerically, and the value of ν_u determined numerically by solving the system of equations. The divergence appearing at the boundary of the monopole comes from the abrupt transition of energy density due to the top-hat approximation. Otherwise, the order of magnitude of the Hamiltonian constraint corresponds to what we expect from the numerical precision.

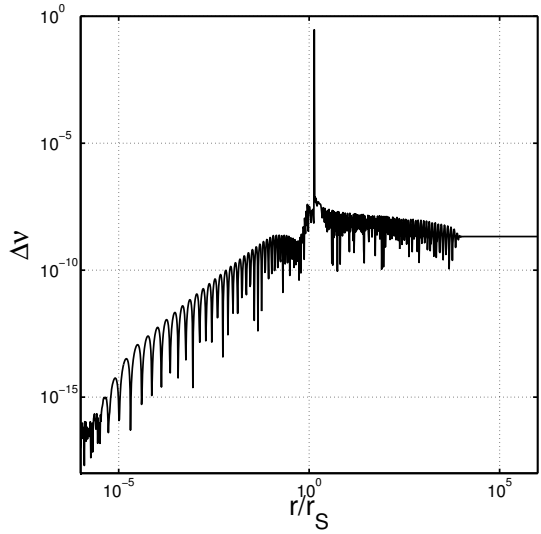

Figure D.1: Hamiltonian constraint for the same monopole solution as represented in Fig. 5.2 ($\xi = 10$, $m = 10^6$ kg and $s = 0.75$) obtained with the full numerical method.

D.4 Comparison between the full integration method and the simplified one

In Sec. 5.3.3 we argue that we can safely neglect the Higgs field inside the body as long as it is sufficiently constant and not too much displaced from its vev. This means that, instead of integrating the whole system of equations, we could use the inner Schwarzschild expressions for λ and ν (Eqs. (5.3.46) and (5.3.47)) and integrate only the Klein-Gordon equation as an IVP. We now demonstrate the correctness of this claim by comparing our results with a complete numerical integration. We first plot on Fig. D.2 the contribution of each term appearing in the trace of Eq. (5.3.2) obtained with the full numerical integration in the case when $m = 10^6$ kg, $s = 0.75$ and $\xi = 10$. In the dimensionless unit system, the contributions of the trace of the stress-energy tensor are given by,

$$\frac{r_{\rm s}^2}{m_{\rm pl}^2} T^{(h)} = -h_u^2 + 2V(h), \tag{D.4.1}$$

and,

$$\frac{r_{\rm s}^2}{m_{\rm pl}^2} T^{(\xi)} = \frac{3\xi}{4\pi}\left\{ h_u^2 + h\mathrm{e}^{-2\lambda}\left[h_{uu} - h_u\left(\lambda_u - \nu_u - \frac{2}{u}\right)\right]\right\}. \tag{D.4.2}$$

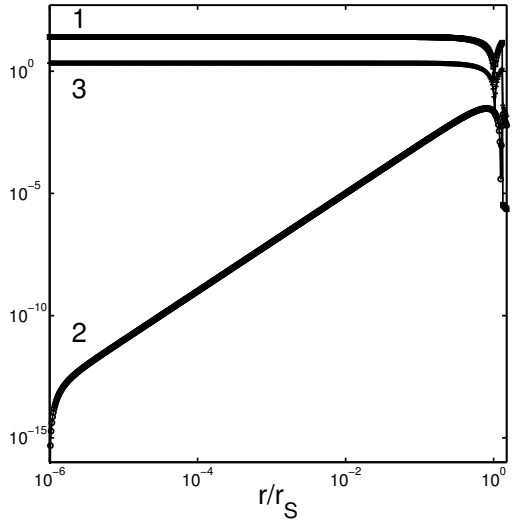

Figure D.2: Plot of the trace of the stress-energy tensor contributions $T^{(h)}$ (curve 2), $T^{(\xi)}$ (curve 3) and of the left-hand side of Eq. (5.3.2) (curve 1). The parameters are chosen as $m = 10^6$ kg, $s = 0.75$, and $\xi = 10$.

We observe in Fig. D.2 that the geometric part is clearly dominant while the contribution coming from the stress-energy tensor components of the scalar field is negligible. This result is confirmed by the comparison of the Ricci scalar given by Eq. (5.3.48) and Eq. (D.1.5) evaluated numerically. In Fig. D.3 we plotted the absolute value of the difference between the two expressions in function of the radial distance for the same parameters as in Fig. D.2. The difference is clearly negligible while the peak at the boundary of the body is caused only by the top-hat approximation for the energy density.

As a further check, we plot the Higgs field profiles obtained with the two numerical methods in Fig. D.4 for $\xi = 10$, $m = 10^6$ kg, and $s = 0.75$. The discrepancy inside the body appears only because the scalar field contribution is neglected in the simplified model. In order to get a quantitative result, we plot on Fig. D.5 the relative errors between the Higgs field solutions obtained with the full numerical method and the simplified one for various monopole solutions. In general, we see that there is a very good agreement between numerical and approximate solutions only for small compactness.

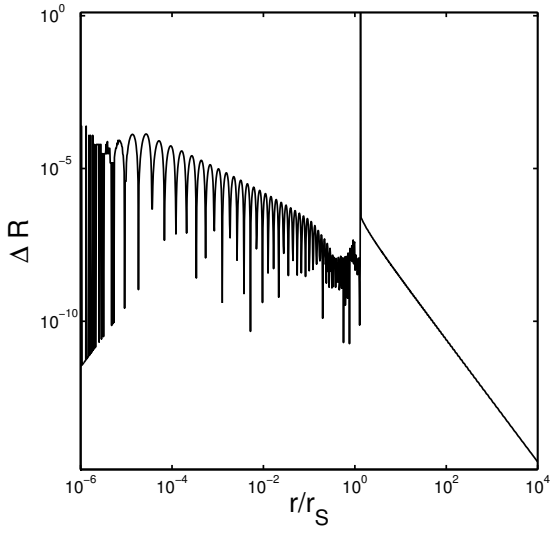

Figure D.3: Absolute value of the difference between the standard GR curvature scalar and its value calculated with our numerical algorithm for $m = 10^6$ kg, $s = 0.75$ and $\xi = 10$.

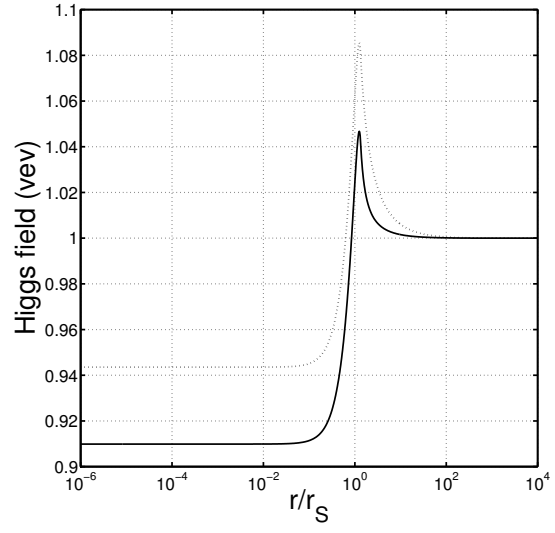

Figure D.4: Numerical solutions for the monopole with $m = 10^6$ kg, $s = 0.75$, and $\xi = 10$ obtained with the full numerical integration and the simplified one. The difference between the two solutions becomes apparent only inside the body and is negligible outside the body.

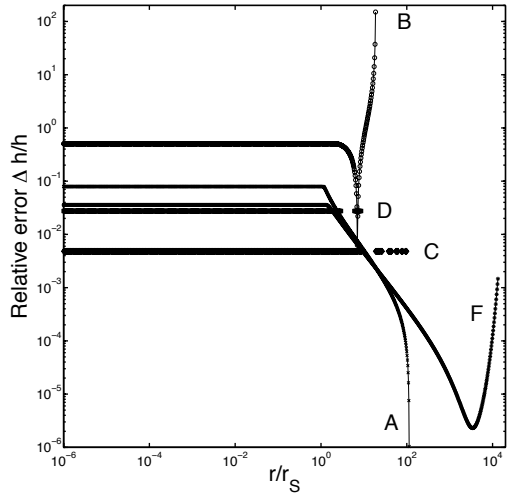

Figure D.5: Relative error between the Higgs field solutions obtained with the full numerical method and the simplified one. Labels refer to Higgs monopoles listed in Tab. 5.1.

Appendix E

Fab Two: equations of motion and ghosts conditions

We report in this appendix some of the calculations used in Chap. 6.

E.1 Equations of motion for the Fab Two

In this section, we focus on the non-standard kinetic term of the Fab-Four Lagrangian,

$$\begin{aligned} S_{\rm John} &= \int \mathrm{d}^4x\,\sqrt{-g}\,\phi^\alpha\phi^\beta\,G_{\alpha\beta}, \\ &= \int \mathrm{d}^4x\,\sqrt{-g}\,g^{\rho\alpha}g^{\sigma\beta}\,\phi_\rho\phi_\sigma\left(R_{\alpha\beta}-\frac{1}{2}R\,g_{\alpha\beta}\right), \end{aligned} \tag{E.1.1}$$

where we adopted the convention $\phi_\alpha = \nabla_\alpha\phi$. The variation of $S_{\rm John}$ reads,

$$\begin{aligned} E_{\mu\nu} \equiv \frac{1}{\sqrt{-g}}\frac{\delta S_{\rm John}}{\delta g^{\mu\nu}} &= \phi^\rho\phi^\sigma G_{\rho\sigma}\frac{\delta\sqrt{-g}}{\delta g^{\mu\nu}} + \phi_\rho\phi^\beta G_{\alpha\beta}\frac{\delta g^{\rho\alpha}}{\delta g^{\mu\nu}} + \phi^\alpha\phi_\sigma G_{\alpha\beta}\frac{\delta g^{\sigma\beta}}{\delta g^{\mu\nu}} \\ &\quad + \phi^\alpha\phi^\beta\frac{\delta R_{\alpha\beta}}{\delta g^{\mu\nu}} - \frac{1}{2}\phi^\alpha\phi_\alpha\frac{\delta R}{\delta g^{\mu\nu}} - \frac{1}{2}\phi^\alpha\phi^\beta R\frac{\delta g_{\alpha\beta}}{\delta g^{\mu\nu}}, \\ &= -\frac{1}{2}g_{\mu\nu}\,\phi^\rho\phi^\sigma\,G_{\rho\sigma} + 2\,\phi_{(\mu}R_{\nu)\alpha}\,\phi^\alpha \\ &\quad -\frac{1}{2}\,R\,\phi_\mu\phi_\nu \underbrace{+\phi^\rho\phi^\sigma\frac{\delta R_{\rho\sigma}}{\delta g^{\mu\nu}}}_{(\mathcal{T}_1)} \underbrace{-\frac{1}{2}\phi_\alpha\phi^\alpha\frac{\delta R}{\delta g^{\mu\nu}}}_{(\mathcal{T}_2)}, \end{aligned} \tag{E.1.2}$$

using Eqs. (1.2.4)–(1.2.5) and adopting the convention on the symmetrization of indices,

$$T_{(\mu\nu)} \equiv \frac{1}{2}\left(T_{\mu\nu}+T_{\nu\mu}\right), \tag{E.1.3}$$

for any tensor $\mathbf{T}$. The variation of the Ricci scalar is given by Eq. (1.2.6) while the one of the Ricci tensor reads,

$$\frac{\delta R_{\rho\sigma}}{\delta g^{\mu\nu}} = \frac{1}{2}\left[g_{\rho\mu}g_{\sigma\nu}\Box + g_{\mu\nu}\nabla_\rho\nabla_\sigma - 2\,g_{\mu(\rho}\nabla_{\sigma}\nabla_{\nu)}\right]. \tag{E.1.4}$$

The term $(\mathcal{T}_1)$ becomes,

$$\begin{aligned}(\mathcal{T}_1) &= \frac{1}{2}\,\phi_\mu\phi_\nu\Box + \frac{1}{2}\phi^\rho\phi^\sigma g_{\mu\nu}\nabla_\rho\nabla_\sigma - \phi_{(\mu}\phi^\sigma\nabla_\sigma\nabla_{\nu)}, &\text{(E.1.5)}\\ &= \frac{1}{2}\Box\left(\phi_\mu\phi_\nu\right) + \frac{1}{2}\,g_{\mu\nu}\,\nabla_\sigma\nabla_\rho\left(\phi^\rho\phi^\sigma\right) - \nabla_\sigma\nabla_{(\nu}\left(\phi_{\mu)}\phi^\sigma\right), &\text{(E.1.6)}\end{aligned}$$

by integrating by parts twice the expression and neglecting the boundary terms. Using the commutation relations between the covariant derivatives,

$$\begin{aligned}\left[\nabla_\mu,\nabla_\nu\right]\phi &= 0, &\text{(E.1.7)}\\ \left[\nabla_\mu,\nabla_\nu\right]V^\rho &= R^\rho_{\kappa\mu\nu}V^\kappa, &\text{(E.1.8)}\end{aligned}$$

for any vector field $\mathbf{V}$, the term $(\mathcal{T}_1)$ eventually yields,

$$\begin{aligned}(\mathcal{T}_1) = &-\phi_{\mu\nu}\Box\phi - \phi_{\mu\nu\sigma}\phi^\sigma\\ &+\frac{1}{2}g_{\mu\nu}\left[\left(\Box\phi\right)^2 + \phi^{\rho\sigma}\phi_{\rho\sigma} + \phi^\rho\left(\phi^\sigma_{\ \rho\sigma} + \phi^\sigma_{\ \sigma\rho}\right)\right].\end{aligned} \tag{E.1.9}$$

In the same way, the term $(\mathcal{T}_2)$ becomes,

$$\begin{aligned}(\mathcal{T}_2) &= -\frac{1}{2}\left[R_{\mu\nu}\left(\partial\phi\right)^2 + \phi_\alpha\phi^\alpha\left(g_{\mu\nu}\Box - \nabla_\mu\nabla_\nu\right)\right], &\text{(E.1.10)}\\ &= -\frac{1}{2}\left[R_{\mu\nu}\left(\partial\phi\right)^2 + g_{\mu\nu}\Box\left(\phi_\alpha\phi^\alpha\right) - \nabla_\nu\nabla_\mu\left(\phi_\alpha\phi^\alpha\right)\right], &\text{(E.1.11)}\\ &= -\frac{1}{2}\Big[R_{\mu\nu}\left(\partial\phi\right)^2 + 2\,g_{\mu\nu}\left(\phi_{\rho\zeta}^{\ \ \zeta}\phi^\rho + \phi_{\rho\zeta}\phi^{\rho\zeta}\right)\\ &\qquad - 2\left(\phi_{\rho\mu\nu}\phi^\rho + \phi_{\rho\mu}\phi^\rho_{\ \nu}\right)\Big]. &\text{(E.1.12)}\end{aligned}$$

By recombining all the terms we finally obtain,

$$\begin{aligned}E_{\mu\nu} &= -\frac{1}{2}R\,\phi_\mu\phi_\nu + 2\,\phi_{(\mu}R_{\nu)\alpha}\,\phi^\alpha - \frac{1}{2}G_{\mu\nu}\left(\nabla\phi\right)^2 + R_{\mu\alpha\nu\beta}\phi^\alpha\phi^\beta + \phi_{\rho\mu}\phi^\rho_{\ \nu}\\ &\quad -\phi_{\mu\nu}\Box\phi + \frac{g_{\mu\nu}}{2}\left[-\phi^{\alpha\beta}\phi_{\alpha\beta} + \left(\Box\phi\right)^2 - 2\,\phi^\alpha\phi^\beta\,R_{\alpha\beta}\right].\end{aligned} \tag{E.1.13}$$

The Klein-Gordon equation is derived by computing the variation of $\mathcal{L}_{\rm John}$ with respect to the scalar field,

$$\begin{aligned}\frac{\partial\mathcal{L}_{\rm John}}{\partial\phi} &= 0, &\text{(E.1.14)}\\ \nabla_\rho\frac{\partial\mathcal{L}_{\rm John}}{\partial\phi_\rho} &= \nabla_\rho\left(2G^{\rho\nu}\phi_\nu\right) = 2G^{\rho\nu}\phi_{\nu\rho}, &\text{(E.1.15)}\end{aligned}$$

using the second Bianchi identity for the last equality.

E.2 Cosmological equations

In terms of the reduced variables $x(t) = \kappa\dot{\phi}$, $y(t) = \sqrt{\kappa}\dot{\alpha}$ and $z(t) = 1 + \epsilon\sqrt{\kappa}\phi(t)$, the equations of motion for a flat and empty universe derived from action (6.3.1) are,

$$6\epsilon xy + x^2\left(-1 + 9\gamma y^2\right) + 6y^2 z = 0, \tag{E.2.1}$$

$$4x\left(\epsilon + \gamma\sqrt{\kappa}\dot{x}\right)y + x^2\left(1 + 3\gamma y^2 + 2\gamma\sqrt{\kappa}\dot{y}\right) + 6y^2 z + 2\sqrt{\kappa}(\epsilon\dot{x} + 2\dot{y}z) = 0, \tag{E.2.2}$$

$$3y\left(x - 2\epsilon y - 3\gamma x y^2\right) + \sqrt{\kappa}\left(\dot{x} - 3\gamma\dot{x}y^2 - 3(\epsilon + 2\gamma xy)\dot{y}\right) = 0, \tag{E.2.3}$$

which can be decoupled in the following way,

$$\dot{x} = \frac{-3x\left[\epsilon x + 4\left(\epsilon^2 + \gamma x^2\right)y + 7\epsilon\gamma xy^2\right] + 6y(-2x + \epsilon y)z}{2\kappa^{1/2}\left(3\epsilon^2 + 12\epsilon\gamma xy + \gamma x^2\left(1 + 9\gamma y^2\right) + \left(2 - 6\gamma y^2\right)z\right)}, \tag{E.2.4}$$

$$\dot{y} = \frac{2\epsilon xy\left(1 - 15\gamma y^2\right) + x^2\left[-1 + 3\gamma y^2\left(4 - 9\gamma y^2\right)\right] - 6y^2\left(2\epsilon^2 + z - 3\gamma y^2 z\right)}{2\kappa^{1/2}\left[3\epsilon^2 + 12\epsilon\gamma xy + \gamma x^2\left(1 + 9\gamma y^2\right) + \left(2 - 6\gamma y^2\right)z\right]}. \tag{E.2.5}$$

The scalar field EoS is given by,

$$w_\phi = -x\left(3\gamma x^2 + 2z\right)\frac{N}{D}, \tag{E.2.6}$$

with,

$$\begin{aligned} N &= 6x\left(\gamma x^2 - z\right)\left(3\gamma x^2 + 2z\right)^2 + 6\sqrt{3}\epsilon^3\sqrt{x^2\left(3\epsilon^2 + 3\gamma x^2 + 2z\right)}\left(7\gamma x^2 + 2z\right) \\ &\quad -2\sqrt{3}\epsilon\sqrt{x^2\left(3\epsilon^2 + 3\gamma x^2 + 2z\right)}\left(33\gamma^2 x^4 + 16\gamma x^2 z - 4z^2\right) \\ &\quad +9\epsilon^2\left(15\gamma^2 x^5 + 4\gamma x^3 z - 4xz^2\right) - 18\epsilon^4\left(7\gamma x^3 + 2xz\right), \end{aligned} \tag{E.2.7}$$

$$\begin{aligned} D &= \left[-3\epsilon x + \sqrt{3}\sqrt{x^2\left(3\epsilon^2 + 3\gamma x^2 + 2z\right)}\right]^2 \times \\ &\quad \Big[18\gamma^3 x^6 + 30\gamma^2 x^4 z + 24\gamma x^2 z^2 + 8z^3 \\ &\quad +6\sqrt{3}\epsilon\gamma x\left(\gamma x^2 + 2z\right)\sqrt{x^2\left(3\epsilon^2 + 3\gamma x^2 + 2z\right)} + 3\epsilon^2\left(3\gamma^2 x^4 + 4z^2\right)\Big]. \end{aligned} \tag{E.2.8}$$

E.3 Stability conditions

We derive the metric perturbations based on Eqs. (23) and (25-27) of [De Felice12],

$$Q_{\rm T} > 0 \quad \Rightarrow \quad z + \frac{\gamma x^2}{2} > 0, \tag{E.3.1}$$

$$c_{\rm T}^2 \geq 0 \quad \Rightarrow \quad z - \frac{\gamma x^2}{2} \geq 0, \tag{E.3.2}$$

for the tensorial part, and,

$$Q_{\rm S} \ > 0 \ \Rightarrow 3\epsilon^2 + 12\epsilon\gamma xy + 9\gamma^2 x^2 y^2 + 2z + \gamma\left(x^2 - 6y^2 z\right) > 0, \qquad \text{(E.3.3)}$$

for the scalar part of the metric perturbations, while the condition on the squared speed $c_{\rm S}^2 \geq 0$ leads to,

$$\begin{aligned} &2x\left(\epsilon + \gamma\sqrt{\kappa}\dot{x}\right)\left(\gamma x^2 + 2z\right)\left(\epsilon x + 3\gamma x^2 y + 2yz\right) \\ &\quad +2y\left(\frac{\gamma x^2}{2} + z\right)^2\left(\epsilon x + 3\gamma x^2 y + 2yz\right) + \frac{1}{2}\left(\gamma x^2 - 2z\right)\left(\epsilon x + 3\gamma x^2 y + 2yz\right)^2 \\ &\quad\quad -2\sqrt{\kappa}\left(\frac{\gamma x^2}{2} + z\right)^2\left[\epsilon\left(\dot{x} + \frac{2xy}{\sqrt{\kappa}}\right) + 3\gamma x(2\dot{x}y + x\dot{y}) + 2\dot{y}z\right] \geq 0. \qquad \text{(E.3.4)} \end{aligned}$$

E.4 Spherically symmetric equations of motion

We derive the equations of motion for the action (6.3.1) in the vacuum for a spherically symmetric and static field configuration, assuming the metric ansatz (6.3.9),

$$\begin{aligned} 0 \ &= \ \Big(2\varphi'^2 B r^2 B'' + 4\varphi' B^2 r\varphi'' + 4\varphi' B r^2 \varphi'' B' - 5\varphi'^2 B'^2 r^2 + 2\varphi'^2 B^2\Big)\gamma\kappa^2 \\ &- \ \Big(4B^3\varphi B'' r^2 + 2B^3 B' r^2\varphi' + 4B^4\varphi' r + 8B^3\varphi B' r + 2B^4 r^2\varphi'' \\ &- \ 2B^2\varphi B'^2 r^2\Big)\epsilon\kappa^{1/2} - 8B^3 r B' - 4B^3 r^2 B'' + 2B^2 r^2 B'^2 - \varphi'^2\kappa^2 B^4 r^2, \end{aligned}$$

$$\begin{aligned} 0 \ &= \ \Big(4\varphi'^2 B' A r B + 2\varphi'^2 B^2 A - 3\varphi'^2 B'^2 A r^2 + 4\varphi' B r^2\varphi'' A B' + 8\varphi'^2 B^2 r A' \\ &+ \ 2\varphi'^2 B' A' B r^2 + 2\varphi'^2 A'' r^2 B^2 + 4\varphi' B^2 r\varphi'' A + 4\varphi' A' r^2\varphi'' B^2 \\ &+ \ 2\varphi'^2 A B r^2 B''\Big)\gamma\kappa^2 - \Big(4B^3 A B' r^2\varphi' - 2B^2 A\varphi B'^2 r^2 + 8B^4 A\varphi' r \\ &+ \ 8\varphi r A' B^4 + 8B^3 A\varphi B' r + 4B^3 A\varphi B'' r^2 + 4\varphi B' A' r^2 B^3 + 6A' r^2\varphi' B^4 \\ &+ \ 4\varphi A'' r^2 B^4 + 4B^4 A r^2\varphi''\Big)\epsilon\kappa^{1/2} - 4B^3 A r^2 B'' - 4r^2 A'' B^4 - 8r A' B^4 \\ &- \ 8B^3 A r B' - 4A' r^2 B' B^3 + 2B^2 A r^2 B'^2 - \varphi'^2\kappa^2 B^4 A r^2, \end{aligned}$$

$$
\begin{aligned}
0 &= \Big(4\varphi' A' B^3 + 4\varphi' A B' B^2 + 4\varphi' B' A r^2 B'' B + 4\varphi' B'' A' r^2 B^2 \\
&+ 4\varphi'' r A' B^3 + 4\varphi' r A'' B^3 + 4\varphi'' B' A' r^2 B^2 + 8\varphi' B' A' r B^2 + 4\varphi' B'' A r B^2 \\
&+ 4\varphi'' B' A r B^2 - 4\varphi' B'^2 A r B - 6\varphi' B'^2 A' r^2 B - 6\varphi' B'^3 A r^2 \\
&+ 4\varphi' B' A'' r^2 B^2 + 2\varphi'' B'^2 A r^2 B\Big)\gamma\kappa - \Big(8B' A r B^4 + 4B^5 r A' \\
&+ 4r^2 A B'' B^4 + 2B' A' r^2 B^4 + 2B^5 r^2 A'' - 2B'^2 A r^2 B^3\Big)\epsilon\kappa^{-1/2} \\
&+ 2A' r^2 \varphi' B^5 + 2B^5 r^2 \varphi'' A + 4\varphi' B^5 A r + 2B' r^2 \varphi' A B^4,
\end{aligned}
$$

$$
\begin{aligned}
0 &= \Big(2\varphi'^2 A' B^2 + 2r\varphi'^2 A'' B^2 - 6\varphi'^2 B'^2 A r + 4\varphi' A \varphi'' B^2 - 2\varphi'^2 B' A B \\
&- 4\varphi'^2 A' B' r B + 4\varphi' r B' A \varphi'' B + 4r\varphi' A' \varphi'' B^2 + 2\varphi'^2 r B'' A B\Big)\gamma\kappa^2 \\
&- \Big(4\varphi B' A B^3 - 4r\varphi B'^2 A B^2 + 4B^4 r A' \varphi' + 4B^4 \varphi A'' r + 4B^4 \varphi'' A r \\
&+ 4B^4 \varphi A' + 4B^4 \varphi' A + 4\varphi B'' A r B^3\Big)\epsilon\kappa^{1/2} + 4r B'^2 A B^2 - 4r A B'' B^3 \\
&- 4B' A B^3 - 4B^4 A' - 4B^4 A'' r - 2B^4 \varphi'^2 A r \kappa^2.
\end{aligned}
$$

For the numerical integration the metric ansatz (2.3.1) is preferred and the matter sector must be included. The three Einstein equations and the Klein-Gordon equation then read respectively,

$$\begin{aligned}
&\nu''\left[-\frac{(1+\epsilon\sqrt{\kappa}\phi)}{\kappa}r+\frac{\kappa\gamma}{2}\,\mathrm{e}^{-2\lambda}\phi'^2 r\right]+\phi''\left(-\frac{\epsilon}{\sqrt{\kappa}}r+\kappa\gamma\mathrm{e}^{-2\lambda}\phi'+\kappa\gamma\mathrm{e}^{-2\lambda}\phi'\nu' r\right)\\
&\quad+\lambda'\left[\left(-\frac{3\,\kappa\gamma}{2}r\mathrm{e}^{-2\lambda}\phi'^2+\frac{(1+\epsilon\sqrt{\kappa}\phi)}{\kappa}r\right)\nu'-\frac{3\,\kappa\gamma}{2}\mathrm{e}^{-2\lambda}\phi'^2+\frac{1+\epsilon\sqrt{\kappa}\phi}{\kappa}+\frac{\epsilon}{\sqrt{\kappa}}\phi' r\right]\\
&\quad=\nu'^2\left[\frac{(1+\epsilon\sqrt{\kappa}\phi)}{\kappa}r-\frac{\kappa\gamma}{2}\phi'^2\mathrm{e}^{-2\lambda}r\right]+\nu'\left(\frac{1+\epsilon\sqrt{\kappa}\phi}{\kappa}+\frac{\epsilon}{\sqrt{\kappa}}r\phi'-\frac{\kappa\gamma}{2}\mathrm{e}^{-2\lambda}\phi'^2\right)+\frac{\epsilon}{\sqrt{\kappa}}\phi'+\frac{\phi'^2 r}{2}+\mathrm{e}^{2\lambda}r\left(-\frac{3}{\tilde{R}^2}\frac{p}{\rho}\right),
\end{aligned}\tag{E.4.1}$$

$$\begin{aligned}
&\phi''\left[-\frac{\epsilon}{\sqrt{\kappa}}\,\mathrm{e}^{2\lambda}r^2+2\,\kappa\gamma\phi' r\right]+\lambda'\left[\frac{\epsilon}{\sqrt{\kappa}}\,\mathrm{e}^{2\lambda}\phi' r^2+2\,r\mathrm{e}^{2\lambda}\frac{(1+\epsilon\sqrt{\kappa}\phi)}{\kappa}-3\,\kappa\gamma\phi'^2 r\right]\\
&\qquad=\frac{\phi'^2}{2}\left[\mathrm{e}^{2\lambda}r^2-\kappa\gamma\left(1+\mathrm{e}^{2\lambda}\right)\right]+2\,\frac{\epsilon}{\sqrt{\kappa}}\mathrm{e}^{2\lambda}\phi' r+\left(\mathrm{e}^{2\lambda}-\mathrm{e}^{4\lambda}\right)\frac{(1+\epsilon\sqrt{\kappa}\phi)}{\kappa}+r^2\mathrm{e}^{2\lambda}\left(\frac{3}{\tilde{R}^2}\right),
\end{aligned}\tag{E.4.2}$$

$$\begin{aligned}
&\nu'\left[-2\,r\frac{(1+\epsilon\sqrt{\kappa}\phi)}{\kappa}+3\,\kappa\gamma\mathrm{e}^{-2\lambda}\phi'^2 r-\frac{\epsilon}{\sqrt{\kappa}}\,\phi' r^2\right]+\frac{\phi'^2}{2}\left(3\,\kappa\gamma\mathrm{e}^{-2\lambda}+r^2-\kappa\gamma\right)-2\,\frac{\epsilon}{\sqrt{\kappa}}\phi' r\\
&\qquad-\left(1-\mathrm{e}^{2\lambda}\right)\frac{(1+\epsilon\sqrt{\kappa}\phi)}{\kappa}+\frac{3}{\tilde{R}^2}\frac{p}{\rho}\mathrm{e}^{2\lambda}r^2=0,
\end{aligned}\tag{E.4.3}$$

$$\begin{aligned}
&\nu''\left(2\,\kappa\gamma r\phi'-\frac{\epsilon}{\sqrt{\kappa}}\,\mathrm{e}^{2\lambda}r^2\right)+\phi''\left(2\,\kappa\gamma r\nu'+\mathrm{e}^{2\lambda}r^2+\kappa\gamma-\kappa\gamma\mathrm{e}^{2\lambda}\right)\\
&\quad+\lambda'\left[\nu'\left(-6\,\kappa\gamma r\phi'+\frac{\epsilon}{\sqrt{\kappa}}\,\mathrm{e}^{2\lambda}r^2\right)+\phi'\left(-\mathrm{e}^{2\lambda}r^2-3\,\kappa\gamma+\kappa\gamma\mathrm{e}^{2\lambda}\right)+2\,\frac{\epsilon}{\sqrt{\kappa}}\mathrm{e}^{2\lambda}r\right]\\
&\quad=-\nu'^2\left(2\,\kappa\gamma r\phi'-\frac{\epsilon}{\sqrt{\kappa}}\,\mathrm{e}^{2\lambda}r^2\right)-\nu'\left[\phi'\left(3\,\kappa\gamma-\kappa\gamma\mathrm{e}^{2\lambda}+\mathrm{e}^{2\lambda}r^2\right)-2\,\frac{\epsilon}{\sqrt{\kappa}}\mathrm{e}^{2\lambda}r\right]-2\,\phi'\mathrm{e}^{2\lambda}r-\frac{\epsilon}{\sqrt{\kappa}}\mathrm{e}^{2\lambda}\left(\mathrm{e}^{2\lambda}-1\right),
\end{aligned}\tag{E.4.4}$$

with $\tilde{R}=3/(\kappa\rho)=\mathcal{R}^3/r_{\mathrm{s}}$.

Bibliography

[Aad12] AAD, G. et al. [ATLAS Collaboration]. Observation of a new particle in the search for the Standard Model Higgs boson with the ATLAS detector at the LHC. *Phys. Lett.* B716:1–29 (2012).

[Abbott16a] ABBOTT, B.P. et al. [LIGO Scientific Collaboration and Virgo Collaboration]. GW151226: Observation of gravitational waves from a 22-solar-mass binary black hole coalescence. *Phys. Rev. Lett.* 116:241103 (2016).

[Abbott16b] ABBOTT, B.P. et al. [LIGO Scientific Collaboration and Virgo Collaboration]. Observation of gravitational waves from a binary black hole merger. *Phys. Rev. Lett.* 116:061102 (2016).

[Abbott16c] ABBOTT, B.P. et al. [LIGO Scientific and Virgo Collaborations]. Tests of general relativity with gw150914. *Phys. Rev. Lett.* 116:221101 (2016).

[Ade15a] ADE, P.A.R. et al. [BICEP2, Planck Collaboration]. Joint Analysis of BICEP2/Keck Array and Planck Data. *Phys. Rev. Lett.* 114:101301 (2015).

[Ade15b] ADE, P.A.R. et al. [Planck Collaboration]. Planck 2015 results. XIII. Cosmological parameters. *arXiv:1502.01589* (2015).

[Ade15c] ADE, P.A.R. et al. [Planck Collaboration]. Planck 2015 results. XIV. Dark energy and modified gravity. *arXiv:1502.01590* (2015).

[Ade15d] ADE, P.A.R. et al. [Planck Collaboration]. Planck 2015 results. XVII. Constraints on primordial non-Gaussianity. *arXiv:1502.01592* (2015).

[Ade15e] ADE, P.A.R. et al. [Planck Collaboration]. Planck 2015 results. XX. Constraints on inflation. *arXiv:1502.02114* (2015).

[Adelberger02] ADELBERGER, E.G. Sub-millimeter tests of the gravitational inverse square law. In *CPT and Lorentz symmetry. Proceedings: 2nd Meeting, Bloomington, USA, Aug 15-18, 2001* pages 9–15. (2002).

[Adelberger03] ADELBERGER, E.G., HECKEL, B.R., and NELSON, A.E. Tests of the gravitational inverse square law. *Ann. Rev. Nucl. Part. Sci.* 53:77–121 (2003).

[Adelberger07] ADELBERGER, E.G., HECKEL, B.R., HOEDL, S.A., et al. Particle Physics Implications of a Recent Test of the Gravitational Inverse Sqaure Law. *Phys. Rev. Lett.* 98:131104 (2007).

[Aldama15] ALDAMA, M.E. The gravity apple tree. *J. Phys. Conf. Ser.* 600(1):012050 (2015).

[Alexander77] ALEXANDER, H.G. *The Leibniz-Clarcke Correspondence, With extracts from Newton's 'Principia' and 'Optiks'*. Manchester University Press (1977).

[Alimi08] ALIMI, J.M. and FUZFA, A. The Abnormally Weighting Energy Hypothesis: the Missing Link between Dark Matter and Dark Energy. *JCAP* 0809:014 (2008).

[Amaro-Seoane13] AMARO-SEOANE, P. et al. eLISA/NGO: Astrophysics and cosmology in the gravitational-wave millihertz regime. *GW Notes* 6:4–110 (2013).

[Amendola10] AMENDOLA, L. and TSUJIKAWA, S. *Dark energy: theory and observations, Cambridge University Press*. Cambridge University Press (2010).

[Amendola13] AMENDOLA, L. et al. [Euclid Theory Working Group Collaboration]. Cosmology and fundamental physics with the Euclid satellite. *Living Rev. Rel.* 16:6 (2013).

[Amendola16] AMENDOLA, L. et al. Cosmology and Fundamental Physics with the Euclid Satellite. *arXiv:1606.00180* (2016).

[Anastassopoulos15] ANASTASSOPOULOS, V. et al. [CAST Collaboration]. Search for chameleons with CAST. *Phys. Lett.* B749:172–180 (2015).

[Anderson88] ANDERSON, A., HAROCHE, S., HINDS, E.A., et al. Measuring the van der waals forces between a rydberg atom and a metallic surface. *Phys. Rev. A* 37:3594–3597 (1988).

[Anderson14] ANDERSON, L. et al. [BOSS Collaboration]. The clustering of galaxies in the SDSS-III Baryon Oscillation Spectroscopic Survey: baryon acoustic oscillations in the Data Releases 10 and 11 Galaxy samples. *Mon. Not. Roy. Astron. Soc.* 441(1):24–62 (2014).

[Andre13] ANDRE, P. et al. [PRISM Collaboration]. PRISM (Polarized Radiation Imaging and Spectroscopy Mission): A White Paper on the Ultimate Polarimetric Spectro-Imaging of the Microwave and Far-Infrared Sky. *arXiv:1306.2259* (2013).

[Angus07] ANGUS, G.W., SHAN, H., ZHAO, H., et al. On the Law of Gravity, the Mass of Neutrinos and the Proof of Dark Matter. *Astrophys. J.* 654:L13–L16 (2007).

[Antoniadis13] ANTONIADIS, J. et al. A Massive Pulsar in a Compact Relativistic Binary. *Science* 340:6131 (2013).

[Armano16] ARMANO, M. et al. Sub-femto-g free fall for space-based gravitational wave observatories: Lisa pathfinder results. *Phys. Rev. Lett.* 116:231101 (2016).

[Armitage-Caplan11] ARMITAGE-CAPLAN, C. et al. [COrE Collaboration]. COrE (Cosmic Origins Explorer) A White Paper. *arXiv:1102.2181* (2011).

[Atkins13] ATKINS, M. and CALMET, X. Bounds on the Nonminimal Coupling of the Higgs Boson to Gravity. *Phys. Rev. Lett.* 110(5):051301 (2013).

[Babichev09] BABICHEV, E., DEFFAYET, C., and ZIOUR, R. k-Mouflage gravity. *Int. J. Mod. Phys.* D18:2147–2154 (2009).

[Babichev13] BABICHEV, E. and DEFFAYET, C. An introduction to the Vainshtein mechanism. *Class. Quant. Grav.* 30:184001 (2013).

[Babichev14] BABICHEV, E. and CHARMOUSIS, C. Dressing a black hole with a time-dependent Galileon. *JHEP* 08:106 (2014).

[Baker15] BAKER, T., PSALTIS, D., and SKORDIS, C. Linking Tests of Gravity On All Scales: from the Strong-Field Regime to Cosmology. *Astrophys. J.* 802:63 (2015).

[Baker16] BAKER, T. Lovelock's theorem. `http://users.ox.ac.uk/~lady2729/Research_files/landscape_TBaker.pdf` (2016). [Online; accessed 12-June-2016].

[Barbon09] BARBON, J.L.F. and ESPINOSA, J.R. On the Naturalness of Higgs Inflation. *Phys. Rev.* D79:081302 (2009).

[Barreira13] BARREIRA, A., LI, B., HELLWING, W.A., et al. Nonlinear structure formation in the Cubic Galileon gravity model. *JCAP* 1310:027 (2013).

[Bartnik88] BARTNIK, R. and MCKINNON, J. Particlelike solutions of the Einstein-Yang-Mills equations. *Phys. Rev. Lett.* 61:141–144 (1988).

[Barvinsky08] BARVINSKY, A.O., KAMENSHCHIK, A.YU., and STAROBINSKY, A.A. Inflation scenario via the Standard Model Higgs boson and LHC. *JCAP* 0811:021 (2008).

[Bauch02] BAUCH, A. and WEYERS, S. New experimental limit on the validity of local position invariance. *Phys. Rev. D* 65:081101 (2002).

[Baumgärtner10] BAUMGÄRTNER, F., SEWELL, R.J., ERIKSSON, S., et al. Measuring energy differences by bec interferometry on a chip. *Phys. Rev. Lett.* 105:243003 (2010).

[Bednyakov15] BEDNYAKOV, A.V., KNIEHL, B.A., PIKELNER, A.F., et al. Stability of the electroweak vacuum: Gauge independence and advanced precision. *Phys. Rev. Lett.* 115:201802 (2015).

[Bekenstein72] BEKENSTEIN, J.D. Nonexistence of baryon number for static black holes. *Phys. Rev. D* 5:1239–1246 (1972).

[Bekenstein93] BEKENSTEIN, J.D. The Relation between physical and gravitational geometry. *Phys. Rev.* D48:3641–3647 (1993).

[Bekenstein95] BEKENSTEIN, J.D. Novel "no-scalar-hair" theorem for black holes. *Phys. Rev. D* 51:R6608–R6611 (1995).

[Bekenstein04] BEKENSTEIN, J.D. Relativistic gravitation theory for the MOND paradigm. *Phys. Rev.* D70:083509 (2004). [Erratum: Phys. Rev.D71,069901(2005)].

[Beltrán Jiménez15] BELTRÁN JIMÉNEZ, J. Lectures on Modified Gravity (2015).

[Bento02] BENTO, M.C., BERTOLAMI, O., and SEN, A.A. Generalized Chaplygin gas, accelerated expansion and dark energy matter unification. *Phys. Rev.* D66:043507 (2002).

[Berti15] BERTI, E. et al. Testing General Relativity with Present and Future Astrophysical Observations. *Class. Quant. Grav.* 32:243001 (2015).

[Bertotti03] BERTOTTI, B., IESS, L., and TORTORA, P. A test of general relativity using radio links with the Cassini spacecraft. *Nature* 425(6956):374–376 (2003).

[Bertschinger02] BERTSCHINGER, E. Symmetry Transformations, the Einstein-Hilbert Action, and Gauge Invariance (2002).

[Bezrukov08] BEZRUKOV, F.L. and SHAPOSHNIKOV, M. The Standard Model Higgs boson as the inflaton. *Phys. Lett.* B659:703–706 (2008).

[Bezrukov09a] BEZRUKOV, F. and SHAPOSHNIKOV, M. Standard Model Higgs boson mass from inflation: Two loop analysis. *JHEP* 07:089 (2009).

[Bezrukov09b] BEZRUKOV, F.L., MAGNIN, A., and SHAPOSHNIKOV, M. Standard Model Higgs boson mass from inflation. *Phys. Lett.* B675:88–92 (2009).

[Bezrukov11] BEZRUKOV, F., MAGNIN, A., SHAPOSHNIKOV, M., et al. Higgs inflation: consistency and generalisations. *JHEP* 01:016 (2011).

[Bezrukov12] BEZRUKOV, F.L. and GORBUNOV, D.S. Distinguishing between R^2-inflation and Higgs-inflation. *Phys. Lett.* B713:365–368 (2012).

[Bezrukov13] BEZRUKOV, F., KARANANAS, G.K., RUBIO, J., et al. Higgs-Dilaton Cosmology: an effective field theory approach. *Phys. Rev.* D87(9):096001 (2013).

[Bird16] BIRD, S., CHOLIS, I., MUÑOZ, J.B., et al. Did LIGO detect dark matter? *Phys. Rev. Lett.* 116(20):201301 (2016).

[Birkhoff23] BIRKHOFF, G. *Relativity and Modern Physics*. Harvard University Press (1923).

[Boehmer07] BOEHMER, C.G. The Einstein-Elko system: Can dark matter drive inflation? *Annalen Phys.* 16:325–341 (2007).

[Bonvin06] BONVIN, C., CAPRINI, C., and DURRER, R. A no-go theorem for k-essence dark energy. *Phys. Rev. Lett.* 97:081303 (2006).

[Brandenberger11] BRANDENBERGER, R.H. Alternatives to the inflationary paradigm of structure formation. *Int. J. Mod. Phys. Conf. Ser.* 01:67–79 (2011).

[Brandenberger16] BRANDENBERGER, R. and PETER, P. Bouncing Cosmologies: Progress and Problems. *arXiv:1603.05834* (2016).

[Brans61] BRANS, C. and DICKE, R.H. Mach's principle and a relativistic theory of gravitation. *Phys. Rev.* 124:925–935 (1961).

[Brans08] BRANS, C.H. Scalar-tensor theories of gravity: Some personal history. *AIP Conf. Proc.* 1083:34–46 (2008).

[Brax04] BRAX, P., VAN DE BRUCK, C., DAVIS, A.C., et al. Detecting dark energy in orbit - The Cosmological chameleon. *Phys.Rev.* D70:123518 (2004).

[Brax06] BRAX, P., VAN DE BRUCK, C., DAVIS, A.C., et al. Small scale structure formation in chameleon cosmology. *Phys. Lett.* B633:441–446 (2006).

[Brax07a] BRAX, P., VAN DE BRUCK, C., and DAVIS, A.C. Compatibility of the chameleon-field model with fifth-force experiments, cosmology, and PVLAS and CAST results. *Phys. Rev. Lett.* 99:121103 (2007).

[Brax07b] BRAX, P., VAN DE BRUCK, C., DAVIS, A.C., et al. Detecting chameleons through Casimir force measurements. *Phys.Rev.* D76:124034 (2007).

[Brax10] BRAX, P., VAN DE BRUCK, C., DAVIS, A.C., et al. Tuning the Mass of Chameleon Fields in Casimir Force Experiments. *Phys. Rev. Lett.* 104:241101 (2010).

[Brax11a] BRAX, P. and BURRAGE, C. Atomic Precision Tests and Light Scalar Couplings. *Phys.Rev.* D83:035020 (2011).

[Brax11b] BRAX, P. and PIGNOL, G. Strongly Coupled Chameleons and the Neutronic Quantum Bouncer. *Phys.Rev.Lett.* 107:111301 (2011).

[Brax13a] BRAX, P., CLESSE, S., and DAVIS, A.C. Signatures of Modified Gravity on the 21-cm Power Spectrum at Reionisation. *JCAP* 1301:003 (2013).

[Brax13b] BRAX, P., DAVIS, A.C., LI, B., et al. Systematic simulations of modified gravity: chameleon models. *JCAP* 1304:029 (2013).

[Brax13c] BRAX, P., PIGNOL, G., and ROULIER, D. Probing Strongly Coupled Chameleons with Slow Neutrons. *Phys.Rev.* D88:083004 (2013).

[Breu16] BREU, C. and REZZOLLA, L. Maximum mass, moment of inertia and compactness of relativistic stars. *Mon. Not. Roy. Astron. Soc.* 459(1):646–656 (2016).

[Brihaye15] BRIHAYE, Y. and VERBIN, Y. Self-gravitating spherical solutions of the nonminimally coupled non-Abelian Higgs model. *Phys. Rev.* D91(6):064021 (2015).

[Brout78] BROUT, R., ENGLERT, F., and GUNZIG, E. The creation of the universe as a quantum phenomenon. *Annals of Physics* 115(1):78 – 106 (1978).

[Bruneton07] BRUNETON, J.P. On causality and superluminal behavior in classical field theories: Applications to k-essence theories and MOND-like theories of gravity. *Phys. Rev.* D75:085013 (2007).

[Bruneton12] BRUNETON, J.P., RINALDI, M., KANFON, A., et al. Fab Four: When John and George play gravitation and cosmology. *Adv. Astron.* 2012:430694 (2012).

[Buchdahl59] BUCHDAHL, H.A. General relativistic fluid spheres. *Phys. Rev.* 116:1027–1034 (1959).

[Buchert12] BUCHERT, T. and RÄSÄNEN, S. Backreaction in late-time cosmology. *Ann. Rev. Nucl. Part. Sci.* 62:57–79 (2012).

[Burgess09] BURGESS, C.P., LEE, H.M., and TROTT, M. Power-counting and the Validity of the Classical Approximation During Inflation. *JHEP* 09:103 (2009).

[Burrage15] BURRAGE, C., COPELAND, E.J., and HINDS, E. Probing Dark Energy with Atom Interferometry. *JCAP* 1503(03):042 (2015).

[Burrage16] BURRAGE, C., COPELAND, E.J., and STEVENSON, J.A. A Proposed Experimental Search for Chameleons using Asymmetric Parallel Plates. *arXiv:1604.00342* (2016).

[Cacciapuoti09] CACCIAPUOTI, L. and SALOMON, C. Space clocks and fundamental tests: The ACES experiment. *The European Physical Journal Special Topics* (2009).

[Callan70] CALLAN, JR., C.G., COLEMAN, S., and JACKIW, R. A new improved energy-momentum tensor. *Annals of Physics* 59:42–73 (1970).

[Capozziello06] CAPOZZIELLO, S., NOJIRI, S., ODINTSOV, S.D., et al. Cosmological viability of f(R)-gravity as an ideal fluid and its compatibility with a matter dominated phase. *Phys. Lett.* B639:135–143 (2006).

[Carr74] CARR, B.J. and HAWKING, S.W. Black holes in the early universe. *Monthly Notices of the Royal Astronomical Society* 168(2):399–415 (1974).

[Carr75] CARR, B.J. The primordial black hole mass spectrum. *APJ* 201:1–19 (1975).

[Carr07] CARR, B. *Universe Or Multiverse?* Cambridge University Press (2007).

[Carroll04] CARROLL, S.M. *Spacetime and geometry: An introduction to general relativity*. Addison-Wesley Publishing Company (2004).

[Casoli00] CASOLI, F., LEQUEUX, J., and DAVID, F. *Infrared space astronomy, today and tomorrow: 3-28 August 1998*. Springer Berlin Heidelberg (2000).

[Cervantes-Cota95] CERVANTES-COTA, J.L. and DEHNEN, H. Induced gravity inflation in the standard model of particle physics. *Nucl. Phys.* B442:391–412 (1995).

[Chamel13] CHAMEL, N., HAENSEL, P., ZDUNIK, J.L., et al. On the Maximum Mass of Neutron Stars. *Int. J. Mod. Phys.* E22:1330018 (2013).

[Chamel15] CHAMEL, N. and T., D. Etoiles à neutrons, laboratoires de l'extrême (2015).

[Chandrasekhar83] CHANDRASEKHAR, S. *The Mathematical Theory of Black Holes*. Oxford University Press (1983).

[Chang11] CHANG, P. and HUI, L. Stellar Structure and Tests of Modified Gravity. *Astrophys. J.* 732:25 (2011).

[Charmousis12a] CHARMOUSIS, C., COPELAND, E.J., PADILLA, A., et al. General second order scalar-tensor theory, self tuning, and the Fab Four. *Phys. Rev. Lett.* 108:051101 (2012).

[Charmousis12b] CHARMOUSIS, C., COPELAND, E.J., PADILLA, A., et al. Self-tuning and the derivation of a class of scalar-tensor theories. *Phys.Rev.* D85:104040 (2012).

[Chatrchyan12] CHATRCHYAN, S. et al. [CMS Collaboration]. Observation of a new boson at a mass of 125 GeV with the CMS experiment at the LHC. *Phys. Lett.* B716:30–61 (2012).

[Chiba13] CHIBA, T. and YAMAGUCHI, M. Conformal-Frame (In)dependence of Cosmological Observations in Scalar-Tensor Theory. *JCAP* 1310:040 (2013).

[Chow09] CHOW, N. and KHOURY, J. Galileon Cosmology. *Phys.Rev.* D80:024037 (2009).

[Chrusciel12] CHRUSCIEL, P.T., COSTA, J.L., and HEUSLER, M. Stationary Black Holes: Uniqueness and Beyond. *Living Rev. Rel.* 15:7 (2012).

[Cisterna16] CISTERNA, A., DELSATE, T., DUCOBU, L., et al. Slowly rotating neutron stars in the nonminimal derivative coupling sector of Horndeski gravity. *Phys. Rev.* D93(8):084046 (2016).

[Clesse11] CLESSE, S. *Hybrid Inflation: Multi-field Dynamics and Cosmological Constraints*. Ph.D. thesis Brussels U. (2011).

[Clesse16] CLESSE, S. and GARCÍA-BELLIDO, J. The clustering of massive Primordial Black Holes as Dark Matter: measuring their mass distribution with Advanced LIGO. *arXiv:1603.05234* (2016).

[Clifton12] CLIFTON, T., FERREIRA, P.G., PADILLA, A., et al. Modified Gravity and Cosmology. *Phys. Rept.* 513:1–189 (2012).

[Clowe06] CLOWE, D., BRADAC, M., GONZALEZ, A.H., et al. A direct empirical proof of the existence of dark matter. *Astrophys. J.* 648:L109–L113 (2006).

[Colella75] COLELLA, R., OVERHAUSER, A.W., and WERNER, S.A. Observation of gravitationally induced quantum interference. *Phys. Rev. Lett.* 34:1472–1474 (1975).

[Coleman85] COLEMAN, S. Q-balls. *Nuclear Physics B* 262:263–283 (1985).

[Colpi86] COLPI, M., SHAPIRO, S.L., and WASSERMAN, I. Boson stars: Gravitational equilibria of self-interacting scalar fields. *Phys. Rev. Lett.* 57:2485–2488 (1986).

[Copeland06] COPELAND, E.J., SAMI, M., and TSUJIKAWA, S. Dynamics of dark energy. *Int. J. Mod. Phys.* D15:1753–1936 (2006).

[Copeland12] COPELAND, E.J., PADILLA, A., and SAFFIN, P.M. The cosmology of the Fab-Four. *JCAP* 1212:026 (2012).

[Creminelli10] CREMINELLI, P., NICOLIS, A., and TRINCHERINI, E. Galilean Genesis: An Alternative to inflation. *JCAP* 1011:021 (2010).

[Cronin09] CRONIN, A.D., SCHMIEDMAYER, J., and PRITCHARD, D.E. Optics and interferometry with atoms and molecules. *Rev.Mod.Phys.* 81:1051–1129 (2009).

[Cyburt16] CYBURT, R.H., FIELDS, B.D., OLIVE, K.A., et al. Big Bang Nucleosynthesis: 2015. *Rev. Mod. Phys.* 88:015004 (2016).

[Damour92] DAMOUR, T. and ESPOSITO-FARESE, G. Tensor multi-scalar theories of gravitation. *Class. Quant. Grav.* 9:2093–2176 (1992).

[Damour93a] DAMOUR, T. and ESPOSITO-FARÈSE, G. Nonperturbative strong-field effects in tensor-scalar theories of gravitation. *Phys. Rev. Lett.* 70:2220–2223 (1993).

[Damour93b] DAMOUR, T. and NORDTVEDT, K. Tensor - scalar cosmological models and their relaxation toward general relativity. *Phys.Rev.* D48:3436–3450 (1993).

[Damour96] DAMOUR, T. and ESPOSITO-FARESE, G. Tensor - scalar gravity and binary pulsar experiments. *Phys. Rev.* D54:1474–1491 (1996).

[Davis12] DAVIS, A.C., LIM, E.A., SAKSTEIN, J., et al. Modified Gravity Makes Galaxies Brighter. *Phys. Rev.* D85:123006 (2012).

[De Felice10] DE FELICE, A. and TSUJIKAWA, S. f(R) theories. *Living Rev. Rel.* 13:3 (2010).

[De Felice12] DE FELICE, A. and TSUJIKAWA, S. Conditions for the cosmological viability of the most general scalar-tensor theories and their applications to extended Galileon dark energy models. *JCAP* 1202:007 (2012).

[De Simone09] DE SIMONE, A., HERTZBERG, M.P., and WILCZEK, F. Running Inflation in the Standard Model. *Phys. Lett.* B678:1–8 (2009).

[Deffayet09a] DEFFAYET, C., DESER, S., and ESPOSITO-FARESE, G. Generalized Galileons: All scalar models whose curved background extensions maintain second-order field equations and stress-tensors. *Phys.Rev.* D80:064015 (2009).

[Deffayet09b] DEFFAYET, C., ESPOSITO-FARESE, G., and VIKMAN, A. Covariant Galileon. *Phys.Rev.* D79:084003 (2009).

[Deffayet11] DEFFAYET, C., GAO, X., STEER, D.A., et al. From k-essence to generalised Galileons. *Phys. Rev.* D84:064039 (2011).

[Degrassi12] DEGRASSI, G., DI VITA, S., ELIAS-MIRO, J., et al. Higgs mass and vacuum stability in the Standard Model at NNLO. *JHEP* 08:098 (2012).

[Delva15] DELVA, P., HEES, A., BERTONE, S., et al. Test of the gravitational redshift with stable clocks in eccentric orbits: application to Galileo satellites 5 and 6. *Class. Quant. Grav.* 32(23):232003 (2015).

[Demorest10] DEMOREST, P., PENNUCCI, T., RANSOM, S., et al. Shapiro Delay Measurement of A Two Solar Mass Neutron Star. *Nature* 467:1081–1083 (2010).

[deRham12] DE RHAM, C. Galileons in the Sky. *Comptes Rendus Physique* 13:666–681 (2012).

[deRham14] DE RHAM, C. Massive gravity. *Living Rev. Rel.* 17(7) (2014).

[Durrer08a] DURRER, R. *The Cosmic Microwave Background*. Cambridge University Press (2008).

[Durrer08b] DURRER, R. and MAARTENS, R. Dark Energy and Dark Gravity. *Gen. Rel. Grav.* 40:301–328 (2008).

[Dvali00] DVALI, G.R., GABADADZE, G., and PORRATI, M. 4-D gravity on a brane in 5-D Minkowski space. *Phys. Lett.* B485:208–214 (2000).

[Eddington57] EDDINGTON, A.S. *The Mathematical Theory of Relativity*. Cambridge University Press, Cambridge (1957).

[Einhorn80] EINHORN, M.B., STEIN, D.L., and TOUSSAINT, D. Are grand unified theories compatible with standard cosmology? *Phys. Rev. D* 21:3295–3298 (1980).

[Einstein16] EINSTEIN, A. Die Grundlage der allgemeinen Relativitätstheorie. *Annalen der Physik* 49:769–822 (1916).

[Eisenhauer11] EISENHAUER, F., PERRIN, G., BRANDNER, W., et al. GRAVITY: Observing the Universe in Motion. *The Messenger* 143:16–24 (2011).

[Eisenstein05] EISENSTEIN, D.J. et al. [SDSS Collaboration]. Detection of the baryon acoustic peak in the large-scale correlation function of SDSS luminous red galaxies. *Astrophys. J.* 633:560–574 (2005).

[Elder16] ELDER, B., KHOURY, J., HASLINGER, P., et al. Chameleon Dark Energy and Atom Interferometry. *Phys. Rev.* D94(4):044051 (2016).

[Espinoza11] ESPINOZA, C.M., LYNE, A.G., STAPPERS, B.W., et al. A study of 315 glitches in the rotation of 102 pulsars. *MNRAS* 414:1679–1704 (2011).

[Esposito-Farèse06] ESPOSITO-FARÈSE, G. Gravitation: Theories and Experiment (Part II) (2006).

[Fairlie92] FAIRLIE, D.B. and GOVAERTS, J. Universal field equations with reparametrization invariance. *Phys. Lett.* B281:49–53 (1992).

[Fairlie11] FAIRLIE, D. Comments on Galileons. *J. Phys.* A44:305201 (2011).

[Fakir90] FAKIR, R. and UNRUH, W.G. Induced-gravity inflation. *Phys. Rev. D* 41:1792–1795 (1990).

[Famaey12] FAMAEY, B. and MCGAUGH, S. Modified Newtonian Dynamics (MOND): Observational Phenomenology and Relativistic Extensions. *Living Rev. Rel.* 15:10 (2012).

[Fardon04] FARDON, R., NELSON, A.E., and WEINER, N. Dark energy from mass varying neutrinos. *JCAP* 0410:005 (2004).

[Fienga11] FIENGA, A., LASKAR, J., KUCHYNKA, P., et al. The INPOP10a planetary ephemeris and its applications in fundamental physics. *Celest. Mech. Dyn. Astron.* 111:363–385 (2011).

[Fischbach98] FISCHBACH, E. and TALMADGE, C.L. *The Search for Non-Newtonian Gravity*. Springer, New York (1998).

[Fixler07] FIXLER, J., FOSTER, G., MCGUIRK, J., et al. Atom interferometer measurement of the Newtonian constant of gravity. *Science* 315:74–77 (2007).

[Flanagan04] FLANAGAN, E.E. The Conformal frame freedom in theories of gravitation. *Class. Quant. Grav.* 21:3817 (2004).

[Fray04] FRAY, S., DIEZ, C.A., HÄNSCH, T.W., et al. Atomic Interferometer with Amplitude Gratings of Light and Its Applications to Atom Based Tests of the Equivalence Principle. *Phys. Rev. Lett.* 93:240404 (2004).

[Freire12] FREIRE, P.C.C., WEX, N., ESPOSITO-FARESE, G., et al. The relativistic pulsar-white dwarf binary PSR J1738+0333 II. The most stringent test of scalar-tensor gravity. *Mon. Not. Roy. Astron. Soc.* 423:3328 (2012).

[Friedrich00] FRIEDRICH, H. and RENDALL, A.D. The Cauchy problem for the Einstein equations. *Lect. Notes Phys.* 540:127–224 (2000).

[Füzfa02] FÜZFA, A., GERARD, J.M., and LAMBERT, D. The Lemaitre-Schwarzschild problem revisited. *Gen. Rel. Grav.* 34:1411–1422 (2002).

[Füzfa13] FÜZFA, A., RINALDI, M., and SCHLÖGEL, S. Particlelike distributions of the Higgs field nonminimally coupled to gravity. *Phys. Rev. Lett.* 111(12):121103 (2013).

[Gair13] GAIR, J.R., VALLISNERI, M., LARSON, S.L., et al. Testing General Relativity with Low-Frequency, Space-Based Gravitational-Wave Detectors. *Living Rev. Rel.* 16:7 (2013).

[Galley13] GALLEY, C.R. Classical Mechanics of Nonconservative Systems. *Phys. Rev. Lett.* 110(17):174301 (2013).

[Galley14] GALLEY, C.R., TSANG, D., and STEIN, L.C. The principle of stationary nonconservative action for classical mechanics and field theories. *arXiv:1412.3082* (2014).

[Gannouji10] GANNOUJI, R., MORAES, B., MOTA, D.F., et al. Chameleon dark energy models with characteristic signatures. *Phys. Rev.* D82:124006 (2010).

[Garcia-Bellido09] GARCIA-BELLIDO, J., FIGUEROA, D.G., and RUBIO, J. Preheating in the Standard Model with the Higgs-Inflaton coupled to gravity. *Phys. Rev.* D79:063531 (2009).

[Garcia-Bellido11] GARCIA-BELLIDO, J., RUBIO, J., SHAPOSHNIKOV, M., et al. Higgs-Dilaton Cosmology: From the Early to the Late Universe. *Phys. Rev.* D84:123504 (2011).

[Gaul00] GAUL, M. and ROVELLI, C. Loop quantum gravity and the meaning of diffeomorphism invariance. *Lect. Notes Phys.* 541:277–324 (2000).

[Georgi84] GEORGI, H. and KAPLAN, D.B. Composite Higgs and custodial SU(2). *Physics Letters B* 145(3):216–220 (1984).

[Germani10a] GERMANI, C. and KEHAGIAS, A. Cosmological perturbations in the new Higgs inflation. *JCAP* 5:019 (2010).

[Germani10b] GERMANI, C. and KEHAGIAS, A. New Model of Inflation with Non-minimal Derivative Coupling of Standard Model Higgs Boson to Gravity. *Phys.Rev.Lett.* 105:011302 (2010).

[Germani11] GERMANI, C. and KEHAGIAS, A. UV-Protected Inflation. *Phys.Rev.Lett.* 106:161302 (2011).

[Gibbons77] GIBBONS, G.W. and HAWKING, S.W. Cosmological event horizons, thermodynamics, and particle creation. *Phys. Rev. D* 15:2738–2751 (1977).

[Gleyzes15] GLEYZES, J., LANGLOIS, D., PIAZZA, F., et al. Healthy theories beyond Horndeski. *Phys. Rev. Lett.* 114(21):211101 (2015).

[Gödel49] GÖDEL, K. An example of a new type of cosmological solutions of einstein's field equations of gravitation. *Rev. Mod. Phys.* 21:447–450 (1949).

[Gorbar04] GORBAR, E.V. and SHAPIRO, I.L. Renormalization group and decoupling in curved space. 3. The Case of spontaneous symmetry breaking. *JHEP* 02:060 (2004).

[Gourgoulhon12] GOURGOULHON, É. *3+1 Formalism in General Relativity: Bases of Numerical Relativity*. Springer Berlin Heidelberg (2012).

[Gourgoulhon14] GOURGOULHON, E. Cours de relativité générale (2013-2014).

[Govaerts08] GOVAERTS, J. Lecture notes on Quantum Field Theory II (2008).

[Graham15] GRAHAM, P.W., KAPLAN, D.E., and RAJENDRAN, S. Cosmological Relaxation of the Electroweak Scale. *Phys. Rev. Lett.* 115(22):221801 (2015).

[Greenwood13] GREENWOOD, R.N., KAISER, D.I., and SFAKIANAKIS, E.I. Multifield Dynamics of Higgs Inflation. *Phys. Rev.* D87:064021 (2013).

[Gubser04] GUBSER, S.S. and KHOURY, J. Scalar self-interactions loosen constraints from fifth force searches. *Phys.Rev.* D70:104001 (2004).

[Guth81] GUTH, A.H. Inflationary universe: A possible solution to the horizon and flatness problems. *Phys. Rev. D* 23:347–356 (1981).

[Hamber05] HAMBER, H.W. and WILLIAMS, R.M. Nonlocal effective gravitational field equations and the running of Newton's G. *Phys. Rev.* D72:044026 (2005).

[Hamilton15] HAMILTON, P., JAFFE, M., HASLINGER, P., et al. Atom-interferometry constraints on dark energy. *Science* 349:849–851 (2015).

[Harber05] HARBER, D.M., OBRECHT, J.M., MCGUIRK, J.M., et al. Measurement of the casimir-polder force through center-of-mass oscillations of a bose-einstein condensate. *Phys. Rev. A* 72:033610 (2005).

[Hawking73] HAWKING, S. and ELLIS, G. *The Large Scale Structure of Space-Time*. Cambridge University Press (1973).

[Hees12a] HEES, A. and FÜZFA, A. Combined cosmological and solar system constraints on chameleon mechanism. *Phys.Rev.* D85:103005 (2012).

[Hees12b] HEES, A., LAMINE, B., REYNAUD, S., et al. Radioscience simulations in General Relativity and in alternative theories of gravity. *Class. Quant. Grav.* 29:235027 (2012).

[Hees15] HEES, A., HESTROFFER, D., LE PONCIN-LAFITTE, C., et al. Tests of gravitation with GAIA observations of Solar System Objects. In F. Martins, S. Boissier, V. Buat, L. Cambrésy, and P. Petit, editors, *SF2A-2015: Proceedings of the Annual meeting of the French Society of Astronomy and Astrophysics* pages 125–131. (2015).

[Hinterbichler10] HINTERBICHLER, K. and KHOURY, J. Symmetron Fields: Screening Long-Range Forces Through Local Symmetry Restoration. *Phys.Rev.Lett.* 104:231301 (2010).

[Hinterbichler11] HINTERBICHLER, K., KHOURY, J., LEVY, A., et al. Symmetron Cosmology. *Phys.Rev.* D84:103521 (2011).

[Hobbs09] HOBBS, D., HOLL, B., LINDEGREN, L., et al. Determining PPN γ with Gaia's astrometric core solution. In *Relativity in Fundamental Astronomy: Dynamics, Reference Frames, and Data Analysis* volume 5 of *Proceedings of the International Astronomical Union* pages 315–319. (2009).

[Hobson06] HOBSON, M., EFSTATHIOU, G., and LASENBY, A. *General Relativity: An Introduction for Physicists*. Cambridge University Press (2006).

[Hojjati16] HOJJATI, A., PLAHN, A., ZUCCA, A., et al. Searching for scalar gravitational interactions in current and future cosmological data. *Phys. Rev.* D93(4):043531 (2016).

[Horndeski74] HORNDESKI, G.W. Second-order scalar-tensor field equations in a four-dimensional space. *International Journal of Theoretical Physics* 10(6):363–384 (1974).

[Hu01] HU, W. Intermediate Guide to the Acoustic Peaks and Polarization (2001).

[Hui09] HUI, L., NICOLIS, A., and STUBBS, C. Equivalence Principle Implications of Modified Gravity Models. *Phys. Rev.* D80:104002 (2009).

[Ivanov13] IVANOV, A.N., HÖLLWIESER, R., JENKE, T., et al. Influence of the chameleon field potential on transition frequencies of gravitationally bound quantum states of ultracold neutrons. *Phys. Rev. D* 87:105013 (2013).

[Jacobson96] JACOBSON, T. Introductory Lectures on Black Hole Thermodynamics (1996).

[Jacobson01] JACOBSON, T. and MATTINGLY, D. Gravity with a dynamical preferred frame. *Phys. Rev.* D64:024028 (2001).

[Jaekel05] JAEKEL, M.T. and REYNAUD, S. Post-Einsteinian tests of linearized gravitation. *Class. Quant. Grav.* 22:2135–2158 (2005).

[Jain13] JAIN, B., VIKRAM, V., and SAKSTEIN, J. Astrophysical Tests of Modified Gravity: Constraints from Distance Indicators in the Nearby Universe. *Astrophys.J.* 779:39 (2013).

[Jebsen21] JEBSEN, J. Über die allgemeinen kugelsymmetrischen Lösungen der Einsteinschen Gravitationsgleichungen im Vakuum. *Ark. Mat. Ast. Fys. (Stockholm)* 15:1–9 (1921).

[Jenke14] JENKE, T., CRONENBERG, G., BURGDORFER, J., et al. Gravity Resonance Spectroscopy Constrains Dark Energy and Dark Matter Scenarios. *Phys.Rev.Lett.* 112:151105 (2014).

[Johannsen11] JOHANNSEN, T. and PSALTIS, D. Metric for rapidly spinning black holes suitable for strong-field tests of the no-hair theorem. *Phys. Rev. D* 83:124015 (2011).

[Jordan55] JORDAN, P. *Schwerkraft und Weltall* volume 133. Vieweg, Braunschweig 2nd edition (1955).

[José98] JOSÉ, J. and SALETAN, E. *Classical Dynamics: A Contemporary Approach*. Cambridge University Press (1998).

[Joyce15] JOYCE, A., JAIN, B., KHOURY, J., et al. Beyond the Cosmological Standard Model. *Phys. Rept.* 568:1–98 (2015).

[Kaiser95] KAISER, D.I. Primordial spectral indices from generalized Einstein theories. *Phys. Rev.* D52:4295–4306 (1995).

[Kaiser07] KAISER, D. When Fields Collide. *Scientific American* (2007).

[Kaiser14] KAISER, D.I. and SFAKIANAKIS, E.I. Multifield Inflation after Planck: The Case for Nonminimal Couplings. *Phys. Rev. Lett.* 112(1):011302 (2014).

[Kaluza21] KALUZA, T. Zum Unitätsproblem in der Physik. *Sitzungsber. Preuss. Akad. Wiss. Berlin. (Math. Phys.):* page 966–972 (1921).

[Kapner07] KAPNER, D., COOK, T., ADELBERGER, E., et al. Tests of the gravitational inverse-square law below the dark-energy length scale. *Phys.Rev.Lett.* 98:021101 (2007).

[Kasevich91] KASEVICH, M. and CHU, S. Atomic interferometry using stimulated Raman transitions. *Phys. Rev. Lett.* 67:181–184 (1991).

[Kehagias14] KEHAGIAS, A., DIZGAH, A.M., and RIOTTO, A. Remarks on the Starobinsky model of inflation and its descendants. *Phys. Rev.* D89(4):043527 (2014).

[Kerr63] KERR, R.P. Gravitational field of a spinning mass as an example of algebraically special metrics. *Phys. Rev. Lett.* 11:237–238 (1963).

[Khoury04a] KHOURY, J. and WELTMAN, A. Chameleon cosmology. *Phys.Rev.* D69:044026 (2004).

[Khoury04b] KHOURY, J. and WELTMAN, A. Chameleon fields: Awaiting surprises for tests of gravity in space. *Phys.Rev.Lett.* 93:171104 (2004).

[Klein26a] KLEIN, O. The atomicity of electricity as a quantum theory law. *Nature* 118:516 (1926).

[Klein26b] KLEIN, O. Quantentheorie und fünfdimensionale Relativitätstheorie. *Zeitschrift fur Physik* 37:895–906 (1926).

[Kobayashi11] KOBAYASHI, T., YAMAGUCHI, M., and YOKOYAMA, J. Generalized G-inflation: Inflation with the most general second-order field equations. *Prog.Theor.Phys.* 126:511–529 (2011).

[Kokkotas99] KOKKOTAS, K.D. and SCHMIDT, B.G. Quasinormal modes of stars and black holes. *Living Rev. Rel.* 2:2 (1999).

[Kostelecky11] KOSTELECKY, V.A. and RUSSELL, N. Data Tables for Lorentz and CPT Violation. *Rev. Mod. Phys.* 83:11–31 (2011).

[Kostelecký16] KOSTELECKÝ, V.A. and MEWES, M. Testing local Lorentz invariance with gravitational waves. *Phys. Lett.* B757:510–514 (2016).

[Kowalski08] KOWALSKI, M. et al. [Supernova Cosmology Project Collaboration]. Improved Cosmological Constraints from New, Old and Combined Supernova Datasets. *Astrophys. J.* 686:749–778 (2008).

[Kramer04] KRAMER, 2, M., BACKER, D.C., CORDES, J.M., et al. Strong-field tests of gravity using pulsars and black holes. *New Astron. Rev.* 48:993–1002 (2004).

[Kramer06] KRAMER, M. et al. Tests of general relativity from timing the double pulsar. *Science* 314:97–102 (2006).

[Lamporesi08] LAMPORESI, G., BERTOLDI, A., CACCIAPUOTI, L., et al. Determination of the Newtonian Gravitational Constant Using Atom Interferometry. *Phys.Rev.Lett.* 100:050801 (2008).

[Larena07] LARENA, J. *Champs scalaires en cosmologie: Discussions sur les principes d'équivalence et cosmologique*. Ph.D. thesis Université Paris VII-Denis Diderot (2007).

[Lee89] LEE, K., STEIN-SCHABES, J.A., WATKINS, R., et al. Gauged *Q* balls. *Phys. Rev. D* 39:1665–1673 (1989).

[Lemaître33] LEMAÎTRE, G. L'univers en expansion. *Ann. Soc. Sci. Bruxelles* 53A:51–83 (1933).

[Lerner10] LERNER, R.N. and MCDONALD, J. A Unitarity-Conserving Higgs Inflation Model. *Phys. Rev.* D82:103525 (2010).

[Li16] LI, K. et al. Neutron Limit on the Strongly-Coupled Chameleon Field. *Phys. Rev.* D93(6):062001 (2016).

[Liddle94] LIDDLE, A.R., PARSONS, P., and BARROW, J.D. Formalizing the slow roll approximation in inflation. *Phys. Rev.* D50:7222–7232 (1994).

[Lidsey00] LIDSEY, J.E., WANDS, D., and COPELAND, E.J. Superstring cosmology. *Phys. Rept.* 337:343–492 (2000).

[Liebling12] LIEBLING, S.L. and PALENZUELA, C. Dynamical Boson Stars. *Living Rev. Rel.* 15:6 (2012).

[Lima10] LIMA, W.C.C., MATSAS, G.E.A., and VANZELLA, D.A.T. Awaking the vacuum in relativistic stars. *Phys. Rev. Lett.* 105:151102 (2010).

[Linde82] LINDE, A.D. A new inflationary universe scenario: A possible solution of the horizon, flatness, homogeneity, isotropy and primordial monopole problems. *Physics Letters B* 108:389–393 (1982).

[Linde83] LINDE, A.D. Chaotic inflation. *Physics Letters B* 129:177–181 (1983).

[Llinares13] LLINARES, C. and MOTA, D. Releasing scalar fields: cosmological simulations of scalar-tensor theories for gravity beyond the static approximation. *Phys. Rev. Lett.* 110(16):161101 (2013).

[Lovelock69] LOVELOCK, D. The uniqueness of the Einstein field equations in a four-dimensional space. *Archive for Rational Mechanics and Analysis* 33(1):54–70 (1969).

[Lovelock71] LOVELOCK, D. The Einstein Tensor and Its Generalizations. *Journal of Mathematical Physics* 12:498–501 (1971).

[Lyth99] LYTH, D.H. and RIOTTO, A. Particle physics models of inflation and the cosmological density perturbation. *Phys. Rept.* 314:1–146 (1999).

[Maartens11] MAARTENS, R. Is the Universe homogeneous? *Phil. Trans. Roy. Soc. Lond.* A369:5115–5137 (2011).

[Mach83] MACH, E. Die Mechanik in ihrer Entwicklung Historisch. *Kritisch Dargerstellt, Leipzig: Brockhaus* (1883).

[Maggiore14] MAGGIORE, M. and MANCARELLA, M. Nonlocal gravity and dark energy. *Phys. Rev.* D90(2):023005 (2014).

[Markevitch04] MARKEVITCH, M., GONZALEZ, A.H., CLOWE, D., et al. Direct constraints on the dark matter self-interaction cross-section from the merging galaxy cluster 1E0657-56. *Astrophys. J.* 606:819–824 (2004).

[Martin14a] MARTIN, J., RINGEVAL, C., TROTTA, R., et al. The Best Inflationary Models After Planck. *JCAP* 1403:039 (2014).

[Martin14b] MARTIN, J., RINGEVAL, C., and VENNIN, V. Encyclopædia Inflationaris. *Phys. Dark Univ.* 5-6:75–235 (2014).

[Maselli16] MASELLI, A., SILVA, H.O., MINAMITSUJI, M., et al. Neutron stars in Horndeski gravity. *Phys. Rev.* D93(12):124056 (2016).

[Massey07] MASSEY, R. et al. Dark matter maps reveal cosmic scaffolding. *Nature* 445:286 (2007).

[Matsumura14] MATSUMURA, T. et al. Mission design of LiteBIRD. *J. Low. Temp. Phys.176,733* (2014).

[Mattingly05] MATTINGLY, D. Modern tests of Lorentz invariance. *Living Rev. Rel.* 8:5 (2005).

[Meyer12] MEYER, L., GHEZ, A.M., SCHÖDEL, R., et al. The Shortest-Known-Period Star Orbiting Our Galaxy's Supermassive Black Hole. *Science* 338:84 (2012).

[Michimura13] MICHIMURA, Y., MATSUMOTO, N., OHMAE, N., et al. New limit on lorentz violation using a double-pass optical ring cavity. *Phys. Rev. Lett.* 110:200401 (2013).

[Milani02] MILANI, A., VOKROUHLICKÝ, D., VILLANI, D., et al. Testing general relativity with the BepiColombo radio science experiment. *Phys. Rev. D* 66:082001 (2002).

[Milgrom83] MILGROM, M. A modification of the Newtonian dynamics as a possible alternative to the hidden mass hypothesis. *APJ* 270:365–370 (1983).

[Misner73] MISNER, C., THORNE, K., and WHEELER, J. *Gravitation*. W.H. Freeman and Company (1973).

[Mitsou15] MITSOU, E. *Aspects of Infrared Non-local Modifications of General Relativity*. Ph.D. thesis Geneva U. (2015).

[Mortonson13] MORTONSON, M.J., WEINBERG, D.H., and WHITE, M. Dark Energy: A Short Review. *arXiv:1401.0046* (2013).

[Mota06] MOTA, D.F. and SHAW, D.J. Strongly coupled chameleon fields: New horizons in scalar field theory. *Phys.Rev.Lett.* 97:151102 (2006).

[Mota07] MOTA, D.F. and SHAW, D.J. Evading Equivalence Principle Violations, Cosmological and other Experimental Constraints in Scalar Field Theories with a Strong Coupling to Matter. *Phys.Rev.* D75:063501 (2007).

[Mota11] MOTA, D.F. and WINTHER, H.A. Cosmology of Chameleons with Power-Law Couplings. *Astrophys. J.* 733:7 (2011).

[Motohashi15] MOTOHASHI, H. and SUYAMA, T. Third order equations of motion and the Ostrogradsky instability. *Phys. Rev.* D91(8):085009 (2015).

[Mukhanov05] MUKHANOV, V. *Physical Foundations of Cosmology*. Cambridge University Press (2005).

[Newman65] NEWMAN, E.T., COUCH, E., CHINNAPARED, K., et al. Metric of a rotating, charged mass. *Journal of Mathematical Physics* 6(6) (1965).

[Ni72] NI, W.T. Theoretical Frameworks for Testing Relativistic Gravity.IV. a Compendium of Metric Theories of Gravity and their post-Newtonian Limits. *APJ* 176:769 (1972).

[Nicolis09] NICOLIS, A., RATTAZZI, R., and TRINCHERINI, E. The Galileon as a local modification of gravity. *Phys. Rev.* D79:064036 (2009).

[Nordström18] NORDSTRÖM, G. On the energy of the gravitational field in einstein's theory. *Verhandl. Koninkl. Ned. Akad. Wetenschap., Afdel. Natuurk., Amsterdam* 26:1201–1208 (1918).

[Nordtvedt68a] NORDTVEDT, K. Equivalence principle for massive bodies. i. phenomenology. *Phys. Rev.* 169:1014–1016 (1968).

[Nordtvedt68b] NORDTVEDT, K. Equivalence principle for massive bodies. ii. theory. *Phys. Rev.* 169:1017–1025 (1968).

[Nordtvedt68c] NORDTVEDT, K. Testing relativity with laser ranging to the moon. *Phys. Rev.* 170:1186–1187 (1968).

[Norton93] NORTON, J.D. General covariance and the foundations of general relativity: eight decades of dispute. *Reports on Progress in Physics* 56(7):791+ (1993).

[Nutku69] NUTKU, Y. The Post-Newtonian Equations of Hydrodynamics in the Brans-Dicke Theory. *APJ* 155:999 (1969).

[Olive14] OLIVE, K.A. et al. [Particle Data Group Collaboration]. Review of Particle Physics. *Chin. Phys.* C38:090001 (2014).

[Ostrogradsky50] OSTROGRADSKY, M. Mémoire sur les équations différentielles relatives au problème des isopérimètres. *Mem. Ac. St. Petersbourg* 4:385 (1850).

[Padilla11] PADILLA, A., SAFFIN, P.M., and ZHOU, S.Y. Bi-galileon theory II: Phenomenology. *JHEP* 01:099 (2011).

[Pani11] PANI, P., CARDOSO, V., BERTI, E., et al. The vacuum revealed: the final state of vacuum instabilities in compact stars. *Phys. Rev.* D83:081501 (2011).

[Penrose65] PENROSE, R. Gravitational collapse and space-time singularities. *Phys. Rev. Lett.* 14:57–59 (1965).

[Perlmutter99] PERLMUTTER, S. et al. [Supernova Cosmology Project Collaboration]. Measurements of Omega and Lambda from 42 high redshift supernovae. *Astrophys. J.* 517:565–586 (1999).

[Peskin95] PESKIN, M. and SCHROEDER, D. *An Introduction to Quantum Field Theory*. Addison-Wesley Publishing Company (1995).

[Peter09] PETER, P. and UZAN, J. *Primordial cosmology*. Oxford University Press (2009).

[Peters99] PETERS, A., CHUNG, K.Y., and CHU, S. Measurement of gravitational acceleration by dropping atoms. *Nature* 400(6747):849–852 (1999).

[Pines85] PINES, D. and ALPAR, M.A. Superfluidity in neutron stars. *Nature* 316(6023):27–32 (1985).

[Ponti07] PONTI, C. *Mille secrets de poussins*. L'Ecole des Loisirs (2007).

[Pound60] POUND, R.V. and REBKA, G.A. Apparent Weight of Photons. *Phys. Rev. Lett.* 4:337–341 (1960).

[Pound64] POUND, R.V. and SNIDER, J.L. Effect of Gravity on Nuclear Resonance. *Phys. Rev. Lett.* 13:539–540 (1964).

[Preskill79] PRESKILL, J.P. Cosmological Production of Superheavy Magnetic Monopoles. *Phys. Rev. Lett.* 43:1365–1368 (1979).

[Radhakrishnan69] RADHAKRISHNAN, V. and MANCHESTER, R.N. Detection of a Change of State in the Pulsar PSR 0833-45. *Nature* 222:228–229 (1969).

[Reissner16] REISSNER, H. Über die eigengravitation des elektrischen feldes nach der einsteinschen theorie. *Annalen der Physik* 355(9):106–120 (1916).

[Ricotti08] RICOTTI, M., OSTRIKER, J.P., and MACK, K.J. Effect of Primordial Black Holes on the Cosmic Microwave Background and Cosmological Parameter Estimates. *Astrophys. J.* 680:829 (2008).

[Riess98] RIESS, A.G. et al. [Supernova Search Team Collaboration]. Observational evidence from supernovae for an accelerating universe and a cosmological constant. *Astron.J.* 116:1009–1038 (1998).

[Rinaldi12] RINALDI, M. Black holes with non-minimal derivative coupling. *Phys. Rev.* D86:084048 (2012).

[Rinaldi14] RINALDI, M. The dark aftermath of Higgs inflation. *Eur. Phys. J. Plus* 129:56 (2014).

[Rinaldi15a] RINALDI, M. Dark energy as a fixed point of the Einstein Yang-Mills Higgs Equations. *JCAP* 1510(10):023 (2015).

[Rinaldi15b] RINALDI, M. Higgs Dark Energy. *Class. Quant. Grav.* 32:045002 (2015).

[Ringeval05] RINGEVAL, C. and ROMBOUTS, J.W. Metastable gravity on classical defects. *Phys. Rev.* D71:044001 (2005).

[Rovelli04] ROVELLI, C. *Quantum Gravity*. Cambridge University Press (2004).

[Rubin70] RUBIN, V.C. and FORD, JR., W.K. Rotation of the Andromeda Nebula from a Spectroscopic Survey of Emission Regions. *APJ* 159:379 (1970).

[Ruffini69] RUFFINI, R. and BONAZZOLA, S. Systems of self-gravitating particles in general relativity and the concept of an equation of state. *Phys. Rev.* 187:1767–1783 (1969).

[Rybka10] RYBKA, G., HOTZ, M., ROSENBERG, L.J., et al. Search for chameleon scalar fields with the axion dark matter experiment. *Phys. Rev. Lett.* 105:051801 (2010).

[Sadeghian11] SADEGHIAN, L. and WILL, C.M. Testing the black hole no-hair theorem at the galactic center: Perturbing effects of stars in the surrounding cluster. *Class. Quant. Grav.* 28:225029 (2011).

[Sakharov68] SAKHAROV, A.D. Vacuum quantum fluctuations in curved space and the theory of gravitation. *Sov. Phys. Dokl.* 12:1040–1041 (1968). [Gen. Rel. Grav.32,365(2000)].

[Sakstein14] SAKSTEIN, J., JAIN, B., and VIKRAM, V. Detecting modified gravity in the stars. *Int. J. Mod. Phys.* D23(12):1442002 (2014).

[Salgado98] SALGADO, M., SUDARSKY, D., and NUCAMENDI, U. On spontaneous scalarization. *Phys. Rev.* D58:124003 (1998).

[Sato81] SATO, K. First-order phase transition of a vacuum and the expansion of the universe. *Mon. Not. Roy. Astron. Soc.* 195(3):467–479 (1981).

[Schimd07] SCHIMD, C., TERENO, I., UZAN, J.P., et al. Tracking quintessence by cosmic shear - constraints from virmos-descart and cfhtls and future prospects. *Astron.Astrophys.* 463:405–421 (2007).

[Schlamminger08] SCHLAMMINGER, S., CHOI, K.Y., WAGNER, T.A., et al. Test of the equivalence principle using a rotating torsion balance. *Phys. Rev. Lett.* 100:041101 (2008).

[Schlippert14] SCHLIPPERT, D., HARTWIG, J., ALBERS, H., et al. Quantum test of the universality of free fall. *Phys. Rev. Lett.* 112:203002 (2014).

[Schlögel14] SCHLÖGEL, S., RINALDI, M., STAELENS, F., et al. Particle-like solutions in modified gravity: the Higgs monopole. *Phys. Rev.* D90(4):044056 (2014).

[Schlögel16] SCHLÖGEL, S., CLESSE, S., and FÜZFA, A. Probing Modified Gravity with Atom-Interferometry: a Numerical Approach. *Phys. Rev.* D93(10):104036 (2016).

[Schmidt09] SCHMIDT, F., LIMA, M.V., OYAIZU, H., et al. Non-linear Evolution of f(R) Cosmologies III: Halo Statistics. *Phys. Rev.* D79:083518 (2009).

[Schneider16] SCHNEIDER, A. Astrophysical constraints on resonantly produced sterile neutrino dark matter. *JCAP* 1604(04):059 (2016).

[Schunck03] SCHUNCK, F.E. and MIELKE, E.W. General relativistic boson stars. *Class. Quant. Grav.* 20:R301–R356 (2003).

[Schwarz16] SCHWARZ, D.J., COPI, C.J., HUTERER, D., et al. CMB Anomalies after Planck. *Class. Quant. Grav.* 33(18):184001 (2016).

[Schwarzschild16a] SCHWARZSCHILD, K. On the gravitational field of a mass point according to Einstein's theory. *Sitzungsber. Preuss. Akad. Wiss. Berlin (Math. Phys.)* 1916:189–196 (1916).

[Schwarzschild16b] SCHWARZSCHILD, K. Über das gravitationsfeld einer kugel aus inkompressibler flüssigkeit nach der einsteinschen theorie. *Sitzber. Preuss. Akad. Wiss. Berlin (Math.-Phys.)* 1916:424–434 (1916).

[Shifman78] SHIFMAN, M., VAINSHTEIN, A., and ZAKHAROV, V. Remarks on Higgs-boson interactions with nucleons. *Physics Letters B* 78(4):443–446 (1978).

[Shih74] SHIH, A. van der waals forces between a cs atom or a cscl molecule and metal or dielectric surfaces. *Phys. Rev. A* 9:1507–1514 (1974).

[Shih75] SHIH, A. and PARSEGIAN, V.A. Van der waals forces between heavy alkali atoms and gold surfaces: Comparison of measured and predicted values. *Phys. Rev. A* 12:835–841 (1975).

[Shternin11] SHTERNIN, P.S., YAKOVLEV, D.G., HEINKE, C.O., et al. Cooling neutron star in the Cassiopeia A supernova remnant: evidence for superfluidity in the core. *MNRAS* 412:L108–L112 (2011).

[Silva15] SILVA, H.O., MACEDO, C.F.B., BERTI, E., et al. Slowly rotating anisotropic neutron stars in general relativity and scalar–tensor theory. *Class. Quant. Grav.* 32:145008 (2015).

[Smolin79] SMOLIN, L. Towards a Theory of Space-Time Structure at Very Short Distances. *Nucl. Phys.* B160:253 (1979).

[Sotiriou10] SOTIRIOU, T.P. and FARAONI, V. f(R) Theories Of Gravity. *Rev. Mod. Phys.* 82:451–497 (2010).

[Sotiriou12] SOTIRIOU, T.P. and FARAONI, V. Black holes in scalar-tensor gravity. *Phys. Rev. Lett.* 108:081103 (2012).

[Starobinsky80] STAROBINSKY, A.A. A new type of isotropic cosmological models without singularity. *Physics Letters B* 91:99–102 (1980).

[Steffen10] STEFFEN, J.H. [GammeV-CHASE Collaboration]. The CHASE laboratory search for chameleon dark energy. *PoS* ICHEP2010:446 (2010).

[Steinhardt02] STEINHARDT, P.J. and TUROK, N. Cosmic evolution in a cyclic universe. *Phys. Rev.* D65:126003 (2002).

[Steinwachs12] STEINWACHS, C.F. and KAMENSHCHIK, A.YU. Non-minimal Higgs Inflation and Frame Dependence in Cosmology. *AIP Conf. Proc.1514,161* (2012).

[Sukenik93] SUKENIK, C., BOSHIER, M., CHO, D., et al. Measurement of the Casimir-Polder force. *Phys.Rev.Lett.* 70:560–563 (1993).

[Surace16] SURACE, M., KOKKOTAS, K.D., and PNIGOURAS, P. The stochastic background of gravitational waves due to the f-mode instability in neutron stars. *Astron. Astrophys.* 586:A86 (2016).

[Sushkov09] SUSHKOV, S.V. Exact cosmological solutions with non-minimal derivative coupling. *Phys.Rev.* D80:103505 (2009).

[Tarallo14] TARALLO, M.G., MAZZONI, T., POLI, N., et al. Test of Einstein Equivalence Principle for 0-spin and half-integer-spin atoms: Search for spin-gravity coupling effects. *Phys. Rev. Lett.* 113:023005 (2014).

[Taylor92] TAYLOR, J.H., WOLSZZAN, A., DAMOUR, T., et al. Experimental constraints on strong-field relativistic gravity. *Nature* 355(6356):132–136 (1992).

[Teukolsky15] TEUKOLSKY, S.A. The Kerr Metric. *Class. Quant. Grav.* 32(12):124006 (2015).

[Theisen86] THEISEN, S. Fourth order supergravity. *Nuclear Physics B* 269:744–744 (1986).

[Thorne94] THORNE, K. *Black Holes and Time Warps: Einstein's Outrageous Legacy*. W.W. Norton (1994).

[Tolman39] TOLMAN, R.C. Static solutions of einstein's field equations for spheres of fluid. *Phys. Rev.* 55:364–373 (1939).

[Tsamis14] TSAMIS, N.C. and WOODARD, R.P. A Caveat on Building Nonlocal Models of Cosmology. *JCAP* 1409:008 (2014).

[Tsujikawa12] TSUJIKAWA, S. Observational tests of inflation with a field derivative coupling to gravity. *Phys. Rev.* D85:083518 (2012).

[Upadhye12a] UPADHYE, A. Dark energy fifth forces in torsion pendulum experiments. *Phys.Rev.* D86:102003 (2012).

[Upadhye12b] UPADHYE, A. Dark energy fifth forces in torsion pendulum experiments. *Phys. Rev.* D86:102003 (2012).

[Upadhye12c] UPADHYE, A., HU, W., and KHOURY, J. Quantum Stability of Chameleon Field Theories. *Phys. Rev. Lett.* 109:041301 (2012).

[Uzan11] UZAN, J.P. Varying Constants, Gravitation and Cosmology. *Living Rev. Rel.* 14:2 (2011).

[Vainshtein72] VAINSHTEIN, A.I. To the problem of nonvanishing gravitation mass. *Phys. Lett.* B39:393–394 (1972).

[Van Acoleyen11] VAN ACOLEYEN, K. and VAN DOORSSELAERE, J. Galileons from Lovelock actions. *Phys. Rev.* D83:084025 (2011).

[vanderBij87] VAN DER BIJ, J.J. and GLEISER, M. Stars of Bosons with Nonminimal Energy Momentum Tensor. *Phys. Lett.* B194:482 (1987).

[vanderBij00] VAN DER BIJ, J.J. and RADU, E. Regular and black hole solutions of the Einstein-Yang-Mills-Higgs equations: The Case of nonminimal coupling. *Nucl. Phys.* B585:637–665 (2000).

[Vessot80] VESSOT, R.F.C., LEVINE, M.W., MATTISON, E.M., et al. Test of Relativistic Gravitation with a Space-Borne Hydrogen Maser. *Phys. Rev. Lett.* 45:2081–2084 (1980).

[Voje Johansen06] VOJE JOHANSEN, N. and RAVNDAL, F. On the discovery of Birkhoff's theorem. *Gen. Rel. Grav.* 38:537–540 (2006).

[Volkov99] VOLKOV, M.S. and GAL'TSOV, D.V. Gravitating non-Abelian solitons and black holes with Yang-Mills fields. *Phys. Rept.* 319:1–83 (1999).

[Wald84] WALD, R. *General Relativity*. University of Chicago Press (1984).

[Weinberg89] WEINBERG, S. The cosmological constant problem. *Rev. Mod. Phys.* 61:1–23 (1989).

[Weinberg02] WEINBERG, E.J. Black holes with hair. *NATO Sci. Ser. II* 60:523–544 (2002).

[Weinberg08] WEINBERG, S. *Cosmology*. Oxford University Press (2008).

[Weisberg10] WEISBERG, J.M., NICE, D.J., and TAYLOR, J.H. Timing Measurements of the Relativistic Binary Pulsar PSR B1913+16. *Astrophys. J.* 722:1030–1034 (2010).

[Wex14] WEX, N. Testing Relativistic Gravity with Radio Pulsars. *arXiv:1402.5594* (2014).

[Whitt84] WHITT, B. Fourth-order gravity as general relativity plus matter. *Physics Letters B* 145(3):176–178 (1984).

[Will93] WILL, C.M. *Theory and experiment in gravitational physics*. Cambridge University Press (1993).

[Will08] WILL, C. The Confrontation Between General Relativity and Experiment. *EAS Publ.Ser.* 30:3–13 (2008).

[Williams04] WILLIAMS, J.G., TURYSHEV, S.G., and BOGGS, D.H. Progress in lunar laser ranging tests of relativistic gravity. *Phys. Rev. Lett.* 93:261101 (2004).

[Williams09] WILLIAMS, J.G., TURYSHEV, S.G., and BOGGS, D.H. Lunar laser ranging tests of the equivalence principle with the earth and moon. *Int. J. Mod. Phys.* D18:1129–1175 (2009).

[Wiltshire09] WILTSHIRE, D.L., VISSER, M., and SCOTT, S. *The Kerr spacetime : rotating black holes in general relativity*. Cambridge University Press (2009).

[Woodard14] WOODARD, R.P. Nonlocal Models of Cosmic Acceleration. *Found. Phys.* 44:213–233 (2014).

[Woodard15] WOODARD, R.P. Ostrogradsky's theorem on Hamiltonian instability. *Scholarpedia* 10(8):32243 (2015).

[Yagi13] YAGI, K. and YUNES, N. I-Love-Q. *Science* 341:365–368 (2013).

[Yunes13] YUNES, N. and SIEMENS, X. Gravitational-Wave Tests of General Relativity with Ground-Based Detectors and Pulsar Timing-Arrays. *Living Rev. Rel.* 16:9 (2013).

[Zee79] ZEE, A. Broken-symmetric theory of gravity. *Phys. Rev. Lett.* 42:417–421 (1979).

[Zee80] ZEE, A. Horizon problem and the broken-symmetric theory of gravity. *Phys. Rev. Lett.* 44:703–706 (1980).

[Zeldovich78] ZELDOVICH, Y.B. and KHLOPOV, M.Y. On the concentration of relic magnetic monopoles in the universe. *Physics Letters B* 79:239–241 (1978).

[Zhang16] ZHANG, X., ZHAO, W., HUANG, H., et al. Post-Newtonian parameters and cosmological constant of screened modified gravity. *Phys. Rev.* D93(12):124003 (2016).

[Zlatev99] ZLATEV, I., WANG, L., and STEINHARDT, P.J. Quintessence, cosmic coincidence, and the cosmological constant. *Phys. Rev. Lett.* 82:896–899 (1999).

[Zumalacárregui14] ZUMALACÁRREGUI, M. and GARCÍA-BELLIDO, J. Transforming gravity: from derivative couplings to matter to second-order scalar-tensor theories beyond the Horndeski Lagrangian. *Phys. Rev.* D89:064046 (2014).

[Zwicky33] ZWICKY, F. Die Rotverschiebung von extragalaktischen Nebeln. *Helvetica Physica Acta* 6:110–127 (1933).